The University of Nottingham
UNITED KINGDOM · CHINA · MALAYSIA

Department of Mechanical, Materials and Manufacturing Engineering

The effect of oil feed pressure on friction and cavitation in plain bearings

Yousuf Ali Mansoor

(BEng)

Thesis submitted to the University of Nottingham for the degree of Doctor of Philosophy

September 2017

Abstract

Experimental and theoretical studies of the influence of oil supply pressure on the friction torque in plain bearings have been carried out. The focus of the work has been the reduction in bearing friction that might be achieved by reducing oil supply pressure and the mechanisms by which the changes in friction occur, with potential applications to reducing bearing friction in internal combustion engines.

A single bearing test rig has been used to investigate the impact of feed oil pressure on the extent of cavitation and the role of increased film cavitation on friction under light, steady loads for a bearing with a 180° groove, using an SAE 5W-30 oil. Film visualization shows that cavitation area increases when the oil feed pressure is reduced and the extent of the full width film reduces primarily as the angle of film reformation is retarded. Both load and speed increases reduce the full width film extent.

At constant film viscosity, friction torque was reduced by up to 20% by increased cavitation which reduced the film area and the eccentricity ratio. The latter reduces the surface shear stress in the load-bearing region of the film and overall, the circumferential average. As load increases, the reduction in film area accounts for an increasing proportion of the friction torque reduction.

The effect of load, speed, lubricant formulation and clearance on bearing friction and film pressure has been investigated. Increases in load led to increases in friction and peak film pressures with smaller percent reductions in friction torque as the supply pressure was reduced. Bearing friction torque was found to show a linear dependence on oil viscosity in the hydrodynamic regime where friction could be substantially reduced by using low viscosity oils. The effect of increased clearance was to reduce bearing friction and increase peak film pressures.

The effects of reduced oil supply pressure on friction in crankshaft main bearings during cold-start warm-ups has been investigated. Friction reductions have been found to be most significant during cold running conditions at light loads. The thermal coupling between the bearing films and engine structure influences the film

warm-up. Initially there is a rapid rise in film temperatures after which the warm-up is held back by the temperature of the surrounding metal. In addition to reducing bearing friction, reducing oil supply pressure also reduces the oil pumping work required; this represents an additional benefit which can be particularly significant under cold operating conditions.

Contents

Abstract i

Nomenclature viii

Acknowledgements xiii

Chapter 1- Introduction 1

1.1 Background: CO_2 Emissions and the Automotive Industry 3

1.2 Lubricated Friction 6

1.3 Aims and Objectives of the Investigation 8

1.4 Thesis Layout 9

1.5 Contribution to Knowledge 10

Chapter 2- Literature Review 12

2.1 Introduction 12

2.2 Fundamentals of Hydrodynamic Plain Bearings 13

2.2.1 Basics of Design 13

2.2.2 Hydrodynamic Lubrication 16

2.2.3 Behaviour of Loaded Bearings 18

2.2.4 Plain Bearing Friction Torque 20

2.2.5 Lubricant Cavitation and Modelling 24

2.2.6 Effects of Reduced Supply Pressure on Bearing Performance 30

2.2.7 Bearing Wear 31

2.2.8 Failure Modes 32

2.3 Viscometrics of Lubrication Oil 33

2.3.1 Introduction 33

2.3.2 SAE Oil Standard 34

2.3.3 Viscosity-Temperature Equations 34

2.3.4 Viscosity Variation with Shear Rate 35

2.3.5 Viscosity Variation with Pressure 38
2.4 Oil Lubrication System of Engines 39
2.4.1 Requirements 39
2.4.2 Oil System Layout 40
2.4.3 Pump Types and System Operation 41
2.5 Friction in Engines 45
2.5.1 Introduction 45
2.5.2 Engine Rubbing Friction Regimes 45
2.5.3 Definitions of Friction Terms 47
2.5.4 Friction Measurement Methods 48
2.5.5 Recent Developments in Reducing Engine Bearing Friction 49
2.6 Discussion and Concluding Remarks 53
Chapter 3- A Single-Bearing Friction Rig and Setup for Visual Studies of Bearing Film Area and Extent 55
3.1 Introduction 55
3.2 Overview of Test Rig Design and Measurement Techniques Employed in Literature 56
3.2.1 Test Rigs 56
3.2.2 Measurement Techniques 57
3.3 Single-Bearing Rig Design and General Assembly 57
3.3.1 Shaft Assembly 58
3.3.2 Loading System 59
3.3.3 Rig Lubricant Supply System 60
3.3.4 Calibration of the Torque Measurement 61
3.3.5 Bearing Test Bushes and Design 62
3.3.6 Test Rig Instrumentation and Calibration 65

3.4 Observation of Cavitation and Determination of Cavitation Area 66
3.5 Operation of Facility and Data Analysis Methods 69
3.6 Discussion 70
Chapter 4- Oil Film Cavitation Patterns Under Light Load Operating Conditions 73
4.1 Introduction 73
4.2 Range of Experiments for Visual Investigation 73
4.3 Cavitation Patterns and Changes in Film Extent with Feed Pressure 73
4.4 Stages of Hydrodynamic Film Failure and Recovery of Film 82
4.5 Discussion 86
4.6 Conclusions 91
Chapter 5- Influence of Cavitation on Bearing Friction 92
5.1 Introduction 92
5.2 Cavitation Area and Friction Changes 92
5.3 Cavitation Friction Assessment 95
5.4 Mechanism of Friction Reduction with Reducing Feed Pressure at Light Loads 97
5.4.1 A Numerical Model for the Analysis of Feed Conditions on a 180° Circumferentially Grooved Bearing 98
5.4.2 Solution Procedure 99
5.4.3 Analysis of Friction Reduction Mechanisms with Feed Pressure 100
5.4.4 Variation in %Torque Reduction Against %Cavitation Area with Drop in Feed Pressure, Comparison between Experiment and Friction Model 102
5.5 Discussion 105
5.6 Conclusions 107
Chapter 6- Effects of Load, Speed, Oil Formulation and Clearance on Friction and Pressure Distributions 108
6.1 Introduction 108

6.2 Estimation of Load Capacity from Film Pressure Measurement 109

6.3 Effect of Steady Load on Bearing Friction and Performance Characteristics and Changes with Feed Pressure 111

6.4 Effect of Shaft Speed on Bearing Friction and Performance Characteristics and Changes with Feed Pressure 115

6.5 Effect of Lubricant Formulation on Bearing Operating Characteristics 120

6.5.1 Friction Torque 121

6.5.2 Pressure Profiles 123

6.5.3 Flow Rates 127

6.5.4 Film Temperature 128

6.6 Effect of Radial Clearance on Bearing Friction and Film Pressure 129

6.7 Discussion 132

6.8 Conclusions 139

Chapter 7- Studies of Motored Friction of Crankshaft Main Bearings in a Cylinder Block 140

7.1 Introduction 140

7.2 Multi-Bearing Rig Design, Specification and Data Acquisition 140

7.2.1 Test Rig Instrumentation and Calibration 144

7.2.2 Friction Measurement 146

7.2.3 Main Bearing Gas Load Distribution 147

7.3 Crankshaft Friction and Warm-Up Results under Reduced Oil Supply Pressures 148

7.3.1 Crankshaft Bearing Friction Variation with Feed Pressure 148

7.3.2 Main Bearing and Bulk Oil Thermal Interaction with Feed Pressure 153

7.3.3 Film Pressure Variation 155

7.3.4 Bearing Friction and Failure at No Flow Condition 156

7.4 Response of Oil Film Temperature and Pressure to Increase in Main Gallery Pressure 157
7.5 Effect of Load and Reduction in Oil Supply Pressures on Crankshaft Friction . 159
7.6 Reductions in Oil Pump Work 162
7.7 Discussion 163
7.8 Conclusions 166
Chapter 8- Discussion and Conclusions 167
8.1 Discussion 167
8.2 Future Work 174
8.3 Conclusions 176
Appendix 178
References 179

Nomenclature

A	Area	(m^2)
a	Groove width	(m)
b	Bearing width	(m)
barA	Absolute pressure	
barG	Gauge pressure	
C_r	Mean Radial clearance	(m)
CW	Clockwise	
c_1	Vogel constant 2	(°C)
c_2	Vogel constant 3	(°C)
d	Shaft diameter	(m)
D	Bearing diameter	(m)
e	Eccentricity	(m)
F	Friction force	(N)
P_f	Supply pressure	(Pa)
F_g	Piston steady gas force	(N)
h	Film thickness	(m)
h*	Dimensionless film thickness	
k_v	Vogel constant 1	(Pa.s)
M_v	Vogelpohl parameter	
N	Journal speed	(rpm)
p	Pressure	(Pa)

p*	Dimensionless pressure	
P	Power loss	(W)
Q	Bearing flow rate	(m^3/s)
Q_p	Feed pressure flow	(m^3/s)
R	Bearing radius	(m)
SL	Specific load	(bar)
t	Time	(s)
T	Temperature	(°C)
τ	Torque	(N m)
U	Journal tangential velocity	(m/s)
$\dot{V}$	Volume flow rate of oil	(lpm)
V_s	Swept volume	(m^3)
W	Applied load	(N)
W_1	Walther constant 1	
W_2	Walther constant 2	
W*	Dimensionless load capacity	
$\dot{W}_h$	Oil pump hydraulic power	(W)
x	Circumferential coordinate	(m)
x*	Dimensionless circumferential coordinate	
y	Axial coordinate	(m)
y*	Dimensionless axial coordinate	

Greek Symbols

α	Pressure-viscosity coefficient	
β	Oil inlet angle relative to y-axis	(°)
Ɛ	Eccentricity ratio	
ω	Angular velocity	(rad/s)
φ	Attitude angle	(°)
ϕ	Angle of film reformation front	
Θ	Bearing polar coordinate	(rad)
θ	Clockwise angle relative to y-axis	(°)
τ	Shear stress	(Pa)
ν	Kinematic viscosity	(m^2/s)
μ	Dynamic viscosity	(Pa.s)
γ	Shear rate	(s^{-1})

Subscripts

atm	atmospheric pressure
bush	Test Bush
CL	Centreline
c	cavitation
f	film
j	journal

max	Maximum
min	Minimum
r	Radial
sh	Shear
sq	Squeeze

Abbreviations

ADEPT	Advanced Diesel Electric Powertrain
BDC	Bottom Dead Centre
BMEP	Brake Mean Effective Pressure
CCS	Cold Crank Simulator
CMM	Coordinate Measuring Machine
CW	Clockwise
DAQ	Data Acquisition
ECU	Engine Control Unit
EGR	Exhaust Gas Recirculation
EU	European Union
FDM	Finite Difference Method
FMEP	Friction Mean Effective Pressure
FP	Feed Pressure (bar)
HTHS	High Temperature High Shear
ICE	Internal Combustion Engine

IMEP	Indicated Mean Effective Pressure
JFO	Jakobsson, Floberg and Olsson
LCV	Low Carbon Vehicle
MEP	Mean Effective Pressure
MOFT	Minimum Oil Film Thickness
NEDC	New European Drive Cycle
NI	National Instruments
OSV	Oil Switching Valve
PCJ	Piston Cooling Jet
PL	Specific bearing load based on piston projected area
SL	Specific bearing load based on bearing projected area
THD	Thermohydrodynamic
UK	United Kingdom
VDOP	Variable Displacement Oil Pump

Acknowledgements

I would like to express my sincerest gratitude to my thesis supervisor, Professor Paul Shayler for providing me with this opportunity and for his guidance and support throughout my time at the University of Nottingham. I could not have envisaged a better mentor for my PhD study. Thank you so much for your support, encouragement and inspiring ideas.

Many thanks to Dr. Jean Paul Zammit and Dr. Michael McGhee for their help, suggestions and assistance especially in my first year of PhD at Nottingham. Thank you for training me and helping me settle down when I started. My special thanks go to my colleagues in the Engine Research Group, particularly Gianluca and Chen for their friendship.

I would like to thank the technical staff at the University of Nottingham including Paul Bramman, Nigel Sykes and John Lane for all their support and helping me setup and maintain the test rigs.

I wish to acknowledge the financial support I received through the Dean of Engineering Scholarship for Research Excellence from the University of Nottingham.

Most of all, I am tremendously indebted to my parents (Mansoor Siddique and Salma Mansoor) and my siblings (Mujtaba and Fatima) for their unwavering love, care and counsel throughout my life. I will never be able to repay you for all you have done for me.

Chapter 1- Introduction

The investigations reported in this thesis are concerned with the friction torque of plain bearings and what influences this, particularly with regards to the effects of the pressure of the oil feed and also the mechanisms by which this changes friction torque.

The form of plain, hydrodynamic bearing of interest consists of a journal rotating within a bush with the clearance between them occupied by a lubricant. The relative motion and eccentricity of the journal to the bush leads to generation of hydrodynamic pressures which allows the bearing to support an externally applied load while maintaining low friction motion. The Reynolds hydrodynamic equation, derived by Osborne Reynolds in 1886 [1], defines the pressure distribution of such bearings and is presented in more detail in Chapter 2.

The motivation for the research has been to investigate the possibility of improving the fuel economy of light duty automotive engines by reducing frictional losses in the plain bearings used in the crankshaft and camshaft assemblies of engines. In particular, the thesis is concerned with the effects of the pressure of the oil feed to bearings and the mechanisms by which the friction in the bearings might be reduced when this pressure is reduced.

Engine rubbing friction is a substantial source of engine inefficiency. Mechanical friction accounts for approximately 25 percent of the indicated work output of a vehicle engine under urban driving conditions [2] and is strongly dependent on the lubricant temperature. Shayler [3] investigated crankshaft main bearing friction during warm-up and observed that after the early few seconds of engine operation, the variation of engine friction followed a power-law dependence on oil viscosity determined at the oil feed. When the engine is running cold, the oil viscosity can be several times higher than under warm conditions, therefore, the penalty associated with frictional losses is highest when the engine is running cold, contributing to higher fuel consumption.

The main sources of engine rubbing friction are the piston assembly, the crankshaft assembly and the valve train assembly. Heywood [4] reported that of the total engine rubbing friction, 50 percent can be attributed to the piston assembly, 30 percent to the crankshaft bearings and seals and 20 percent to the valve train. Therefore, the short journal bearings used in the crankshaft assemblies of internal combustion engines make a significant contribution to engine friction losses and reduction of these losses would contribute to substantial fuel savings.

Commonly in automotive lubrication systems, oil is delivered to engine bearings via a fixed displacement mechanical pump coupled to the engine crankshaft directly or by a belt drive. The pump delivery is dependent upon engine speed and the pressure of the oil feed to the bearings is maintained at or above the setting required to maintain flooded conditions. If the oil feed pressure and oil flow to the bearings is reduced, a reduction in friction torque may be observed. Ultimately, if the bearings are run dry, contact between the bearing journal and shell or bush occurs and failure can quickly result. However, between the fully-flooded and completely starved conditions, it is possible to run the bearings in a partly-flooded condition. It is of considerable interest to understand this behaviour and whether it might be safely exploited as a route to improving engine efficiency.

Furthermore, the use of fixed displacement pumps leads to high power consumption and poor flow control. When the engine speed is high, the volume displaced by the pump may be more than required, leading to the use of flow reducers and relief valves diverting oil back to the engine sump. However, this incurs energy losses and oil aeration and degradation. With improved oil flow control in the lubricant circuit a reduction of parasitic loads on the engine can also be achieved.

In the investigations reported in this thesis, the effect of reduced feed pressure on main bearing friction under steady load conditions was tested on two bespoke bearing test rigs. The first rig consisted of a single main bearing based on a 1.5 litre Ford diesel production engine and was developed to explore in more detail the relationship of friction torque to oil feed conditions and changes in conditions of the bearing film for a range of bearing loads, journal speeds and oil viscosities. Typically,

tests covered a range of film temperature from ambient to a final steady value. Investigations were carried out with a bronze or Perspex bush; the latter allowed oil film cavitation to be visualised and the mechanism of friction reduction to be explored in further detail.

The second test rig made use of specially manufactured shafts with the five plain journal bearings of a crankshaft from a 4 cylinder, light duty diesel engine. The shaft was motored in the engine block to investigate the friction torque changes during a warm-up process. The oil temperature in the main gallery increased from initial temperatures of 5 °C to around 20 °C and from -10 °C to around 60 °C. Tests were carried out at engine speeds of 1000 rev/min and steady piston gas loads of 1bar to 7bar. In each set of tests, the main bearing feed pressure was progressively reduced from a high baseline main gallery pressure down to low pressure. The reduction in main bearing friction with feed pressure as well as thermal interaction in a multi-bearing engine rig has been, therefore, experimentally determined over sub-zero cold start and warm conditions for a range of loads from the results.

A major theme of the investigations carried out has been cavitation in fluid film bearings. Generally, cavitation is associated with vapour formation due to generation of very low fluid pressures. In the field of bearing tribology, however, formation of cavities in thin films due to outgassing of dissolved air as well as vaporising of lubricant are both regarded as cavitation [5]. In this thesis, following the terminology of tribology literature, outgassing of dissolved air is also referred to as cavitation.

1.1 Background: CO_2 Emissions and the Automotive Industry

Concerns regarding global warming have put increased pressure on automotive manufacturers worldwide to reduce CO_2 emissions from vehicles. In the European Union (EU) passenger cars account for approximately 12 percent of total EU emissions of carbon dioxide (CO_2) which is the primary greenhouse gas [6].

The reduction in CO_2 emissions is one of the main incentives behind the ACEA's (European Automobile Manufacturers' Association) continuous efforts to reduce

vehicle fuel consumption since there is a distinct link between CO_2 emission and fuel consumption. Combustion of a litre of diesel produces nearly 3000 grams of CO_2.

In 2008, the EU set mandatory targets on CO_2 emissions per km for new cars [7]. The law requires that by 2015 new cars registered in the EU do no emit on average more than 130 grams of CO_2. This equates to an average fuel consumption of about 4.9 l/100 km for diesel fuel. The limiting value of 130 g/km is an average value to be achieved over a manufacturer's fleet and a 'limit value curve' sets emission limits according to the mass of vehicle. Since only the fleet average is regulated, manufacturers can still produce heavier vehicles with emissions above their indicative targets given that they are balanced by the vehicles below the curve. An example limit value curve is given in Figure 1.1. The target of 130g/km was gradually introduced between 2012 to 2015. After 2015, a manufacturer's fleet must comply with the regulation or otherwise an excess emissions premium has to be paid for each car registered. This premium equals €5 for the first g/km over the target, €15 for the second g/km, €25 for the third g/km, and €95 for each subsequent g/km. From 2019, each excess gram of CO_2 per kilometre would be penalised at €95.

By the year 2020, the fleet average to be achieved by 95 percent of all new cars has been set to 95 grams of CO_2 per kilometre. By 2021, 100 percent of each manufacturer's new cars will have to comply with the limit value curve.

Vehicle fuel consumption and CO_2 emissions are measured over the New European Drive Cycle (NEDC) which intends to represent typical car usage in Europe. Measuring over a drive cycle allows assessment of fuel consumption and emissions of a vehicle in a normalized way, so that different vehicles can be compared. The NEDC is shown in Figure 1.2. It consists of four repeated ECE-15 urban driving cycles (UDC) and one Extra-Urban driving cycle (EUDC). The UDC represents typical driving conditions in the city characterised by low speed and low engine load while the EUDC represents high load, high speed conditions.

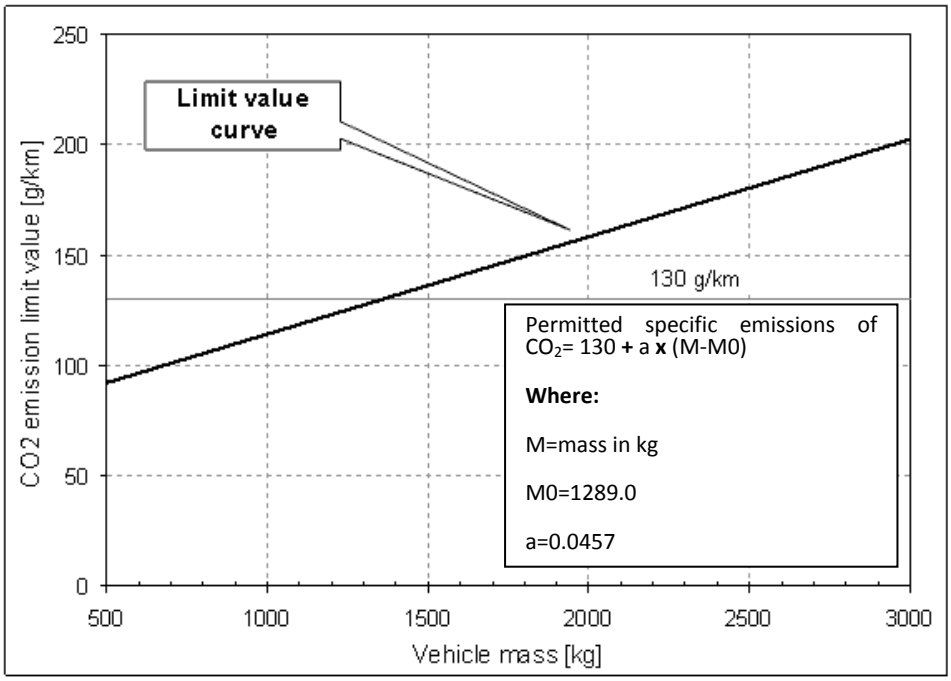


Figure 1.1: Limit value curve [6]

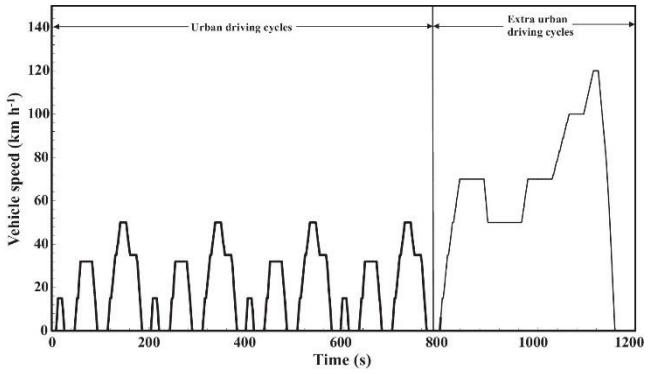


Figure 1.2: New European driving cycle

Part of the work undertaken in this thesis was in connection with the Advanced Diesel Electric Powertrain (ADEPT) project. The project was part of the Low Carbon Vehicle (LCV) programme of Innovate UK (formerly the Technology Strategy Board). Participating members of the consortium working on the project consisted of Ricardo, Ford Motor Company, Controlled Power Technologies (CPT), the European Advanced Lead Acid Battery Consortium (EALABC), Faurecia and the University of Nottingham. The project aimed to apply the low voltage concept of 'intelligent

electrification' to a diesel car for the first time. The consortium was to apply a 48V mild hybridisation to a diesel engine with additional application of synergistic 48V ancillaries and advanced thermal systems/waste heat recovery technologies. A Ford Focus estate demonstrator vehicle was targeted at 75 g/km CO_2 as measured on European Drive Cycle, with a CO_2 walk through to less than 70 g/km, whilst maintaining a CO_2/cost superior to an equivalent Hybrid Electric Vehicle. The Nottingham University component involved investigation of bearing performance and conditions over a range of speeds and loads to quantify the friction reduction possible under cold running conditions, to identify what this is due to and to identify what constraints must be observed to avoid bearing damage. As part of this series of investigations, tests were also carried out on a firing diesel engine which have been occasionally referred to. However, in this thesis steadily loaded bearings have been the focus.

1.2 Lubricated Friction

Friction losses in an engine mainly occur in the piston assembly (piston rings, piston skirt and piston liner), big end and small end bearings, crankshaft main bearings and oil seals, camshaft bearings and valve train assembly and the belts and pulleys required to run engine ancillaries [4].

A variety of lubrication regimes exist in these components due to differing operating conditions of load, speed and viscosity [4]. The different lubrication regimes are typically explained using the Stribeck diagram [8] in Figure 1.3 which characterises friction coefficient, which is the ratio of the instantaneous friction force to the normal load, against a duty parameter, μU/W, where μ is the viscosity, U is the sliding speed and W is the normal load.

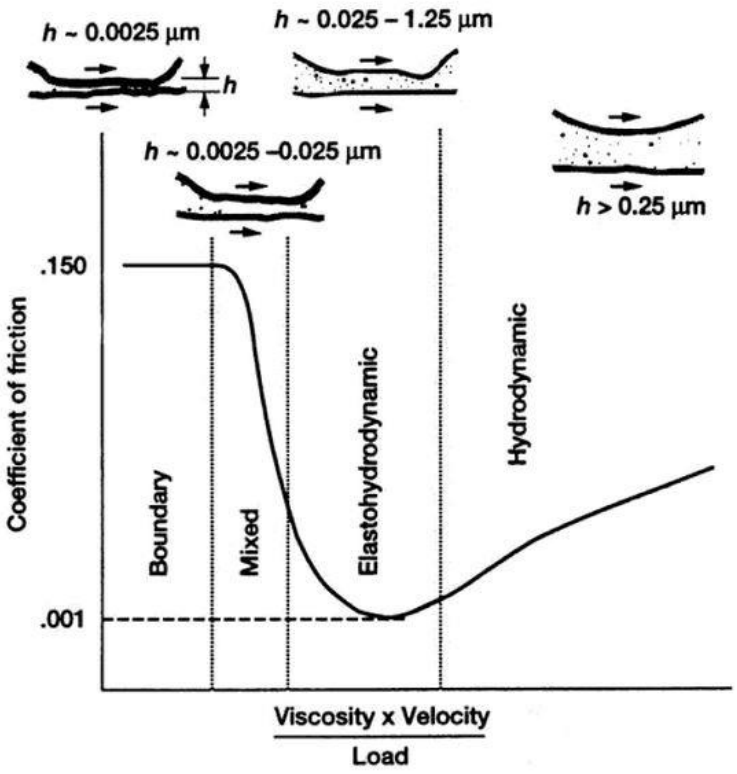


Figure 1.3: Stribeck curve showing the different lubrication regimes [8]

On the left side of the curve lies the boundary lubrication regime where the friction coefficient for many systems is of the order 0.1 [9]. Here the mean oil film thickness is less than the combined surface roughness of the opposite surfaces and friction depends on surface properties. In this regime the friction coefficient is dependent upon non-hydrodynamic characteristics. The friction coefficient becomes a function of the shear strength of the absorbed oil layer and yield stress of the softer material in the pair of sliding surfaces. Oil viscosity does not play a dominant role in dictating the friction force and friction can be reduced by use of additives to a mineral oil [10, 11]. An oxidised layer of boundary film, 1 to 3 nm in thickness prevents excessive wear of the rubbing surfaces [12-14]. If the boundary film breaks down, the friction coefficient may rise to 1 or more eventually resulting in seizure of components.

On the right side of the curve lies the hydrodynamic region where the friction coefficient can be of the order of 0.002 [9]. The friction here depends on viscous shearing of the lubricant rather than the interaction between surface irregularities since and the surfaces are completely separated by a thick oil film [13]. In this region film thicknesses are more than 0.25 µm and generally between 5 to 500 µm [14]. In

non-conforming contacts, local pressures in the contact area can become very high and the load is supported by an increase in lubricant viscosity due to pressure and the elastic deformation of the surfaces [13]. This region is known as the elastohydrodynamic zone. In between boundary and hydrodynamic lubrication lies the mixed regime where intermittent contact between the surfaces takes place [12, 14]. Here the oil film thickness is reduced and is similar in size to the surface irregularities. The film thickness in this zone typically lies between 0.0025 to 0.25 μm [14].

Whilst parts of the piston assembly experience metal-metal contact, the main and big end bearings in the crankshaft assembly operate mostly in the hydrodynamic regime. However, mixed lubrication does occur in bearings during start-ups and stops leading to wear [15]. The friction in the hydrodynamic film exists due to shearing of the lubricant and increases with viscosity, speed and load. The minimum allowable film thickness between the journal and shell (MOFT) is typically designed to be 2 μm [16]. Minimum film thicknesses of less than 1 μm would result in some asperity contact during an engine cycle [17]. Friction contributions from individual engine components are further discussed in Section 2.5.

1.3 Aims and Objectives of the Investigation

The focus of this work has been the determination of friction benefits of controlled oil flow to engine main journal bearings over a range of operating conditions and different oil formulations which can be achieved on the engine through electrification of the oil pump and to determine the limitations of operating at reduced flow. Another main aim of the study was to determine the mechanisms of friction reduction under reduced flow.

These aims have been pursued with the realization of the following objectives:

- Design and development of a novel, single main bearing test facility which is able to provide controlled feed pressure to a test bearing and measure bearing friction.

- Examine friction reduction on an isolated, steadily loaded journal bearing with reduction in feed pressure over a range of loads and speeds.
- Investigate the source of friction benefit with reduction in feed pressure using transparent Perspex bushes on the single bearing rig. Two possible mechanisms of friction reduction have been suggested in literature: reduction in film shear area and increase in film temperature as the flow is reduced. This investigation involved visualisation of the bearing film using transparent bushes in order to connect the relationship between torque reduction and increase in film cavitation area and examine what are the other sources contributing to the total benefit.
- Undertaking of motored experimental studies on a modified engine rig to quantify the reduction in engine main bearing friction with flow control to crankshaft main bearings during cold running and warm conditions in an engine environment. Flow control is achieved by use of an electric oil pump which allows bearing feed pressure to be kept lower than required for flooded conditions.
- Using the isolated bearing test facility, investigate the effect of lubricant formulation on main bearing friction at different supply pressures, temperatures and loads.

From the work carried out it has been found that friction torque reduces as feed pressure is reduced, the main sources of which have been determined to be a reduction in film area, decrease in the film shear rate at light load and increase in film temperature. Substantial reductions in friction of up to 20% are achievable especially under cold conditions where oil viscosity is high and friction losses are highest.

1.4 Thesis Layout

The thesis is presented in eight chapters. The chapters following the introduction chapter are listed below:

- *Chapter 2*: The content of this chapter covers a general background on journal bearing design and lubrication as well as friction and the factors affecting friction. Emphasis is given to cavitation in journal bearings as it influences

bearing friction significantly. Further topics covered include a description of engine friction and the lubrication system as a whole, components of total engine friction, friction regimes characterised on the Stribeck curve and methods to measure engine friction. The effect of different design features on main bearing friction is reviewed as well as a discussion of thermal and non-thermal methods towards reducing engine bearing friction.

- *Chapter 3*: In this chapter the single-bearing test facility is described which was designed to investigate in more detail the relationship of friction torque to oil feed conditions and changes in conditions of the bearing film for a range of bearing loads and speeds on an isolated main bearing.
- *Chapter 4*: This chapter is concerned with the presentation of the investigations, results and interpretation of results of cavitation patterns obtained from visual studies performed on Perspex test bushes.
- *Chapter 5*: An experimental and theoretical investigation is presented in this chapter to identify the main mechanisms of friction reduction with decrease in feed pressure.
- *Chapter 6:* In this chapter the effect of different parameters including load, speed and lubricant viscosity on bearing friction is presented and discussed.
- *Chapter 7*: This chapter introduces a multi-bearing engine rig that has been used to experimentally investigate effects of gallery oil pressure on crankshaft bearing friction from cold, sub-zero temperatures to warm running conditions. Results are presented and analysed for various loads and temperatures.
- *Chapter 8*: This chapter presents an overall discussion and main conclusions drawn from the work carried out in this thesis, as well as suggestions for any future work relevant to the subject matter.

1.5 Contribution to Knowledge

Contribution towards knowledge from the current thesis consisted of experimental studies on the effects of feed pressure on engine crankshaft bearing friction carried out on test facilities specifically designed for this purpose and the processing and

interpretation of the friction data. Friction tests were carried out on both an isolated bearing as well as a modified engine crankshaft covering a wide range of temperatures. Apart from that visual studies of film conditions were also performed to investigate the effect of supply pressure on cavitation patterns and friction reduction mechanisms.

Previous experimental studies on the effects of supply pressure on various journal bearing performance parameters including friction torque, film pressure, flow rate and eccentricity ratio have mostly concentrated on single feed hole, single axial or twin axial groove bearings [18-22] and there is little experimental information available for journal bearings with a 180° circumferential groove. Grooving arrangements can have a significant impact on film extent, flow, friction and eccentricity ratio [23, 24]. The investigations carried out in this thesis provide data and analysis for a 180° circumferentially grooved journal bearing for a range of operating conditions which added new dimensions in understanding engine main bearing film friction.

Similarly, there is a lack of visual studies detailing cavitation patterns and film extents for the 180° circumferential groove type journal bearing. The use of Perspex bushes on the single bearing test facility not only allowed film visualisation to be performed on 180° circumferentially grooved bearings for which data is scarcely available in literature, but along with simultaneous measurement of friction torque and film temperature also provided experimental evidence which, along with the use of a theoretical model, was used in explaining the factors that to lead to friction reduction with reduction in supply oil pressure.

Data has been collected on an isolated bearing which allows the effects of supply conditions on friction to be investigated on one bearing, thus simplifying the analysis. Friction data has also been collected using a multi-bearing engine rig which allows the effects of supply conditions to be investigated in an engine environment and over a range of operating temperature- from sub-zero to warm conditions.

Chapter 2- Literature Review

2.1 Introduction

The material presented in this chapter provides an overview of past and current work relevant either directly or indirectly to friction in journal bearings and the influences of operating conditions including oil viscometrics and supply pressure on bearing performance.

The chapter begins with a description of the basics of hydrodynamic journal bearings providing a brief overview of the hydrodynamic theory including a description of different grooving arrangements and the effects of bearing eccentricity on load capacity and friction. Thin film cavitation is discussed since it plays a significant role in determining bearing friction and its extent is greatly influenced by feed pressure.

The next section discusses oil viscometrics and the effects of temperature, shear rate and pressure on oil viscosity and friction. An overview of the lubrication circuit and system in engines is presented as well as recent developments in oil pump technology to provide improved oil flow control and reduce parasitic losses.

The section after this provides a description of the different sources of engine friction and the various friction regimes encountered during engine operation. A summary of the experimental methods employed in measuring crankshaft and bearing friction is presented. An overview is presented on the current trends in the approaches used to reduce engine bearing friction including the effects of oil feed pressure control on bearing film behaviour and fuel economy as evidenced in literature.

2.2 Fundamentals of Hydrodynamic Plain Bearings

2.2.1 Basics of Design

Plain journal bearings fall into the category of fluid film bearings and play a vital role in the lubrication system of automotive engines to prevent friction between parts during relative movement. They typically operate in the hydrodynamic lubrication regime and are essential elements of the crankshaft, con-rod and cam shaft assemblies. The main reasons for their use in crankshaft assemblies is their ability to absorb strong shock-like loads, their suitability for high speeds and long operating life as well as their simple configuration and potential for cost effective manufacturing [25].

The design principle of a journal rotating inside a stationary bush is illustrated in Figure 2.1. The clearance between the two is mostly occupied by the lubricant. Lubricant is fed continuously to the bearing via a groove or hole typically under pressure. A lubricating wedge is formed due to relative motion between the journal and bush leading to generation of hydrodynamic pressure within the film which acts as a 'spring' force [25] supporting the applied steady load. The centres of the journal and bearing are offset by a value, e, known as the eccentricity. The eccentricity ratio which is given by e/C_r, where C_r is the mean radial clearance, is an important dimensionless parameter characterising the circumferential shape of the film. The angle between the load vector and the point of minimum film thickness (Point B in Figure 2.1) is known as the attitude angle.

The shape of the circumferential film pressure is of the profile shown in Figure 2.1. Engine journal bearings are generally of the 'short' type where the bearing width is less than the diameter [26]. For such bearings, assuming perfect alignment, an axial pressure profile parabolic in nature exists [27] shown in Figure 2.2.

In cases where the load vector is constant, a plain bearing may be supplied via a feed hole or an axial feed groove of small angular extent. For unidirectional loads, the common practice is to position grooves on the unloaded bearing side [28]. Experiments carried out by Okamoto et al. [23] have shown a significant reduction in bearing oil flow and film extent as the feed hole is placed closer to the load vector

hence making bearing operation less safe. Figure 2.3 depicts some of the feed groove designs employed in journal bearings. Longer or wider groove extents result in increased fluid flow through the bearing by providing a larger film area over which supply pressure can act [28]. Axial grooves are used in bearings which are relatively long [16] to distribute oil over the entire bearing width to improve lubrication and control the temperature field [29]. Circumferential grooves are used if the load or shaft rotation direction is variable [16]. Engine main bearings typically have a large 180^{o} circumferential groove extent and this is to prevent starvation because the load direction keeps varying and to supply the connecting rod bearings with oil via the crankshaft drillings [16, 27]. In oil lubrication, the supply pressure is typically insignificant compared to the pressures generated within the film [16].

A plain bearings performance characteristics including load capacity and friction are closely related to the bearing diameter and width (affecting available shear area), clearance, shaft speed and oil viscosity [11, 30]. An increase in bearing diameter results in increased entraining velocity (shear rate) and length of oil film (shear area) while an increase in bearing width increases the film width (shear area) [31]. Both lead to increased shear losses due to rotation. Decrease in radial clearance results in smaller film thickness around the bearing resulting in increased shear losses [32].

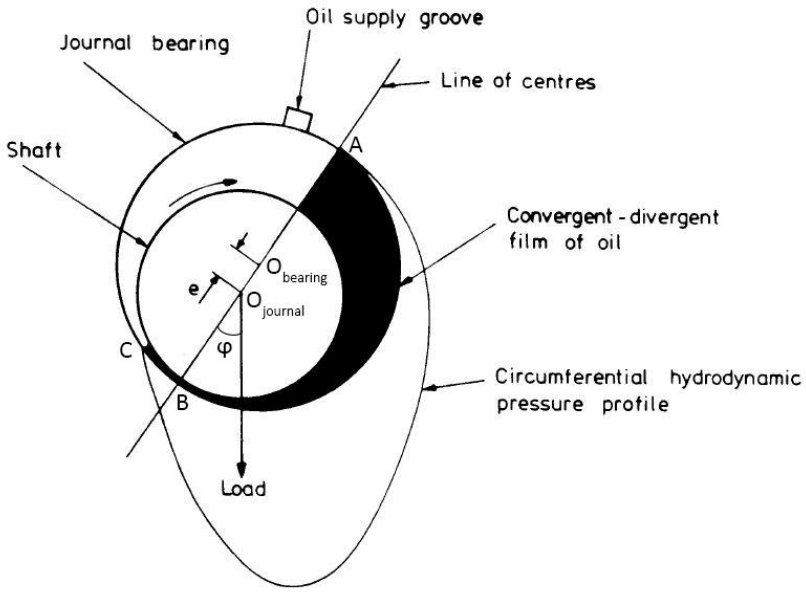


Figure 2.1: Journal bearing operation [27]

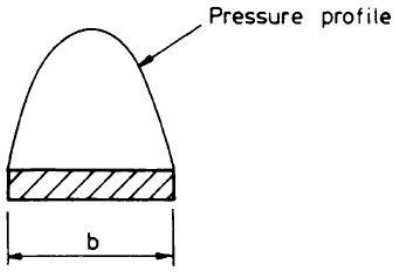


Figure 2.2: Ideal axial pressure profile in a hydrodynamic journal bearing [27]

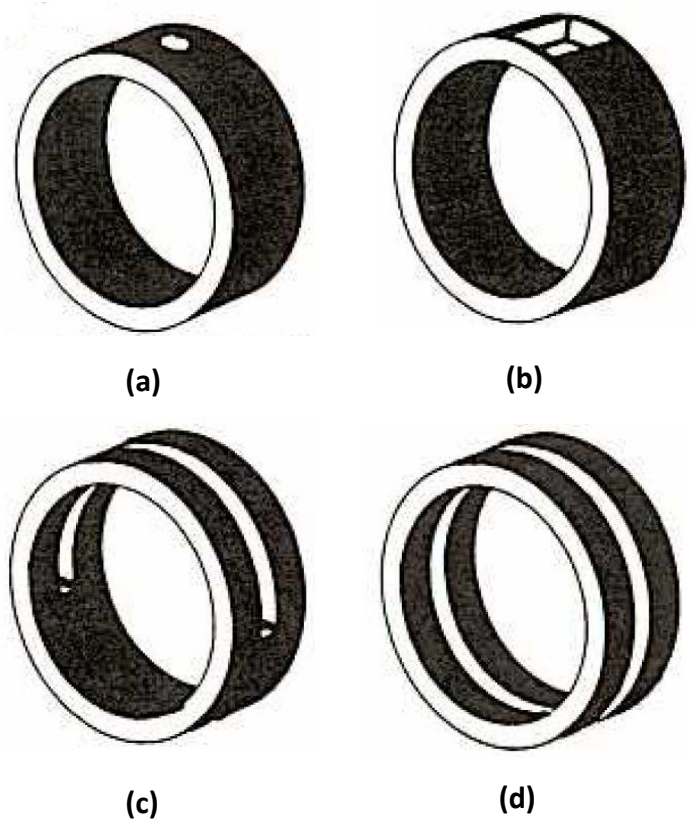


Figure 2.3: Journal bearing oil feed designs (a) single feed hole (b) Axial feed hole (c) 180° circumferential feed hole (d) Full-circumferential feed hole [33]

2.2.2 Hydrodynamic Lubrication

Crankshaft bearings operate mostly in the hydrodynamic lubrication regime where the lubricant film is thicker than the combined surface roughness of the opposite load carrying surfaces of the bearing [17, 25]. There are two basic conditions required for generation of thick film lubrication [34]:

- Sufficient relative velocity should exist between two surfaces for a load carrying film to be generated.
- Surfaces should have some inclination angle with respect to each other or a step.

Hydrodynamic lubrication does not necessarily depend on the supply of pressurised lubricant, however, an adequate supply of lubricant is required for operation. Hydrodynamic lubrication can lead to large drag torque which arises from the shearing of the lubricant, especially at high eccentricity ratios [11]. There are three mechanisms leading to the generation of hydrodynamic lubrication, namely the

pressure driven flow effect, wedge effect and the squeeze film effect [25, 34, 35]. Load support generated by the wedge effect can be explained using the example of a simple pad bearing where the bottom surface covered with lubricant is sliding at a relative velocity, U, along another inclined surface as shown in Figure 2.4 [34]. As the bottom surface moves, lubricant is dragged along it towards a converging wedge, consequently a pressure field is generated which separates the two surfaces. At the entry of the wedge increase in pressure restricts entry of flow causing the velocity profile to bend inwards while at the exit of the wedge, the pressure gradient is negative (promoting exit flow) and causing the velocity profile to bend outwards.

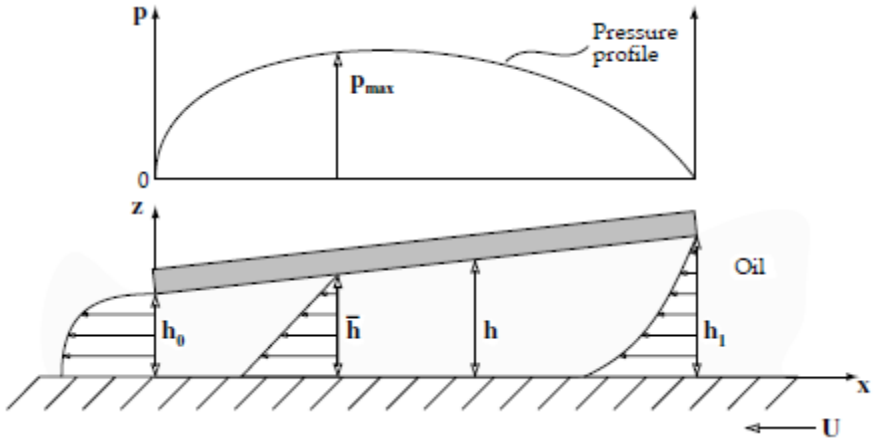


Figure 2.4 Film pressure generation due to the wedge effect [34]

Squeeze film effect occurs as a result of opposing surfaces approaching each other due to loading conditions that are varying with time [34]. Due to this fluctuation in load, the lubricant is expelled from the gap, generating film pressure and providing a contribution to load-carrying capacity which is independent of the relative sliding motion between the opposite surfaces. The pressure field produced by this process results in a damping force [25].

For crankshaft journal bearings both the wedge and squeeze mechanisms are important [25, 34, 36] and the pressure distributions from the wedge and squeeze effects superimpose each other to give the resultant reaction force. The wedge effect occurs due to the rotational velocity of the journal with respect to the bearing shell

which results in a converging wedge (the pressurized zone) and a diverging wedge (where film pressure drops below ambient leading to cavitation). Cavitation is described in further detail in Section 2.2.5. Squeeze film effect is essential in the operation of crankcase bearings which have to support transient combustion forces as it provides increased load capacity albeit for a very short period of time. Significant squeeze film effects can be generated by relatively small squeeze velocities [16].

Hydrodynamic lubrication is one of the three main regimes characterised by the Stribeck diagram [8] shown in Figure 1.3. The friction coefficient in the hydrodynamic regime is determined by hydrodynamic theory (associated with viscous shearing within the fluid film and not from the interaction between surface irregularities). Friction here significantly depends on lubricant viscosity and shear rate as proved by numerous experimental studies carried out [3, 11, 30, 37]. Hydrodynamic friction for plain journal bearings is further explored in Section 2.2.4.

2.2.3 Behaviour of Loaded Bearings

The Reynolds equation defines the pressure distribution in the full film region of loaded journal bearings [1]. The most frequently cited form of Reynolds hydrodynamic equation in literature is the laminar, iso-viscous form as for many practical engineering applications it is assumed that the film viscosity remains constant over the bearing circumference.

$$\frac{\partial}{\partial x}\left(h^3\frac{\partial p}{\partial x}\right)+\frac{\partial}{\partial y}\left(h^3\frac{\partial p}{\partial y}\right)=6\mu U\frac{\partial h}{\partial x}+12\mu\frac{\partial h}{\partial t} \qquad (2.1)$$

In this, x and y are the coordinates of the lubricating plane, h is the oil film thickness, U is the journal surface speed, μ is the lubricant dynamic viscosity and p is the oil film pressure. The first term on the right hand side (RHS) in equation 2.1 is the wedge effect while the second term represents the squeeze effect. The complete solution to the Reynolds equation requires use of numerical methods e.g. Finite Difference (FDM) or Finite Element (FEM) and boundary conditions for determining film rupture and reformation [34] due to film cavitation (Section 2.2.5). An approximate solution known as the 'Short Bearing Theory' is used to provide a simplified analysis of loaded bearing performance with reasonable accuracy. It is assumed that, for bearings with

length to diameter (b/D) less than ½ [38], the pressure gradient acting in the circumferential direction, *dp/dx*, is small compared to that in the axial direction, *dp/dy*, due to the small bearing length. Consequently, the term with *dp/dx* is neglected in equation 2.1. The model provides accurate results for plain cylindrical bearings of slenderness ratios b/D less than ½ and for low to medium values of bearing eccentricity ratio, Ɛ≤0.75 [38]. The short bearing approximation assumes that the positive pressure region always has an extent of 180° where the film starts at the maximum film thickness point and ends at the minimum film thickness point. This approach is also known as the 'half-Sommerfeld' or 'pi-film' solution and was first developed by Gumbel in 1914 [39].

From the short bearing theory, the load capacity of a steadily loaded bearing can be determined by the following equation:

$$W = \frac{U\mu\varepsilon b^3}{{C_r}^2(1-\varepsilon^2)^2}\frac{\pi}{4}\sqrt{\left(\frac{16}{\pi^2}-1\right)\varepsilon^2+1} \qquad (2.2)$$

In dimensionless terms load capacity can be represented as follows:

$$W^* = \frac{W{C_r}^2}{U\mu b^3} \qquad (2.3)$$

Figure 2.5 shows the relationship between dimensionless load capacity and eccentricity ratio. It can be seen that load capacity starts to increase significantly at Ɛ>0.7. This theory suggests that load capacity would become infinite as zero minimum film thickness is achieved. However, a number of factors like surface finish and maximum operating film temperature determine the maximum eccentricity ratio a bearing can operate at [40]. Theoretical and experimental studies show that for dynamically loaded engine bearings, the value of Ɛ lies between 0.6 to 0.7 for unloaded bearings and between 0.8 to 0.9 for loaded bearings [11].

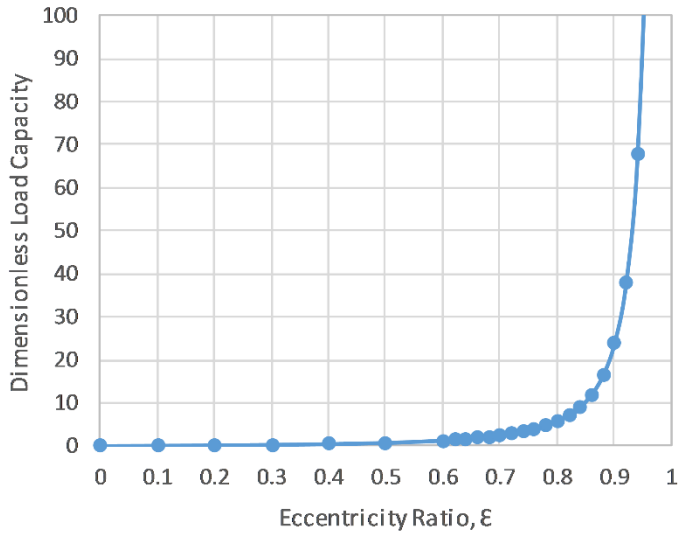


Figure 2.5: Variation between dimensionless load capacity and eccentricity ratio

Lubricant side leakage of a 180° load carrying film varies linearly with eccentricity ratio according to the short bearing assumption:

$$Q = UC_r b\varepsilon \tag{2.4}$$

If lubricant is supplied at a rate lower than this, the theoretical full width film extent would become less than 180° and starvation would occur [34].

2.2.4 Plain Bearing Friction Torque

Lubricant shearing which takes place in the bearing clearance results in power dissipation increasing the temperature of shaft and bearing surfaces and that of the lubricant. The film frictional force in hydrodynamic regime for a steadily loaded bearing is calculated by integrating the shear stress 'τ' over the film area as given by equation 2.5 [26, 34, 41]:

$$F = \int \tau dA \tag{2.5}$$

Where the shear stress according to the hydrodynamic Reynolds equation for a finite width bearing is given by [34]:

$$\tau = \frac{\mu U}{h} + \frac{h}{2}\frac{dp}{dx} \tag{2.6}$$

The first term of equation 2.6 is the 'Couette' term representing shear stress due to pure shear of the film. The second term is known as the 'Poiseulle' term which accounts for the effects of circumferential film pressure gradient on the shear stress of the lubricant. According to this equation, surface properties have no effect on the hydrodynamic friction levels.

The Petrov equation can be used to estimate the bearing force [42]. It neglects any effects of bearing eccentricity, circumferential pressure gradient and cavitation on the friction force and assumes a complete '2 pi' film. The Petrov equation is given as:

$$F = \frac{2\pi\mu UbR}{C_r} \tag{2.7}$$

The 'short bearing' approximation provides an improved estimate of the bearing friction which takes into account the effects of eccentricity (load) and cavitation by assuming a 'pi' film extent- the assumption is that the load carrying film exists throughout the converging part and ruptures at the minimum film thickness point. The following equation results for the full film region [34, 43]:

$$F_{full\ film} = \frac{\pi\mu UbR}{C_r}\frac{1}{(1-\varepsilon^2)^{0.5}} \tag{2.8}$$

In the divergent film zone, a constant volume of oil (dictated by the minimum film thickness point) carried in the form of streamers can be assumed to be under shear, resulting in the following equation for the cavitation zone [43]:

$$F_{cavitation} = \frac{\pi\mu UbR}{C_r}\frac{1}{(1-\varepsilon^2)^{0.5}}\frac{1}{(1+\varepsilon)} \tag{2.9}$$

There is also a torque contribution due to hydrodynamic film pressure which is a function of journal position and load. It has been referred to as the 'offset term' [41]:

$$F_{offset} = \frac{\varepsilon C_r W}{2R}\sin\varphi \tag{2.10}$$

The total bearing torque can be estimated by summation of the three terms above:

$$F_{total} = F_{full\ film} + F_{cavitation} + F_{offset} \tag{2.11}$$

Martin [43] schematized the friction loss components under steady loads comparing the '2-pi' (no cavitation) and 'pi' film solutions. Figure 2.6 shows that most of the friction contribution comes from the full film region and cavitation reduces the overall bearing friction. The offset term contributes a small amount to the total power loss. Power loss is more strongly affected by eccentricity ratio in the region ε >0.7 similar to the effect of ε on load capacity.

The loads experienced by the big end and main bearings are dynamic in nature. For big end bearings, the load consists of the gas force acting on the piston assembly, the reciprocating inertia of the piston assembly and the connecting-rod upper part and the rotational inertia forces created by the lower connecting rod. The loads acting on the main bearings are mainly due to force reactions from the big-end bearings as well as out of balance forces of the crankshaft [31]. The squeeze film action resulting because of dynamic loads adds to the bearing power loss due to rotation of the shaft [43].

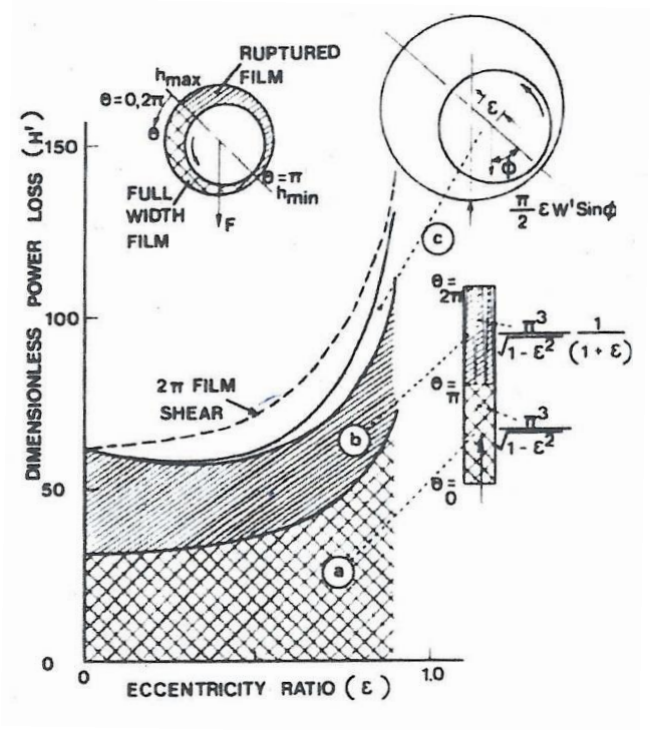


Figure 2.6: Schematic diagram showing power loss components for steady load conditions (a)Full-film friction (b) cavitation zone friction (c)offset term friction [43]

Ozasa et al. [44] performed numerical calculations of hydrodynamic lubrication for con-rod bearings under engine dynamic loads calculating the shear, squeeze and

total power losses over an engine cycle. The total power loss is the arithmetic sum of the shear and squeeze power losses given by the Reynolds equation:

$$P = P_{sh} + P_{sq} \tag{2.12}$$

Where

$$P_{sh} = R\omega \iint \tau R \, d\Theta \, dy \tag{2.13}$$

$$P_{sq} = -\iint p \frac{dh}{dt} R d\Theta \, dy \tag{2.14}$$

where τ is the shear stress, R is the journal radius, Θ is the bearing angle, y is the axial coordinate, p is the film pressure, h is the film thickness and t is time. The author's results have been used to show the relative contributions from the shear and squeeze terms towards total engine cycle friction and are shown in Figure 2.7.

The numerical analysis showed that the average power loss over an engine cycle significantly depended on film shear rather than the squeeze film effect under dynamic loads. Friction from film shear contributed to near 75% at 1000rpm and the contribution increased to 90% at a speed of 6000rpm.

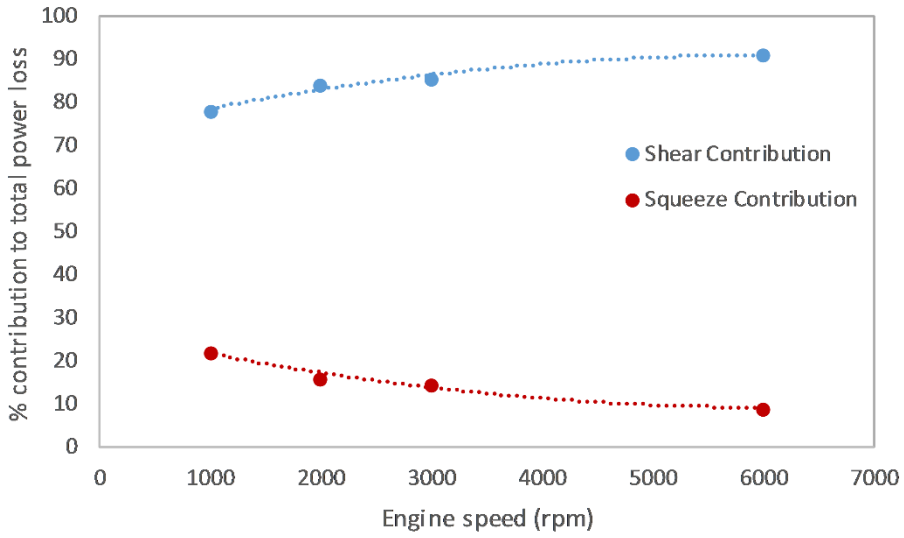


Figure 2.7 Relative contributions from the shear and squeeze terms towards total power loss averaged over an engine cycle (data from [44])

2.2.5 Lubricant Cavitation and Modelling

Cavitation in partially flooded hydrodynamic bearings has a significant effect on the friction torque. In steadily loaded fluid film bearings the cavitation zone is defined as the region between film rupture and reformation points where the full film ruptures and gas cavities exist as strips surrounded by the liquid as shown in the photographs obtained by Cole et al. [45]. The angular extent of the film where cavities do not exist is known as the full width film region.

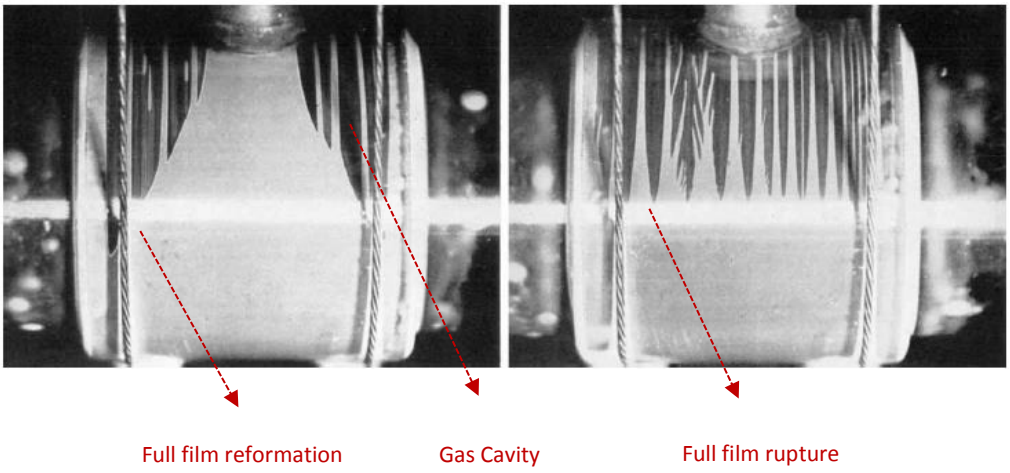


Figure 2.8: Film reformation, rupture and cavitation streamers in a steadily loaded bearing [45]

The phenomenon of cavitation is not restricted to journal bearings. It occurs in many narrow channels where a diverging film section exists, such as found in slider bearings, thrust bearings, rolling element bearings, squeeze film dampers and gears. In engines, lubricant cavitation also occurs at the piston-ring conjunction where the ring acts as a parabolic wedge bearing against the cylinder liner and pressure drops in the divergent film region. The development of cavitation in the piston ring assembly has been experimentally visualized in works carried out by Dellis and Arcoumanis [46] and Dhunput et al. [47] where the development and size of the cavities is shown to be dependent on piston speed and load. The mechanisms of cavity development are the same as that for journal bearings as are explained in the following section.

2.2.5.1 Types of Cavitation

Two main categories of cavitation mechanisms have been discussed in literature [5, 48-50]. The first, gaseous cavitation, is sub-divided into ‘degassing’ and ‘pseudo-

cavitation'. 'Degassing' occurs when dissolved gases diffuse from the liquid phase into an existing gaseous bubble nucleus forming a stable gas cavity. This occurs in the divergent region of the journal bearing where the lubricant is pulled apart and the fluid film pressure may fall below the saturation pressure of the dissolved gases (which is almost equal to the ambient pressure). Most mineral oils contain around 8-12 % in volume of dissolved air [51]. 'Pseudo-cavitation' occurs when an existing gas bubble expands due to depressurization without further gas mass diffusion from the liquid to the gas phase [52]. The former 'degassing' process results in a very rapid bubble growth. Gaseous cavitation results in streamers of oil forming in the cavitation zone.

The second type of cavitation is known as vaporous cavitation in which lubricant vapour is generated when the film pressure drops below its vapour pressure. There is a higher probability of vaporous cavitation occurring as the bearing speed and load increases [53]. Unlike gaseous cavitation, vaporous cavitation results in bearing damage by cavitation erosion as the vapour-filled cavities collapse and the cavities are short lived and unstable [54-56]. Vaporous cavitation normally occurs in dynamic and high load conditions such as the main bearings of the engine crankshaft. Cavitation damage in bearings under dynamic load conditions has been evidenced by Soda et al. [57]. Under dynamic loads, the bearing is more prone to ventilation as the sharp rate of divergence of the film generates negative pressures allowing suction of ambient air [58].

2.2.5.2 Cavitation Behaviour and Factors Affecting the Extent of Cavitation Zones

A number of researchers have observed the behaviour and extent of the oil film experimentally and amongst the factors shown to affect the extent of gaseous cavitation zones in journal bearings are the supply pressure and the type and location of grooving arrangement. Visual studies in steadily loaded fluid film bearings have shown a decrease in full width film extent and increase in the extent of cavitation zones with a decrease in supply pressure [22, 58-60]. The pioneering work of Cole and Hughes [45] on the cavitation behaviour of steadily loaded bearings showed a reduction in full film extent and oil flow with reduction in oil supply pressure,

although the effect on friction torque was not investigated. Dowson and Taylor [50] confirmed that cavitation occurs in the divergent film region and discussed the different boundary conditions for film rupture and reformation. Braun and Hendricks [49] photographed the finger like patterns in the cavitation zone of submerged journal bearings under steady-state conditions and measured the pressures in the cavitation zone to be moderately sub-atmospheric. Mitsui et al. [61] observed the film flow near the oil groove region and cavitation of an axial groove bearing. Works by Mokhtar et al. [59] on steadily loaded Perspex bushes with three different grooving arrangements (single feed hole, axial and circumferential grooves) suggested that cavitation in journal bearings is inevitable and that it increases with journal speed and decreases with increase in load and supply pressure. Dowson et al. [62] performed film visualisation studies over a range of eccentricities and speeds for an axial groove bearing to validate their numerical analysis [63] which took into account film rupture and reformation. Using single hole and axial groove bearings, the influence of reducing oil pressure was to extend the cavitation region downstream of the inlet. Film visualising experiments carried out by Okamoto et al. [23] for a single feed hole bearing and Heshmat et al. [58, 64] and Tanaka [22] on axial groove bearings have similarly shown reductions in full width film extent with decrease in oil supply pressure and this has been related to reduced oil flow through the bearing. More recently, Wang et al. [60] visualised the shape of the cavitation zone in spiral oil wedge journal bearings using high speed cameras for different speeds and inlet pressures. They demonstrated increases in cavitation area with speed and decrease in inlet pressure with inlet pressure showing a stronger influence on cavitation.

Under reduced oil flow conditions, the amount of oil issuing from the groove is insufficient to fully fill the clearance therefore the continuous film is formed a certain distance away from the inlet where the clearance is sufficiently reduced and the extent of the cavitation zone increases. The cavitation fingers consist of released gasses and ambient air when steadily loaded [65].

The presence of oil feed grooves in the high-pressure film zone or use of smaller feed grooves e.g. feed holes compared with axial or circumferential grooves similarly reduces the flow of oil into the bearing and has been shown to result in smaller full width film extents and larger cavitation zones [23, 66]. Okamoto et al. [23] studied the influence of the positioning of the feed oil hole on bearing oil flow and found a significant reduction in flow rate and reduction in film thickness as the oil hole became closer to the loading direction.

2.2.5.3 Effects of the Extent of Cavitation Zone on Bearing Friction and Load Capacity

The existence of cavitation streamers in the film rupture zone leads to a reduction in bearing friction torque since the viscosities of gas/vapour and lubricant are significantly different (Section 5.3). The extent of cavitation streamers is greatly influenced by supply oil pressure and excessive cavitation either due to flow starvation or aeration of lubricant can have a deleterious effect on the load carrying capacity of a bearing due to a reduction in load bearing film extent (flow starvation) [64, 66] and weakening of the oil film because of the compressibility of air (aeration) [67].

Theoretical studies performed by Heshmat [65] on the effects of reduced film extent due to inlet flow reduction on sleeve bearings have shown that the load capacity and maximum hydrodynamic pressure dropped significantly after inlet flow fell below 70 percent of flooded requirement leading to increased eccentricity ratios. A schematic of the reduced film extent and increased cavitation in shown in Figure 2.9 for a two-lobed bearing. Power losses at the same time were seen to reduce by as much as 40% at 10% full flow due to reduced film extent. He et al. [68] performed a thermohydrodynamic (THD) analysis of leading-edge groove (LEG) bearings under starved conditions and demonstrated a 30% reduction in power loss at 30% flooded flow. Reductions in power losses and increases in eccentricity with increased extent of the cavitation zone when supply pressure/flow reduction is reduced are shown in the numerical results of Vijayaraghavan et al. [66], Tanaka [22], Vincent et al. [69] and Brito et al. [70] for axially grooved bearings. The reductions in power losses have been attributed to reduced shearing losses in the film as well as increased film

temperatures due to smaller volume of oil present leading to lower oil viscosities. Increases in bearing eccentricity with reduced film extent indicate a reduction in the load capacity of the bearing. The reductions in friction loss as well as reductions in minimum film thickness with supply pressure have been found to be more significant at light loads compared with high loads [66]. Vijayaraghavan et al. [66], using a THD model based on Elrod's cavitation algorithm [71] which implicitly applies Jacobsson Floberg Olsson (JFO) mass conserving boundary conditions [72, 73] for cavitation rupture and reformation boundary determination, reported power loss reductions of 10-15% for high loads and 15-20% for low loads at 50% of fully flooded flow.

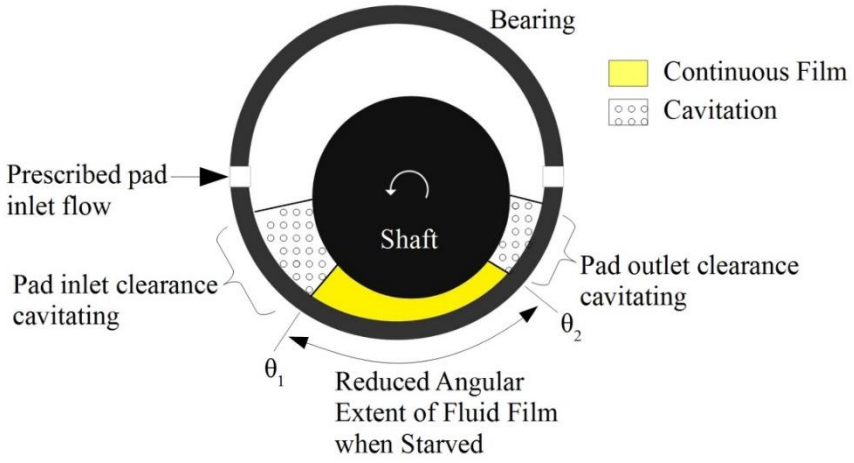


Figure 2.9: Schematic of the changes in film extent and increase in cavitation with reduction in inlet flow rate for a two-lobe bearing

2.2.5.4 Cavitation Modelling

Cavitation in the bearing represents a rupture in the continuity of the liquid film and this needs to be considered when solving the hydrodynamic Reynolds equation. Different solutions have been proposed in the literature. Sommerfeld (1904) [74] offered a solution which neglected film rupture leading to predicted negative pressures and a zero net load bearing capacity. Gumbel [39] modified Sommerfeld's approach, assuming that film rupture started at the minimum film thickness point while film reformation occurred at the maximum film thickness point. This approach is also known as the 'half-Sommerfeld' or 'pi-film' solution and it does not account for mass continuity at the end of the pressure curve or at its beginning. This boundary condition is applied in the 'short bearing' approximation.

Swift (1932) [75] and Stieber (1933) [76] offered an improved alternative to the half-Sommerfeld condition, assuming a zero-pressure gradient continuity condition at the inception of cavitation. This film rupture condition is known as the Reynolds boundary condition and while it sufficiently predicts film rupture (mass conserved at rupture), film reformation is not properly taken into account as it is assumed to reform at the maximum film thickness point. This model implied that lubricant would be carried between gas fingers in the cavitation zone. Mass conservation is not taken into account in the rupture zone (where Reynolds equation is not applicable) and the pressure in the cavitation zone remains constant at the cavitation pressure, p_{cav}. The Reynolds boundary condition is usually implemented using numerical methods and one such application will be described in Section 5.4 where a grooved journal bearing model is described. According to the above boundary conditions, within the cavitation zone the pressure driven flow (Poiseulle flow) is equal to zero and fluid is carried between gas streamers by the shaft rotation (Couette flow) to the point of film reformation.

Prediction of the film reformation front creates significant difficulty in numerical modelling and neither the 'pi-film' nor the 'Reynolds model' account for mass conservation. One of the successful mass conserving models is the Jakobsson and Floberg and Olson (JFO) model [72, 73, 77]. The model assumes the cavitation zone to be at a constant cavitation pressure with an infinite number lubricant streamers being purely driven by Couette flow and the spaces between the streamers to be filled with a gaseous mixture as shown in Figure 2.10.

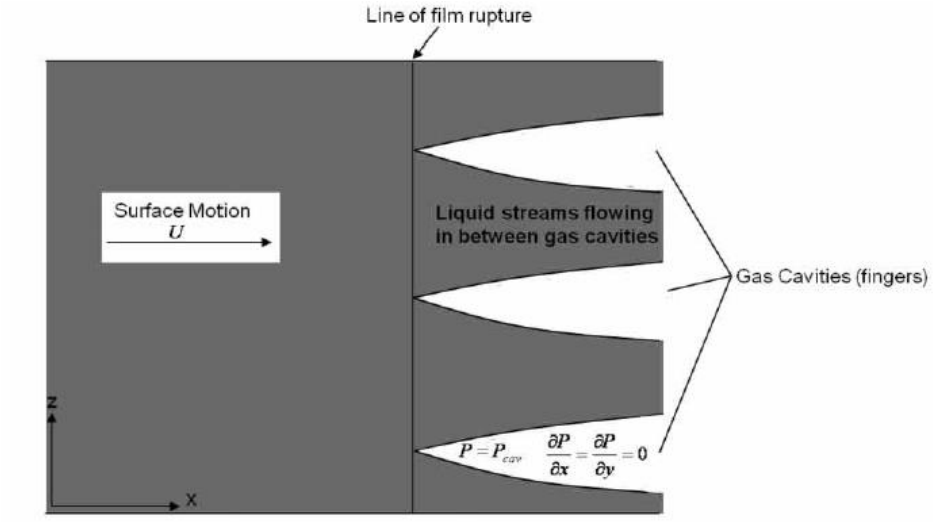


Figure 2.10: Striated gas and liquid fingers assumed in the JFO cavitation model [5]

The model provides boundary conditions which satisfy the continuity condition for any geometry of reformation fronts and is described further in Section 5.4.1.

Elrod and Adams [78] and Elrod [71] proposed mass conserving algorithms which implement the JFO boundary conditions implicitly. In this approach, a modified single Reynolds equation is used which is valid in both the full film and cavitation regions using a switch function which suppresses the Reynolds pressure-driven flow term in the cavitation zone. The solution of the modified Reynolds equation results in a relative density field $\left(\rho/\rho_{cav}\right)$. In the full film region, the lubricant pressure and density are related through the bulk modulus of the fluid. In the cavitation region, density ratios represent the fractional film content. Later, studies have been carried out on validating and advancing the Elrod's algorithm [62, 63, 79-81].

2.2.6 Effects of Reduced Supply Pressure on Bearing Performance

Experimental studies on the effects of supply pressure on various journal bearing performance parameters including friction torque, film pressure, flow rate and eccentricity ratio have mostly concentrated on single feed hole, single axial or twin axial groove bearings [18-22]. Brito et al. [20] found using a twin axially grooved bearing that friction torque decreases as the supply pressure is reduced, the effect of which is more pronounced at lighter loads compared with higher loads. Increases in

peak film temperatures and significant reductions in flow rate have been recorded with reduction in oil supply pressure [19, 20, 23, 24]. As described in the previous section, a reduction in supply pressure is also experimentally shown to reduce the film extent.

Eccentricity ratio and peak film pressure measurements for a bearing with a single axial groove at 90° to load line [19] and two-axial grooves at ±90° [20] to load line have been shown to increase with decrease in supply pressure as a result of decreased film angular extent. The increase in peak film pressure indicates lowering of minimum film thickness and increased operating eccentricity. However, for a single axial groove at 0° to the load line, a decrease in supply pressure led to decrease in peak film pressure [18, 82]. This has been shown to be related to increases in film thickness due to a reduction in hydrostatic load as the supply pressure is reduced even under heavily loaded conditions [24]. Therefore, different arrangement of grooves can impact the eccentricity ratio in different ways as the supply pressure is reduced although Ahmad et al. [82] reported the decreases in peak film pressure to be more significant at light loads.

Overall the reduction in supply pressure has shown to reduce the friction torque which can be related to reductions in film extent from other visual studies carried out.

2.2.7 Bearing Wear

Bearing wear leads to increases in operating clearance and disruption in continuous hydrodynamic film due to surface irregularities which leads to reduced load capacity and loss of oil supply pressure. If untreated, excessive wear can lead to bearing seizure.

Vaporous cavitation in dynamically loaded bearings, such as IC engine bearings, results in erosion damage as very large implosive forces are created as the vapour bubbles collapse [79]. Erosive wear also occurs because of hard foreign particles e.g. dirt and debris in the lubricating oil which can score the bearing surface.

Bearing abrasive wear occurs when mixed lubrication occurs instead of the wear free hydrodynamic lubrication. Abrasive wear can result because of low rotation speed, high loads, oil starvation, high temperatures leading to low oil viscosity and geometrical distortions and misalignments [83]. This happens most commonly during engine starts and stops when the shaft speed is insufficient to generate a hydrodynamic film and scoring results due to interaction of surface roughness' between opposite surfaces.

2.2.8 Failure Modes

Garner [84, 85] schematized the safe operating region of hydrodynamic journal bearings indicating four modes of failure as shown in Figure 2.11. The thin oil film limit signifies metal to metal contact when the bearing eccentricity becomes so high that surface asperities come into contact. The increase in eccentricity, for a given load and speed, can be a result of low oil viscosity, use of very tight clearances (causing starvation) or very big clearances due to wear (causing loss of supply pressure and lowering of load carrying capacity) and reducing oil supply pressure significantly resulting in oil starvation and insufficient load carrying film extents [66, 69].

At high speeds and high loads, the bearing metal may experience plastic flow (well below the melting point) because of the high temperature (due to high shear) and pressure conditions in the film [40].

Failure can also occur due to lubricant oxidation and subsequent degradation under high shear and temperature conditions which promote oil oxidation [84, 86]. Oxidation inhibitors are added to lubricants to retard the oxidation process [86].

Under conditions of high speed and/or low load, a steadily loaded journal can experience vibrational instability known as half-speed whirl, in which the journal centre precesses around the bearing centre at around half the journal speed [16, 84, 87]. In such conditions the bearing loses its hydrodynamic ability and boundary contact occurs. This can also happen in the case of rotating loads, such as engine main bearings. During some section of the engine cycle the angular velocity of the

rotating load may be half the angular velocity of the journal resulting in a zero effective surface velocity. This causes a loss in hydrodynamic wedge effect though load can still be supported by squeeze motion temporarily [16, 34]. Seizure can occur if such condition exists for more than 20° of shaft rotation.

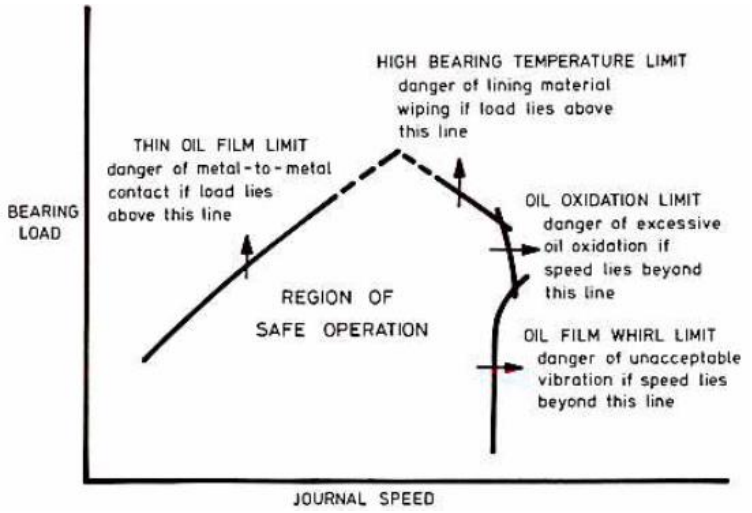


Figure 2.11: Hydrodynamic bearing modes of failure and safe operating zone [85]

2.3 Viscometrics of Lubrication Oil

2.3.1 Introduction

Viscosity of a lubricant greatly influences hydrodynamic frictional dissipation and is strongly affected by temperature. It is a measure of a fluid's resistance to gradual deformation by shear or tensile stress and describes the internal friction of a moving fluid. The friction coefficient due to thin film shear is particularly sensitive to fluid viscosity in the hydrodynamic regime as evidenced in the Stribeck curve (Figure 1.3).

Engines currently make use of mineral or synthetic oils to achieve low friction and wear rates between rubbing components. Oil temperatures during operation typically vary from sub-zero (during winter in UK) up to 100 ˚C resulting in a big variation in viscosity. Viscosity is also a function of shear rate as high shear rates result in a loss of viscosity in multigrade oils and is also affected by fluid pressure as is described in the following sections.

2.3.2 SAE Oil Standard

The SAE (Society of Automotive Engineers) J300 standard is an internationally accepted standard for grading lubricants according to viscosity values [88]. Single grade lubricants are stated as SAE XX while multigrade lubricants are stated as SAE XW-XX where XX represents a number. The number including the letter 'W' (Winter) represents a range of viscosity at -18 ˚C while the number without 'W' represents a range of viscosity at 100 ˚C. A lubricant is required to be tested using several recognized test procedures to be classified as an SAE grade. For low temperature performance, lubricants are tested in a Cold Cranking Simulator (CCS) between -35 ˚C and -10 ˚C and shear rates of approximately 10^4 to 10^5 s^{-1} [89]. For high temperature performance under high shear conditions (HTHS), engine oils are tested at 150 ˚C at a shear rate of 10^6 s^{-1} [90].

2.3.3 Viscosity-Temperature Equations

Several equations are available for predicting lubricant viscosity at a given temperature.

The Walther equation is used to calculate the kinematic viscosity, ν, of oil at any given temperature and it forms the basis of the ASTM D341 viscosity-temperature charts [91]. The Walther equation is of the form:

$$log(log(\nu + 0.6) = W_1 + W_2\, log(T) \qquad (2.15)$$

Here ν is the kinematic viscosity of the oil in centistoke (cS), W_1, W_2 are constants which depend on the oil and T (°C) is the temperature.

The Vogel equation generally provides a more accurate fit to oil viscosity variation with temperature at low shear rates and atmospheric pressure [34].

$$\mu = k_v e^{\left(\frac{c_1}{T+c_2}\right)} \qquad (2.16)$$

Here μ is the dynamic viscosity of oil in Pas, k_v (Pas), c_1 (°C), c_2 (°C) are constants specific to the oil and T (°C) is the temperature. To determine the three constants in the equation, three viscosity measurements at different temperatures are needed for a specific oil.

2.3.4 Viscosity Variation with Shear Rate

The Cross equation [92] can be used to estimate the variation in the viscosity with shear rate for multigrade oils:

$$\mu(\gamma) = \mu_\infty + \frac{\mu_0 - \mu_\infty}{1+\left(\frac{\gamma}{\gamma_c}\right)^m} \quad (2.17)$$

where μ is the viscosity at a given shear rate, γ, μ_∞ is the fully shear thinned viscosity, μ_0 is the viscosity at low shear, γ_c is the shear rate at the mean value of μ_∞ and μ_0 and *m* is an empirically determined parameter. For most multi-grade oils, the value of *m* may lie between 0.5 and 1 [93]. For a 10W/30 oil, the viscosity ratio of μ_∞ to μ_0 has been given value of 0.76 in literature [93].

Figure 2.12 shows typical viscosity-shear behaviour for three oils at 100 °C, SAE 30 mono-grade oil, SAE15W/40 multigrade oil and SAE10W/30 multigrade oil [93]. The drop in viscosity at high shear rates occurs as long polymer chains which are randomly orientated tend to align themselves. This process is normally reversible. Viscosity-shear thinning is expected in multigrade oils between shear rates of 10^4 and 10^5 s^{-1} depending on the temperature [94] as polymer additives in the oil lose their effectiveness. One outcome of shear thinning in multigrade oils is that it results in lower friction and improved fuel economy compared with single grade oils [95].

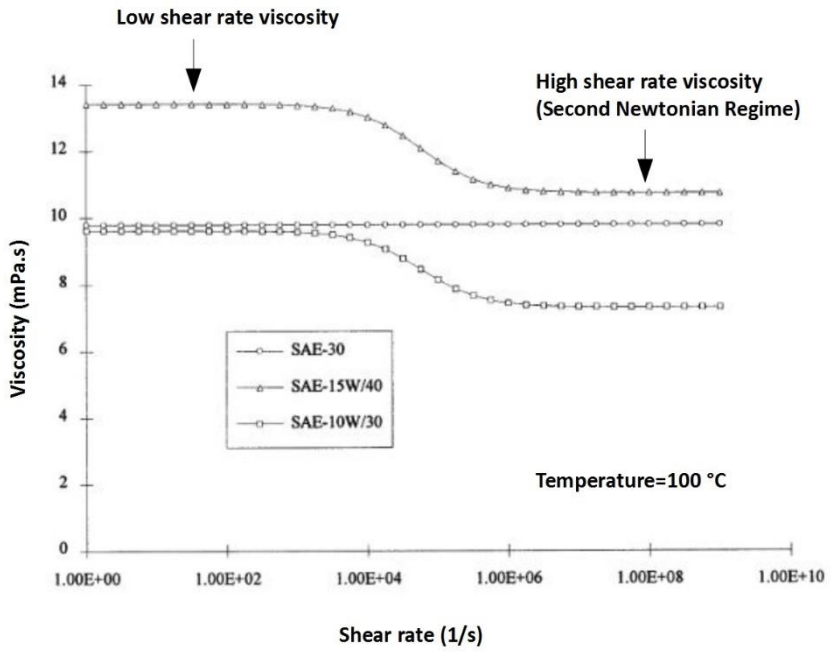


Figure 2.12 Shear thinning behaviour in multigrade lubricating oils [93]

In engine bearings, as the clearances are generally around only 40-50 microns wide and journal rotation speeds are high, high shear rates exist in the film leading to a lower effective viscosity. Figure 2.13 shows the variation in average shear rates experienced with speed for a bearing with 40 µm clearance. Average shear rates are seen to lie between $5x10^4$ to $3x10^5$ for a speed range of 800 rpm to 5000 rpm, therefore, a multigrade lubricant may experience effects of shear thinning during operation in the bearings.

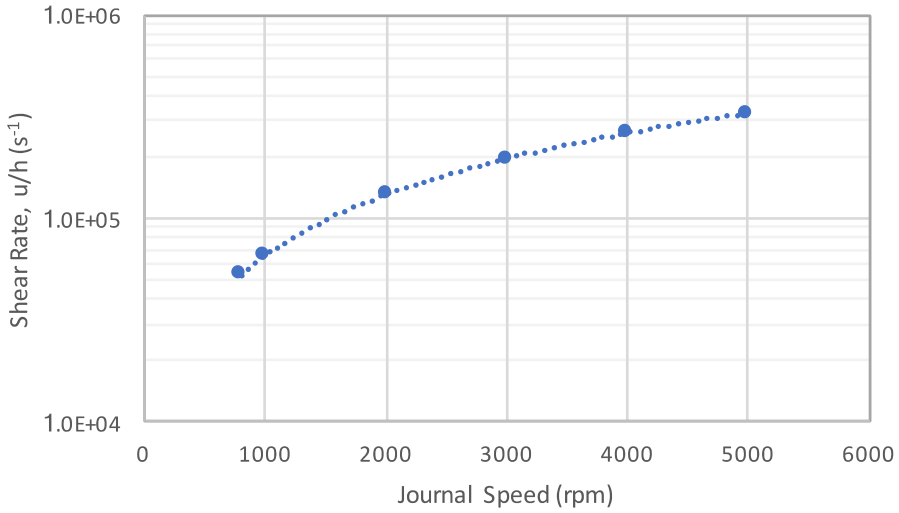


Figure 2.13: Variation in shear rate for a journal bearing with C_r=50 µm

Shayler et al.[96] modified the low shear Vogel equation to account for the effects of high shear on oil viscosity to better predict the lubricant viscosity at rubbing surfaces. This effective viscosity is based on Cold Cranking Simulator measurements (CCS) at -30 ˚C, High Temperature High Shear (HTHS) viscosity at 150 ˚C and viscosity measurements at three intermediate temperatures.

The effective viscosity equation is given as:

$$\mu = k_v e^{\left(\frac{\theta_1}{T+\theta_2}\right)}(de^{(fT)}) \tag{2.18}$$

Where

$$f = \frac{ln\left[\left(\frac{\mu_{CCS}}{\mu_{HTHS}}\right)\left(\frac{\mu_{vogelt1}}{\mu_{vogelt2}}\right)\right]}{T_1 - T_2} \tag{2.19}$$

And

$$d = \left(\frac{\mu_{CCS}}{\mu_{vogelt1}}\right) exp(-fT_1) \tag{2.20}$$

A MATLAB script found in [34] allows determination of Vogel coefficients from viscosity data of a lubricant. The script has been modified to calculate coefficients for the effective viscosity. The calculation of the coefficients requires CCS and HTHS

viscosities along with dynamic viscosity values at three temperatures. For the stock 5W/30 lubricants used in this research, the Vogel coefficients as well as the modified Vogel coefficients (where CCS and HTHS viscosities were available) have been summarised in Table 2.1. Figure 2.14 shows the predicted variation of lubricant dynamic viscosity with temperature. Viscosity increases logarithmically with decrease in temperature and therefore friction losses become very significant under cold running conditions [97].

2.3.5 Viscosity Variation with Pressure

In bearings, film pressures reach very high values and this has an effect of increasing the local film viscosity. To account for pressure effects on viscosity, the Barus' equation is often used which is accurate up to a 1000 bar,

$$\mu_p = \mu_{atm} e^{\alpha p} \tag{2.21}$$

where μ_p is the pressure compensated viscosity, μ_{atm} is the viscosity at atmospheric pressure, p is the pressure under consideration and α is the pressure-viscosity coefficient. There are various formulae available to calculate this, one of common ones is by Wu [98]:

$$\alpha = m_0(0.1657 + 0.2332 log_{v_0}) \tag{2.22}$$

Where m_0 is equal to the lubricant ASTM slope/0.2 and v_0 is the atmospheric kinematic viscosity at the temperature of interest. For the stock 5W-30 lubricant used mainly in this study, α is calculated to be 2×10^{-8} m^2/N and the variation in viscosity with pressure is shown in Figure 2.15. In the current testing, film pressures up to 60 bar have been measured. Over this range, the oil viscosity would increase by ~12% compared with ambient pressure. High loads leading to increased local viscosity would contribute to increased engine friction.

Table 2.1 Vogel coefficients for the stock lubricants used

Test Rig	Lubricant Grade	Vogel Coefficients			Modified Vogel Coefficients	
		k_v	θ_1	θ_2	f	d
Single Bearing Rig	5W/30	5.17e-05	1142	130	-	-
Crankshaft Bearing Rig	5W/30	4.71e-05	1190	131.7	0.8371	0.000559

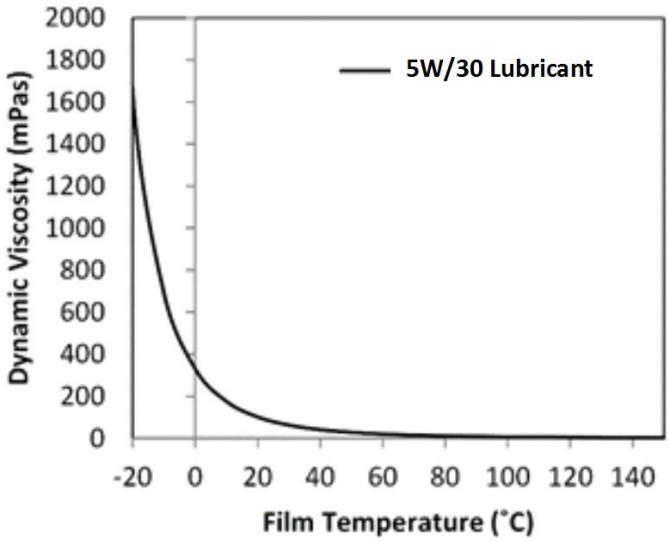


Figure 2.14 Dynamic viscosity prediction using the Vogel equation for the stock 5W/30 lubricant

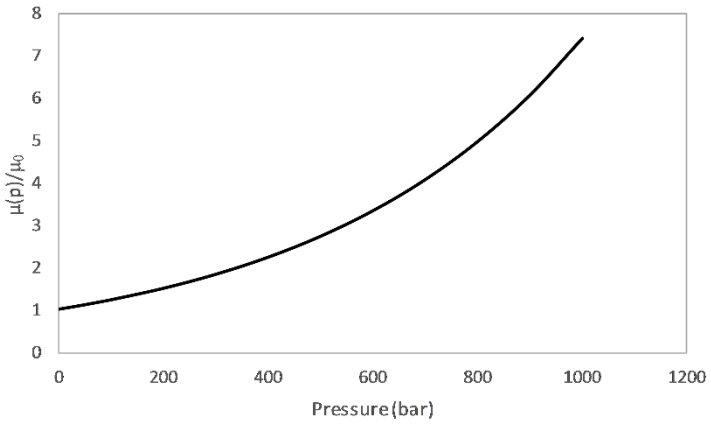


Figure 2.15 Variation in dynamic viscosity at given pressure compared to dynamic viscosity at atmospheric pressure

2.4 Oil Lubrication System of Engines

2.4.1 Requirements

The prime function of the oil lubrication system in an internal combustion engine is to minimise levels of friction and wear between rubbing surfaces by supplying

adequate amounts of lubricant to the required components. This results in reduced wear and heat dissipation [25]. The supplied lubricant also prevents metal damage by preventing oxidation and corrosion, improves sealing of the combustion chamber by forming an oil film between the piston rings and the cylinder wall, dampens shock loads protecting engine parts and provides hydraulic power transfer to activate components for example variable valve timing and timing chain tensioning systems [25, 86].

In addition to this, the lubrication system ensures cooling of several engine components and rubbing surfaces. Heat can be a result of frictional dissipation between rubbing surfaces or conduction to components which are near to the combustion heat source. Heat is convected away from bearings by the oil flowing through them especially under warm running conditions [3]. Heat is also transferred to oil from the head structure, piston assembly (via oil splash and piston cooling jets), coolant during warmup in the filter cooler assembly as well as the exhaust gases within some exhaust gas recirculation (EGR) coolers [99-101].

2.4.2 Oil System Layout

The oil distribution system of an engine consists of an oil pump and a network of drillings and pipes within the engine structure including the crankshaft, connecting rods and camshaft to distribute the oil contained in the engine sump [102]. An example of a typical lubrication network is presented in Figure 2.16.

Oil is drawn by the pump from the engine sump and delivered to the oil cooler and filter assembly and is then directed towards the main oil gallery. Pressurised oil is then fed either directly from the main gallery via drillings in the engine structure to components such as the crankshaft main bearings, camshaft bearings and timing chain or via secondary, smaller passages within components such as the crankshaft which transport oil from the main bearing circumferential grooves towards the big end bearings and piston cooling jets. A schematic of the oil passage from the main bearing to the big end bearing is presented in Figure 2.17. The small end bearings and cylinder walls get lubricated via oil splashing off from the rotating crankshaft instead of having a line feeding oil.

For cooling the pistons under high speed high load conditions, nozzles connected to the main bearings spray oil jets to the piston undersides. These piston cooling jets are controlled by spring loaded ball valves which remain closed under low load and engine speed conditions to ensure sufficient pressure in the oil system.

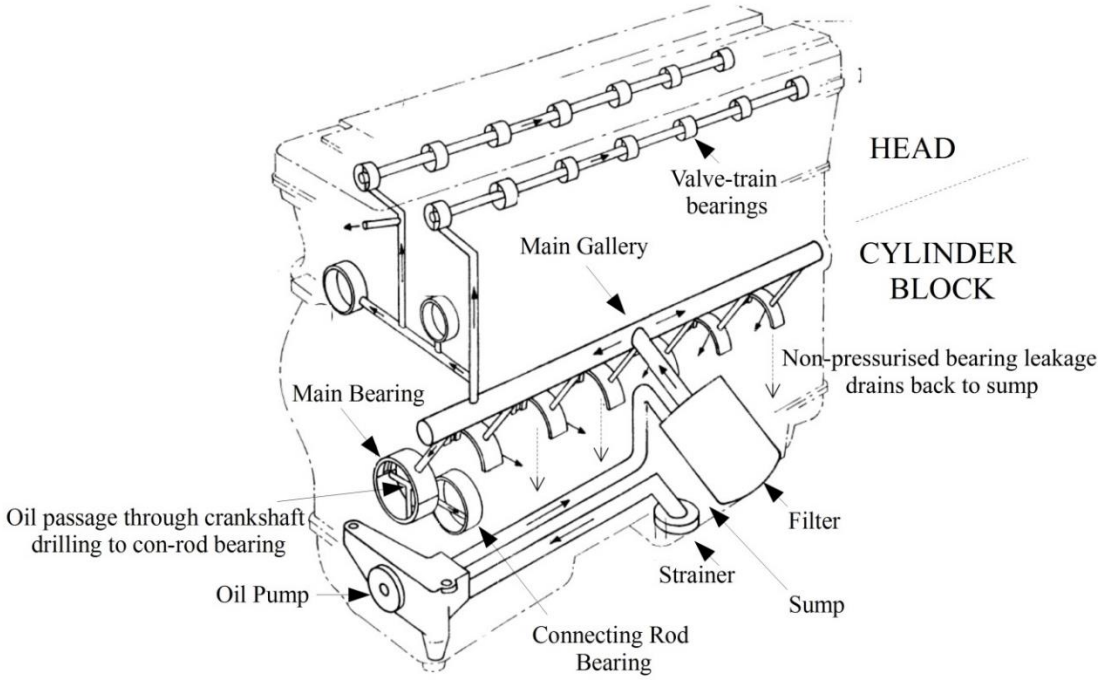


Figure 2.16: Typical engine lubrication network (adapted from [27])

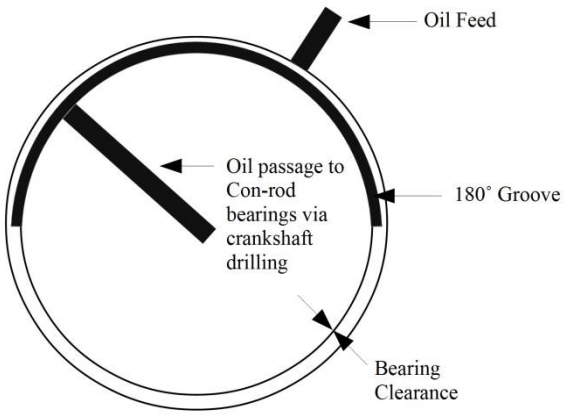


Figure 2.17: Schematic of oil passage from main bearing groove to connecting rod bearings via crankshaft drillings

2.4.3 Pump Types and System Operation

Commonly, engine lubrication systems have a positive displacement pump driven by mechanical gear trains from the crankshaft [102]. Pumping capacity is designed to

ensure sufficient oil delivery to the critical parts of the engine at low engine speed and high operating oil temperature (hot idling condition) [103, 104]. As the engine speed increases, the pump speed and flow rate also increase and the oil circuit pressure rises. This is to some degree beneficial for the system as higher engine speeds generally mean higher bearing loads and thus larger oil flow requirement. Spring-loaded relief valves allow safe operating pressures to be maintained by allowing oil to be expelled back in to the pan or the inlet of the oil pump [104, 105]. A schematic of a fixed displacement pump with a spring-loaded relief valve is presented in Figure 2.18. Engine tests carried out at the University of Nottingham have shown that during warmup from ambient conditions main gallery pressures can vary from 6barA to 3barA when idling and from 7barA to 5barA at a high speed of 3000rpm.

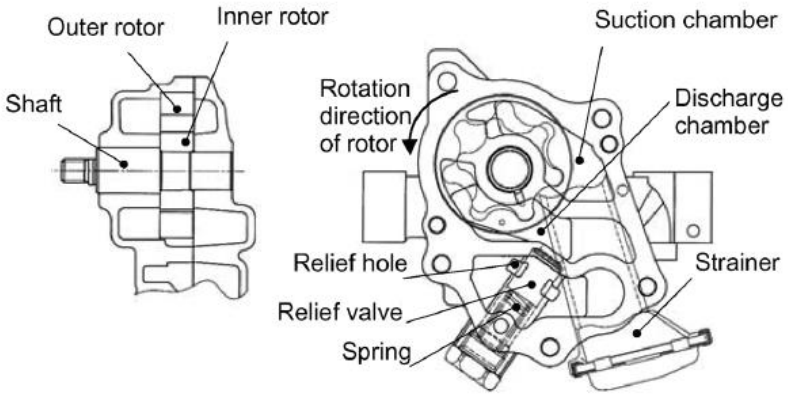


Figure 2.18: Schematic of a fixed displacement pump [104]

Variable displacement oil pumps (VDOPs) which control oil circuit pressure by varying pump delivery instead of using relief valves offer engine fuel economy gains over the use of fixed displacement pumps. VDOPs are gaining popularity amongst engine designers [103, 104, 106, 107].

Variable displacement pumps are driven off the crankshaft, however, they employ a hydraulically or electrically actuated control system to regulate the output supply pressure. An example of a hydraulically actuated system was presented by Toyoda et al. [104] in which a variable discharge type relief valve fitted within a trochoidal oil pump body opened or closed a relief hole (depending on the load exerted on the

relief valve by the pressure in the output chamber) thus varying the output system pressure.

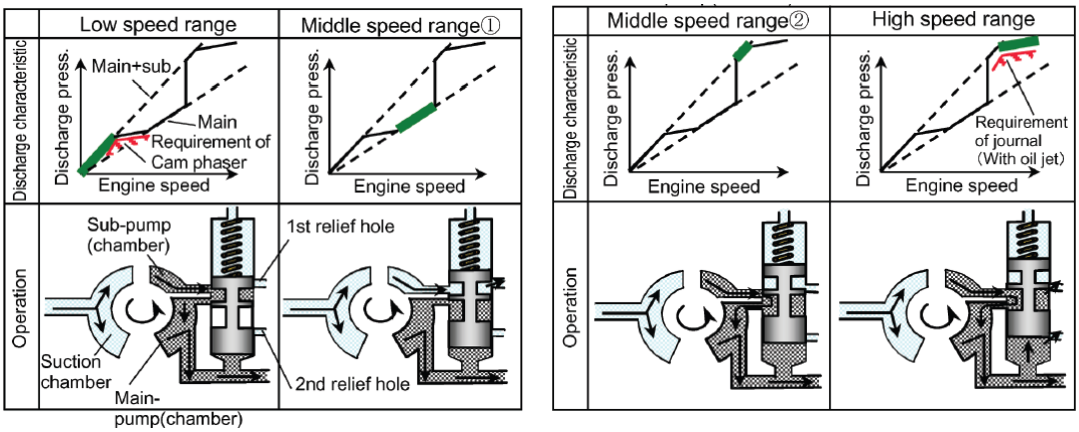
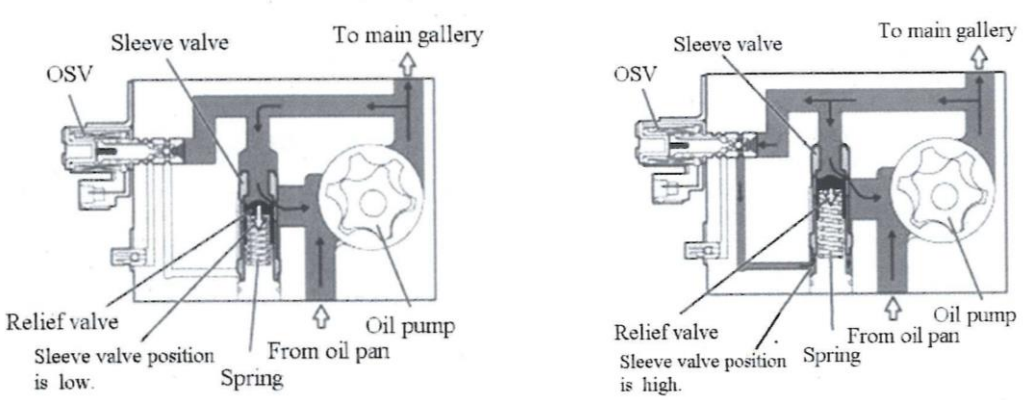


Figure 2.19: Operation of a hydraulically actuated variable output pump [104]

Toyota motor corporation [108] developed a variable oil pump control system which electronically controlled the oil pressure in two stages: low and high pressure (Figure 2.20). The system utilized a spring-loaded relief valve as well as an oil switching valve (OSV) which received signals from the ECU and was electronically actuated. When the OSV is in the on position, the opening of the relief valve leads to increased relief start oil pressure (Figure 2.20(a)). When in the off position, the closing of the relief valve results in low relief start oil pressure where the piston cooling jets are stopped and mechanical pump losses are reduced (Figure 2.20(b)). It was shown that running at lower oil pressure results in lower oil temperature which contributes to an increase in friction, however, this penalty was offset by reduction in mechanical loss and higher efficiency resulting in an improvement of fuel efficiency by 0.8% overall.



(a) High oil pressure control **(b) Low oil pressure control**

Figure 2.20: Electronically actuated oil pressure control [108]

A Vane type design in variable flow oil pumps is also common [109, 110]. A schematic is shown in Figure 2.21. Changes in eccentricity between the control ring and centre of the rotor by movement of the control ring allow for adjustment of the oil flow and pressure.

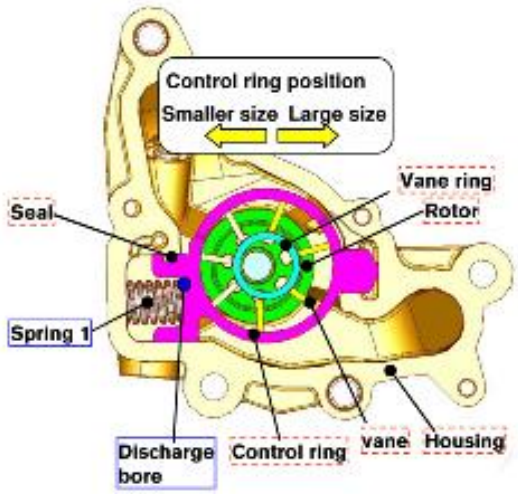


Figure 2.21: Vane type variable displacement oil pump [110]

Considerable improvements in fuel economy can be achieved with use of VDOPs by avoiding excessive oil pressure generation. In a research carried out by Ford [107] control of main gallery pressures to 3barG using a VDOP over cold NEDC led to fuel economy improvements of up to 3.4% compared with a production fixed displacement pump.

Apart from VDOPs, full electric oil pump solutions have also been explored which offer precise control of oil pressure for better efficiency as well as the ability to operate the pump when the engine is switched off providing pre-priming of rubbing surfaces resulting in reduced wear [111].

2.5 Friction in Engines

2.5.1 Introduction

The difference between the net indicated and brake power output of an engine represents the power absorbed by the frictional losses and ancillaries. These power losses account for approximately 10% of the indicated power at full load and 100% when idling [4]. Total engine friction can be subdivided into two categories: rubbing friction and parasitic losses. Rubbing friction is a result of resistance to moving parts of the engine and includes friction in areas such as the crankshaft, piston assembly and valve train. Parasitic losses are due to the energy required to charge the battery using the alternator which is used to drive accessories such as the fan, water pump, fuel pump amongst others.

Rubbing friction, which is the primary interest in this study, accounts for approximately 10 percent of the total power loss and, of that, 50 percent can be attributed to the piston assembly (piston, connecting rod and rings), 30 percent to bearings and seals (hydrodynamic lubrication) and 20 percent to the valve train (mixed lubrication) [4]. According to Priest and Taylor [112], a 10 percent reduction in mechanical losses can lead to a 1.5% reduction in fuel consumption. Frictional losses are dissipated as heat via the engine structure to the coolant and oil and this also influences the warm-up behaviour of the engine.

2.5.2 Engine Rubbing Friction Regimes

Rubbing surfaces in engines lie in one of the four main modes of lubrication, which as previously described in Section 1.2 are known as hydrodynamic, elastohydrodynamic, mixed and boundary. Figure 2.22 (reprinted from [17]) shows a Stribeck curve which identifies the lubrication regimes experienced by individual components in an engine.

Crankshaft journal bearings, which are the focus of this study, operate in the hydrodynamic regime, apart from when the engine is started and stopped where boundary contact may occur due to low shaft rotation speed and insufficient oil flow from the oil pump resulting in wear [17, 86]. The piston ring and cylinder wall interface experience all friction regimes depending on the position of the piston [113]. Normally the nature of lubrication is hydrodynamic at mid-stroke where piston velocity is high, and approaches mixed and ultimately boundary lubrication as the piston velocity approaches zero at the Top Dead Centre (TDC) and Bottom Dead Centre (BDC) [12]. Friction power loss at reversals is not substantial since the piston velocity is low, however, increased wear results because of boundary contact. The valve train also experiences multiple friction regimes where mostly hydrodynamic friction exists in the camshaft bearings, mixed/boundary lubrication at the cam/follower interface and both mixed and hydrodynamic friction in oscillatory components such as the lifters and valves.

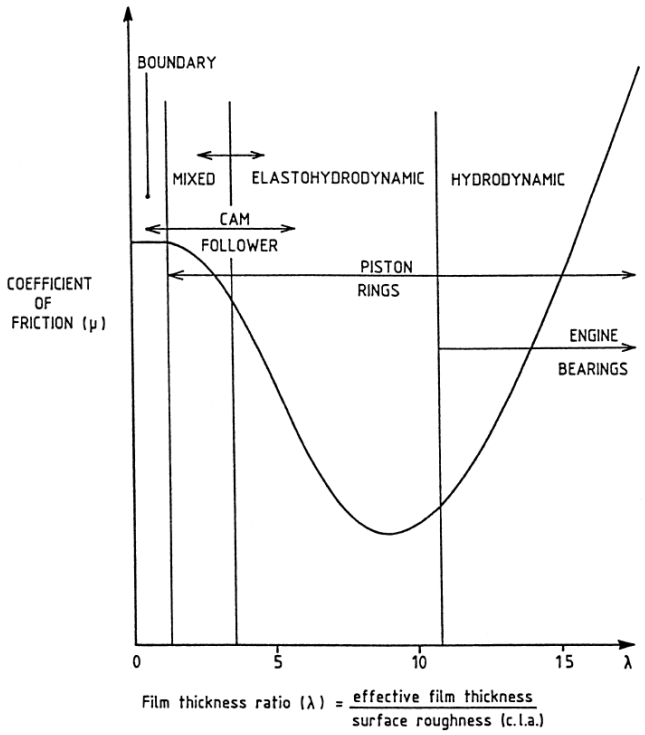


Figure 2.22: Stribeck curve illustrating the regimes experienced by individual components of an engine [17]

2.5.3 Definitions of Friction Terms

For a firing engine, rubbing friction work is calculated by subtracting brake work and auxiliary work from the net indicated work over the engine cycle. Brake work is the work transferred from the engine to the output shaft. Net indicated work is that remaining after allowing for the pumping work done to induct and exhaust gas from the cylinder. Ancillary work is the work required to run ancillaries such as oil pump, fuel pump, water pump, alternator and air conditioning compressor.

For engines, friction data are commonly presented as mean effective pressure (MEP) values. Mean effective pressure allows direct comparison of frictional losses in engines of different displacements and is defined as the work per cycle per unit of engine swept volume.

For a firing engine, the friction mean effective pressure (fmep) is given by:

$$fmep = imep_n - bmep - amep \tag{2.23}$$

Here, $bmep$ is the brake work output per cycle per unit of engine swept volume.

$Amep$ is the mean effective pressure lost due to work done on required ancillaries such as oil pump, fuel pump, water pump, alternator and air conditioner.

$Imep_n$ is the net indicated mep and is the work delivered to the piston over the entire four strokes of the cycle, per unit displaced volume. $Imep_n$ is related to gross indicated mean effective pressure ($imep_g$) by the following equation:

$$imep_n = imep_g - pmep \tag{2.24}$$

Where, $imepg$ is defined as the indicated average constant pressure exerted on the piston during the expansion stroke which will produce the same amount of work as the actual pressure during the compression and expansion strokes. $Pmep$ is the work done to induct and exhaust gas from the cylinder during intake and exhaust strokes of the cycle.

For motored tests of four stroke engines, the fmep can be calculated by [96]:

$$fmep = \frac{4\pi T}{V_s} \quad (2.25)$$

Where T is torque required to motor the crankshaft and V_s is total swept volume of the engine. In this thesis, the units of fmep used are kPa unless otherwise stated.

2.5.4 Friction Measurement Methods

More or less accurate estimation of journal bearing friction can be obtained experimentally, such as [4]:

1. *The Indicator Method*: In a firing engine, in-cylinder pressures measured over the engine cycle are used to calculate the indicated power. Brake power, which is the power transferred from the engine to the output shaft, is measured using a dynamometer and is subtracted from the indicated power giving the friction power.
2. *Direct Motoring Test*: The work input required to motor a non-firing engine is measured, usually using a torque transducer. By progressively disassembling the engine (engine teardown), the contribution of individual components to engine friction can be determined.
3. *Willans Line:* This involves plotting fuel consumption against bmep for a given speed and then extrapolating the line to find the value of bmep for zero fuel flow rate. The corresponding value for bmep is taken to be the engine fmep. This method can be applied to diesel engines.
4. *Morse Test:* In a firing multi-cylinder engine running at constant speed, individual cylinders are cut out in turn and the corresponding reduction in brake torque is recorded.

Friction losses in the crankshaft assembly are measured through the motored breakdown approach, however, there exist some differences between firing and motored engine conditions. Firstly, during motoring there is no combustion hence gas load is due to compression only. Secondly, there is no way to account for increased local temperatures due to combustion which affects lubricant viscosity and expansions of different components and therefore the engine friction measured. Despite these differences, friction data acquired during motoring has been found to

agree well with fired engine friction data in studies conducted at the University of Nottingham [114]. Leong [11] undertook motored breakdown tests to investigate crankshaft and piston assembly friction at different oil temperatures and engine speeds. In his research the brake torque was initially measured for the whole engine assembly with both the piston assembly and crankshaft in place. Later to find the contribution from the crankshaft main bearings, the piston assembly including the piston, connecting rod and big end bearings were removed. A similar setup was used by Baylis [3] in the investigation of main bearing friction during early seconds of cold engine operation where a torque transducer was used to measure the friction from the crankshaft's five main bearings. In both the studies, no load could be applied under the broken down motored conditions and friction was obtained as a cycle average result.

The investigations carried out in this thesis utilize the motored friction measurement technique.

2.5.5 Recent Developments in Reducing Engine Bearing Friction

In this section, current trends in the automotive industry to reduce levels of engine bearing friction are described and examples are presented. Reductions in levels of engine friction lead towards improvements in fuel economy and reductions in CO_2 emissions.

2.5.5.1 Promoting Engine Warm-up and Accelerating Local Temperature Rise

Reduction in engine bearing friction may be achieved by thermal means or non-thermal means. Since viscosity of a lubricant greatly influences engine friction and is strongly affected by temperature, reducing the time taken for an engine to reach fully warm conditions is an effective method to reduce fuel consumption. Engine friction after cold-start friction can be four to five times as much as the fully warm engine friction [10].

Optimization of engine warm-up rates using electronic control (electronic pump, thermostat valve, variable speed fan) to delay thermostat opening in engine coolant circuit has shown to improve fuel economy between 2 to 3% over the NEDC [115,

116]. Increased coolant temperatures also lead to increased lubricant temperatures which reduces the oil viscosity and subsequently the friction at hydrodynamically lubricated rubbing surfaces such as the main bearings.

Another solution proposed by engine designers involves modifications to the oil sump so that some oil is isolated during warm-up [117]. An additional thermostat within the sump allows reduction of the working volume. As the oil temperature reaches a certain value, the thermostat opens allowing oil to flow through the sump again. Fmep reductions of 10% have been measured under cold start conditions.

Modifications can also be made to the engine structure improve the local warm-up rate of rubbing surfaces. Motoring tests on engine main bearing friction previously carried out by Shayler et al. [3] focused on influence of local thermal conditions in and around main bearings on crankshaft friction level and it was shown that changes in viscosity produced by changes in film temperature had a substantial impact on bearing friction during cold running conditions. Up to 20 percent reduction in friction was achieved by increasing thermal contact resistance between bearing shells and the engine structure. Zammit et al. [118] have experimentally investigated the reduction in crankshaft bearings during cold engine operation by heating the oil supply to the main gallery. It was found that heat transfer from the oil film into bearing shells and journal greatly reduced the potential benefit of pre-heating the oil.

2.5.5.2 Lubricant Formulation

Lubricant formulation and additives can significantly impact hydrodynamic friction. Viscosity modifiers are used to vary the lubricant viscosity with temperature and shear rate. As shown in equation 2.6, the hydrodynamic film shear stress is proportional to the lubricant viscosity. Using a thinner oil can result in friction reduction at the same working temperature.

Several studies reported in literature have shown increases in fuel economy with use of lower viscosity lubricants. Taylor et al. [119] reported fuel consumption benefits of 4% and 1.75% for SAE 5W/30 and SAE 10W/40 lubricants respectively when compared with the fuel consumption using SAE 20W/50 on a 2.5 l V6 engine. Fully

warm bearing friction simulations carried out by Taylor [10] have shown a 13% reduction in friction using a SAE 10W/30 oil instead of SAE 20W/50. Allmaier et al. [120] reported reductions in crankshaft bearing friction of 35% when cold and 20% when warm as the oil was switched from SAE 10W/40 to SAE 0W/30.

Friction modifiers are added to lubricants to reduce mixed film and boundary film friction and wear. They are either chemically or physically adsorbed on the rubbing surfaces to form thin films [51, 86]. Molybdenum based additives are common friction modifiers [121] and can help reduce camshaft friction [10, 37].

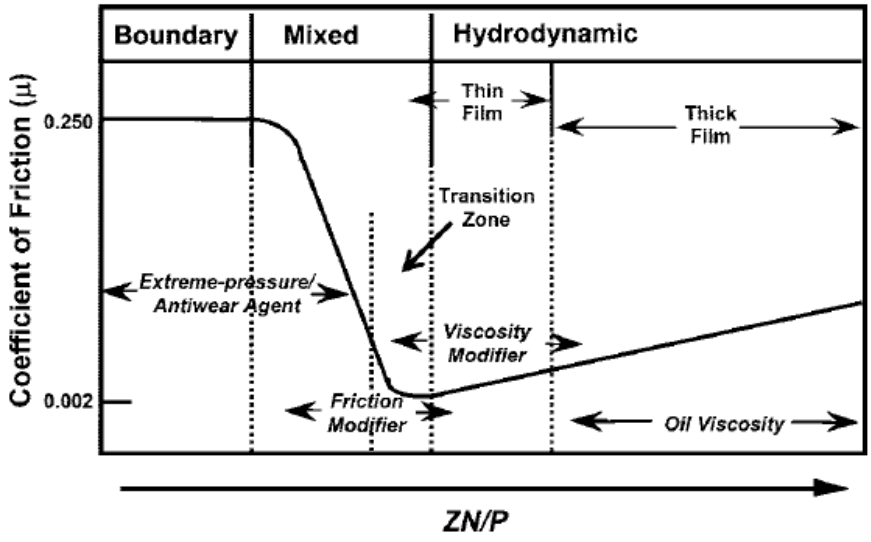


Figure 2.23: Roles of lubricant additives in different lubrication regimes [86]

2.5.5.3 Dimensional Modifications

Dimensional modifications of the crankshaft bearings may also be made to achieve lower friction values. Baylis [3] carried out a series of motoring tests on crankshaft main bearings to investigate the effects of bearing clearance on bearing friction. Radial clearances of 6.6 μm, 26 μm and 44.3 μm were tested and a significant reduction in friction was achieved with increased clearance.

Allmaier et al. [120] showed the effect on reducing bearing width on friction. The bearing width was reduced from 26mm to 16mm. Using a SAE 10W/40 lubricant, narrowing the bearings led to a reduction in friction of 9% under cold conditions and high speeds and a 3% reduction under hot conditions.

2.5.5.4 Surface Texturing

The effect of surface texturing has been explored on the cylinder liner and piston rings has been extensively researched. Dimples on the liner surface and rings created using Laser Surfacing Texturing (LST) have shown to reduce friction. Ryk et al. [122, 123] found a 30% reduction in friction by using flat faced piston rings with micro dimples 80 μm in diameter compared with conventional barrel shaped rings. This has been attributed to increased hydrodynamic effect [124]. Engine tests have shown that textured piston rings can improve fuel economy by up to 4% [125, 126].

Experimental works on the effects of surface texturing on journal bearing friction have been carried out to a lesser extent. Numerical work has shown that lower friction levels can be obtained with dimpled shafts [127, 128]. Dimples with a ratio of depth to minimum film thickness greater than 1 in the high-pressure zone of the film have shown to provide the greatest friction reduction and improvements in bearing performance. Texture design is shown to be very complex with the size, density and angular location of dimples all effecting the bearing load capacity and friction.

2.5.5.5 Improved Oil Flow Control to Crankshaft Bearings

There is an increasing interest from automotive manufacturers to move towards variable displacement and electric oil pumps since tangible reductions in mechanical power losses are possible with the introduction of these technologies. As mentioned earlier in section 2.4.3, use of variable displacement oil pumps offering improved control of oil pressure in the lubricant circuit has led to fuel economy improvements of between 0.8% to 3.4%.

Different sources of fuel efficiency improvement attainable using controlled low oil pressure are summarised in the flow chart diagram (Figure 2.24) presented by Chisaki et al. [108]. The main sources of energy reduction include reduction in parasitic losses via reduction in pump work, reduction in friction losses due to oil windage and splashing on the crankshaft, faster warm-up of the piston liner due to stoppage of the piston cooling jets and as will be shown later in this thesis, reduction in the rubbing friction within the journal bearings themselves due to a reduction in film area under shear and increased film temperatures.

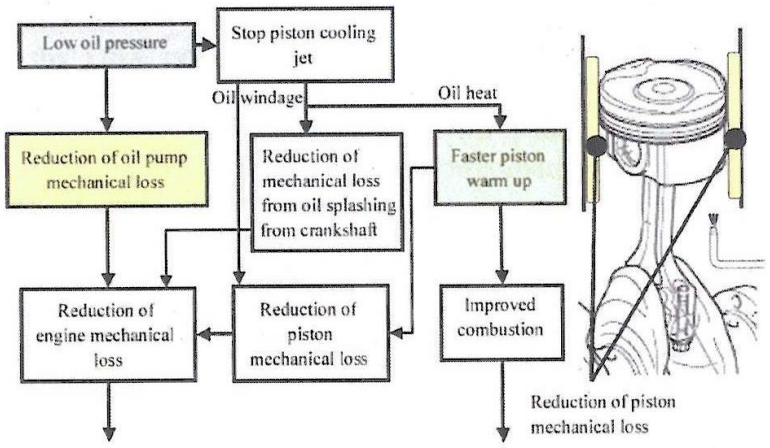


Figure 2.24: Summary of reduction in energy losses in a combustion engine due to low lubricant pressures [108]

2.6 Discussion and Concluding Remarks

A review was presented in this chapter to give a broad picture of journal bearing operation and the factors affecting friction. Crankshaft journal bearings which operate mostly in the hydrodynamic regime are the second largest contributor to total engine rubbing friction therefore reducing the friction contribution from this assembly is of great interest to automotive manufacturers. Friction in dynamically loaded crankshaft journal bearings exists mostly due to shear of the lubricant film rather than the squeeze film effect.

The literature on the effects of lubricant feed conditions on bearing performance is extensive as presented earlier in this Chapter. Reducing feed pressure has been shown to reduce bearing friction under steadily loaded conditions for single, twin-axial groove, leading edge groove and tilting pad journal bearings, particularly at light loads. The reduction in feed pressure has been linked to reductions in flow rate, smaller film extents and increases in peak film temperatures. The effect on peak film pressure, minimum film thickness and oil flow rate depends on the location of oil supply groove. For grooves located opposite the load line, a reduction in oil feed pressure can reduce the hydrostatic force on the bearing and, hence, lead to larger minimum film thicknesses even at high loads.

The presence of cavitation in the lubricant film can lead to reduction in frictional losses due to the difference in viscosities of lubricant and gas cavities. Two types of

cavitation have been identified in literature- gaseous and vaporous cavitation. For steadily loaded bearings, gaseous cavitation is generally prevalent due to degassing of dissolved gases and entrainment of ambient air. For highly loaded dynamically loaded bearings where larger negative pressures may exist in the film, vaporous cavitation can result in bearing damage due to erosive wear.

The presence of cavitation in bearings is greatly influenced by the supply pressure/flow rate. Generally, all steady load journal bearing film visualisation results show that as the flow rate to the bearings is reduced, a shortening of the full-film region is observed and an increase in the cavitation extent in the form of gas streamers occurs. Increases in speed have also shown to lead to increased cavitation areas, however, the influence of feed oil pressure reduction is greater. Experimental measurements and numerical models have shown reductions in power losses as the supply pressure is reduced which has been linked to reduced film extents and increased film temperatures. The shortening of the film extent can lead to increased operating eccentricities and ultimately failure by boundary contact.

It is evident from literature that bearing grooving design influences the response to feed pressure reductions. There is relative scarcity of experimental data or analysis for bearings with the 180^{o} circumferential groove of interest which is addressed in this thesis. In most optical studies reported in literature, though the influence of supply pressure extent on film extent has been measured, the relationship between increased cavitation areas and friction reduction has not been experimentally quantified. For most modelling studies, predictions for friction reductions with supply oil pressure reduction have been made but most have not been confirmed with experimental findings. In the studies reported here, visualisation of the cavitation and torque measurements were carried out simultaneously at fixed film viscosities thereby eliminating any influence of film temperature on friction and allowing the identification of the individual mechanisms leading to the friction reductions with oil supply pressure reduction.

Chapter 3- A Single-Bearing Friction Rig and Setup for Visual Studies of Bearing Film Area and Extent

3.1 Introduction

In this chapter, a single-bearing test facility designed to investigate the relationship between friction torque and oil feed conditions is described. The dimensions of the bearings used in the studies are based on the main bearing design of a 4 cylinder, 1.5 litre turbocharged Ford diesel engine. The use of Perspex bushes made possible the visualization of flow within the bearing which, along with simultaneous measurement of bearing friction using a torque transducer, allowed the connection between bearing friction reduction and film area to be established. This has provided insights to the mechanisms leading to friction reductions with reduction in oil supply pressure. In separate tests, the use of a phosphor bronze bush allowed friction studies at higher loads and oil temperatures. The test rig design allowed the bearing load to be fixed for a given test, while shaft rotation speed and oil supply pressure and temperature could be varied.

Details of the film visualisation setup are presented and the operation of the facility and methodology for calculation of cavitation area on the curved bearing surface are described. It has been shown experimentally and theoretically [34, 129] that the oil film in journal bearings exhibits positive pressures in the converging part and negative pressures in the divergent part of the film. The decrease in pressure is because the oil is being forced to expand after passing through the minimum film thickness point. The drop in pressure in the divergent part of the film results in cavitation, associated either with degassing of air or the formation of vapour, which disrupts the oil film and has a significant effect on the friction within a journal bearing (Section 5.3). The categories of cavitation were described earlier in Section 2.2.5.

3.2 Overview of Test Rig Design and Measurement Techniques Employed in Literature

3.2.1 Test Rigs

Experimental rigs for studies of single journal bearings under steady loads have been described by various investigators including [20, 21, 45, 59, 130]. Usually, test rigs consist of a base frame, an instrumented test bush unit, a loading unit, a lubrication circuit, a motor drive and control and data acquisition systems. The bearing unit consists of the bush, journal and support bearings.

The test bush is normally of a cylindrical design and may in some cases consist of a sleeve to which different bearing geometries can be fitted as implemented by Brito et al. [20]. The journal is commonly supported by high precision roller bearings as they provide adequate stiffness to the system. These have been implemented in several setups including those of Cole et al. [45], Dowson et al. [63], Costa el al. [18], Tanaka [22] and Brito et al. [20]. The journal is more commonly supported by two support bearings, however, designs with a single support have also been used for instance by Tanaka [22].

A loading system is used to apply a steady or oscillating load onto the test bush. Mechanisms for applying steady loads have included use of hydraulic cylinders [64, 131], pneumatic cylinders [18, 20], gearing systems [132], cable-cantilever mechanism utilizing dead weights [21, 22, 59] or fixing the bush eccentricity using support brackets [62]. Where hydraulic or pneumatic load systems are used, it is common to use hydrostatic bearings between the load system and test bush to ensure alignment of the bush. Amongst the mechanisms employed to generate dynamic loads researchers have previously used hydraulic setups applying load at a set frequency to the bush [131, 133] and electromagnets producing impulses [134] to generate pulsating bearing loads.

The drive mechanism on most test rigs consists of an electrically driven direct current (DC) or alternating current (AC) motor and a belt and pulley mechanism. Couplings are used between the drive shaft and test journal to dampen vibrations and avoid

misalignment. The lubrication circuit consists of a tank, oil pump, oil heaters and/or temperature controlled bath.

3.2.2 Measurement Techniques

Bearing friction under varying supplying conditions has been recorded in several research studies using different approaches.

Dowson et al. [132] mounted the whole test machine placed on a swinging cradle supported by two hydrostatic bearings and measured the reaction torque required to prevent cradle rotation. Later test rig designs [15, 20, 135] have employed use of strain gauge torque transducers to measure friction torque and Brito et al. [21] inferred frictional dissipation from motor electrical consumption values, although, accuracy may be compromised by the influence of other factors in this case.

To measure oil film pressure, tappings are generally made within the bush and connected to pressure sensors. Tappings 1 mm in diameter have been conventionally made on the bearing centreline [18, 20, 82]. Film temperatures are measured by thermocouples inserted in holes drilled in the bush and flush with the inner bush surface [20].

For film visualisation transparent bushes have been previously used made from either hardened glass or Perspex [45, 58, 59, 62]. Graduating the shaft or bush is a useful practice to enable the determination of film rupture and reformation boundaries [23, 45, 62]. Dyes added to the oil to make the thin film visible have included ultra-violet dyes [45], graphite additives [59] and colourants [23, 62] which do not impact the fluid viscosity.

3.3 Single-Bearing Rig Design and General Assembly

The test facility designed and built for the investigation reported here is shown schematically in Figure 3.1. Photographs of the test bench and loading system are shown in Figure 3.2. The main elements of the facility were a rotating shaft assembly which includes the journal of a single bearing, a loading system which applies a steady load to the bearing bush, and an oil circulation system. A National Instruments data acquisition system (DAQ) with LabVIEW software was used to record the data.

3.3.1 Shaft Assembly

The shaft assembly was driven by a 2.2kW electric motor through a belt and supported by four SKF 61807 low friction, deep groove ball bearings two of which were found downstream of the torque transducer. The motor was linked to an electronic inverter controller which could provide control over the shaft rotation speed to $\pm$ 10 rpm. The test section of the shaft assembly was machined from mild steel and case hardened. The final radius of 24.9823 mm was measured using a Coordinate Measuring Machine (CMM) at a controlled lab temperature of 20 °C. A Datum Electronics M425 Rotary Torque Transducer with a range of 0-10 Nm was mounted between the belt drive and the test section using two single disc couplings. This gave torque and shaft speed data which were recorded at a sampling rate of 50 samples per half second and was then averaged to provide a value at 0.5 second intervals.

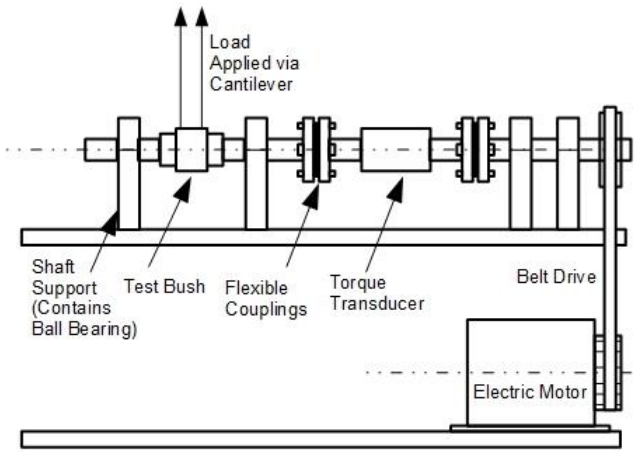
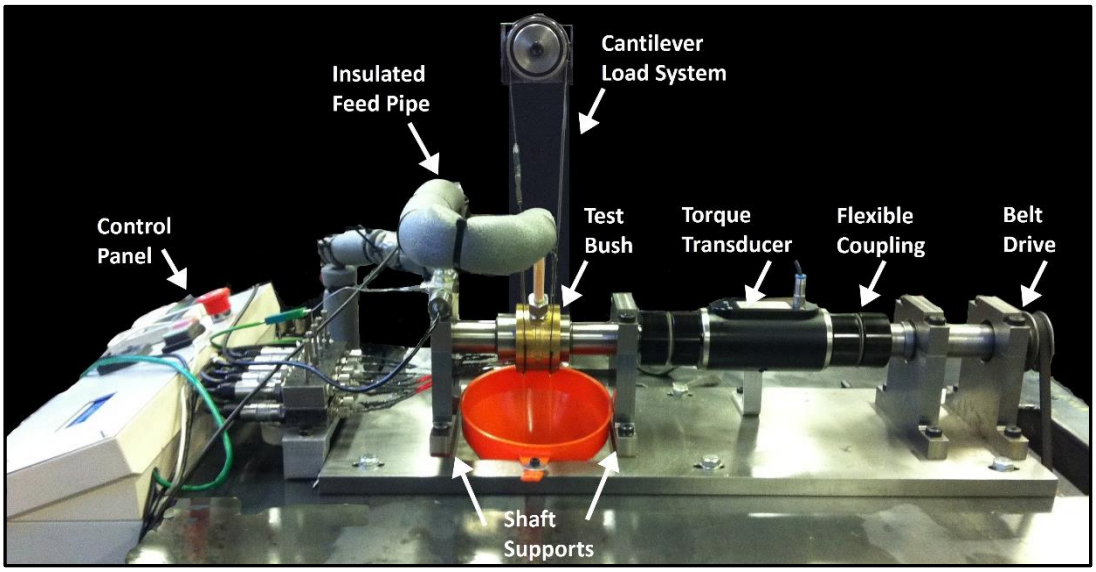
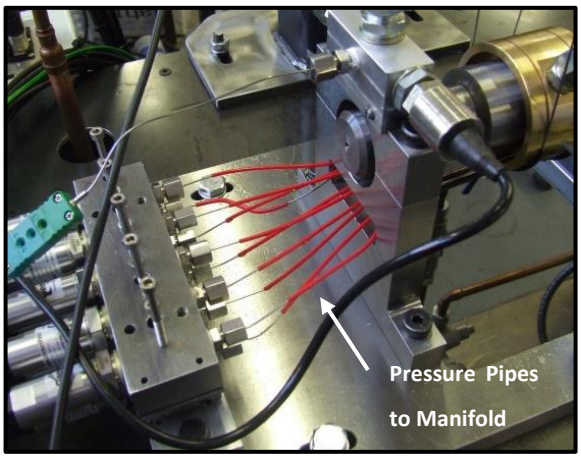


Figure 3.1: Schematic of the Single Bearing Rig



(a)



(b)



(c)

Figure 3.2: (a) Photograph of the test rig (b) Film pressure measurement setup (c) Photograph of loading system

3.3.2 Loading System

The loading system as shown in Figure 3.2(c) was similar to that used by Brito et al. [136]. The system used a balance beam to apply a vertical load to the bush body through a closed-loop of steel cable. The cable ran to one end of the beam and had a weight hanger at the other end. The cable was wrapped around a needle bearing on the beam to ensure that it was not constrained. The load was applied upwards to the bush body through a closed-loop steel cable and an equal and opposite reaction force occurred on the rotating journal. The beam was pivoted on a knife edge and the mechanical advantage for the setup could be varied and this was useful when

applying higher loads. To confirm that the test bearing self-aligned, side leakage oil was collected from each side of the bearing for a specified amount of time. In all cases the maximum difference between the left hand side and right hand side leakage was less than 5%.

This mechanism allowed the bearing to float on the shaft while providing some axial constraint. It also made the setup less obscure, as by applying the load upwards, the tendency of side leakage oil to cover the outer surface of the bush was minimized. This was advantageous for film visualization studies.

The applied load, W_{bush}, can also be represented as a specific load based on the projected area of the main bearing (W_{bush}/A_{bush}). This has been from here onwards referred to as the specific load (SL). Loads of up to 1420 N (SL=13.8 bar) have been tested with this loading design.

3.3.3 Rig Lubricant Supply System

The oil supply system consisted of a reservoir tank with a capacity of approximately 7 litres, an oil pump driven by a 0.75 kW electric motor with variable speed drive, feed pressure regulation valves and a gear flow meter. A schematic of this is shown in Figure 3.3. The feed pressure to the test bearing was controlled by varying the pump speed and pressure regulation valve position.

The oil tank also housed electric cartridge heaters which allowed the oil feed temperature to be raised up to a fully warm 90 °C condition. The lubricant flow from the bearing sides was collected in a tray and gravity fed to the sump to form a closed loop circuit.

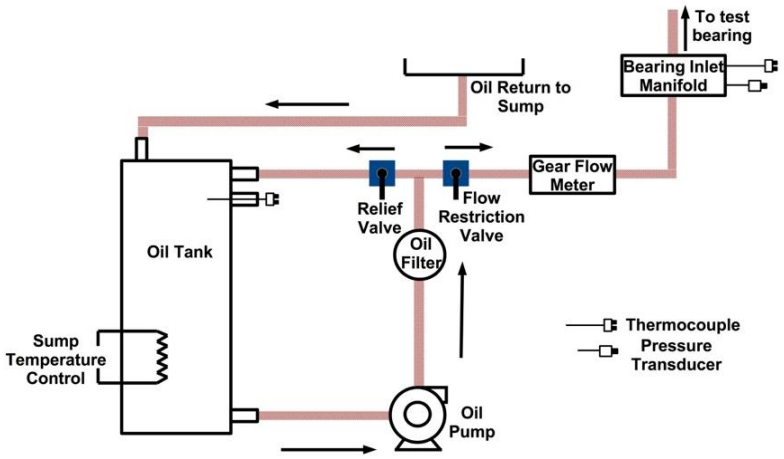


Figure 3.3: Schematic of the oil circuit

3.3.4 Calibration of the Torque Measurement

The torque measured by the torque transducer was typically less than 0.5 N m with an accuracy of ±0.001 N m. Zero errors were checked regularly by decoupling the torque transducer from the shaft assembly. The measured torque to the shaft assembly was corrected to subtract the contribution of two low-friction deep-groove ball bearings supporting the shaft and disc-coupling between the shaft and the torque transducer. In total, the shaft assembly is supported by four of these though only two contribute to the measured torque input to the working section. The correction allows for an increase in ball bearing friction with increasing applied radial load determined through tests on the ball bearings over a range of loads and two speeds using a modified rig assembly. In the modified form, the bush of the test bearing was replaced with a sleeve housing two ball bearings identical to the support bearings as illustrated in Figure 3.4(a). The torque contribution from the two ball bearings was found to be equal to 0.075 N m for unloaded tests at 1000 rpm. In other tests it was found that increase in speed to 1500 rpm had negligible effect on the ball bearing friction. The increase in ball bearing friction torque with load for two ball bearings using the modified assembly is presented in Figure 3.4(b). Typically, the two support bearings contribute approximately 25% of total friction torque under loaded conditions.

The corrected torque is given by the following equation:

$$Torque_{plain\ bearing} = Torque_{measured} - Torque_{2\ ball\ bearings} \quad (3.1)$$

Besides the torque transducer, the only things attached to the test bush from the supporting system included a flexible thermocouple, oil feed tube and hydrodynamic film pressure measurement tubes which were assumed to provide negligible torsional constraint.

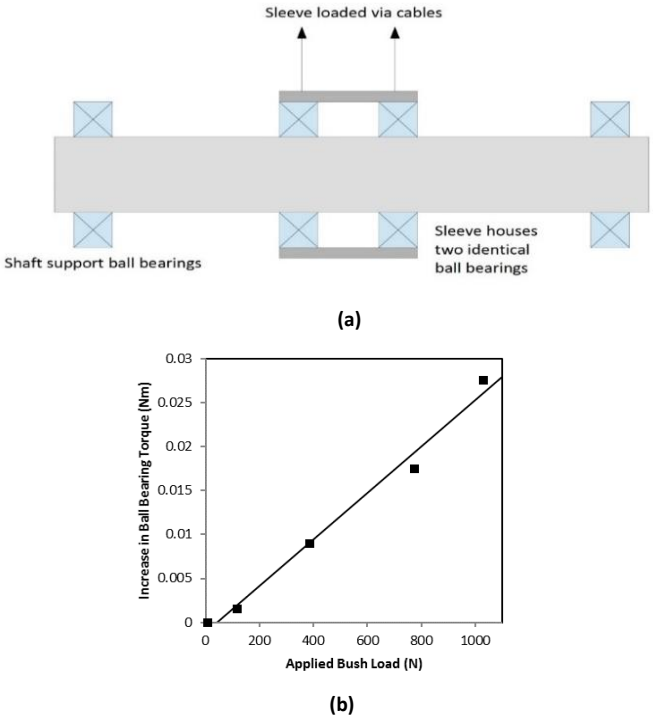


Figure 3.4: (a) Sketch of setup to determine variation in support bearing friction with load (b) Measured increase in the two ball bearing torques with radial load

3.3.5 Bearing Test Bushes and Design

Bushes were manufactured from phosphor bronze and Perspex; the bronze bush served the purpose of high load testing whereas the Perspex bushes allowed visualisation of the film extent and cavitation in the bearing. These have an 180˚ circumferential groove machined in them as found in main bearings of the 1.4 L, 4 cylinder TDI diesel engine used in [137]. Details of the bearing are summarised in Table 3.1, and photographs of the bushes are shown in Figure 3.5.

Perspex was the material used to manufacture the bush because it is more convenient to manufacture compared to glass, especially since the bush required inclusion of features such as a 180˚ groove and grooves for the loading cables that may cause glass to shatter during machining since it is brittle. Still, visualization tests may only be performed at relatively light loads as high loads will cause Perspex to deform and eventually break. Photographs of the test bushes are shown in Figure 3.5 and the bush geometry is presented in Figure 3.6.

The internal diameter of each test bush and the external diameter of the journal were measured using a CMM device to determine the radial clearances which are also summarised in Table 3.1. The design nominal radial clearance value was 50 μm. The bushes were extended at the sides which provided room for slots to be machined in, into which the loading cable would fit. The feed pipe to the supply groove was positioned at 30° clockwise from vertical. The bushes had drillings made for 10 pressure tappings in the mid-plane of the bush for hydrodynamic film pressure measurements according to the distribution shown in Figure 3.6. Tubes were connected from the tappings into a manifold which housed 10 pressure transducers for 10 individual film pressure measurements. Film temperature was also measured with a K-type thermocouple in the mid-plane of the bush close near to the point of minimum film thickness.

Table 3.1: Bearing specifications

Test Bearing Dimensions	
Bearing diameter	50mm
Bearing width	20.5mm
Width/Diameter Ratio	0.41
Bearing groove width	4.9mm
Groove to bearing width ratio	0.239
Groove angular extent	180˚
Angle of oil feed w.r.t. vertical	30˚
Radial clearance, Perspex bush 1	62.7µm
Radial clearance, Perspex bush 2	73.2 µm
Radial clearance, Bronze bush 1	52.7 µm
Radial clearance, Bronze bush 2	47 µm

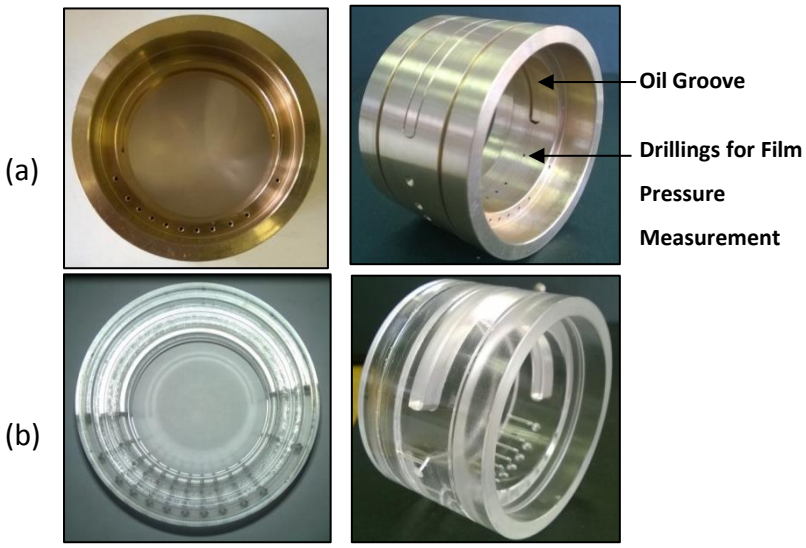


Figure 3.5: (a) Phosphor Bronze bush (b) Perspex bush

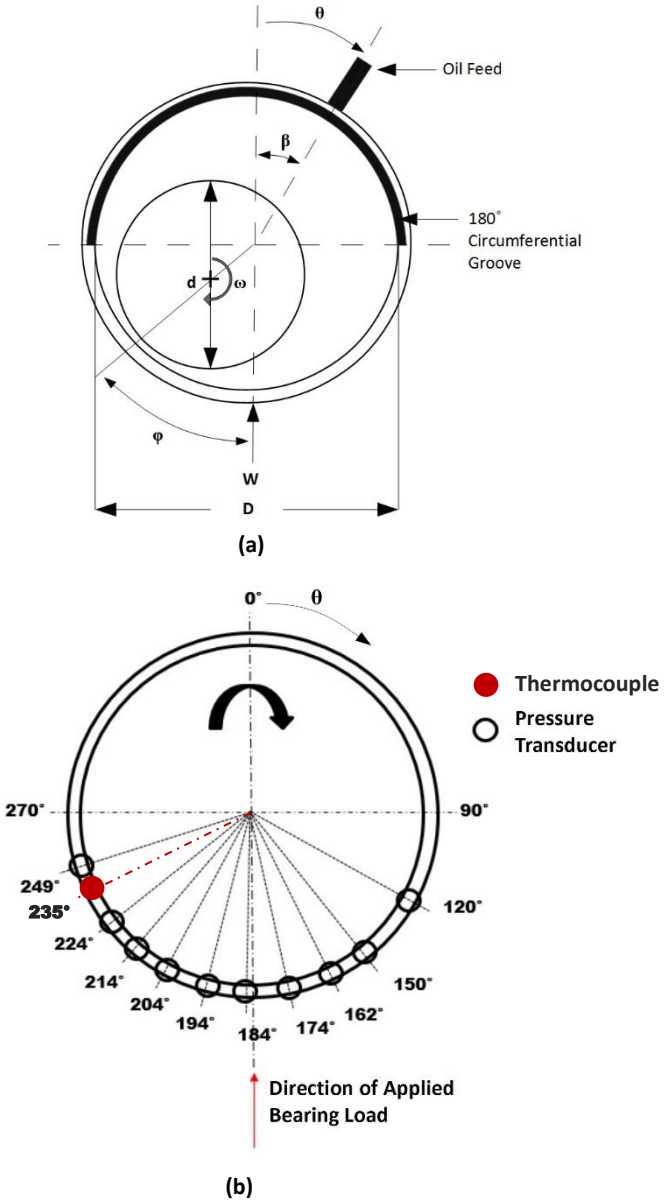


Figure 3.6: (a) Bush geometry and (b) film pressure and temperature measurement angles in the test bush

3.3.6 Test Rig Instrumentation and Calibration

The data acquisition system (DAQ) consisted of a National Instruments NI cDAQ-9178 8-slot USB chassis onto which were connected the following modules: NI 9213 (16-Channel thermocouple input module), NI 9205 (Voltage input module) and NI 9263 (Voltage output module). The DAQ connected to the PC via a USB link. Virtual instruments (VI's) were created in LabVIEW software to record temperature and pressure data from the thermocouples and pressure transducers, respectively.

Four K-type Nickel-Chromium/Nickel-Aluminium thermocouple probes were fitted to the rig for temperature measurements; one in the bearing film, one in the oil sump, one in the bearing inlet manifold just before the feed groove and one measuring the ambient temperature. The film thermocouple was positioned in the mid-plane of the bush close to the expected minimum film thickness point where the film temperature is expected to be the highest as observed by Majumdar and Saha [138].

Lubricant supply pressure was measured by means of an in-house calibrated General Electric Druck PMP 4311 pressure transducer positioned at the inlet manifold to the bearing. The pressure transducer had a range of 0-30 bar with an accuracy of ±0.1% full scale (FS). Film pressure was measured using 10 Gems 3100 series compact high pressure transducers with a 0-250 bar range and an accuracy of ±0.25% full scale.

Shaft speed was controlled via motor frequency selection on the inverter control panel and measured using the torque transducer.

Flow rate to the bearing was measured via a Titan OG1-SU5-VHQ-B oval gear flow meter which has a flow range of 0.01-1 litres per minute for oil of viscosity 3×10^{-5} m^2/s with an accuracy of ±0.75 % of full-scale-deflection (FSD). The flow meter outputs frequency and a calibrated frequency to voltage converter was used to connect the flow meter to the DAQ.

3.4 Observation of Cavitation and Determination of Cavitation Area

When a UV dye was added to the oil the extent of the film could be clearly defined under ultra-violet (UV) light irradiation. The ultra-violet light fluorescent dye used in this work was RLD4 produced by Ring Automotive which is normally used for engine oil and fuel leak detection. Under the light source the film area appeared as bright green while the cavitated areas appeared dark. A total of five high intensity UV torches were focused on the transparent bearing from different angles to make the film visible. Situated approximately 20 cm from the bearing, the lights provided adequate exposure for the cameras to record the film.

Cavitation streamers extended from the rear of the bush to the top (and in some cases to the front of the bush), requiring multiple views of the streamers to calculate

the area. Three digital cameras were used to record high definition video at 30 frames per second. The cameras were positioned to record views of the cavitating region of the film along lines of sight at 270°, 0° and 90° with respect to the vertical as defined in Figure 3.7. Flexible gooseneck clamps were used to position the cameras and UV lights at the appropriate angles.

The positioning of the UV lights was optimised to give the least amount of reflection off the bearing surface. Light diffusing paper was also used to soften the UV light impacting the bush surface. The images were post-processed using Adobe® Photoshop to make the cavitation areas more distinct.

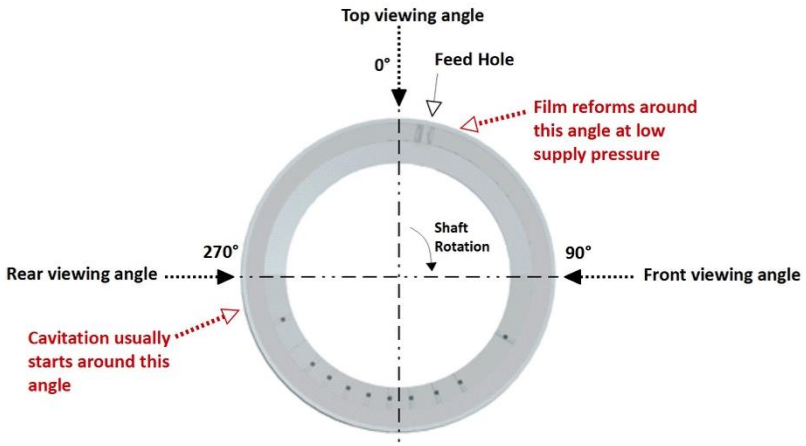


Figure 3.7: Schematic of viewing angles as viewed from the bearing side

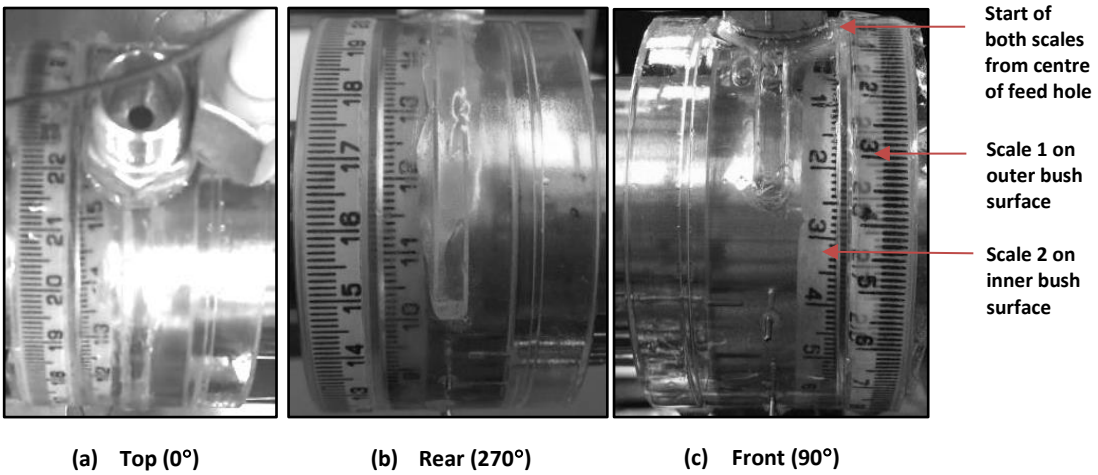


Figure 3.8: (a) Top (b) rear and (c) front camera views used for calibrating the outer scale with respect to the inner scale

The cavitation area determined from the video records required correction for distortion due to the wall thickness and curvature of the bearing bush. To allow for this correction, the angular extent of the film was evaluated using two scales graduated in millimetres with respect to the inlet feed hole. One scale was positioned around the outer surface of the bush. Another scale was fitted in the clearance space between the bush and the shaft when the shaft was stationary. Photographs were taken from the required camera angles to calibrate the inner scale with respect to the outer one at those camera angles. A linear calibration curve was found between the two scales. Figure 3.8 shows both the inner and outer scales from the top, rear and front camera views. Once the relation between the inner and outer scales was determined for the required camera angles, the inner scale was removed.

The cavitation area A_c plus the film area A_f is equal to the journal surface area A_j, so

$$A_c/A_j=1-A_f/A_j \tag{3.2}$$

Or as percentages of the journal surface area,

$$\text{Cavitation Area } A_c\,(\%)=100-\text{Film Area } A_f\,(\%) \tag{3.3}$$

The flow chart presented in Figure 3.9(a) outlines the method developed for percentage cavitation area calculation. A MATLAB script was developed by the author for post-processing of the images of the cavitation streamers to determine the cavitation area. The images were first turned into binary format making the cavitation streamers appear black. The arc lengths of each column of black pixels were then determined using the empirically determined corrections. The arc lengths of each column of black pixels were summed to give the total arc length of the cavitation streamers. The curved surface area of the streamers was then given by multiplying the total arc length with the width of one pixel (which was determined from the image scale).

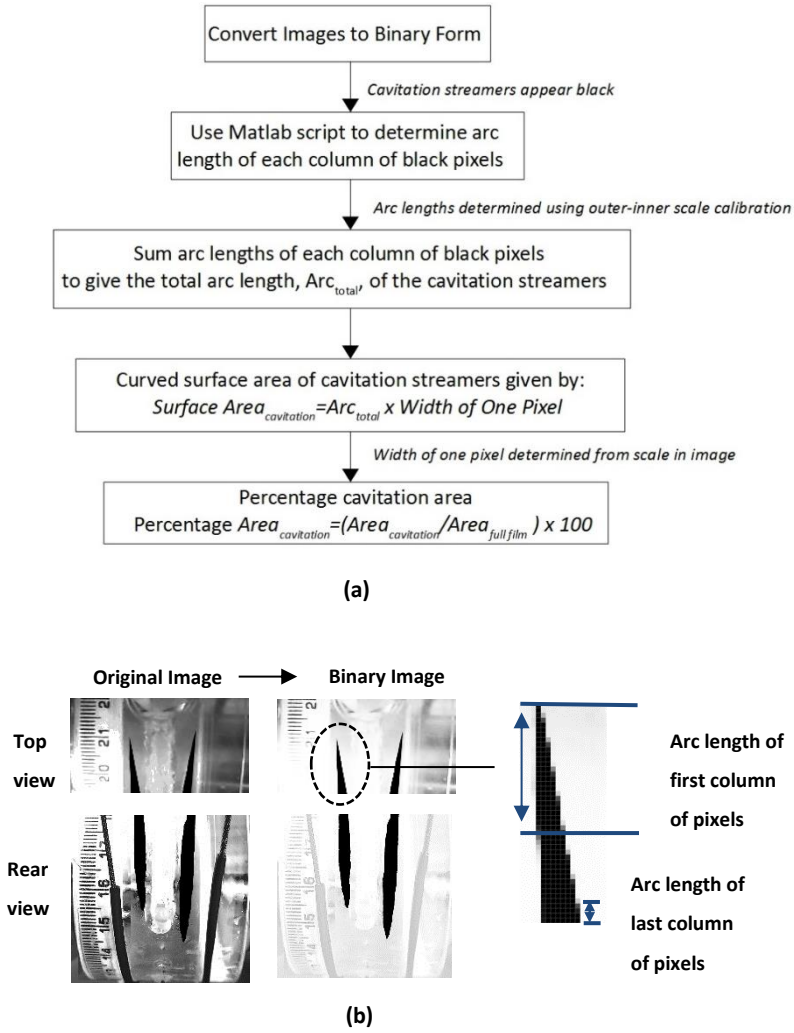


Figure 3.9: Calculation of percentage cavitation area (a) Overall outline of procedure (b) Example of original and binary images and calculation of cavitation arc length

3.5 Operation of Facility and Data Analysis Methods

The zero offset drift in the torque transducer was generally negligible and the repeatability of the torque data was very good and within 0.004 N m. The alignment of the cantilever with respect to the bush was checked using a plumb line to ensure it was centred while a torpedo level was used to check the lever's horizontal alignment.

Tests were performed at fixed speeds, loads and feed temperatures. Higher feed temperatures, achieved using the oil reservoir heaters, were required to raise the film temperature when frictional dissipation was not sufficient on its own to reach the target film temperature. The oil pump was turned on before running the shaft and the feed pressure was adjusted to the desired value using the ball valves and

pump frequency. The shaft was turned on to the desired speed before loading the cantilever with dead weights. Minor feed pressure adjustments were required after loading the shaft. Data was recorded at half second intervals.

Raw data of torque, speed, feed pressure and temperature, film temperature and pressure and oil flow rate was saved after completion of each test and was post processed using a MATLAB script. For comparison of friction data, the film viscosity was used to create plots of torque against viscosity, therefore, eliminating the effects of temperature on friction.

3.6 Discussion

The design and specification of the test rig was described in this chapter which allowed a wide range of operating conditions to be simulated with loads of up to 1500 N and speeds from 400 rpm to 2000 rpm. Bearing torque is measured using a high resolution strain gauge torque transducer as has been employed in previous test rig designs [15, 20, 135].

A number of design features of the rig make it suitable for the wide range of investigations carried out in this thesis including investigating the effects of oil feed pressure, load, speed, feed temperature, oil formulation and clearance on bearing friction and cavitation. The test bushes can be easily swapped over and the ample amount of space and clear line of sight around the bush allow installation of cameras at appropriate viewing angles. The oil in the circuit can be flushed reasonably quickly with a different grade oil and physical access to the rubbing surfaces means that the surfaces can be cleaned by hand to remove surface additives. Precise control over parameters such as supply oil pressure, feed temperature, load and journal speed allows for stable testing conditions. A further advantage of the test rig is that it allows isolation of friction measurements on a single bearing. The only significant external contribution to the total measured bearing friction comes from the shaft support ball bearings which has been accounted for, hence, the friction measurements are due to the journal bearing only.

The repeatability of the test rig is found to be very good with the repeatability of torque, film pressure and film temperature measurements within 0.004 N m, 0.1 bar and 0.3 °C respectively. The rig demonstrated no drifts in readings due to assembly and disassembly of the shaft- the shaft support bearings were clamped down to a fixed torque each time ensuring similar levels of friction in the support ball bearings after each rebuild.

There are a few limitations of the current test rig design. Unlike engine main bearings which experience cyclic loads of varying magnitudes due to combustion forces and inertial forces of the crankshaft assembly, the test rig simulates steady loads and hence squeeze film effects are not accounted for. Also, very high load values could not be achieved with the employed cantilever load mechanism unlike hydraulic or pneumatic loading solutions reported in literature which can provide loads of the order 10^4 N [20].

Engine main bearings generally consist of a backing structure and an overlay material. The backing structure is made from steel which supports the bearing structure during cyclic loads. The overlay lining surface, generally made from an aluminium alloy, provides low friction properties including embeddability and conformability. Further, the main bearings consist of two shells which are clamped together in the engine structure. The shape of the main bearings conforms to the shape of the bearing caps. The clamping force due to tightening of the bearing caps may give rise to a non-circular, elliptic profile of the bearing which can reduce bearing whirl.

The mono-metal test bushes used on the single bearing test rig were made from Phosphor bronze considering its high strength, corrosion resistance and wear resistance. The circularity of the bush was measured using a CMM machine and the maximum deviation from the mean diameter was within 5 µm. When the bush was mounted there was not a reference to indicate the location of this non-circularity, however, the pressure distributions in the load bearing area conform to predicted values indicating that the influence of this was negligible. The surface roughness of the test journal matches that of typical crankshaft journals which is approximately 0.2 µm.

In an engine structure, as will be demonstrated later in the thesis, main bearing film temperatures are thermally clamped to the surrounding metal temperature after an initial period of temperature rise due to frictional dissipation. This is due to heat conduction from the film into the shell and crankshaft. On the single bearing test rig, however, film temperature is not clamped to the bush temperature (due to its smaller mass and since it is exposed to air), hence responses to changes in feed temperature to film temperature will be quicker on the rig. This should not, however, influence the results and data analysis, since friction analysis has been carried out against viscosity eliminating the influence of temperature effects.

Chapter 4- Oil Film Cavitation Patterns Under Light Load Operating Conditions

4.1 Introduction

This chapter is concerned with the presentation of results obtained from experimental studies carried out using the Perspex bush. Through the film visualisation made possible by using the transparent bush, the influence of operating conditions on cavitation and the influence this has on bearing torque was investigated. The oil used was Havoline Energy SAE 5W-30, and in the tests to be described, oil film temperature was within the range 20-30 °C, depending on ambient temperature and operating condition. The study covered a range of oil feed pressures and journal speeds from 400 to 2000 rev/min. The use of Perspex limited the bearing loads to a maximum of 450 N. This corresponds to a specific load (SL) of 4.3 bar, based on projected bearing area.

4.2 Range of Experiments for Visual Investigation

Two Perspex bushes were manufactured for the study, with radial clearances of 62.7 µm and 73.2 µm respectively. Tests were carried out at speeds from 400 to 2000 rpm, oil feed pressures from 3 barA down to 1.1 barA, and specific loads (SL) from 0 to 4.3 bar. For each setting, at least two tests were carried out; differences in the results were generally negligible.

Oil and bearing temperature at the start of a test was typically 20 ˚C. The tests lasted for ~900 s and over this time period the film temperature generally increased to close to 30 °C due to frictional dissipation and heat conduction in the bush and shaft. Over this temperature range and the corresponding range of film viscosity, there were no changes in cavitation pattern.

4.3 Cavitation Patterns and Changes in Film Extent with Feed Pressure

Examples of cavitation patterns are presented in Figures 4.1 for a range of feed pressures and loads. The cavitation area where an oil film does not exist is defined by a black region. Typically, the cavitation area consists of a small number of streamers within a lozenge-shaped area. The start of the streamers marks the rupture angle,

$\Theta_{rupture}$, and end marks the reformation angle, $\Theta_{reformation}$. These are highlighted in Figures 4.2 and 4.3.

Under unloaded conditions and shaft speed of 1000 rpm, no cavitation occurred in the bearing film at all feed pressures tested down to 1.1 barA. As the load was increased to a specific bush load of SL=1.1 bar (W_{bush}=120 N and calculated eccentricity ratio, $\varepsilon_{calculated}$~0.35), a steady pattern of cavitation streamers appeared at the rear of the bush, after the minimum film thickness point and a full-width film appeared at the upper part of the bush where the film reformation angle was influenced by the feed pressure. Under loaded conditions, the amount of cavitation was minimum at 3barA but it was still present. The streamers formed in the upper 180˚ region of the bearing with a single streamer each side of the groove. The appearance of cavitation streamers in the upper unloaded part of the shell is to be expected as the load carrying part of the film lies in the bottom half of the bearing. When the specific load was increased to SL=4.3 bar (W_{bush}=450 N, $\varepsilon_{calculated}$~0.65), the cavitation streamers split into multiple streams with fine oil filaments in between, at all feed pressures tested. Also the oil film area under shear was seen to decrease which is quantified in Chapter 5.

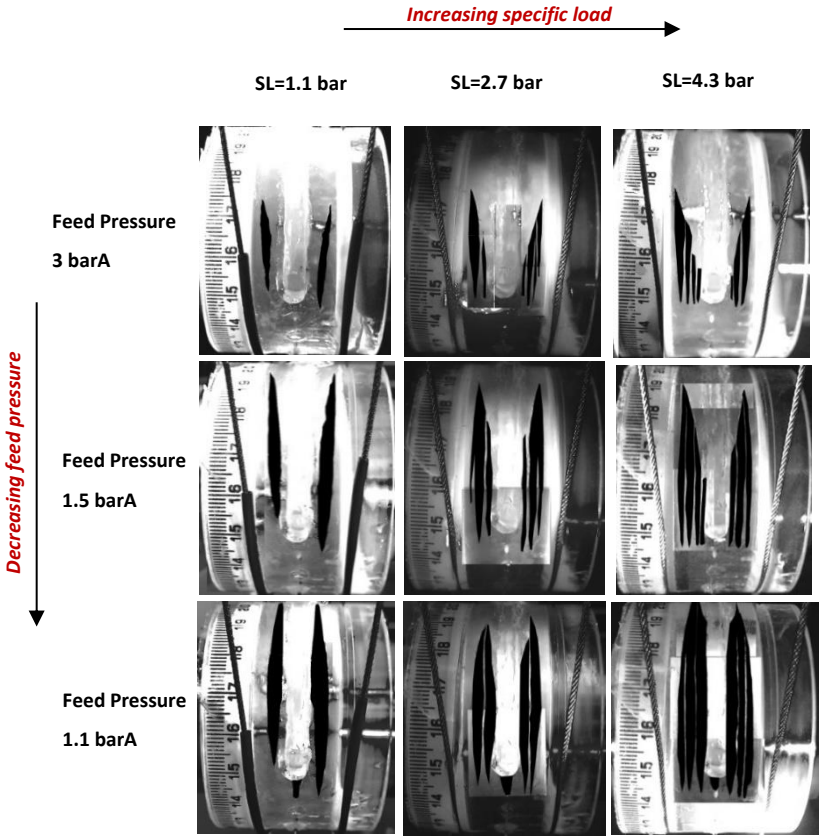


Figure 4.1: Rear viewing angles showing the effect of load and supply pressure on cavitation patterns at N=1000 rpm and C_r=73.2 µm

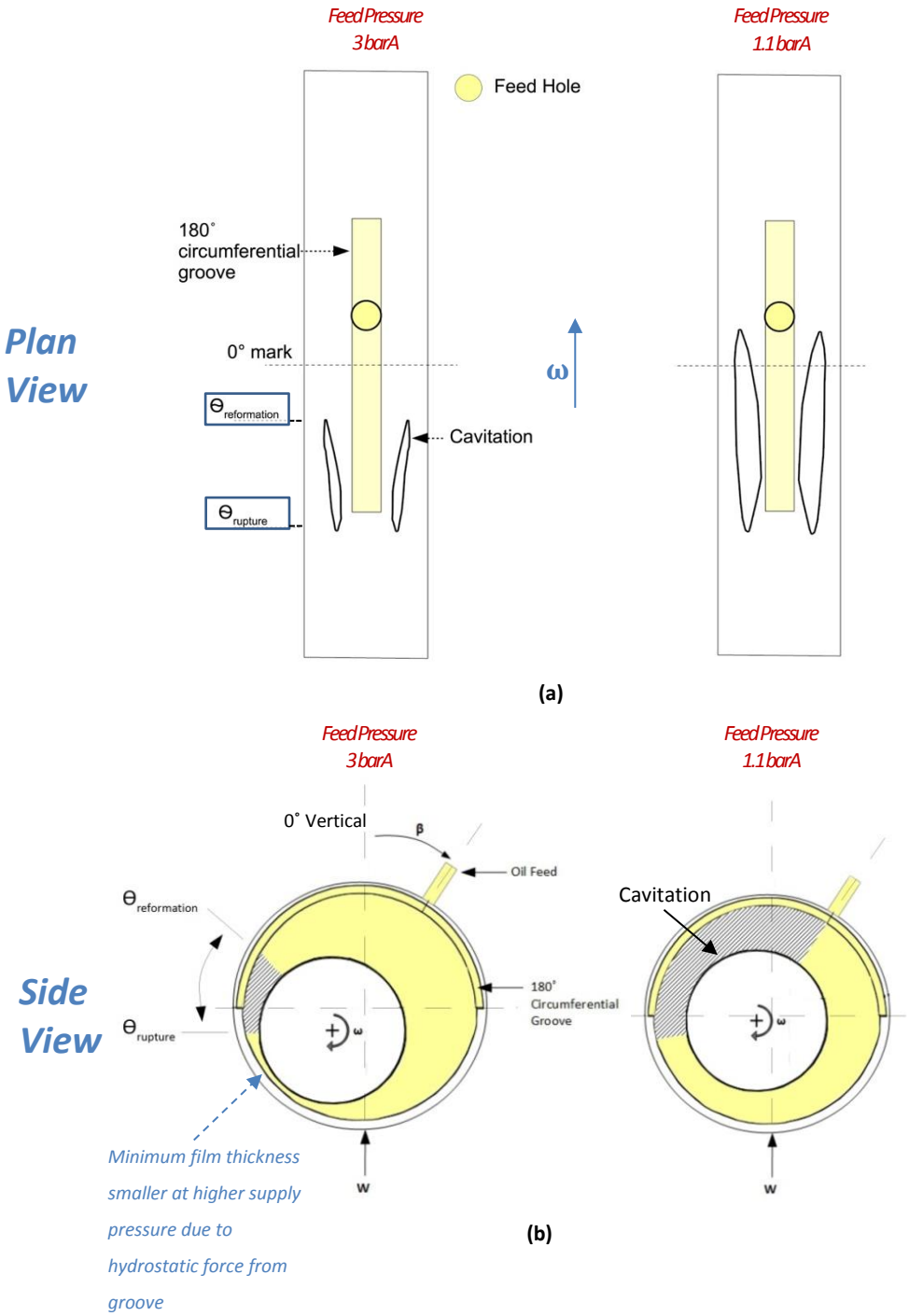


Figure 4.2: Illustrations showing the effect of supply pressure on film extent and minimum film thickness at a light load of SL=1.1bar, N=1000rpm and C_r=73.2 µm (a) plan view (b) side view

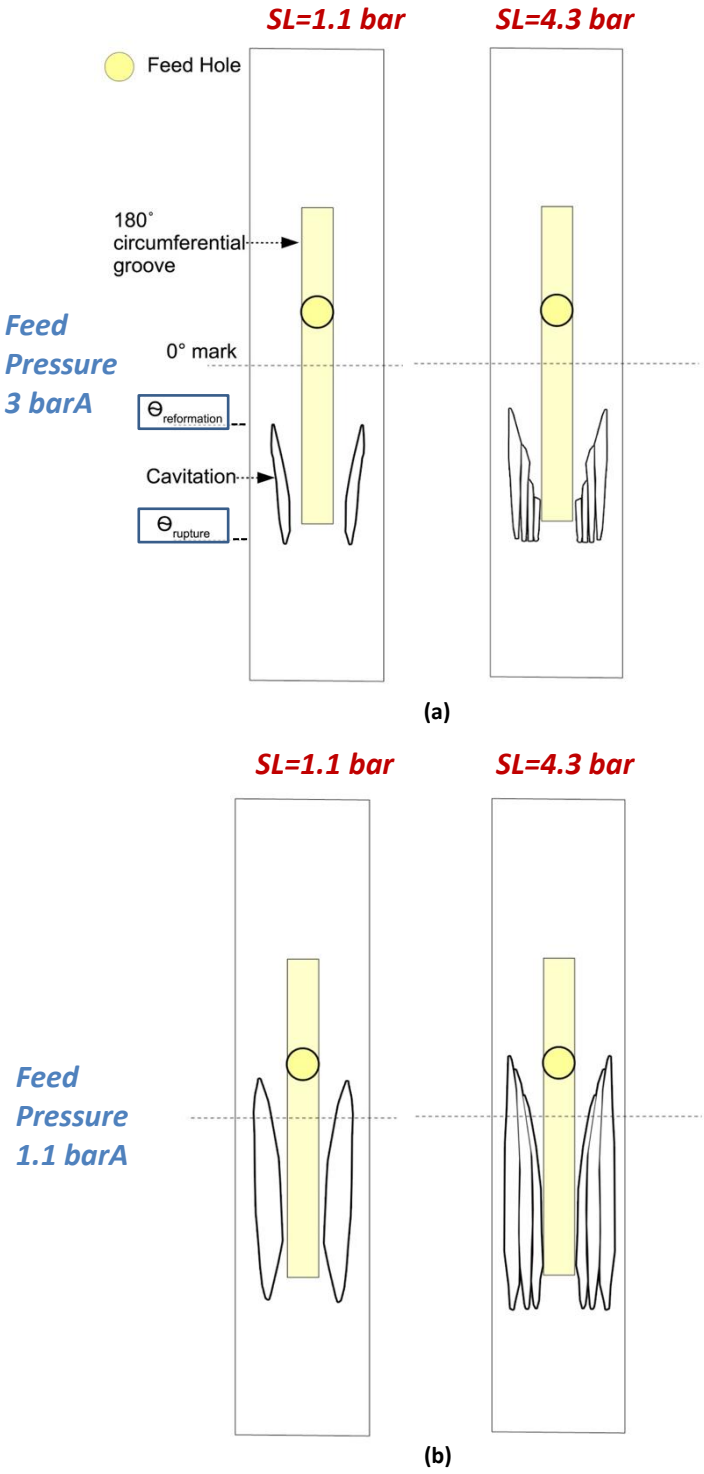


Figure 4.3: Illustrations showing the effect of load on cavitation patterns at two supply pressures (a) 3barA (b) 1.1barA at N=1000rpm and C_r=73.2 µm

Around the reformation point, the film was seen to spread from either side of the groove eventually forming a complete width film. Figure 4.2 illustrates the effect of supply pressure on the film extent and minimum film thickness at a light load of SL=1.1 bar. Minimum film thickness decreases with increase in supply pressure at light loads as will be explained in Section 5.4. The effects of increased load on the splitting of cavitation streamers is shown in Figure 4.3.

A summary of the observed changes in cavitation patterns with changing speed or load is given in Table 4.1.

Table 4.1: Summary of observed changes in cavitation patterns with changes in load and speed

Independent Variable	Circumferential Extent of Cavitation	Axial Width of Cavitation	Number of Cavitation Streamers
Increasing load (SL 1.1 bar to SL 4.3 bar)	Weak increase	Increase	Increase
Increasing speed (400 rpm to 2000 rpm)	Increase	No effect	Weak decrease

In the experiments carried out, no foaming or frothing of oil was observed in the film even at very low feed pressures of 1.1barA. At the edges of the bearing were visible complete rings of oil which have previously been referred to as menisci in the work carried by Cole et al. [45]. It is believed that these menisci act as seals preventing air entrainment into the bearing. The cavities showed a stable behaviour throughout the test suggesting that they are most likely gaseous in nature i.e. due to degassing of non-condensable dissolved gasses in oil. No entrainment giving rise to cavitation extending to the edges of the bearing was observed. This is attributed to the effects of the surface energy of the bearing material and surface tension of the oil. When changing from Perspex to Bronze bush the surface energy increases from 38 mJ/m^2 to approximately 1000 mJ/m^2. The higher value is expected to reduce the likelihood of air entrainment when using the Bronze bush.

In summary, the main conclusion drawn from these results is the experimental confirmation that cavitation area increases as the bearing is progressively starved as well as with increase in load.

The measured changes in film angular extent with drop in feed pressure at a steady specific load of 1.1 bar and speed of 1000 rpm are shown in Figure 4.4 and are consistent with results reported by Dowson et al. [62]. For any applied load tested, the rupture boundary was straight and showed small changes in angular position as the feed pressure was decreased. The reformation boundary, on the other hand, moved significantly in the direction towards the feed hole to the groove as the supply pressure was decreased to 1.1barA. When feed pressure was reduced from 3 barA to 1.1 barA, film reformation occurred approximately 60˚ later whereas the film rupture point moved less than 4°. Therefore, it is the angle of film reformation which dictates the film extent and would have most influence on bearing friction. The full width film extent is defined as:

$$\theta_{full\ width\ film} = 360 - \left(\theta_{reformation} - \theta_{rupture}\right) \quad (4.1)$$

This is diagrammatically shown in yellow in Figure 4.2(b). For all the tests performed, the extent of the full-width film was always greater than 180˚. At the lowest supply pressure of 1.1 barA, the film reformed close to the feed hole.

The results presented in Figure 4.5 and Figure 4.6 show the influence on the film extent of speed and load, respectively. The reported points are averages of two separate tests. The repeatability of data for film rupture and reformation angles was within 1.5°. Figure A1 (appendix) presents images of cavitation patterns recorded at various speeds. As journal speed increases both film rupture and film reformation points occur later (indicating lowering of eccentricity ratio) but the influence of speed is greater on the reformation point. The decrease in bearing eccentricity indicates that the load capacity of the bearing has improved although the full width film extent decreases by about 30° with a five-fold increase in speed from 400 rpm to 2000 rpm. The full width film extent decreases and an increase in cavitation area is visible with an increase in journal speed. Measurements of changes in oil flow rate with speed for

specific loads of 1.1bar and 4.3bar at a feed temperature of 27 °C are presented in Figure 4.7. These show that the flow rate first decreased as speed was increased up to 1000 rpm after which it increased slightly.

As load was increased film rupture occurred earlier due to lower attitude angle and higher ε and the film extent reduced by between ~6° at the highest feed pressure and ~13° at the lowest feed pressure. Increases in flow rate with increasing load are most marked at the higher oil feed pressures (Figure 4.7(c)). The increases are due to increased clearance near the groove region at higher loads i.e. higher eccentricity ratio as is explained in the following discussion section.

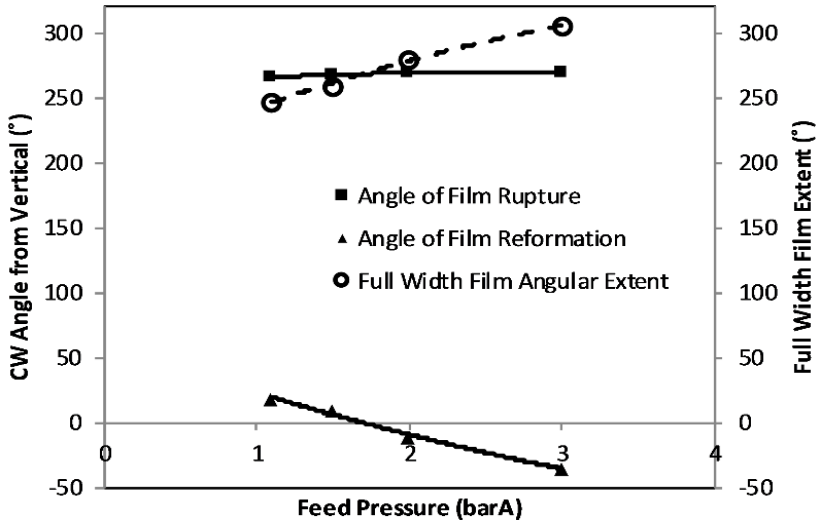
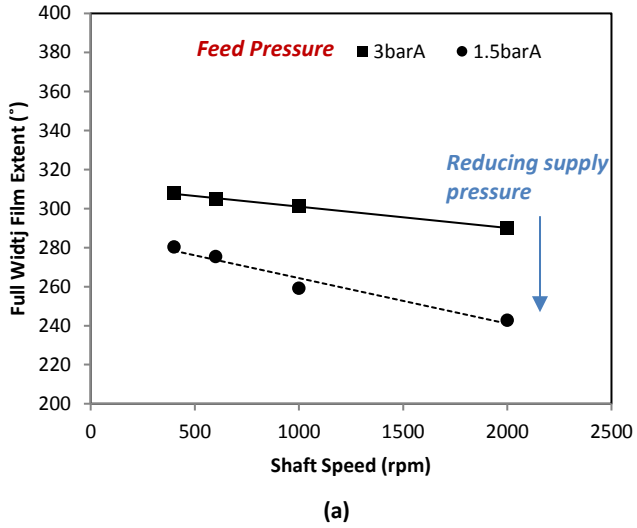
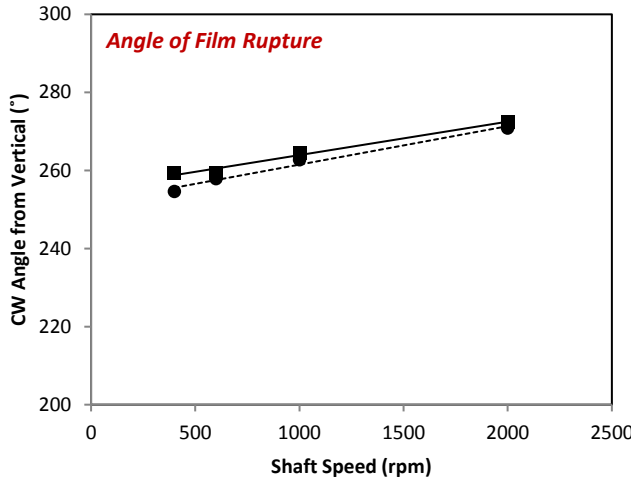


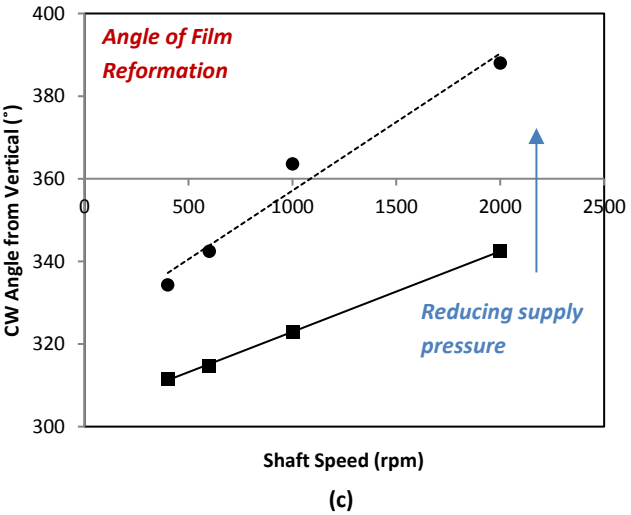
Figure 4.4: Variation in extent of full width fluid film and angle of rupture and reformation at SL=1.1bar, N=1000rpm and C_r=73.2 µm



(a)

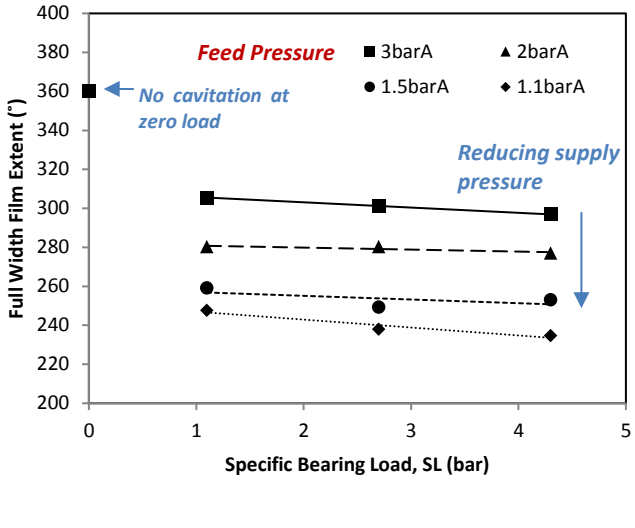


(b)

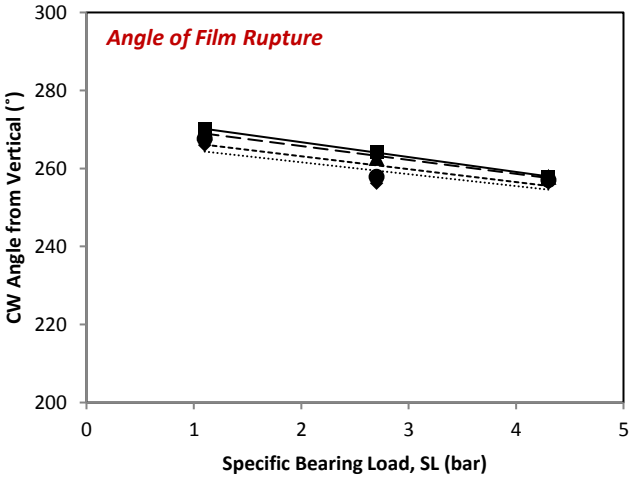


(c)

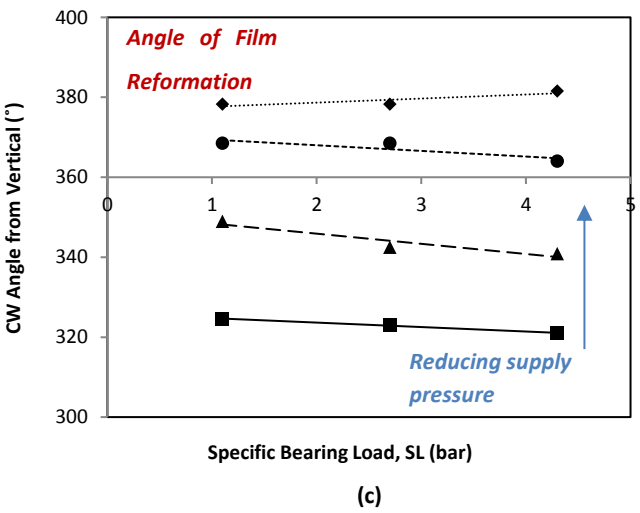
Figure 4.5: Effect of speed on (a) film extent (b) film rupture and (c) film reformation presented at two values of supply pressure at SL=1.1bar, N=1000rpm and C_r=73.2 µm



(a)



(b)



(c)

Figure 4.6: Effect of load on (a) film extent (b) film rupture and (c) film reformation presented at four values of supply pressure at N=1000rpm and C_r=73.2 µm

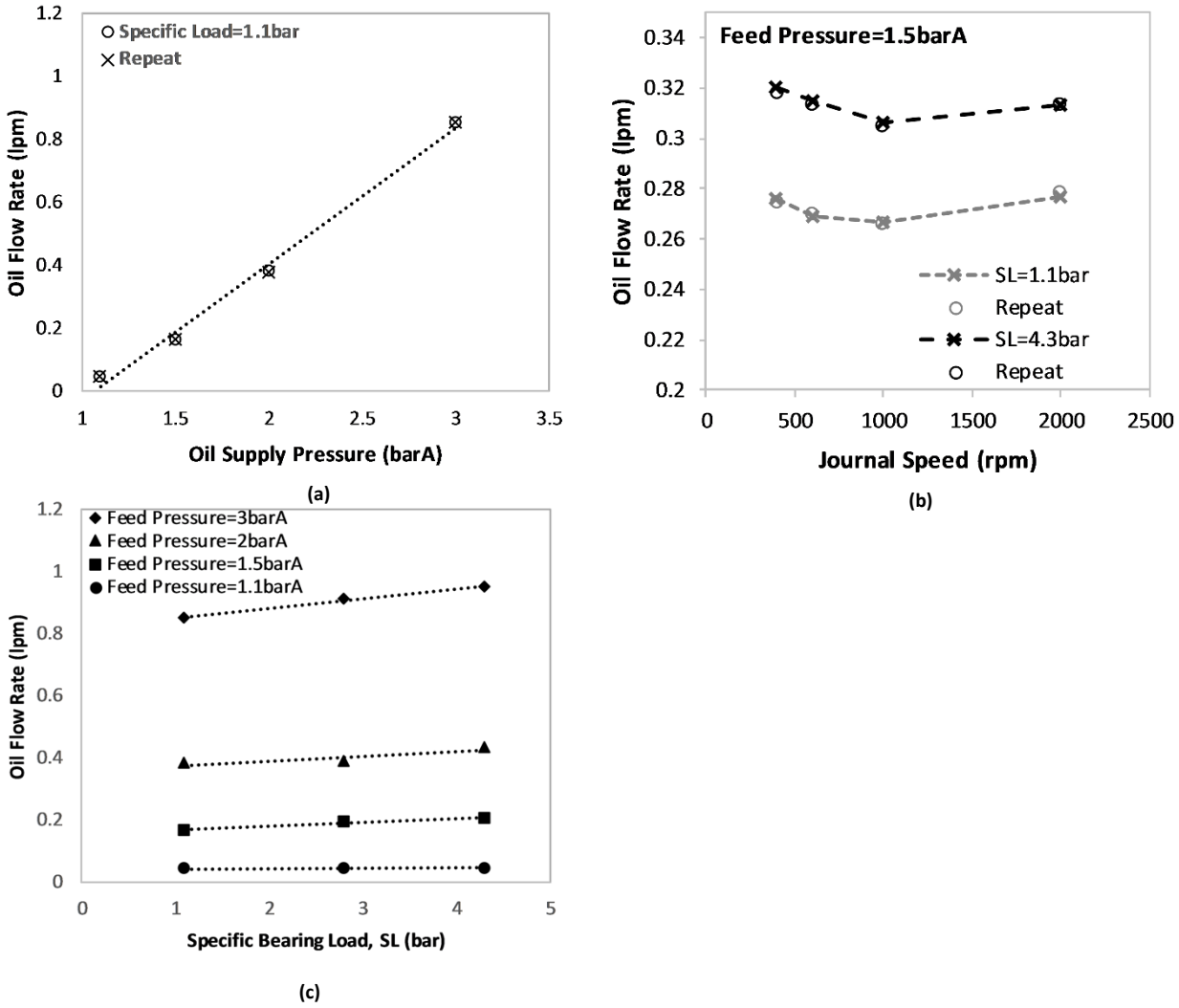


Figure 4.7: (a) Variation in flow rate with supply pressure at 1000rpm (b) Variation in flow rate with speed at feed temperature=27 °C (c) Variation in flow rate with bearing load at feed temperature=22 °C and 1000rpm. Bush radial clearance for all tests =73.2 µm

4.4 Stages of Hydrodynamic Film Failure and Recovery of Film

The Perspex bush was also utilized to observe the film and torque behaviour for an extreme condition when the oil supply was shut off altogether (from 3 barA supply pressure) to understand the failure mechanism. The changes in cavitation patterns are depicted in Figure 4.8. It was observed that the cavitation area increased within the first 4 seconds as the streamers on either side of the feed groove extended to the front side of the bearing. After this time the cavitation area increased quite drastically as the feed pipe was completely depleted of oil. The oil film pattern then inverted as the oil was drawn into the load carrying part of the film from the sides of

the bearing which became narrower as time progressed and the oil in the 'meniscus' was used up. The upper part of the bearing where the groove is situated was found to be completely devoid of oil, and such a scenario in dynamically loaded bearings can result in failure as the load direction continually changes. The film reformation point showed much more significant change compared with the rupture point as shown in Figure 4.9 and overall the film extent decreased significantly (Figure 4.10). The measured torque traces as shown in Figure 4.11 show that at light load, the reduced film extent sustained by oil from the menisci at the sides is able to support the applied bearing load for a period of time. As the load is increased, the reduced film extent is unable to support the load and the lubrication regime shifts from hydrodynamic to boundary condition. The reduction in torque is most significant during the first 5 to 6 seconds after oil pump shut off, as explained by the drastic increase in cavitation area. For higher loads, a minimum torque is achieved at this point after which torque starts to rise again due to boundary contact. At light load, oil is recirculated for longer whereas at high load, it escapes the bearing sooner hence the film breakdown occurs sooner and a critical film extent is reached sooner. The measured film extent at which contact occurred for a specific load of 4bar was ~115°.

Upon switching on the oil supply back to a pressure of 3 barA, it was observed that full recovery of the oil film and reduction of torque values (as lubrication regime changes back to hydrodynamic) occurred within 2 seconds.

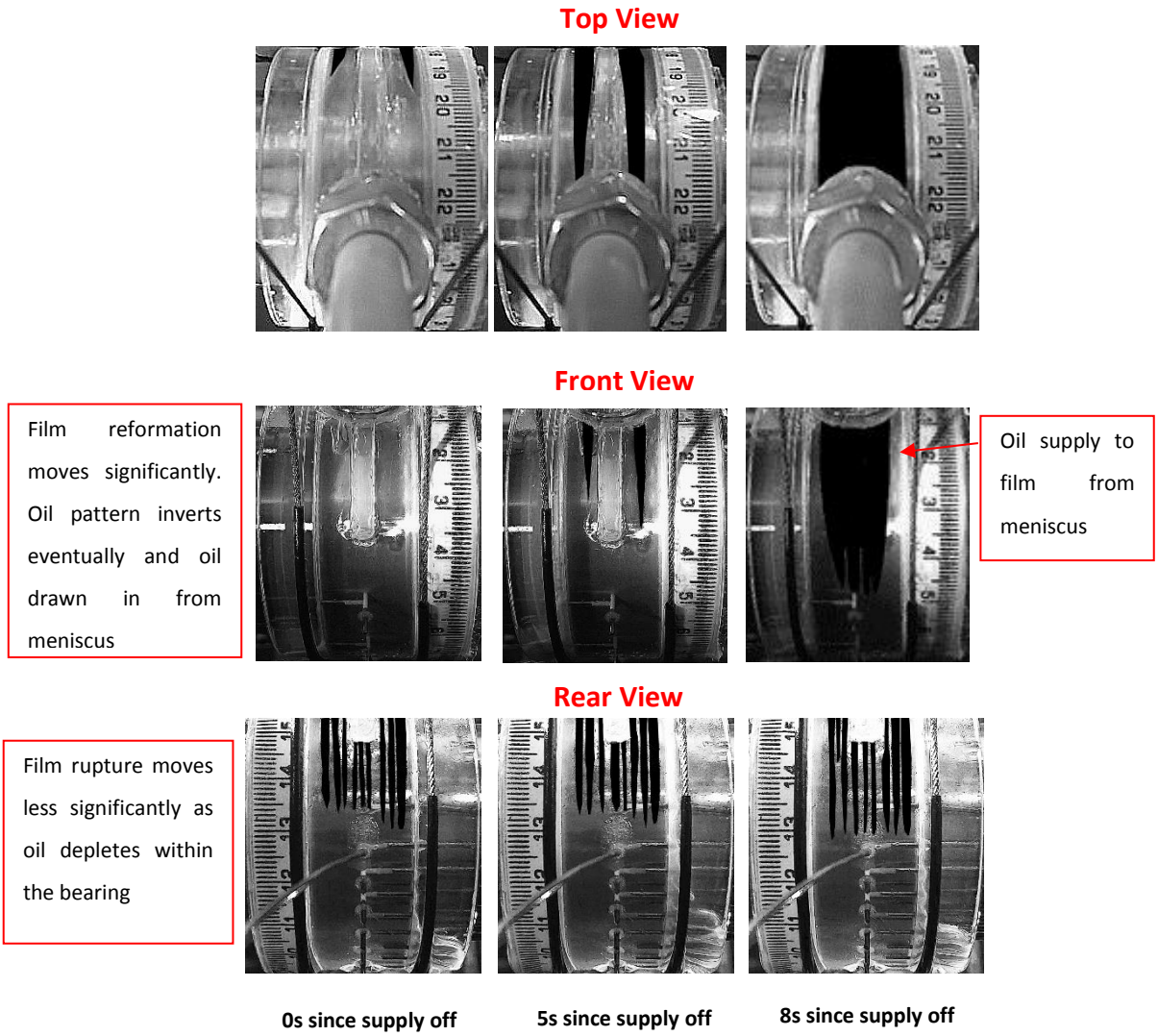


Figure 4.8: Stages of hydrodynamic failure

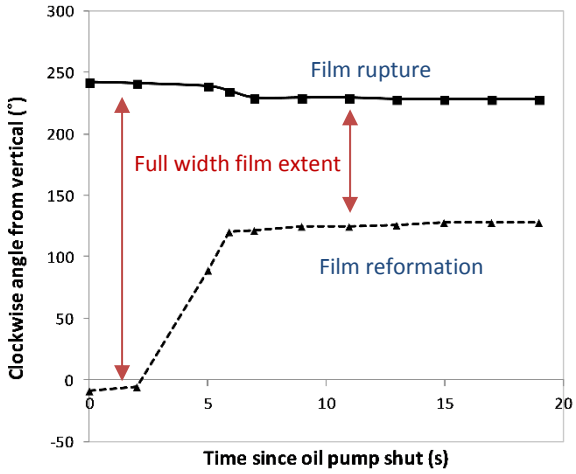


Figure 4.9: Variation in angle of film rupture and reformation as oil supply is switched off, SL=4.3bar

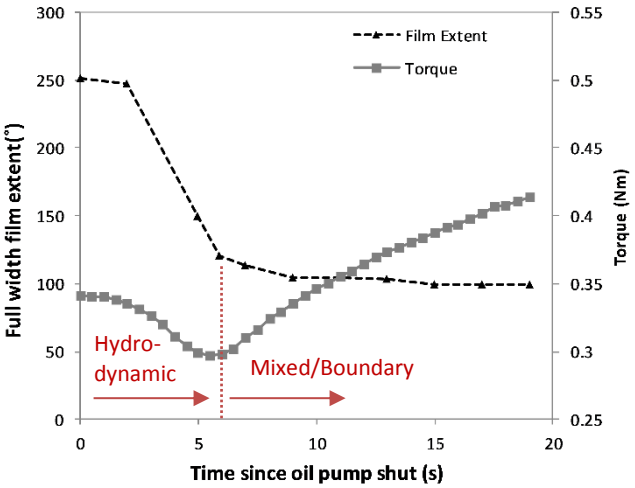


Figure 4.10: Variation in film extent and torque as oil supply is shut off, SL=4.3bar

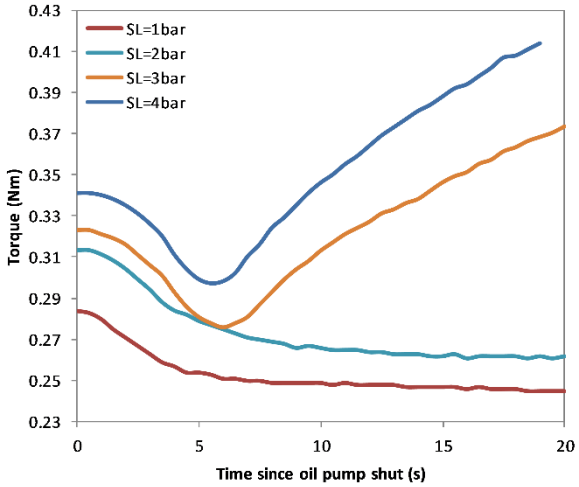


Figure 4.11: Variation in torque as oil pump is switched off for various load values

4.5 Discussion

The influences of supply pressure and operating parameters including load and speed on cavitation behaviour, film extents and flow rate have been reported in this chapter. It was found that cavitation increases with reduction in supply pressure due to less oil being available resulting in smaller full width film angular extents and reduced bearing oil flow. This observation is corroborated by literature [23, 58, 59, 62].

The existence of the cavitation streamers in the low pressure zone occurs as a result of the fluid pressure falling below a critical value depending on the nature of the cavitation process. This can be either dissolved gas coming out of solution, vapour created by phase transformation or compressed gas bubbles expanding into larger bubbles. The last of these can be ruled out because there is more uncertainty in choosing between the first two phenomena since both are pressure driven and require similarly low pressures to initiate. However, there are complementary studies in the literature suggesting degassing is the most likely mechanism.

In the light, steady load tests performed the cavities are expected to be gaseous in nature since they exhibited a stable behaviour. Also no cavitation erosion damage was observed. Swales [139] and Dowson and Taylor [56] demonstrated in their experimental work that under steady load conditions, the stability of the cavitation streamers and lack of pitting damage suggests that the contents of the cavities are gaseous in nature. Also gas saturation pressure, which is typically close to atmospheric [50], is achieved well before the vapour pressure of the lubricant [58]. For the current test oil the vapour saturation pressure is equal to ~2 Pa absolute at 37.8 °C [140]. Film pressure data, which will be later presented in Section 5.4.3, shows that the film pressure in the cavitation zone is slightly sub atmospheric. This validates the gaseous nature of the cavities. The development of these cavities may be aided by entrainment of surrounding air. As Heshmat notes [58], a weak bond exists between the oil streamers and the stationary bush surface compared with the rotating shaft surface which can permit side entrainment of air to the cavitated regions. Heshmat [58] noted an amorphous mixture of oil, foam and gas bubbles

close to the reformation angle of an axially grooved bearing under starved conditions. However, such a film behaviour was not seen in the current tests.

From Figure 4.5 it is observed that the full width film extent decreases as the speed increases and the film reformation boundary moves significantly forward. Okamoto et al. [23], Mokhtar et al. [59], Dowson et al. [62] and Costa et al. [18] have observed the same trends. Okamoto et al. [23] explained that the movement of the film reformation point with speed occurs as a result of the circumferential flow in the oil feed zone becoming dominant over the axial flow. Mokhtar et al. [59] related the reduction in film extent with speed to hydrodynamic action and entrainment and solution of air.

The total flow into a bearing from the feed groove consists of the oil entrained by shaft rotation over the groove region (groove Couette flow) and the flow which is due to the supply pressure. Pressurised flow in bearings with large groove angular extents greatly depends on the shaft eccentricity due to changes in clearance around the groove [34]. For a 180° circumferentially grooved bearing pressurised flow is found to increase with eccentricity ratio according to the feed pressure flow equation proposed by Martin and Lee [33], which was derived by curve-fitting to a large data base of feed pressure flow values obtained using a finite difference model:

$$Q_p = \frac{P_f {C_r}^3}{\mu}\left[\frac{1.25-0.25\left(\frac{a}{b}\right)}{6\left(\frac{b}{a}-1\right)^{0.333}}.f_1 + \frac{\frac{D}{L}}{6\left(1-\frac{a}{b}\right)}.f_2\right] \quad (4.2)$$

With:

$$f_1 = (1+\varepsilon\cos\theta_1)^3 + (1+\varepsilon\cos\theta_2)^3 \quad (4.3)$$

$$f_2 = \left[\theta_2 + 3\varepsilon\sin\theta_2 + \varepsilon^2\left(1.5\theta_2 + \frac{3}{4}\sin 2\theta_2\right) + \varepsilon^3\left(\sin\theta_2 - \frac{\sin^3\theta_2}{3}\right)\right] - \left[\theta_1 + 3\varepsilon\sin\theta_1 + \varepsilon^2\left(1.5\theta_1 + \frac{3}{4}\sin 2\theta_1\right) + \varepsilon^3\left(\sin\theta_1 - \frac{\sin^3\theta_1}{3}\right)\right] \quad (4.4)$$

In these equations a is the groove width, μ is the dynamic viscosity of the feed oil, P_f is the feed pressure. The terms f_1 and f_2 are flow rate functions dependent on the groove geometry. θ_1 and θ_2 are the angles with respect to the attitude angle of the

start and end of the feed groove. An example of the change in calculated pressure flow component for different feed pressures is presented in Figure 4.12. It is found that increases in feed pressure flow are more sensitive to eccentricity ratio at higher supply pressures, which is also confirmed by experimental flow rate measurements as the load is increased in Figure 4.7(c).

Feed pressure flow also provides a much more significant contribution to total flow in to a bearing compared with net groove Couette flow. As the supply pressure is dropped from 3 barA to 1.5 barA the total bearing flow reduces by ~80% at a constant speed of 1000rpm (Figure 4.7(a)).

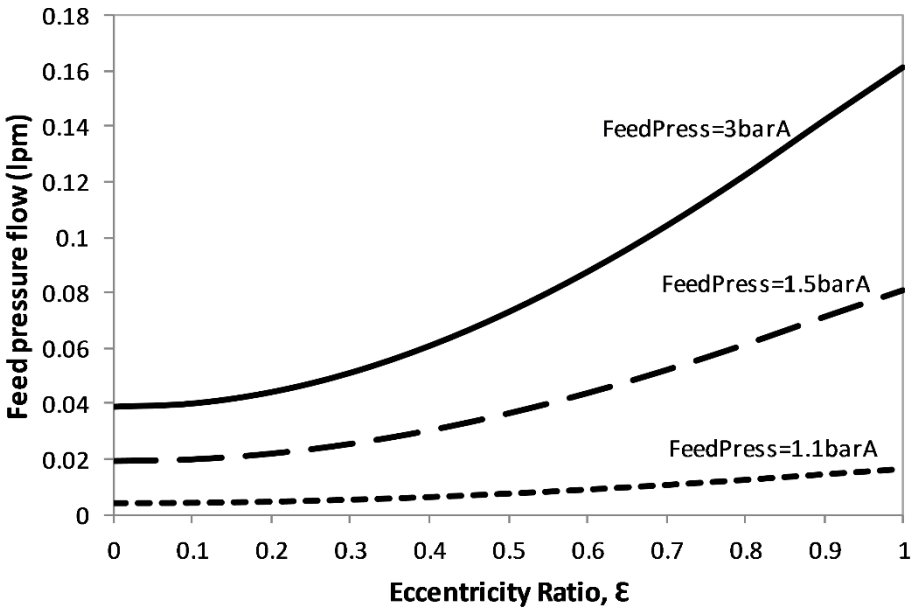


Figure 4.12: Variation in feed pressure flow with eccentricity ratio

To prevent lubricant starvation, according to [34], the sum of these two flow components should match the lubricant consumption of 'full hydrodynamic lubrication' of a 180° load carrying film. According to the 'short bearing' theory, this is given by:

$$Q_{required} = UC_r b\varepsilon \qquad (4.5)$$

This indicates that the hydrodynamic requirement of a bearing increases linearly with speed and eccentricity ratio.

As the journal velocity increases bearing eccentricity decreases due to increased hydrodynamic lift [18-20]. This reduction reduces the feed pressure flow while the increase in shaft speed increases groove Couette flow. At speeds below 1000rpm the former dominates and flow rate is reduced under the lightly loaded conditions as shown in Figure 4.7(b). The reduction in film extent with increasing speed is a consequence of the reduction in flow rate and the increase in the required flow to maintain a full hydrodynamic lubrication (Equation 4.5). The increase in flow rate at speeds above 1000rpm reflects an increase in groove Couette flow and the influence of higher frictional dissipation on film temperature, which is raised by several degrees Celsius, lowering oil viscosity.

With an increase in load, the full width film extent decreases as shown in Figure 4.5(c). Flow rate increases as a result of increased clearance near the groove region. This promotes feed pressure flow into the bearing and the increased axial pressure gradients in the loaded region promote side leakage, further causing an increase in oil flow from the groove. The shortening of film extent, especially at low supply pressure of 1.1barA, is possibly due to the fact the increase in feed pressure flow is insufficient to compensate for the increased requirement for full hydrodynamic lubrication at the higher eccentricity ratio. The increase in cavitation extent and area with increasing load is also attributable to the generation of more negative film pressures at higher eccentricities in the diverging part of the film.

Even under very low supply pressure conditions a relatively large angular film extent was maintained under light load conditions at moderate operating temperatures. Film extents measured are more than a 100° larger than those reported by Okamoto et al. [23] for a similarly dimensioned bearing (b=20 mm, d=53 mm, C_r=45 μm) but with a single feed hole 5 mm in diameter. A possible explanation for this is that a larger groove extent provides greater flow to the film, hence, a larger film extent would be maintained at similar supply pressures. Costa et al. [24] investigated the effect of axial groove width on bearing flow rate and film extent. Their results confirmed a considerably higher flow rate and film extent for the wider axial groove.

Comparing the cavitation patterns for a single hole design [23, 45] and the 180° circumferential design used in the current work (Figure 4.13) shows the streamer pattern for the single feed hole covered the full width of the bearing in the rupture zone. For a 180° circumferentially grooved bearing, the extent of the streamers in the low film pressure zone is reduced by the oil flow from the groove. Big end bearings are normally fed using a single feed hole unlike the crankshaft main bearings which are fed via a circumferential groove. The results indicate that the big end bearings will possibly experience smaller film extents and larger cavitation zones due to lesser flow from the groove compared with main bearings at a similar supply pressure.

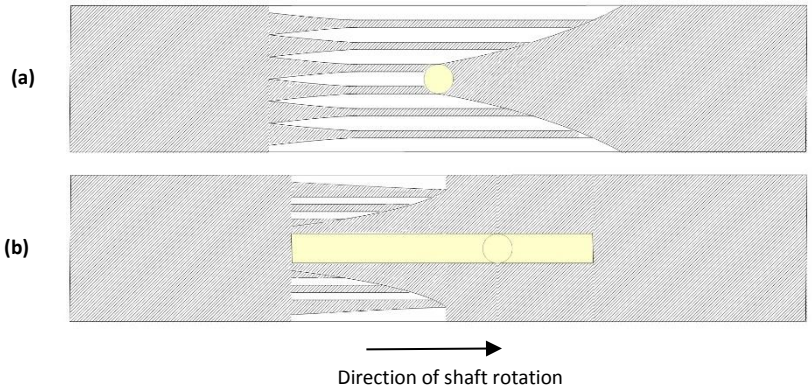


Figure 4.13: Film pattern comparison (a) Single feed hole [23, 45] (b) 180° feed groove (current design)

Bearing film failure was observed as oil supply was completely shut off to the bearing due to a collapse in the load carrying film. It was found that a load carrying film can be maintained for a few seconds by the oil recirculating within the bearing and from the side menisci. At light load, due to lower eccentricity, oil is recirculated within the bearing for longer therefore, it is able to sustain the hydrodynamic film for longer. Also the critical film extent required to maintain hydrodynamic operation for lighter load would be lower. At higher loads, bearing failure occurs quickly as the oil is quickly expelled from the bearing and also a larger critical film extent is required to maintain a higher load. Bearing failure occurs via surface to surface boundary contact in these cases.

In summarising the outcomes of this Chapter, the key figures are Fig. 4.5 and 4.6. If the oil feed pressure is reduced, the full width film extent reduces and cavitation area increases. Decreases in film extent lead to large friction reductions which are demonstrated in Chapter 5.

For a 180° circumferentially grooved bearing a large film extent (greater than 240°) exists even at very low oil pressures enabling safer operation compared with smaller feed groove arrangements e.g. single feed hole or axial grooves of short angular extent. The film extents reduce with increases in load and speed indicating that the minimum feed oil pressure requirement for safe operation will increase as these two parameters increase.

Total restriction of the oil supply to the bearing can result in rapid hydrodynamic failure (in less than 5 seconds) due to diminishing film extent and thickness and hence should be avoided.

4.6 Conclusions

- Reducing the pressure of the oil feed to a plain short bearing leads to increases in the cavitation area and shortening of the full width film extent.
- Cavitation is likely to be of gaseous nature under light, steady load conditions.
- A 180° circumferential groove helps maintain a large film extent at low supply pressures compared with grooves of smaller extent.
- Bearing flow rate is dominated by feed pressure flow and increases with load.
- Film rupture boundary is weakly influenced by oil feed pressure while the film reformation boundary is significantly influenced.
- Increases in load and speed lead to a reduction in full width film extent.
- Hydrodynamic film recovery from a starved film condition can be achieved in less than 2 seconds by increasing oil supply pressure.

Chapter 5- Influence of Cavitation on Bearing Friction

5.1 Introduction

In this chapter, an experimental and computational study aimed at examining the linkage of cavitation to friction torque is presented. The relationship between percentage torque reduction and percentage cavitation area as oil feed pressure is reduced was experimentally determined for a range loads up to SL=4.3 bar at a journal speed of 1000 rpm. A computational Finite Difference Method (FDM) model for a 180° circumferentially grooved bearing was used to provide an explanation for the experimental results and the mechanisms resulting in friction reduction with feed pressure reduction were identified.

5.2 Cavitation Area and Friction Changes

The %torque reduction was effectively independent of viscosity over the small variation of film temperature which occurred during tests. This is illustrated in Figure 5.1. Oil viscosity was calculated from measured film temperature using the Vogel equation where for Havoline Energy 5W-30, k_v is 5.17e-05 Pa s, c_1 is 1142 °C, and c_2 is 130 °C. The coefficient values were determined from experimental oil viscosity data points. The corresponding cavitation area determined from the video records was similarly stable and unchanging throughout a test.

Results relating feed pressure, cavitation area and friction torque reduction are presented in Figure 5.2 for the Perspex bush with radial clearance, C_r=73.2 µm. Reducing feed pressure gives rise to increasingly large changes in cavitation area as shown in Figures 5.2(a). The increases in cavitation area become steeper below 2barA supply pressure. The changes are similar over the range of loads used, but offset to higher levels by increasing load. The corresponding reductions in friction torque with reducing feed pressure are plotted in Figure 5.2(b), showing the largest percentage reductions were recorded at the lightest loads. Also, torque reductions became steeper below 2 barA feed pressure similar to the trend for cavitation area. Up to nearly 20 percent reduction in torque is observed as the feed pressure was reduced from the baseline to 1.1 barA. The relationship between the %torque reduction from

baseline and the calculated %cavitation area is shown in Figure 5.2(c). From this, it is apparent that as feed pressure is reduced, the reduction in friction torque is larger than the increase in cavitation area and one or more other factors are at play. This is most evident at the lightest loads where changes in cavitation area are relatively small. As load increases, the changes in cavitation area and %torque reduction become more equal and the ratio approach unity at the highest load and lowest feed pressure. The same trends are seen in the data recorded using the second bush, with the smaller radial clearance of 62.7 µm compared to 73.2 µm for the first bush. The results for % torque reduction and %cavitation area, shown in Figure 5.3, are very similar and indicate that clearance is not a strong influence on the effect of feed pressure.

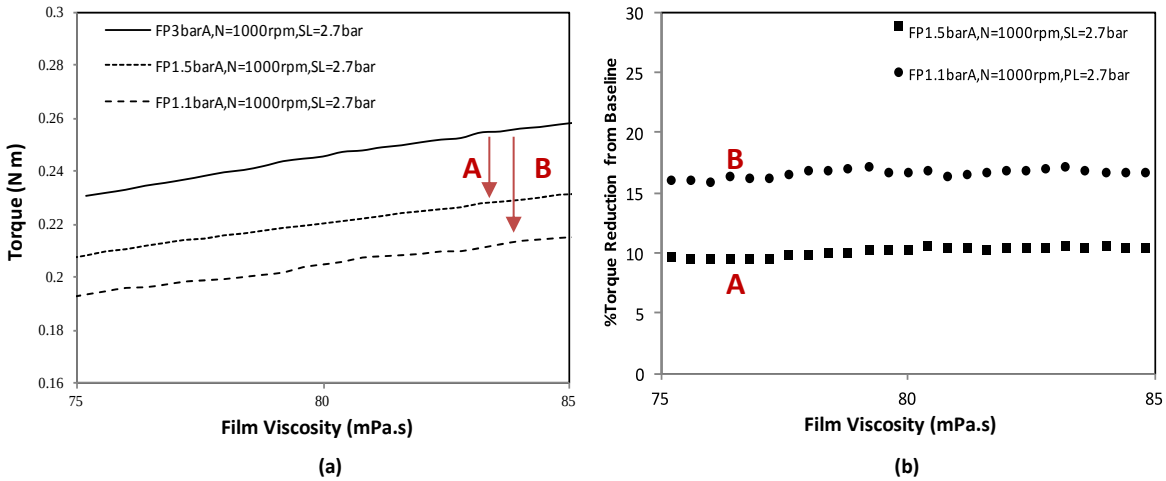
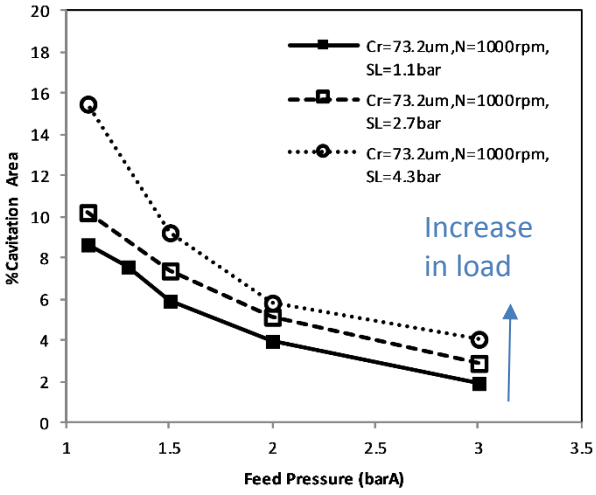
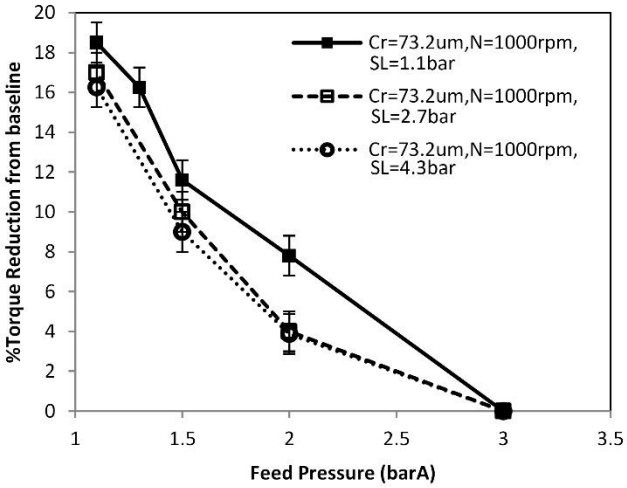


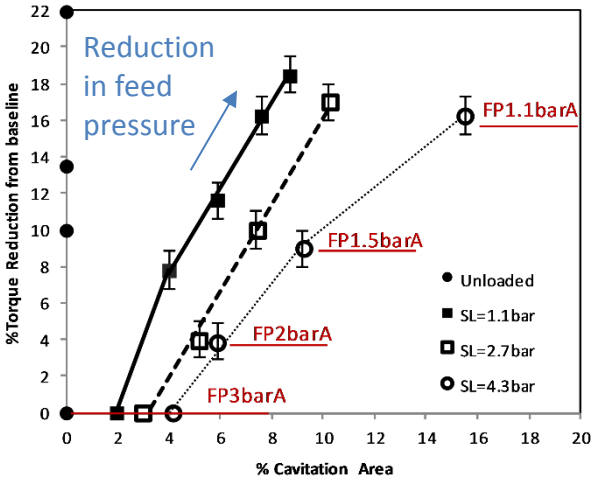
Figure 5.1: Example of (a) measured torque and (b) percentage torque reduction against film viscosity when feed pressure is dropped from 3barA to 1.1barA at SL=2.7bar, N=1000rpm and C_r=73.2 µm



(a)



(b)



(c)

Figure 5.2: Perspex bush with clearance C_r of 73.2 µm. Variation in (a) cavitation area with decrease in feed pressure for increasing load values (b) %torque reduction from baseline with decrease in feed pressure for increasing load values. (c) relation between %torque reduction and %cavitation area for increasing load values

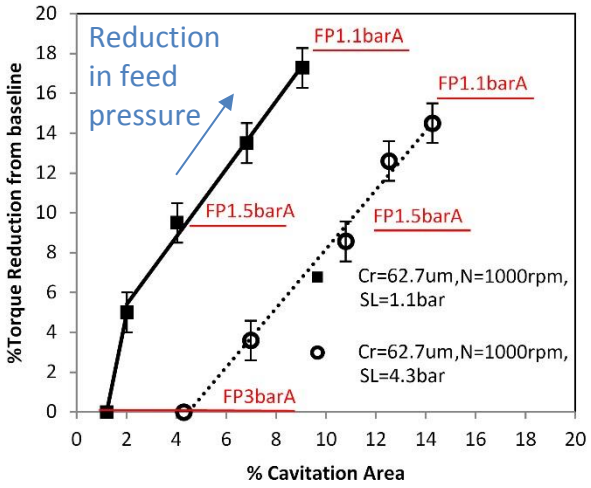


Figure 5.3: Perspex bush with clearance C_r of 62.7 µm. Relation between %torque reduction and %cavitation area for increasing load values

5.3 Cavitation Friction Assessment

In this section, a simple model is considered to determine the significance of cavitation on the friction encountered in the bearing thin film. The velocity profile in the bearing lubricant film assuming pure Couette flow is shown Figure 5.4. The shear stress τ (Pa) acting between layers of viscous fluid in laminar flow is dependent upon the inverse slope of velocity profile as given below

$$\tau = \mu \frac{\partial u}{\partial y} \tag{5.1}$$

$$\tau = \frac{F}{A} \tag{5.2}$$

where μ is the lubricant dynamic viscosity (Pa.s), u is bearing velocity (m/s), y is the local film thickness (m), F is the friction force (N) and A is the area of the rubbing surfaces in contact (m^2).

As described in Section 2.2.5, for a steadily loaded bearing, cavitation streams consist of degassed air from the oil as well as ambient air in a gas cavity within a proportion of clearance space between shaft and bush. The presence of cavitation significantly effects bearing friction as the viscosity of air is much lower than the viscosity of oil at any temperature within the working range of 0 ˚C to 90 ˚C. Table 5.1 lists the viscosity of lubricant oil and air at various temperatures.

Assuming a linear shear rate, the friction resulting from shear within a concentric bearing clearance can be defined by the Petrov friction equation:

$$F = (2\pi Rb)(\mu)(\frac{U}{C_r}) \quad (5.3)$$

$$\tau = (F)(R) \quad (5.4)$$

$$\tau = (2\pi Rb)(\mu)(\frac{U}{C_r})(R) \quad (5.5)$$

Where R is the bearing radius (m), b is the bearing width (m), C_r is the mean radial clearance (m) and τ is friction torque (N m).

Calculations of friction torque were carried out at various temperatures for both oil and air using equation 5.5. The ratio of friction torque resulting from oil as a lubricant versus air is presented in Figure 5.5 for various fluid temperatures. At 20 ˚C the friction torque due to shearing of oil is 3 orders of magnitude higher as compared to air. At 90 ˚C the difference in torque decreases to 2 orders of magnitude as there is a significant drop in oil viscosity. However, still the friction due to shearing of air is negligible compared to that of oil over the entire working temperature range. Therefore, in real bearing operation, the contribution from cavitation areas towards total bearing friction can be neglected.

The main conclusion drawn from this analysis is that bearing friction is significantly affected by the presence of gas cavities in the lubricant film and that an increase in cavitation due to a reduction in full film area will result in a drop in friction torque.

Table 5.1: Dynamic viscosity of air and oil at various temperatures

Temperature (˚C)	Dynamic Viscosity Air (mPa.s)	Dynamic Viscosity Oil (mPa.s)
0	0.0174	331
20	0.0184	103
40	0.0193	42
60	0.0203	21
90	0.0217	9

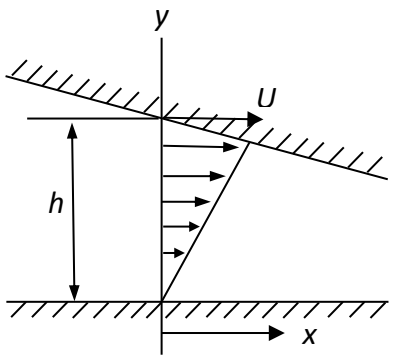


Figure 5.4: Velocity profile in oil film assuming pure Couette flow (linear shear rate)

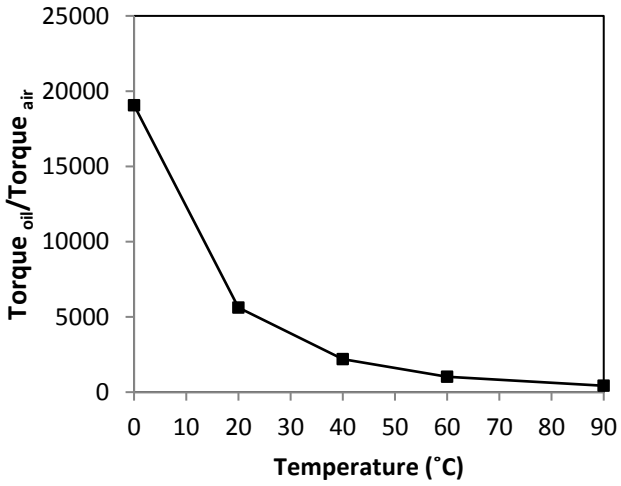


Figure 5.5: Comparison of concentric bearing friction torque due to shearing of oil and air

5.4 Mechanism of Friction Reduction with Reducing Feed Pressure at Light Loads

The mechanisms involved in the reduction of friction torque with oil pressure reduction have been further explored using a computational Finite Difference Method (FDM) model formulated using the numerical procedure presented in [34] but modified to account for a 180° circumferential groove. A summary is presented in the next section. The model was used to compute the eccentricity ratio, film thickness and pressure distribution for values of applied load and feed pressure. The corresponding cavitation area was determined from the experimental film patterns, illustrated by the examples presented in Figure 4.1, and used to define cavitation

areas in the model mesh to calculate overall friction. An example of the digitised film patterns is shown in Figure 5.6.

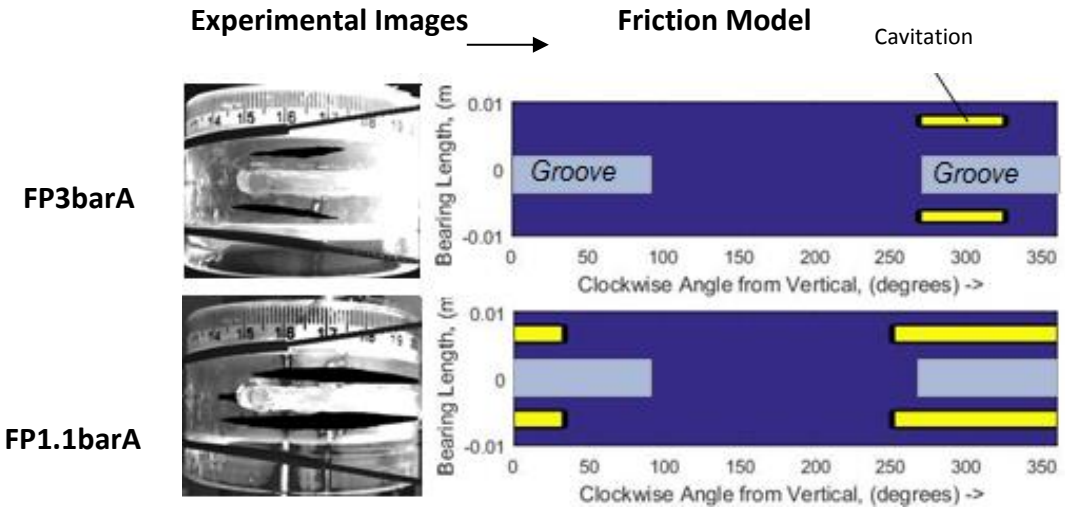


Figure 5.6: Approximated cavitation areas in the friction model considering the effect of eccentricity ratios

The cavitation area was assumed not to contribute any friction as proven in the previous section, and the contribution of the full film areas was determined from equation 5.9.

5.4.1 A Numerical Model for the Analysis of Feed Conditions on a 180° Circumferentially Grooved Bearing

In this model the laminar, iso-viscous Reynolds equation (equation 2.1) is non-dimensionlized to give:

$$\frac{\partial}{\partial x^*}\left(h^{*3}\frac{\partial p^*}{\partial x^*}\right)+\left(\frac{R}{b}\right)^2\frac{\partial}{\partial y^*}\left(h^{*3}\frac{\partial p^*}{\partial y^*}\right)=\frac{\partial h^*}{\partial x^*} \qquad (5.6)$$

where $h^*=\frac{h}{C_r}$, $x^*=\frac{x}{R}$, $y^*=\frac{y}{b}$, and $p^*=\frac{pC_r{}^2}{6U\mu R}$

The Vogelpohl parameter 'M_v' is introduced into the non-dimensional form of Reynolds equation to improve accuracy of the solution.

$$M_v=p^*h^{*1.5} \qquad (5.7)$$

In the numerical analysis of grooved journal bearings, it is important to consider cavitation and reformation of the film in the model. The cavitation front is determined by applying the Reynolds condition that assumes a zero-pressure gradient at the start of the cavitation zone i.e. $\frac{\partial \mathrm{p}}{\partial \mathrm{x}} = 0$ and $p = p_{cav}$.

The reformation front is determined by applying the Jakobsson-Floberg-Olsson model which takes into account mass conservation of lubricant flow from the cavitated and fully reformed oil film. The following mass conservation equation applies at the reformation front as presented in [34] based on the model developed by Jakobsson, Floberg and Olsson [72, 73]:

$$h_c{}^* = h_r{}^* - h_r{}^{*3}\left[\frac{\partial p^*}{\partial x^*} + \left(\frac{R}{b}\right)^2 tan\,\Phi\frac{\partial p^*}{\partial y^*}\right] \qquad (5.8)$$

Where $\mathrm{h_c}^*$ is the film thickness directly upstream of the cavitation front, $\mathrm{h_r}^*$ is the film thickness at the reformation front, and Φ is the angle of the reformation front.

5.4.2 Solution Procedure

A finite difference scheme (FDM) is used to determine the film pressure distribution of a finite width 180˚ grooved bearing under steady load conditions. The solution domain consists of a mesh with 101 by 101 nodes. A zero-gauge pressure boundary condition is applied at the edges of the bearing. The discretised non-dimensional Reynolds equation is solved for every node using the Gauss-Seidel iterative method.

The groove geometry is defined in the mesh by maintaining a constant dimensionless pressure of the groove, equivalent to supply pressure, over the nodes enclosed by the groove. In MATLAB, a variable named SWITCH(i,j) is created having values of 1 or 0. The nodes enclosed by the groove are specified a value of 1 to allow the program distinguish and exclude these nodes from each iteration. The calculation is continued till the change in M_v between two iterations is less than 10^{-6}. At this point a converged steady-state solution is reached.

The computer program is written in MATLAB and is based on the code provided in [34].

5.4.3 Analysis of Friction Reduction Mechanisms with Feed Pressure

The film frictional force for a finite width bearing is calculated by integrating the shear stress 'τ' over the bearing area

$$F = \int_0^b \int_0^{2\pi R} \tau dx dy \quad (5.9)$$

Where the shear stress according to the hydrodynamic Reynolds equation for a finite width bearing is given by

$$\tau = \frac{\mu U}{h} + \frac{h}{2}\frac{dp}{dx} \quad (5.10)$$

According to the above equation, at given oil film viscosity and shaft speed, bearing friction is affected by three components, namely, the film area (in the converging and diverging zones), the film shear rate and the circumferential pressure gradient.

The circumferential variation of film shear rate depends on the variation of film thickness, which in turn depends on the bearing eccentricity ratio. A high eccentricity ratio leads to a higher shear rate in the converging part of the film and higher film friction in the converging zone. The circumferential pressure gradient also depends on journal position and load.

Agreement between model predictions and measurements of rupture and reformation angles, the extent of full-width film, and the centreline pressure variations is generally good, as illustrated by the pressure variations shown in Figure 5.7(a).

In the 180˚ circumferential groove in the upper part of the bearing, the fluid pressure exerts a force on the bush which adds to externally applied load. The force exerted by groove pressure on the test bush was predicted using the FDM model and results are presented in Figure 5.7(b) for a range of feed pressures. At a specific bush load, SL=1.1 bar the applied bush load due to the dead weights equals 120 N which is nearly equal to the hydrostatic load due a feed pressure of 3 barA. Therefore, at light external loads, a feed pressure of 3barA may almost doubles the load on the bush and the bearing eccentricity ratio should increase. The variation of eccentricity ratio with feed pressure and increasing bearing loads, calculated using the model for a

bearing with nominal radial clearance, C_r=73.2 µm, is presented in Figure 5.7(c). With an increase in eccentricity ratio, the shear rate of the converging part of the film will increase, therefore, resulting in a higher friction torque. At light loads (Ɛ<0.35), the change in eccentricity ratio is most significant. The change becomes less as the load increases because the groove hydrostatic pressure becomes a smaller fraction of the hydrodynamic film pressure.

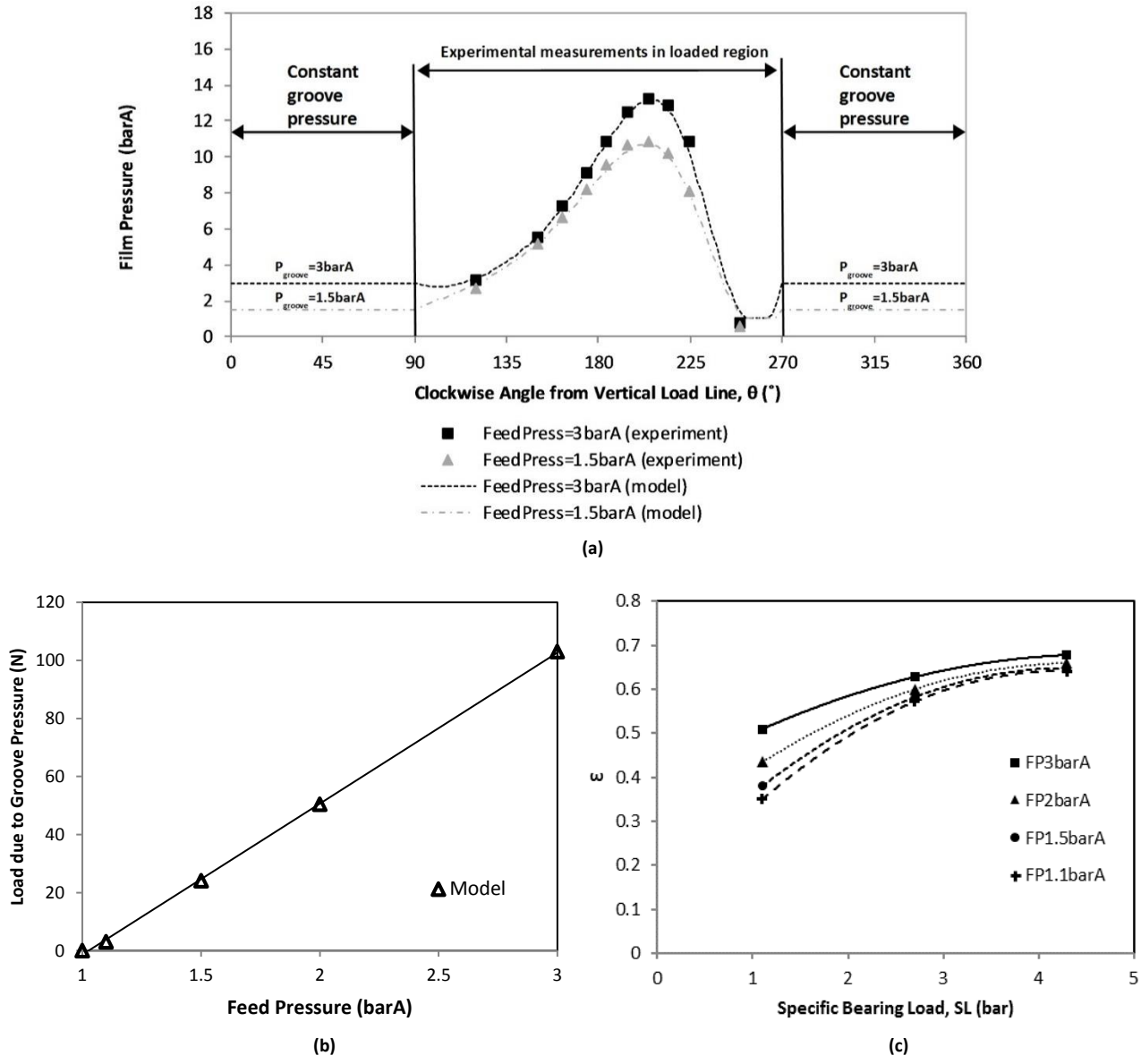


Figure 5.7: (a) Experimental and calculated centreline pressure profiles at steady specific load of 3.5 bar and feed pressures of 3barA and 1.5barA, (b) Load due to hydrostatic groove at given feed pressures (c) calculated variation in eccentricity ratio, Ɛ, with load and feed pressure

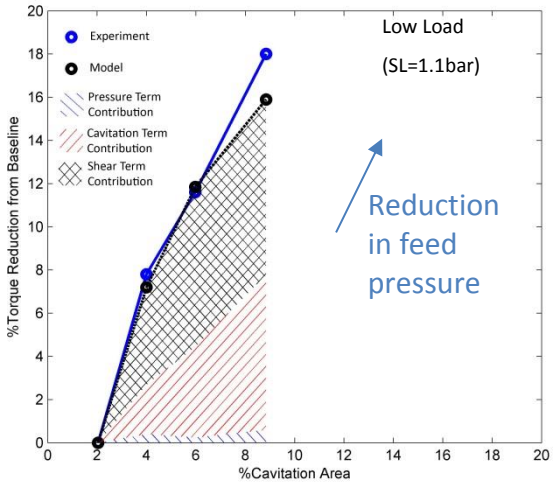
For the range of loads tested it was observed that full film extent was always greater than 180˚ at any given feed pressure. The large film extents may be explained by the presence of the large feed groove in the bearing. There are two changes occurring when the supply pressure is reduced. Firstly, the hydrostatic load due to supply pressure is reduced, which lowers the eccentricity. Secondly, the angular extent of the load bearing film is reduced. A combination of these factors determines the final bearing eccentricity value. At low feed pressure, increasing load will eventually give rise to the extent of the load bearing part of the film becoming less than 180°. After that point the eccentricity ratio may start increasing with drop in feed pressure and the load capacity may also decrease.

5.4.4 Variation in %Torque Reduction Against %Cavitation Area with Drop in Feed Pressure, Comparison between Experiment and Friction Model

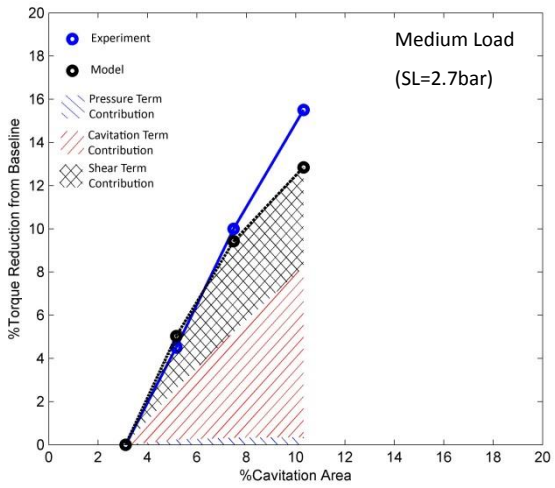
The predicted contributions to friction reduction of film area, film shear rate and the circumferential pressure gradient at a film temperature of 27 °C are plotted along with the experimental values in Figure 5.8 for the low, medium and high loads tested. At very light loads, a bigger change in shear rate (with feed pressure) provides a more significant contribution towards overall %torque reduction as compared with cavitation area. The difference in eccentricity ratio due to feed pressure reduces as the load increases and, consequently, the influence of change in shear rate on %torque reduction decreases with load. As the load increases, the cavitation area increases and coupled with the diminishing contribution from the shear term, the overall contribution from cavitation towards total torque reduction increases. Contribution from change in the film pressure gradient term with feed pressure towards torque reduction is found to be trivial (<1 %). Overall the % torque reduction with supply pressure decreases with increasing load and is corroborated by further studies carried out at higher loads with the bronze bush in Chapter 6.

At light load, around half of the %torque reduction can be associated with the area reduction in the film. At the higher loads, changes in the pressure distribution as the feed pressure is reduced indicate the area reduction associated with cavitation may account for most of the friction torque reduction. The presence of cavitation reduces

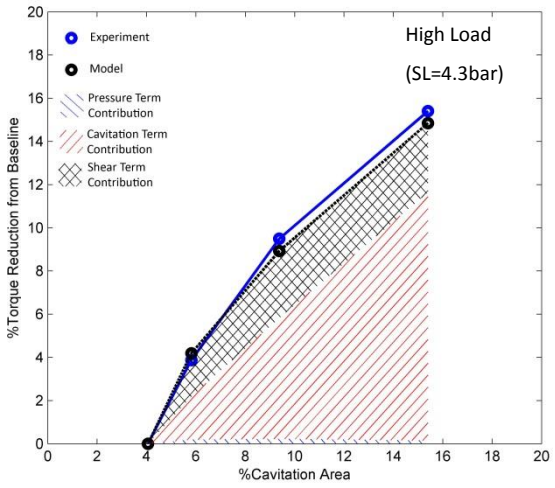
the film area and significantly effects bearing friction since the viscosity of degassed air is 2 to 3 orders of magnitude lower than the viscosity of oil. Therefore, friction contribution from cavitation areas can be neglected.



(a)



(b)



(c)

Figure 5.8: Relative contributions from the shear, cavitation and pressure gradient terms towards total %torque reduction from baseline. Results presented for (a) low, (b) medium and (c) high load.

5.5 Discussion

The reduction in bearing friction resulting from reduction in oil feed pressure have been shown to be closely associated with increased cavitation area. Visualisation of the oil film using transparent bearings shows that the increase in cavitation area is associated with an increase in film reformation angle; the effect on film rupture angle is relatively weak.

According, to the Petrov's equation for a concentric journal bearing, friction would be directly proportional to film area only. However, it is found that changes in bearing eccentricity also provide a change in friction.

For a 180° circumferentially grooved journal bearing, the reduction in friction is produced by the reduction in the film area over which the shear stress acts at the journal surface, and a reduction in eccentricity which reduces the circumferential average shear stress. At light loads these effects are similarly important; as the load is increased, the reduction in film area is more important. The contribution of the 'pressure term' is negligible. Increases in film temperatures due to lower feed pressures lowers oil viscosity and results in a friction reduction. However, in the results presented, film temperature was maintained virtually constant and analysing torque data against film viscosity eliminated any influence of temperature.

In literature, both increases and decreases in eccentricity ratio have been reported with a reduction in supply pressure depending on the groove design and location. Reductions in supply pressure for single or twin axial groove bearings at 90° to the load line have been reported to increase eccentricity and maximum film pressure and decrease the minimum film thickness [19-21]. These trends were observed over a load range of SL=2.5 bar to 12.5 bar as the supply pressure was reduced from 3.1 barA to 1.7 barA in [20]. This reduction in film thickness has been attributed to reduced hydrostatic lift provided by the groove pressure and reduced extent of positive pressure zones.

In other studies by Costa et al. [18, 24] on a single axial bearing at 0° to the load line, a decrease in maximum film pressure and eccentricity ratio has been reported with a

decrease in supply pressure. This has been shown to occur even under high load conditions of SL=12.5 bar as the supply pressure was reduced from 3.8 barA to 1.7 barA in [24]. Decreases in film peak pressure with supply pressure reduction have also been reported by Ahmad et al. [141].

For the current grooving arrangement, the groove covers a wide angular extent and therefore exerts a relatively significant load on the bush at light loads. A change in eccentricity is brought about by two factors with a reduction in feed pressure. Firstly, the hydrostatic load contribution from the groove reduces. Secondly, the angular extent of the film is reduced which would theoretically result in increased eccentricity if the full film extent drops and cavitation extends in to the load bearing region of the film. Results indicate that a reduction in hydrostatic groove pressure force due to reduction in feed pressure provides a greater contribution towards increasing the minimum film thickness compared with a decrease in film extent due to reduced flow rate reducing the minimum film thickness. This is especially true since the measured film extents are relatively large (>240 °) even at low oil feed pressures. In other words, the shear rate within the high-pressure zone reduces with reduction in supply pressure. The measured pressure profiles show a drop in peak film pressures also lending support to this.

The calculated changes in eccentricity ratio are larger at light loads compared with higher loads. These trends also agree well with the trends in published literature where changes in film thickness with supply pressure are more prominent for lightly loaded conditions [66, 70]. At light loads the hydrostatic effect from the groove is of significance compared with the hydrodynamic effect generated hence the changes in minimum film thickness are more significant at the light loads. The reduction in eccentricity at light loads explains the extra measured torque reduction not accounted for by cavitation area at a given film viscosity. The contribution from the change in shear term towards torque reduction is more significant at light loads.

Cavitation area increases with load and the increase is attributable to the generation of more negative film pressures at higher eccentricities in the diverging part of the film as well as increased hydrodynamic requirement. No cavitation occurred for the

unloaded bearing case as the pressures generated in the diverging part of the film are not strong enough to result in cavitation. Up to 16 percent cavitation area has been observed with drop in supply pressure from feed pressure 3 barA to 1.1 barA with torque reductions of up to 20 percent. At light load, around half of the %torque reduction can be associated with the area reduction in the film. At higher loads, cavitation accounts for most of the torque reduction.

5.6 Conclusions

- Friction torque in journal bearings can be significantly reduced by reducing the oil supply pressure. Up to 20% reduction in friction torque has been measured by reducing the feed pressure from 3 barA to 1.1 barA.
- Reducing feed pressure reduces film area and eccentricity ratio for a 180° grooved bearing.
- Friction due to shearing of gas cavities is negligible compared with oil, hence, increases in cavitation area lead to a reduction in friction.
- A reduction in eccentricity reduces the surface shear stress in the load-bearing region of the film and overall, the circumferential average.
- With increase in load, film area reduction accounts for an increasing proportion of torque reduction.

Chapter 6- Effects of Load, Speed, Oil Formulation and Clearance on Friction and Pressure Distributions

6.1 Introduction

Bearing performance depends significantly on operating and supply conditions including supply pressure, temperature, shaft speed and applied load. Most of the performance studies reported in the literature have aimed at bearings with the axial groove inlet design. Vijayaraghavan et al. [66] carried out numerical simulations for an axially grooved bearing and found that the reduction in friction torque with supply pressure reduced with increasing load. This trend has also been reported in experimental studies on axial groove bearings [18, 20, 21]. Other reported effects of increase in load include increases in power loss, flow rate and operating temperatures. Increases in speed generally lead to lower eccentricity ratios, higher friction torques and higher film temperatures [18]. Tighter bearing clearances have shown to increase friction and film temperature [19, 30]. In this chapter, results of parametric studies on bearing friction and performance parameters including film pressure and temperature with changes in supply oil pressure are presented and discussed. The parameters investigated are load, speed, lubricant formulation and clearance.

The results presented in Chapter 5 show that at light loads, when oil feed pressure is reduced, reduction in friction is associated with an increase in cavitation area which reduces the contact area of the film and changes in the pressure distribution which for a given external load reduce eccentricity and the average shear stress at the journal surface. The main aim of the model presented in Chapter 5 was to make a prediction of bearing eccentricity once a given load and feed pressure value was specified and thus extrapolate from a limited amount of experimental data to clarify trends of friction reduction involved. The model is not a fully predictive model and relies on inputs of cavitation area and where the area is relative to the load to determine values of torque reduction with oil supply pressure reduction. In order to quantify friction reduction with oil feed pressure reduction at higher loads, there was a need to perform experimental tests which has been addressed in this chapter.

To examine the higher loads considered here, bronze bushes have been used instead of Perspex ones. Although visualization of the cavitation pattern is sacrificed, the higher loads are more typical of engine main bearing loads under urban driving condition. These tests have been performed on the stock 5W-30 oil at relatively cold operating conditions of around 20 °C.

Experiments have also been conducted to understand the effects of oil formulation on bearing friction torque and the resulting film pressure distribution under warm and fully warm conditions. The tests covered five base oils of different viscosities. Viscosity modifying polymers were added to change the viscosity of the base oils and the variation of viscosity with temperature. Tests were performed at warm (40 °C) and fully warm (90 °C) oil temperatures for light and heavy loads of 100 N (SL=1 bar) and 500 N (SL=5 bar) and for two oil supply pressures of 4 barG (high) and 2 barG (low). The aim of these tests was to acquire experimental friction data and study the influence of varying oil viscometrics and operating conditions for a grooved main bearing.

6.2 Estimation of Load Capacity from Film Pressure Measurement

In order to assess the validity of the experimental film pressure readings an estimate of the load supported by the film is required. This is outlined before presenting the experimental results. The methodology used to determine the bearing load from experimental film pressure data at the bearing centreline is explained in this section and applied later in analysing the data recorded using the bronze bush.

The hydrodynamic pressure generated in the film of a journal bearing supports the load applied by the shaft, maintaining the system in equilibrium. The maximum load that the bearing film is able to sustain without boundary contact for a given geometry is known as the load capacity. The load supported by the film can be obtained by integrating the film pressure around the circumference of the bearing. From the short bearing theory, the load of a 'short' bearing which has a b/D ratio of less than 1 can be calculated by the following equation [34]:

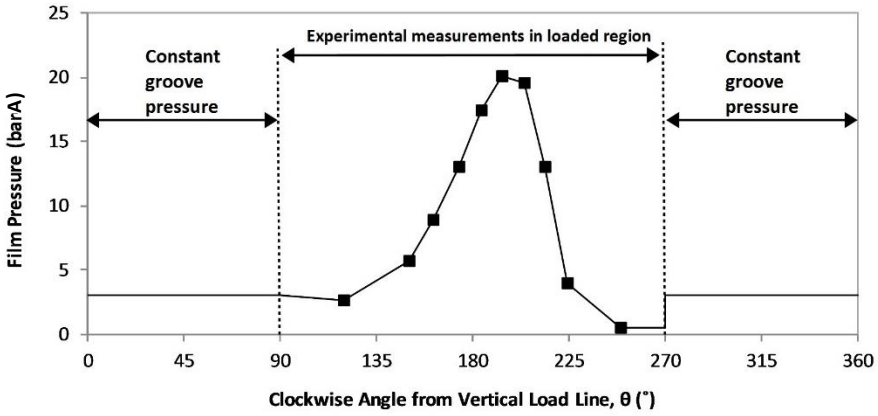
$$W = \frac{U\mu\varepsilon b^3}{{C_r}^2(1-\varepsilon^2)^2}\frac{\pi}{4}\sqrt{\left(\frac{16}{\pi^2}-1\right)\varepsilon^2+1} \qquad (6.1)$$

The bearing load can also be estimated by integrating the experimentally obtained centreline film pressure, P_{CL}, values over the complete bearing surface area. Film pressure measurements were made in the high-pressure zone of the film (lower shell). Film pressure in the axial 'y' coordinate direction is given by the short bearing theory [34] as:

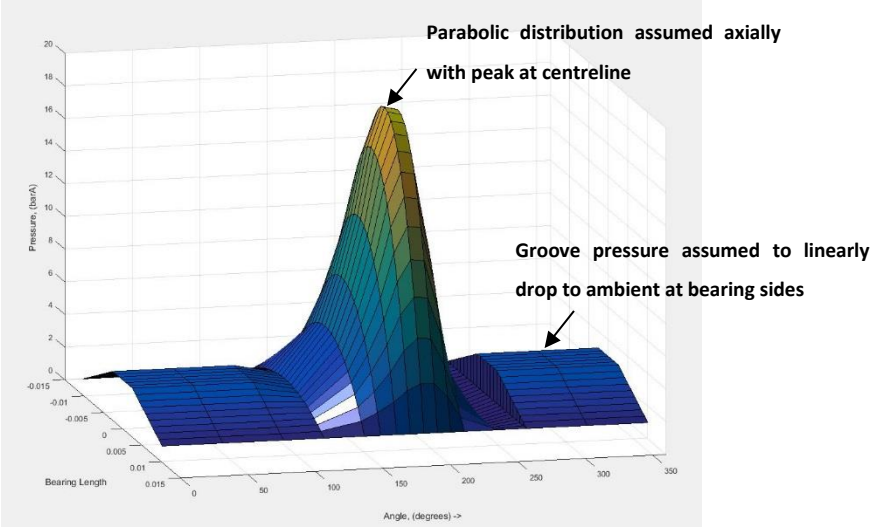
$$P = P_{CL}\left[1 - \left(\frac{2y}{b}\right)^2\right] \tag{6.2}$$

Where $y = \frac{b}{2}$ at the free edges of the bush. All pressures are gauge pressures in this equation.

Using the experimental data for P_{CL}, equation 6.2 to define the axial pressure and assuming in the upper half of the film the pressure reduces linearly from the supply pressure within the feed groove to ambient at the edges of the bearing, a three-dimensional pressure profile can be constructed and then be integrated to give the load of the bearing. An example of the 3D pressure profile is shown in Figure 6.1. The calculated load capacity is in good agreement with the value of applied load as will be shown in the data presented.



(a)



(b)

Figure 6.1: Conversion of (a) 2D centreline pressure profile to (b) 3D pressure distribution for estimation of load capacity.

6.3 Effect of Steady Load on Bearing Friction and Performance Characteristics and Changes with Feed Pressure

Whilst the results for light loads shown in Chapter 5 covered specific loads up to SL=4.3 bar, this has been extended to SL=13.8 bar using a bronze bush. The experimental test matrix is presented in Table 6.1. The effects of changes in feed pressure on torque reduction, hydrodynamic pressure distribution and film temperature were investigated.

The feed temperature was kept at 20 ˚C and over the test period of 900s the film temperature generally increased from 20 °C to close to 30 °C due to frictional

dissipation. Data was processed at a film temperature of 30 °C. For each feed pressure, a separate test was carried out and friction torque results were plotted against film viscosity measurements to eliminate any friction reduction contribution from increased film temperatures at lower oil flow rates.

Table 6.1: Higher load testing on the Bronze bush

Bush Type	Radial Clearance, C_r (µm)	Journal Speed (rpm)	Feed Temperature (˚C)	Specific Load SL (bar)	Bearing Load (N)	Baseline Feed Pressure (barA)
Phosphor Bronze	52.7	1000	20	2.2 to 13.8	225 to 1420	3

Results for the torque required to drive the bearing at 1000 rev/min at three oil feed pressures are shown in Figure 6.2. The torque required to drive the bearing was lower at lower oil feed pressures and increased linearly with increasing load. The percentage reduction in torque produced by reducing oil feed pressure fell as load increased. For example, at a supply pressure of 1.5barA, the %torque reduction fell from close to 18% at SL=2.2 bar to around 13% at SL=13.8 bar.

Although cavitation could not be observed when using a phosphor bronze bush, the film pressure variations shown in Figure 6.3 indicate that cavitation changes continue to be the source of torque reductions through the mechanisms described in Chapter 5. At any given bearing load, the reduction of oil feed pressure produces a reduction of film pressure in the load bearing part of the film without a major change in the pressure profile. This is consistent with a reduction in film pressure in the opposing part of the bearing, with the groove, and a reduction in film area due to increased cavitation. These reduce the contribution to the load supported by the high-pressure region. Integration of the film pressure profiles shows that at both high and low feed pressures the calculated load value is very similar.

The sensitivity of torque to changes in feed pressure decreases as the load increases. Smaller variations in bearing eccentricity and hence the shear contribution towards torque reduction at higher loads can provide an explanation for this. Furthermore, as the applied load increases, the hydrodynamic requirement of the bearing increases

and the load bearing film extent decreases as shown in Chapter 4 results. If the bearing film extent reduces to a sufficient extent at very high loads, then this can result in increased eccentricity ratios for a reduction in supply pressure contributing negatively towards the %torque reduction.

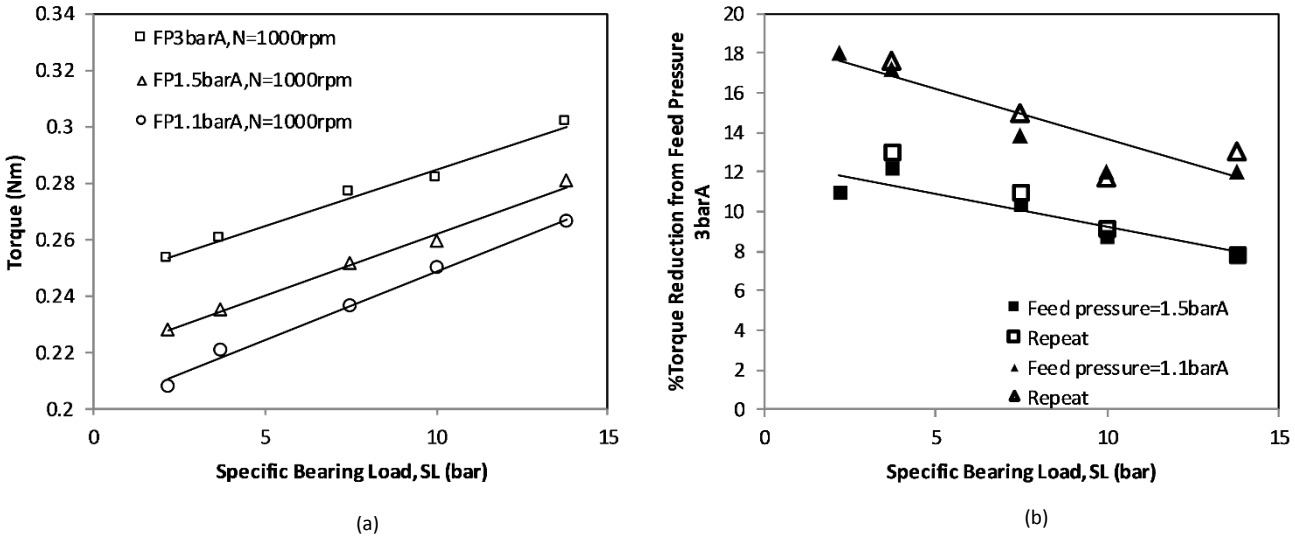


Figure 6.2: (a) Variation in torque at T_{film}=30 ˚C with load and feed pressure (b) Variation in %torque reduction from baseline feed pressure to 1.5barA and 1.1barA with load

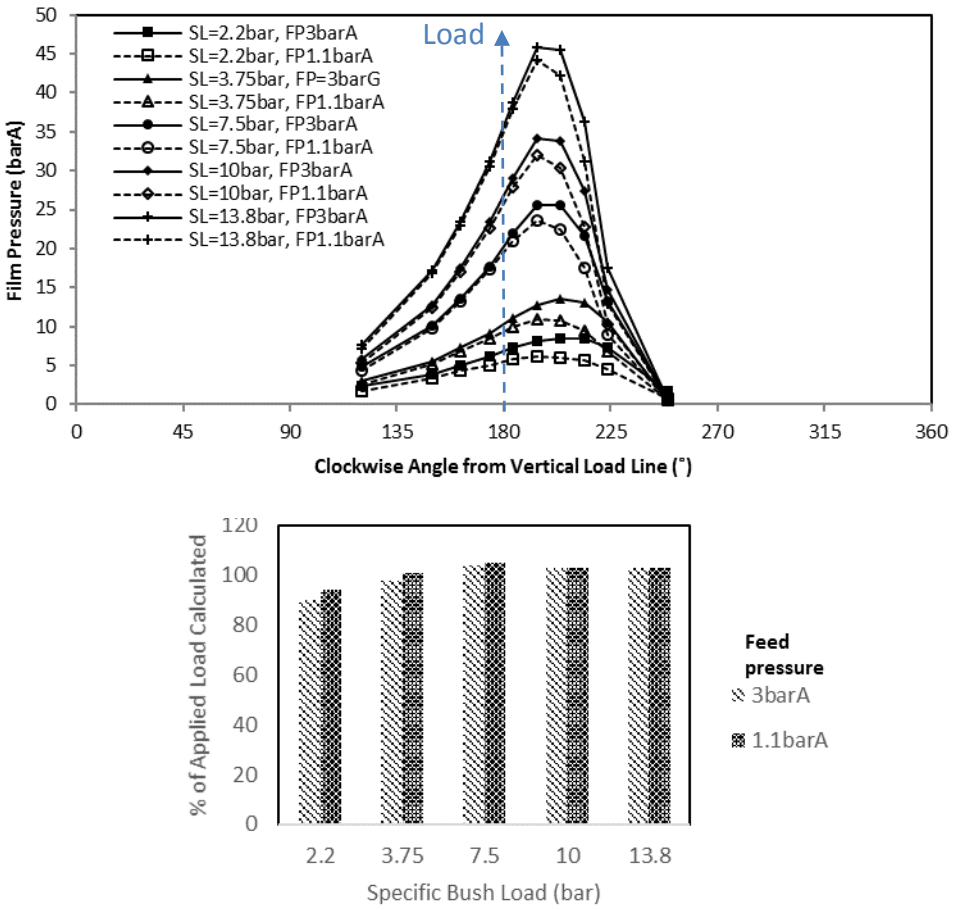


Figure 6.3: Variation in experimental film pressure profile with load. Integration of pressure profile at both supply pressures gives similar load capacity result.

The effect of supply pressure and applied load on the measured film temperatures is shown in Figure 6.4. Film temperature increased by up to 5 °C as a result of reduced flow rate and consequently lower convective heat transfer. Film temperature exhibits a weaker dependence on applied load. As the load increases, the bearing shear rate increases thus giving rise to increased frictional dissipation contributing towards temperature rise. However, this increase in temperature due to increase in frictional dissipation is dampened to an extent by the increase in flow rate with load.

Increases in film temperature under reduced oil supply conditions also result in friction reduction due to a reduction in film viscosity. From the measured torque data on a single bearing, increases of 5 °C in the film temperature over a 900s testing period due to oil flow reduction can provide a further reduction in torque of 9% when the feed pressure is reduced from 3 barA to 1.1 barA. The variation in film

temperature with feed oil flow rate can influence the total friction benefit attained and the effect of this during a cold start warmup in a cylinder block will be explored in Chapter 7.

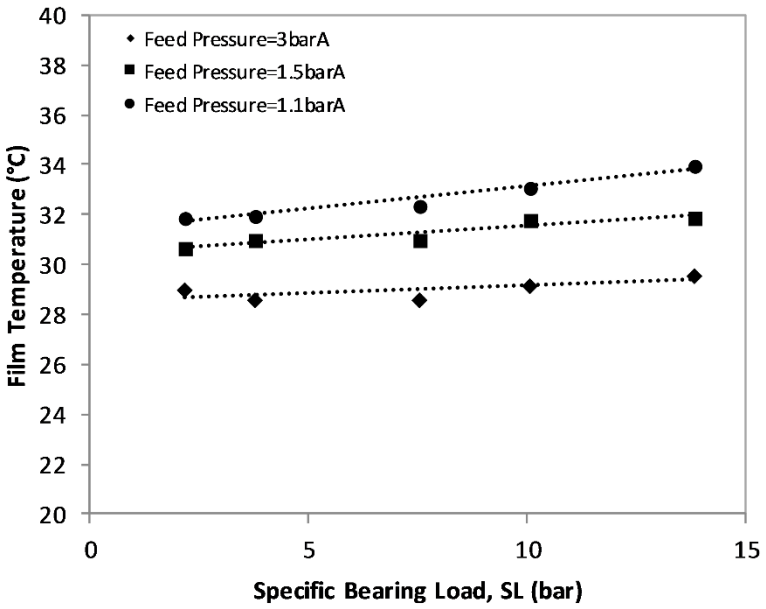


Figure 6.4: Variation in oil film temperature with supply pressure and applied load at a feed temperature of 20°C

6.4 Effect of Shaft Speed on Bearing Friction and Performance Characteristics and Changes with Feed Pressure

The effect of operating speed and feed pressure on bearing friction and performance characteristics was investigated by carrying out tests at combinations of settings given in Table 6.2.

Table 6.2: Test matrix for investigating effect of operating speed on bearing friction and pressure distribution

Test Set #	Inlet Temp (°C)	Specific Load (bar)	Journal Speed (rpm)	Feed Pressure (bar)
1	20, 40, 60	2	1000, 2000	4,3,2,1.5
2	20	1, 8	1000, 1500, 2000	3,1.5

The results presented in Figure 6.5 show that with increasing speed, hydrodynamic friction increases. This is because of increased shear forces within the thin film. As a result, friction shows a steeper gradient with film viscosity and any reductions in oil

viscosity would result in increased benefit at the higher speed. The graph also shows the variation in friction torque at 4 different supply pressures- a friction reduction is noticed for lower supply pressure at each feed temperature. The percentage benefits from the maximum pressure case at each supply temperature are shown Figure 6.6 and the friction benefits at a given supply pressure are found to be similar at the tested feed temperatures and speeds.

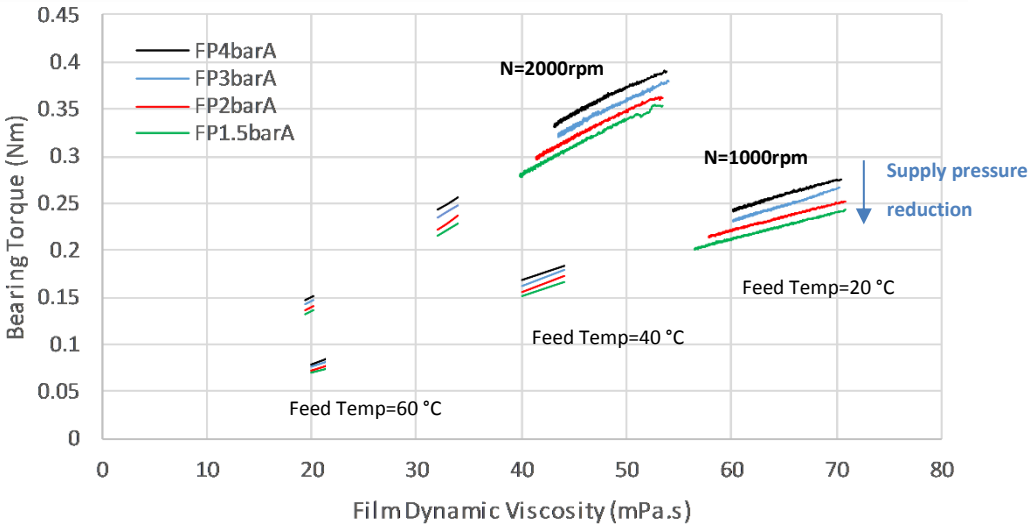


Figure 6.5: Variation in friction torque with speed and supply temperature for 4 different feed pressures, Specific Bearing Load, SL=2bar

Friction power loss decreases with increasing feed temperature, since the viscosity of the oil film decreases, thus reducing lubricant shear rate. The friction torque reduces by approximately 65% from a feed temperature of 20 °C to 60 °C at both tested speeds though bigger differences in the absolute value of torque are observed at the higher speed due to larger hydrodynamic friction contribution.

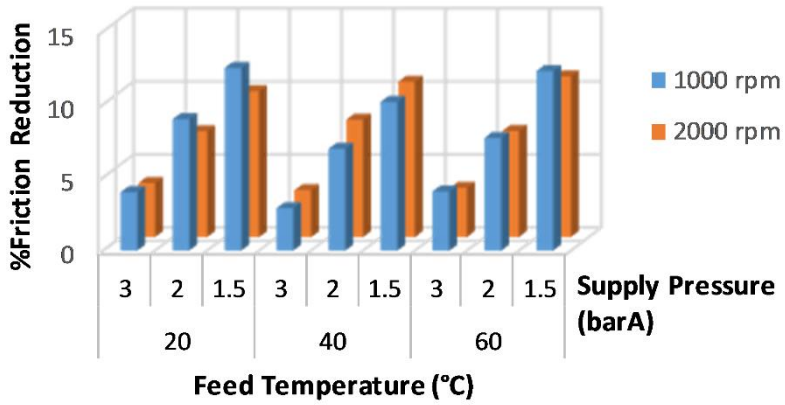


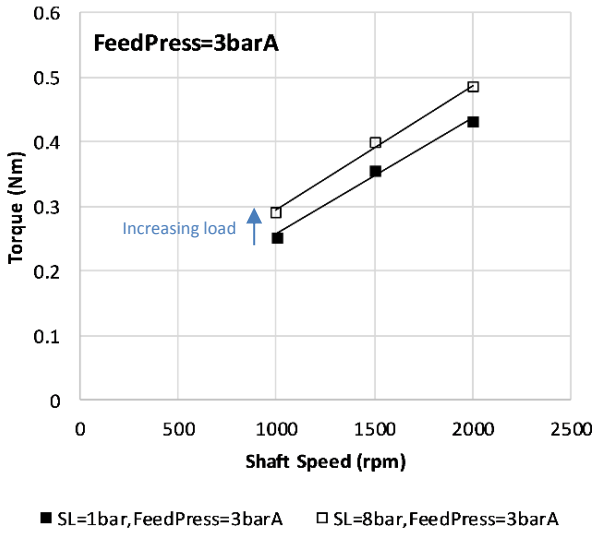
Figure 6.6: %Friction reduction from supply pressure of 4barA at two speeds and three feed temperatures, Specific Bearing Load, SL=2bar

The linear variations in friction torque with speed is shown in Figure 6.7 at a film viscosity of 65 mPa s. Increasing load (Fig. 6.7(a)) raises torque without changing the sensitivity to shaft speed. Reducing supply pressure (Fig. 6.7(b)) from 3 to 1.5 barA reduces torque by ~10% with perhaps a small effect on the sensitivity to supply pressure.

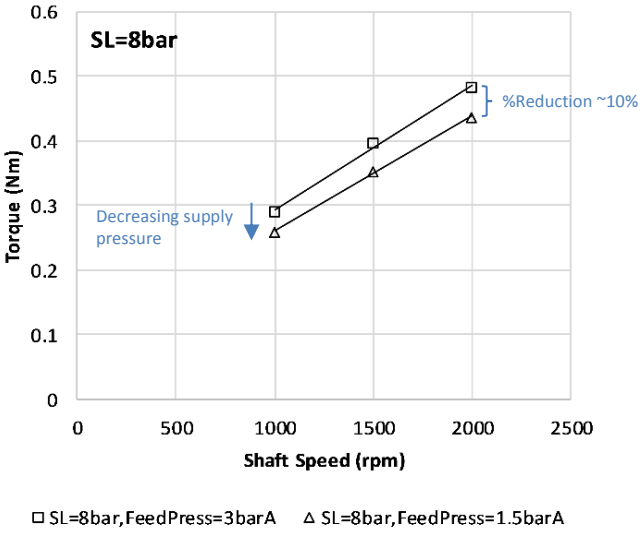
Figure 6.8 shows that the maximum film temperature increased significantly with increase in shaft speed. The effect of supply pressure on film temperature is similar to what was discussed in the previous section. The increase in film temperature is due to the increased frictional dissipation within the film as a result of increased shear rates.

Pressure profiles are presented in Figure 6.9 for the supply pressures of 4 barA and 1.5 barA. Under higher speed conditions, lower peaks and wider positive pressure zones occur at all supply temperatures tested. This signifies an increase in load capacity and decrease in bearing eccentricity. However, as observed in Section 4.3 and [59], a decrease in film extent and increase in cavitation with speed is observed due to increased hydrodynamic flow requirement. Decreases in film extent can lead to increased eccentricity. Higher speeds will provide greater hydrodynamic lift. Overall, the impact of increased hydrodynamic lift is seen to be more significant and reduction in bearing eccentricity is predicted from the results since the peak film pressures drop with increase in speed. With an increase in oil supply temperature greater peak pressures are observed and this results in the positive pressure zones to

have somewhat smaller angular extents. These features are more pronounced at the lower speed and they indicate a reduction in the bearing load capacity and increase in eccentricity due to lower film viscosity at the higher supply temperatures.



(a)



(b)

Figure 6.7: (a) Variation in friction torque with speed at SL=1bar and SL=8bar (b) Variation in friction torque at SL=8bar and feed pressures of 3barA and 1.5barA

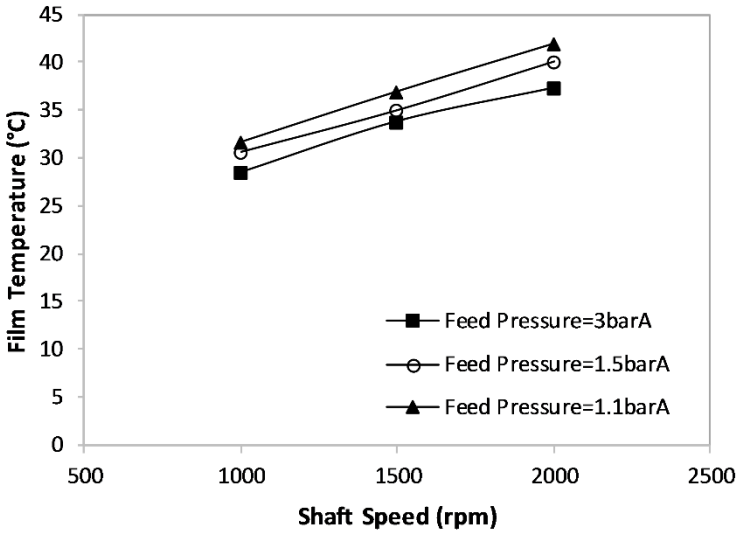


Figure 6.8: Variation in maximum film temperature with shaft speed and supply pressure

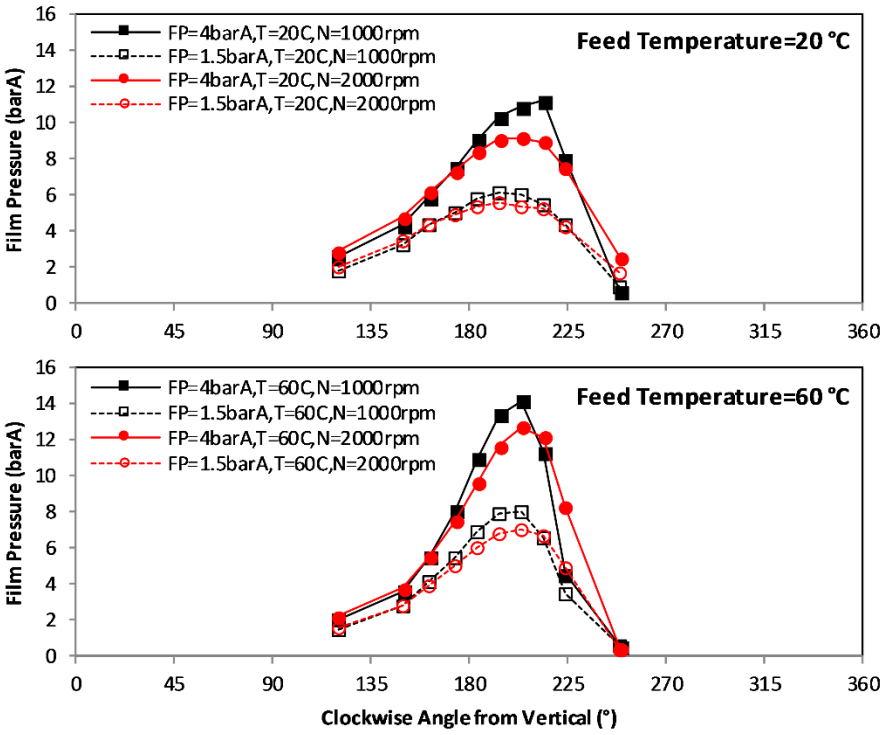


Figure 6.9: Variation in film pressure with increasing speed, Bearing Specific Load, SL=2bar

6.5 Effect of Lubricant Formulation on Bearing Operating Characteristics

The effect of oil formulation on friction, film pressure distribution and flow rates was studied by testing five oils of different viscometrics at different operating conditions. A summary of the oils tested in this study is presented in Table 6.3. Kinematic viscosity and oil density has been measured for 3 temperatures, 40 °C, 60 °C and 90 °C. These data points have been used to calculate the lubricant dynamic viscosity. The Vogel coefficients presented in Table 6.4 for the test oils have been determined from this data and the corresponding predictions of dynamic viscosity using the Vogel equation are shown in Figure 6.10.

Friction torques for these oils were compared at oil supply temperatures of 40 °C and 90 °C and feed pressures of 2 barG and 4 barG at steady bearing loads of 100 N (SL=1 bar) and 500 N (SL=5 bar). The shaft speed was kept constant at 2000 rpm. The tests carried out at high temperature and pressure required rig modifications to collect oil spray from the bearing by encapsulating the entire journal using splash guards. Exhaust facilities were also setup to suck out oil vapour and mist.

Table 6.3: Test oil viscosities and testing conditions

Bush Material	Phosphor Bronze				
Radial Clearance	47 µm				
Lubrication Oils	**Type**	**KV40 (mm^2/s)**	**KV100 (mm^2/s)**	**µ at 40 °C (mPa.s)**	**µ at 100 °C (mPa.s)**
	YUBASE 4	18.86	4.212	15.73	3.51
	E1553A/079A	26.93	5.535	22.77	4.68
	E1553A/079B	31.85	6.293	27.1	5.35
	E1553A/079C	27.32	5.851	22.78	4.88
	Stock 5W-30	51	9.5	42	7.37

Table 6.4: Vogel coefficients of the test oils

Lubricant Type	**Vogel Coefficients**		
	k_v (mPa.s)	**θ_1 (°C)**	**θ_2 (°C)**
YUBASE 4	-	-	-
E1553A/079A/01	0.070811	868.315	110.36
E1553A/079B/01	0.071516	898.5976	110.802
E1553A/079C/01	0.077087	872.6469	112.729
Stock 5W-30	0.051762	1142.07	130.324

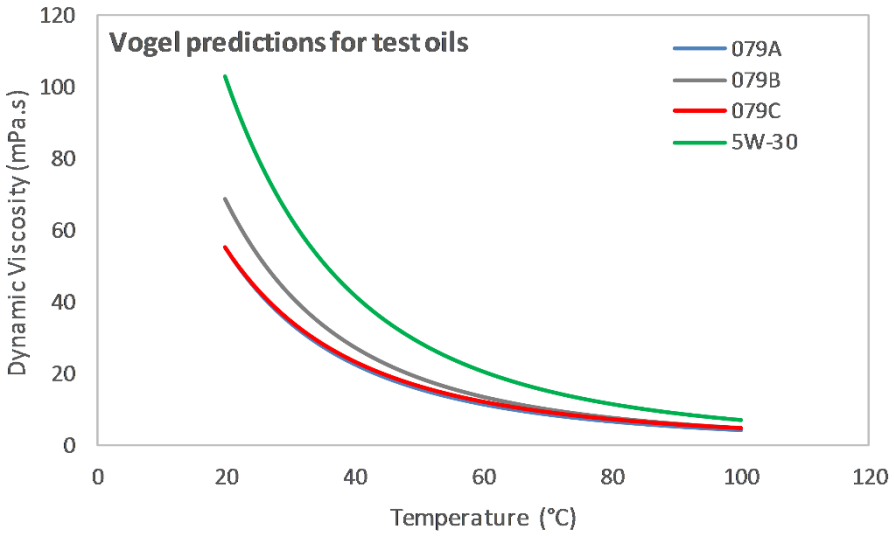


Figure 6.10: Vogel viscosities for the test oils

6.5.1 Friction Torque

Results for measured torque against film viscosity are presented for low load in Figure 6.11 and high load in Figure 6.12. It is seen that the hydrodynamic friction reduces for the lower viscosity oil operating under similar conditions. A near linear relationship of friction against viscosity and similar trends are observed at both low and high loads. Friction data for stock oil 5W-30 is observed to lie slightly off the line at colder feed temperatures.

At light load a maximum decrease in friction torque of ~45% is achieved at a temperature of 40 °C and 90 °C from the thickest (*5W-30*) to thinnest oil (*YUBASE 4*). At high load the maximum decrease is ~45% at 40 °C and ~35% at 90 °C between the thickest and thinnest oil. The viscosity of the thinner oil, YUBASE 4, is nearly 50% lower than the viscosity of the thicker 5W-30 baseline oil at these two temperatures. Therefore, considerable reductions in bearing friction are achievable by modifying the oil viscosity itself. At high temperatures, the difference in viscosities narrows down resulting in closer hydrodynamic friction.

Increase in feed pressure from 2 barG to 4 barG resulted in an increase in friction torque of ~10%. Best fit lines for the two supply pressures are plotted on the torque curves. The increases in torque are explained by a reduction in cavitation area and increase in shear stresses within the bearing film due to the extra force exerted on

the bush by the higher feed pressure as explained in Chapter 5. Data from film pressure profiles confirms increases in film pressure with supply pressure for all the oils tested at both low and high temperatures. An example of this is shown in Figures 6.14 where higher film pressures recorded at all pressure transducers for the higher supply pressure indicate more film area and increased eccentricity ratios, therefore, resulting in more friction losses.

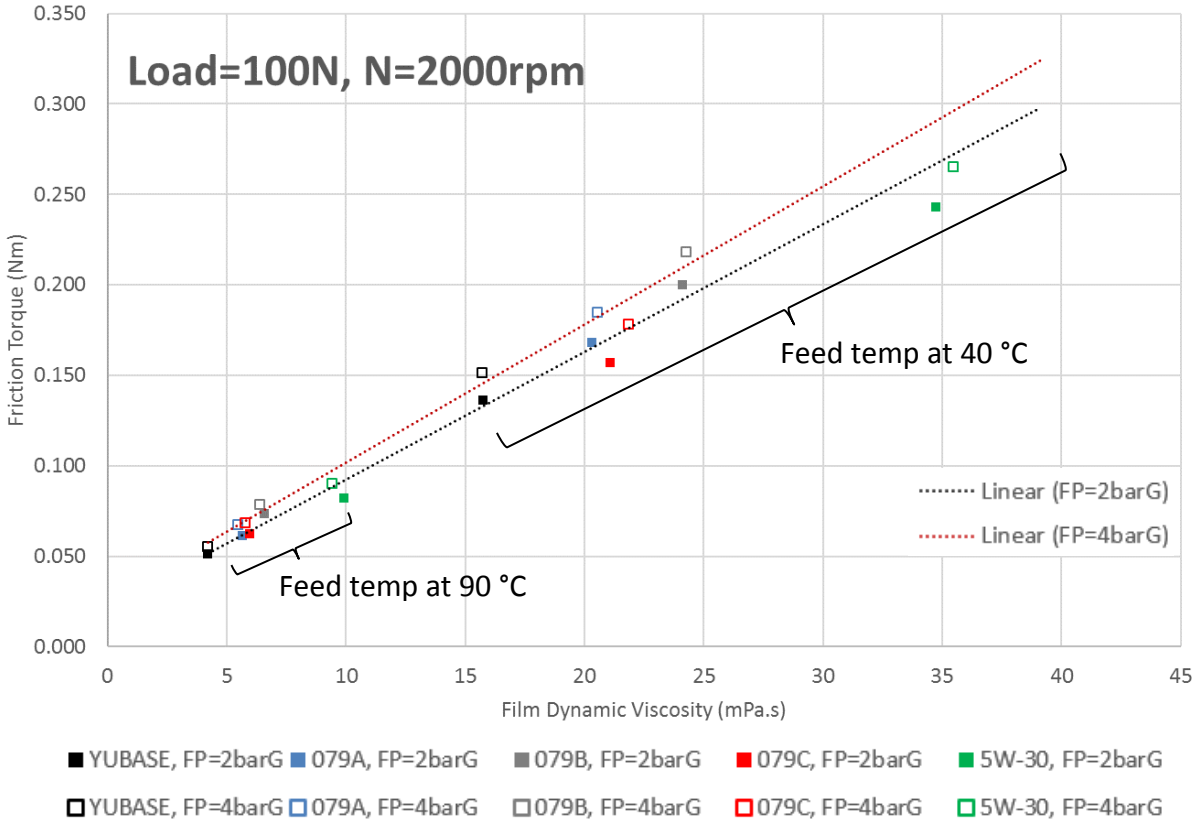


Figure 6.11: Friction torque vs. dynamic viscosity of oil feed at Load=100N, N=2000rpm

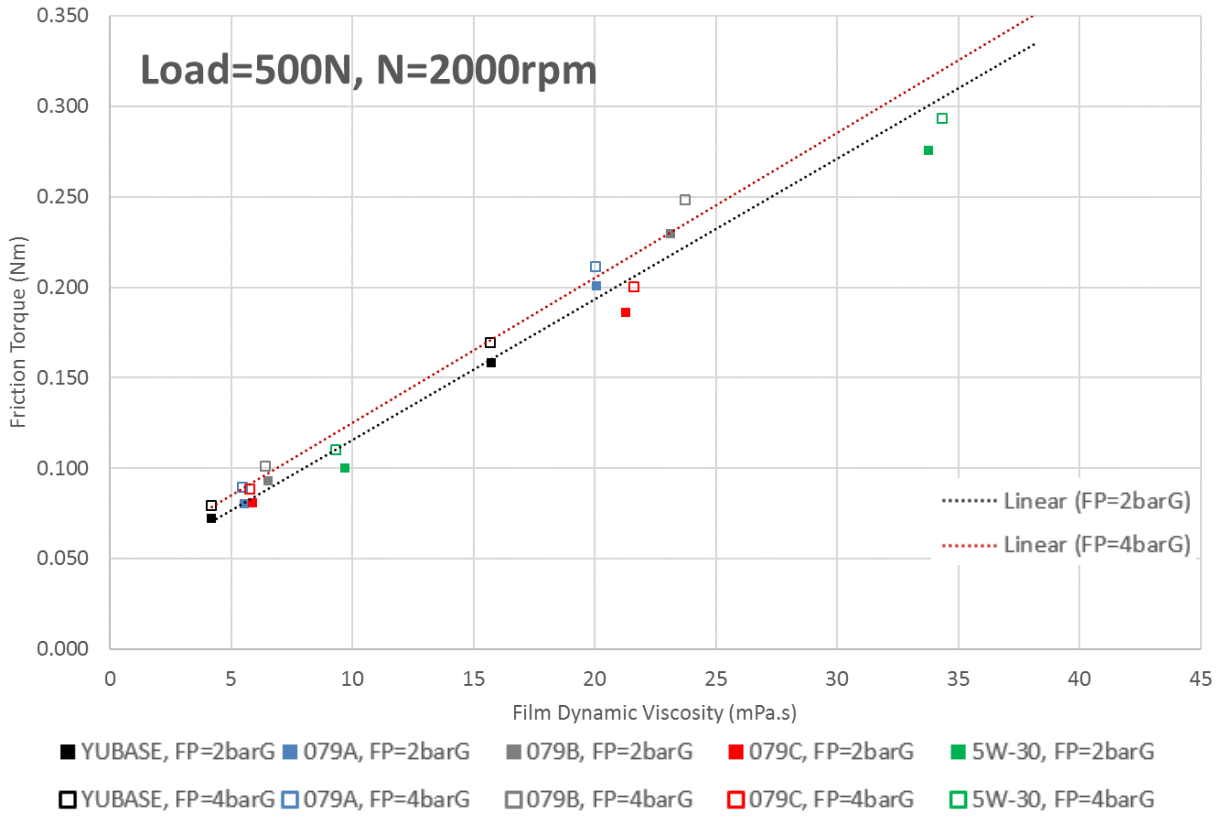


Figure 6.12: Friction torque vs. dynamic viscosity of oil feed at Load=500N, N=2000rpm

6.5.2 Pressure Profiles

Film pressure profiles also show that a lower oil viscosity results in higher peak film pressures and lower attitude angles, both indicating that the bearing is operating at higher eccentricity ratios for similar load, speed and supply temperature conditions. Tests with higher oil viscosity show that the film is spread out more, resulting in positive pressure zones over a large angular extent. Examples of this are shown for two applied loads in Figure 6.13. Pressure readings upstream the film rupture point were extrapolated to estimate the angle at which the film ruptures. This is shown in Figure 6.16 along with the results for the variation in extrapolated film rupture angle against feed oil viscosity. It is found that a decrease in oil viscosity results in film rupture occurring sooner. Increase in bearing load has the same effect. Under light load conditions, the maximum variation in the film rupture angle is greater by ~4° over the viscosity range of the oils.

The numerical bearing model previously described in Section 5.4.1 was used to explain to this behaviour. The film rupture angles calculated using the model have

been plotted in Figure 6.15 along with the experimentally extrapolated points. Model results show a good match with the experimental data. Results in the variation of eccentricity ratio and attitude angle from the model are presented in Figure 6.16. It is observed that the rate of change in eccentricity ratio and attitude angle with oil viscosity is greater at the lighter load. This is because, as described in Section 2.2.3, the sensitivity of the bearing load capacity to eccentricity ratio increases as the latter increases. This also explains the greater variation in the film rupture angle at lighter load since the maximum change in attitude angle is also greater by ~4° compared with the high load case over the same viscosity range.

The variation in peak film pressure with oil viscosity is also plotted in Figure 6.17 which shows an increase in peak pressure with reduction in oil viscosity. The increase in film pressure is more sensitive to decrease in oil viscosity under high temperature, high load conditions. Thicker oils thus increase the load capacity of a journal bearing. These trends are consistent at all the loads, feed pressures and feed temperatures tested.

The accuracy of the film pressure readings was checked by integration of the centreline pressure profile using the short-bearing three-dimensional reconstruction method described in Section 6.2 and all calculated load values were found to be within 90% of the applied load value.

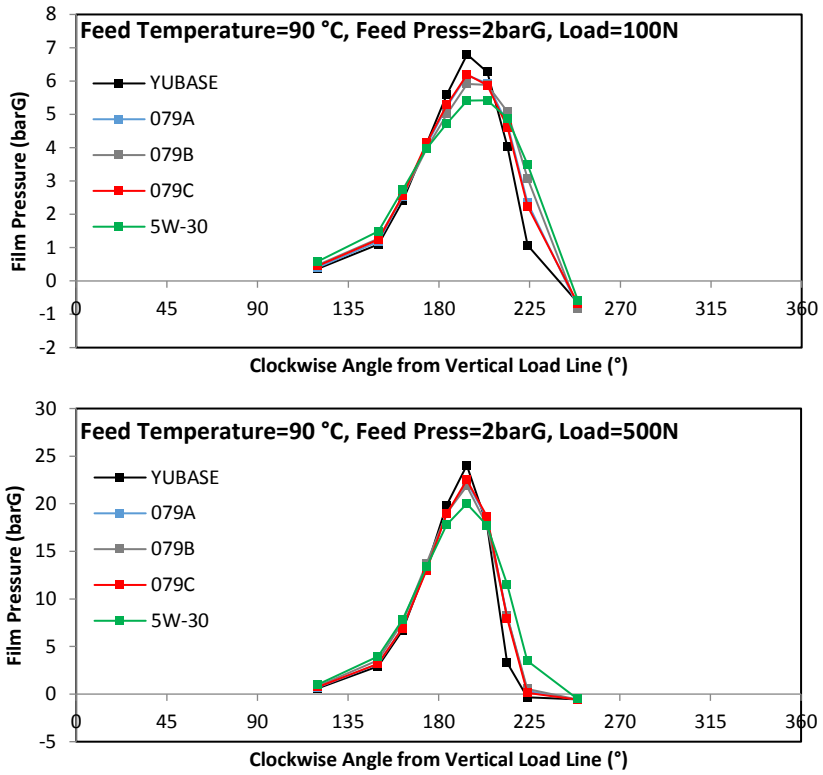


Figure 6.13: Effect of increases in oil viscosity on pressure profiles shown at two load values

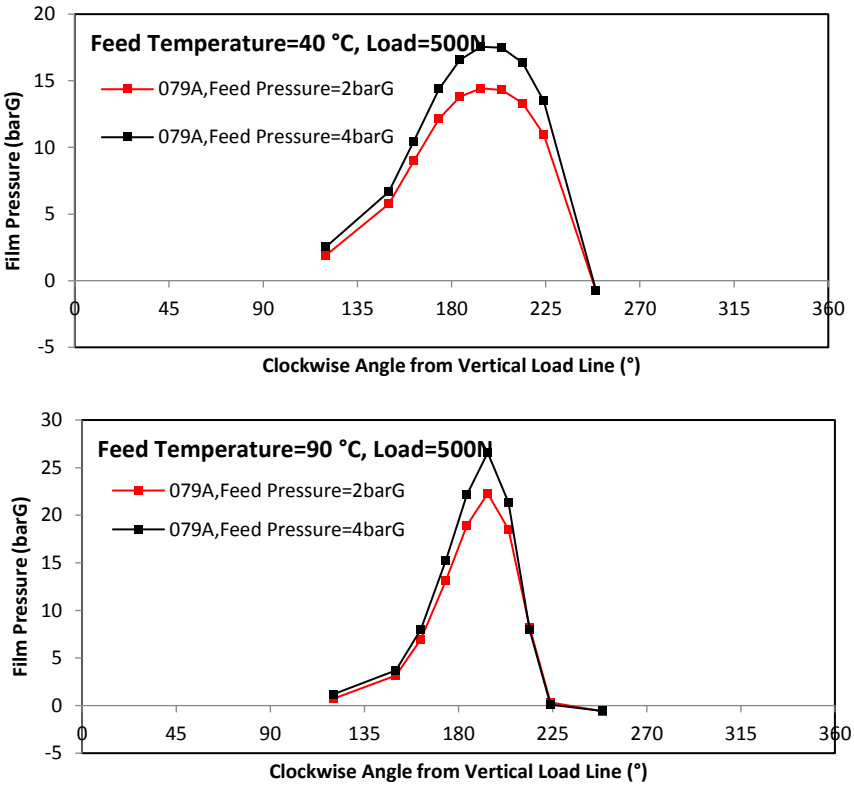


Figure 6.14: Effect of increases in supply pressure on film pressure at two different feed oil temperatures

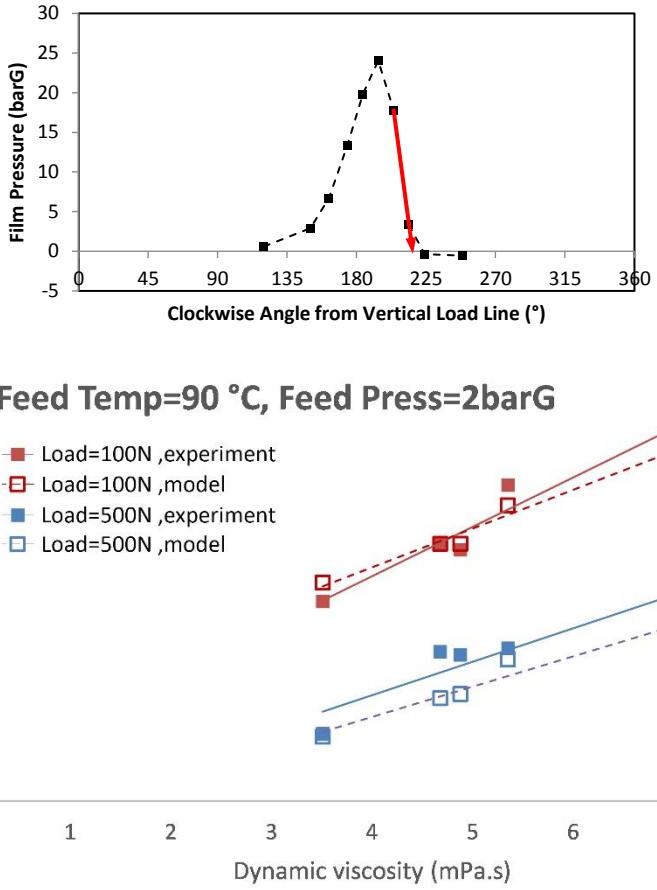


Figure 6.15: Variation in angle of film rupture, $\theta_{rupture}$, with feed dynamic viscosity

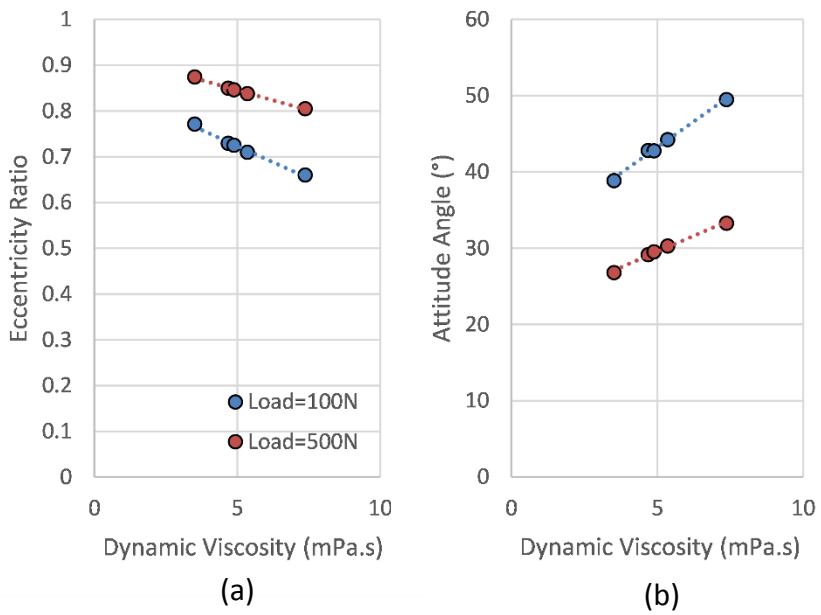


Figure 6.16: Variation in (a) eccentricity ratio (b) attitude angle with lubricant dynamic viscosity

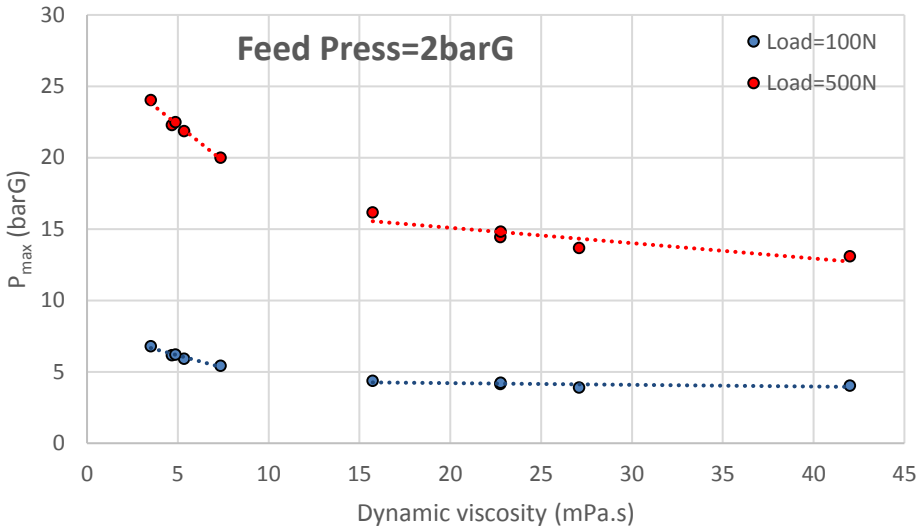


Figure 6.17: Variation in maximum film pressure, P_{max}, with feed dynamic viscosity

6.5.3 Flow Rates

At high oil temperatures, experimental flow rates lied outside the recordable range of the gear flow meter used so an alternative method had to be employed. In order to get an estimate of the flow rates experienced under the test conditions, oil pump speeds were recorded. The oil pump used in the rig was a Tuthill 2LEV-UK positive displacement type with a rotary gear design.

Curves of flow rate (L/min) vs. pump speed for given viscosities published by the pump manufacturer [142] were used to estimate the flow rate behaviour of the oils tested. The results for a load of 100 N at oil temperatures of 40 °C and 90 °C are shown in Figures 6.18 and 6.19.

Oil flow rate increases with a reduction in oil viscosity- flow rate through the bearing increased by nearly 200% when using the thinnest oil (YUBASE) compared with the thickest oil (5W-30). Very high flow rates were experienced under pressurised conditions at fully warm temperature of 90 °C where flow rates reach up to 10 lit/min for the thinnest oil used. By increasing the supply temperature from 40 °C to 90 °C, an approximately 300% increase in flow rate was observed. By increasing the supply pressure from 2 barG to 4 barG, an approximately 200% increase in flow rate was observed.

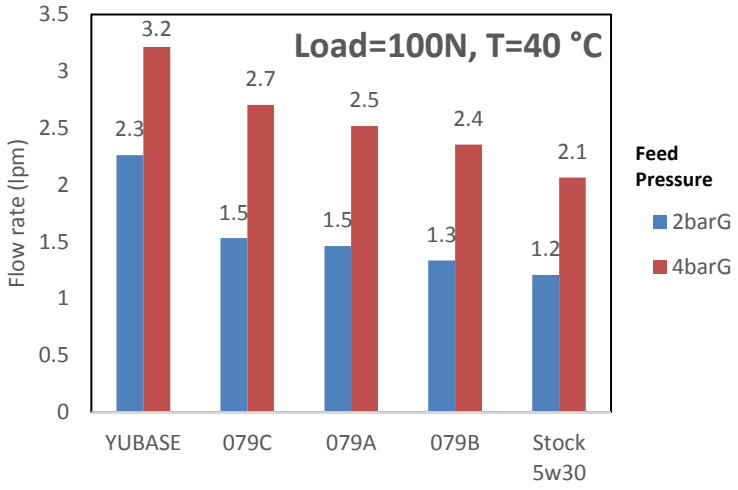


Figure 6.18: Estimated oil flow rate to the bearing at 40 °C feed temperature and 100N load

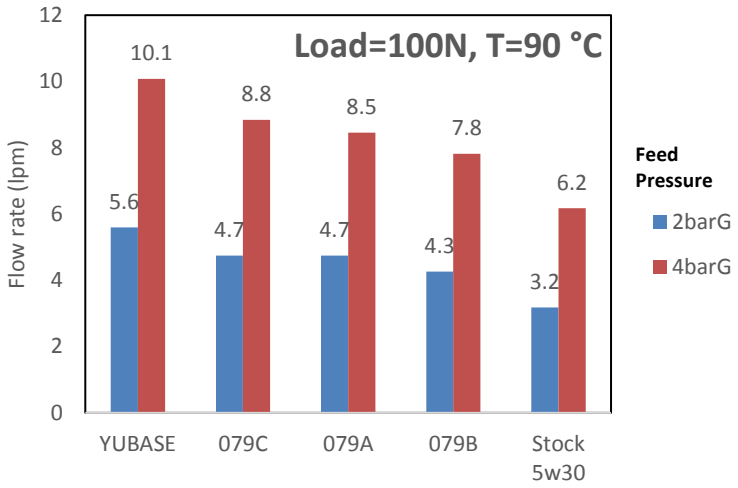


Figure 6.19: Estimated oil flow rate to the bearing at 90 °C feed temperature and 100N load

6.5.4 Film Temperature

Film temperature measurements (Figure 6.20) indicate a modest reduction in film temperature of ~4 °C from the thickest to thinnest oil operating at the same feed temperature of 40 °C. This is due to less convective heat transfer away from the bearing due to a lower flow rate for the thicker oil as shown in the previous section and possibly due to lower viscous dissipation at the lower viscosities. At higher temperature, the difference in film temperatures becomes very small since the difference in oil viscosities also narrows down.

Differences in film temperature, and hence viscosities, for identical feed temperatures indicate the need for using film viscosity values to define friction measurements.

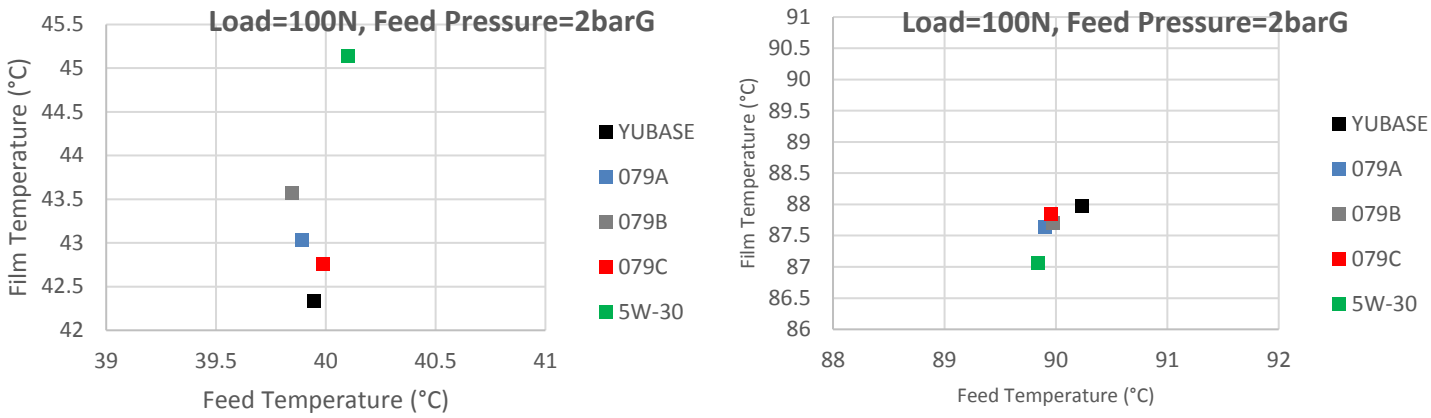


Figure 6.20: Film temperatures at Load=100N, Feed Pressure=2barG, N=2000rpm

6.6 Effect of Radial Clearance on Bearing Friction and Film Pressure

The effect of radial clearance on bearing friction and film pressure profile was investigated through tests covering bearing loads of 100 N (SL=1 bar) and 500N (SL=5 bar) at 2000 rpm and oil supply temperatures of 40 °C and 90 °C. The specifications of the two test bearings utilized are given in Table 6.5. The test oil used in this investigation was YUBASE 4.

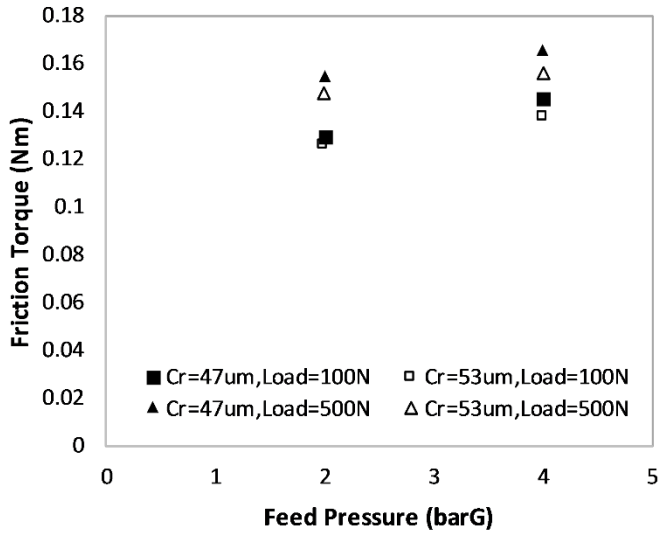
The variation in friction torque for the two clearances at two feed pressures is presented in Figure 6.21. It can be seen in this figure that friction force reduces with increase in radial clearance at both supply pressures and temperatures. An average friction reduction of 5% was achieved with a roughly 10% increase in radial clearance. Friction reductions of between 3 to 6% were measured at all temperatures, supply pressures and loads tested. Reductions in supply pressure from 4 barG to 2 barG resulted in similar friction reductions of close to 10% at light load and 6% at higher load for both the clearances.

Table 6.5: Specification of the test bearings for studying effects of radial clearance

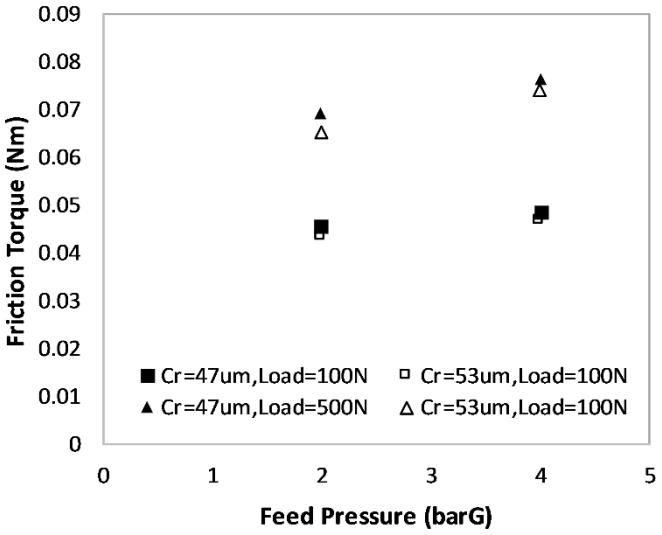
Bush Material	Phosphor Bronze
Bush 1 Radial Clearance	53 µm
Bush 2 Radial Clearance	47 µm
%Difference in Clearance	11%

A tighter clearance results in a lower average film thickness around the bearing circumference, therefore, leading to greater friction losses because of larger shear stresses in the film.

Results for film pressure distributions for the two clearances are shown in Figure 6.22. It is seen that the maximum film pressure decreases with decreasing clearance for similar speed, temperature and load conditions. The film pressure for the smaller clearance is also spread out more, resulting in positive pressure zones over a larger angular extent. For an applied load of 500 N (SL=5 bar) it is clear from a ~50% higher pressure reading at transducer number 9 (at 225°) that film rupture is taking place lower downstream for the smaller clearance. A decrease in bearing clearance has thus improved the load capacity by allowing the bearing to operate at a lower eccentricity ratio.



(a)



(b)

Figure 6.21: Comparison of measured friction torque at radial clearances of 47µm and 53 µm at feed temperatures of (a) 40 °C (b) 90 °C

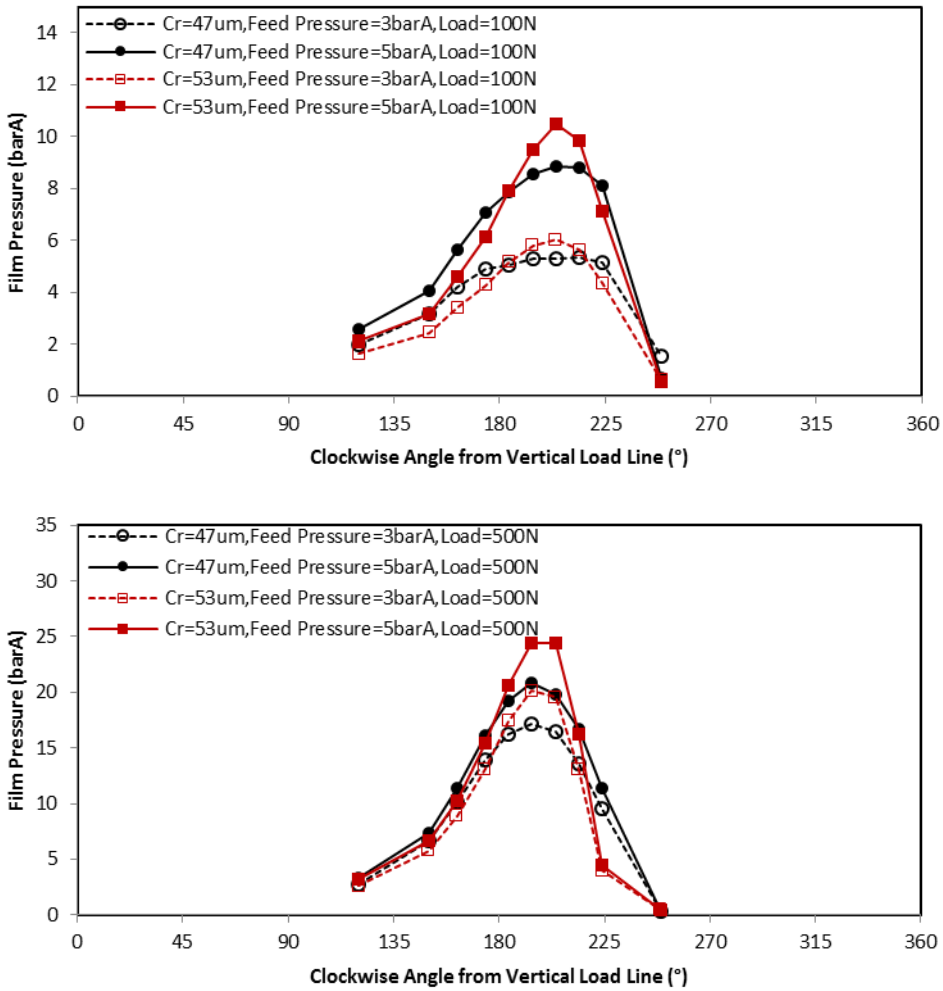


Figure 6.22: Variation in pressure profile with radial clearance at two loads

6.7 Discussion

In this chapter the effects of load, speed, lubricant formulation and clearance on bearing friction were studied along with the effects of supply oil pressure. Higher loads, speeds and lubricant viscosity achieved greater hydrodynamic friction due to greater shear stresses within the hydrodynamic film while increases in bearing clearance achieved the opposite effect. The effect of speed and lubricant viscosity on bearing friction is found to be greater than then effect of load.

For the range of loads tested (SL=2.2 bar to 13.8 bar) bearing friction increased by approximately 22% by increasing load to high values. Over this range the theoretical eccentricity ratio is calculated to change from Ɛ~0.3 to 0.75. The increases in friction are a result of increased eccentricity ratios and the subsequent increases in shear

rates. Compared with the effects of speed, the effect of load on friction is found to be relatively less significant.

Engine friction data presented by Muira et al. [143] suggests that the effect of increases in load on cycle-averaged friction may be even less significant in dynamically loaded bearings. Though instantaneous main bearing friction was shown to increase linearly with peak load (like the current results), cycle averaged friction was barely affected. This is because increases in eccentricity due to increased engine load occur for a very short part of the engine cycle and when averaged over the whole cycle, the effects of the increased eccentricity on friction are less significant.

The percentage reduction in torque achieved by reducing the supply pressure reduced by ~30% by increasing the load to the maximum tested value. Percent reductions in torque with supply pressure reduction have been reported to reduce at increasing load in literature. Vijayaraghavan et al.'s [66] numerical results showed that a 50% reduction in flow rate resulted in a 15-20% reduction in power loss at light load (SL=2.5 bar) and 10-15% at high loads (SL>10 bar). Brito et al. [20] similarly reported a decrease in %torque reduction from in their experimental work over a load range of SL=2.5 bar to 12.5 bar. Torque reduction decreased from ~20% to 10% due to the increase in load as the supply pressure was reduced from 3.1 barA to 1.7 barA. This was explained with the fact that the measured film pressures did not change significantly with supply pressure at high load for a twin axial groove bearing.

The reductions in percentage friction reduction with increase in load can be attributed to the diminishing contribution from the shear term with change in pressure. At high loads, smaller decreases in eccentricity are expected with reductions in supply pressure due to its insignificance compared with the much higher hydrodynamic pressures and also a reduction in the film extent with load especially at low feed pressures. For the current grooving arrangement, the maximum film pressure was always found to decrease with a reduction in supply pressure and no major changes were measured in the pressure profile. Moreover, integration of the experimental pressure profiles gave a good estimate of the

expected load capacity confirming the validity of the approximate method to determine bearing load capacity from experimental film pressure measurements.

Increases in film temperature with reduction in supply pressure and increases in load are consistent with published works [21, 70]. The modest increases in film temperature (less than 5 °C) indicate safe, hydrodynamic bearing operation at low supply pressures even at high loads and relatively cold operating conditions. The increases in film temperature with reduction in supply pressure add to the total friction reduction due to changes in cavitation area and shear rates. However, the extent of this depends on the thermal coupling of the bush to the environment which is explored further in an engine environment in Chapter 7.

Increases in bearing friction with speed are found to be much more significant than increases in bearing load. For a two-fold increase in speed from 1000 rpm to 2000 rpm, bearing friction increased by approximately 90%. This is because increases in friction are directly proportional to the journal speed unlike load. At relatively light loads experimental results have shown that the percent friction benefit with reduction in supply pressure is a weak function of shaft speed. Increases in film temperature are found to be a strong function of speed compared with applied load where the film temperature increased by ~10 °C over the speed range. This can be attributed to the increased frictional dissipation at higher shear rates. A reduction in the maximum film pressure and spread of the high-pressure region confirms that increases in shaft speed improve load capacity of the journal bearing. These results are consistent with Mufti et al's [31] engine friction results where increases in crankshaft speed at high temperature for a low viscosity oil allowed for transition from mixed lubrication to the hydrodynamic regime.

To understand the effects of lubricant formulation on bearing performance, the friction force behaviour of a single main bearing was experimentally observed with 5 oils of different viscosity characteristics. The lower viscosity oils gave lower hydrodynamic friction force due to lower hydrodynamic shear force. From the experimental results, friction reductions of up to 45% have been achieved by reducing the oil viscosity from the stock 5W/30. Given that the crankshaft bearings

contribute to around 30% of the total engine friction [144], this amounts to an approximately 12% reduction in total engine friction. This confirms the strong dependence of hydrodynamic friction on lubricant viscosity and the fact that significant fuel savings that can be achieved by modifying the lubricant viscosity alone.

Using the short bearing approximation, friction in journal bearings can be approximated by [34]:

$$F = \frac{2\pi\mu UbR}{C_r}\frac{1}{(1-\varepsilon^2)^{0.5}} \tag{6.3}$$

Values of eccentricity ratio for given loads and oil viscosities were calculated using equation 2.2. Equation 6.3 was then used to calculate the variation in friction torque for a range of viscosities and two load values of 100 N and 500 N. The variation in friction torque is shown in Figure 6.23. The variation of the friction multiplier term, $\frac{1}{(1-\varepsilon^2)^{0.5}}$, which accounts for the effect of eccentricity on friction against viscosity is also given in Figure 6.24. It is found that down to a viscosity of ~5 mPa s, torque shows a linear dependence on viscosity. Below this value of viscosity, the influence of the friction multiplier term and viscosity gives a non-linearity with the curve eventually passing through zero. If the linear region is extrapolated, an offset on the y-axis is measured which increases with load. A linear dependence of torque on oil viscosity was also observed in the experimental results as shown in Figures 6.11 and 6.12 where an offset on the y-axis is noted if the lines are extrapolated. Reductions in oil viscosity for a given operating temperature, therefore, result in proportional friction reductions without requiring modification to the bearing design or oil supply system.

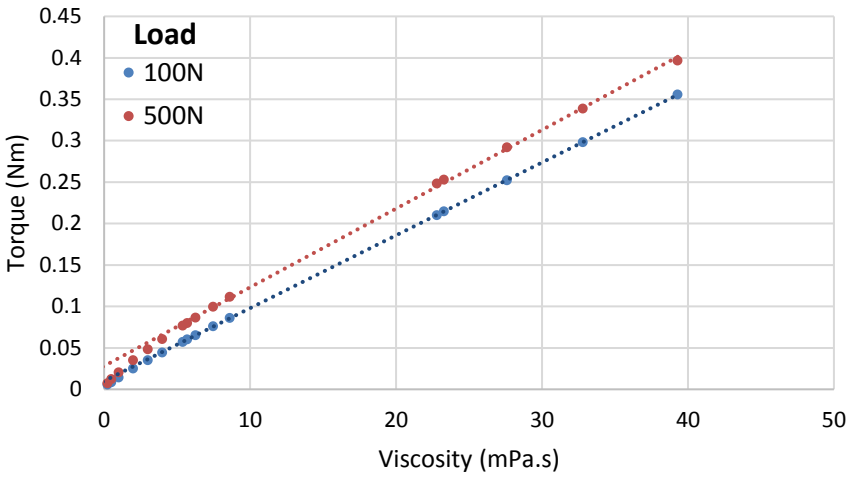


Figure 6.23: Variation in friction torque against viscosity as predicted using the short bearing friction equation

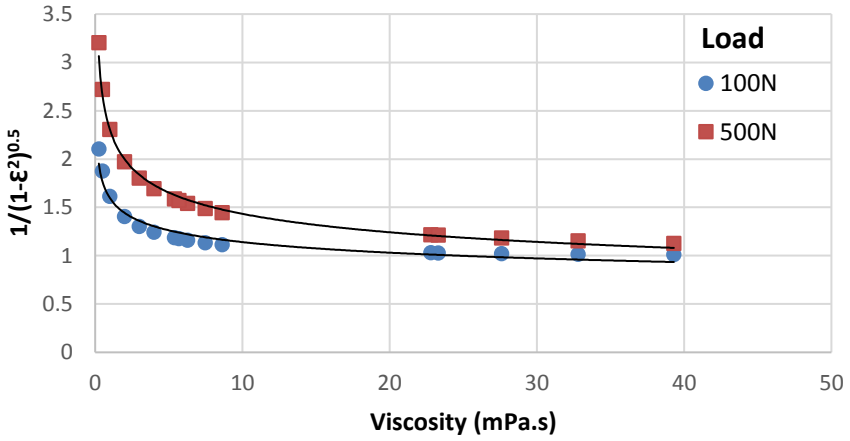


Figure 6.24: Variation in the friction multiplier term against oil viscosity

Reductions in hydrodynamic friction in the crankshaft bearings and piston assembly with use of lower viscosity oils results in reduced engine fmep and this has been previously observed by Leong et al. [11]. The influence of reduced viscosity on the piston assembly has also been researched by Reza [145] where it was similarly found that lower temperatures resulted in greater difference in hydrodynamic friction due to higher difference in viscosity. In the piston assembly, benefits of lower viscosity were only observed in the hydrodynamic regime where friction is viscosity dominated, while the friction characteristics remained very similar in the mixed/boundary friction regimes due to similar additive packages in the tested oils.

Though significant friction reductions are achievable with reduction in lubricant viscosity, lower viscosity fluids require larger capacity oil pumps to maintain similar supply pressures as shown by the flow rate measurements. Large flow rates also lead to increased windage losses due to oil splash and aeration of the lubricant. A compromise is needed in selecting the optimal viscosity grade for the lubricant to keep the friction losses to a minimum and pumping requirements reasonable.

Friction in the main bearings is inversely proportional to film thickness and clearance. The effects of bearing clearance on power loss and film thickness as calculated by Rosenberg [13] are presented in Figure 6.25. Bearing friction is shown to significantly decrease as clearance increases till a value of around 20 μm after which the change in friction becomes less significant. Minimum oil film thickness increases with clearance and then starts to decrease after reaching a maximum value which has been found to be between 20 to 30 μm under warm conditions [13]. The decrease occurs due to less hydrodynamic pressure generation as the surfaces move apart. Increases in radial clearance are desirable to reduce friction as long as hydrodynamic lubrication is maintained. A compromise is required to achieve optimal friction reduction whilst being able to hydrodynamically support the load. Excessive clearances can result in large oil flows (similar to the effect of low oil viscosity) resulting in larger required pump capacities and subsequent oil windage losses and aeration of the lubricant.

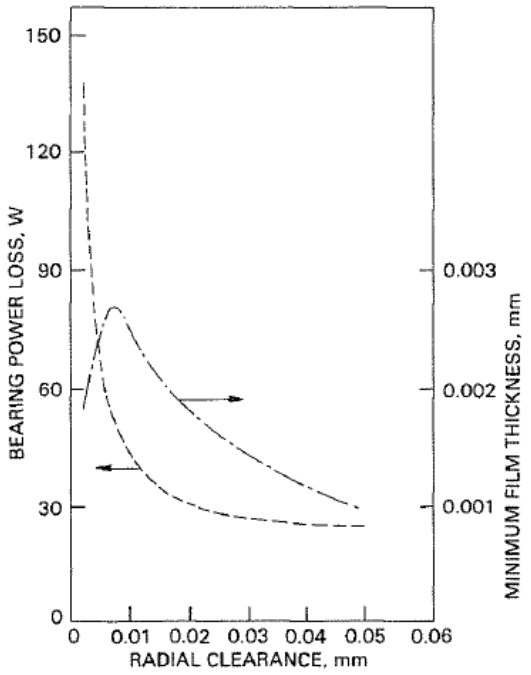


Figure 6.25: Effect of radial clearance on power loss and minimum film thickness [13]

Motoring tests carried out by Baylis [30] on bearings with radial clearances of 6.6, 26.9 and 44.3 µm showed a significant reduction in friction with increased clearances. In the tests carried out in this study bearing clearances were on the larger end of the spectrum (>40 µm) and for a 10% increase in radial clearance, from 47 µm to 52.7 µm, a relatively small friction reduction of around 5% was recorded. Film pressure measurements confirmed a decrease in minimum film thickness as the clearance increased since the peak film pressures increased and the extent of the positive pressure zone decreased. Increases in oil supply temperature results in similar effects on the film pressure distribution also indicating lower minimum film thicknesses.

6.8 Conclusions

- As load increases, reducing oil feed pressure produces a diminishing reduction in friction. This could be attributed to the diminishing contribution from the reduction in average surface shear stress with feed pressure reduction.
- The relationship between oil feed pressure and %friction reduction is found to be less sensitive to increases in speed.
- Peak film pressures and eccentricity ratios increase with applied load, oil feed pressure (unless starved) and radial clearance and decrease with increases in speed and oil viscosity.
- Plain bearing friction is strongly dependent upon oil viscosity and exhibits a linear relationship with film viscosity in the hydrodynamic regime. Significant reductions in friction are possible by reducing the oil viscosity.
- Oil flow rate can increase significantly with reductions in oil viscosity.
- Friction in plain bearings is inversely proportional to clearance, however, the sensitivity of the decrease in friction to increases in clearance becomes less as clearance increases. A relatively small friction reduction of 5 percent was achieved under all operating conditions tested by increasing the radial clearance from 47 μm to 53 μm.

Chapter 7- Studies of Motored Friction of Crankshaft Main Bearings in a Cylinder Block

7.1 Introduction

In this chapter, results for motored rubbing friction in the engine crankshaft main bearings during cold-start warmup under reduced feed pressure conditions are presented and analysed. The aim was to investigate main bearing friction in a cylinder block assembly which more closely represents conditions in an engine than does the single bearing test rig. The interactions between oil flow, thermal changes influencing oil viscosity and oil feed pressure influencing friction, film area and eccentricity are considered. The results were recorded using a second bespoke test rig in which a shaft without crankthrows replaced the crankshaft in a 2.2 litre in-line 4 cylinder diesel engine block. The shaft could be motored and the main bearings subjected to steady loads. This allowed the friction torque, film pressure distribution and film temperature of five main bearings to be measured over a range of temperatures, loads and motoring speeds.

The crankshaft bearing rig allows a better simulation of the thermal conditions in an engine block during cold start warm-ups which is a key area for friction reduction. This allowed predictions to be made of the benefits of reducing oil supply pressure in an engine environment during warm-up compared with the first test rig which focused on an isolated main bearing and data processing at fixed viscosities. Moreover, even higher loads could be applied and a maximum specific bearing load value of up to 30 bar has been tested.

7.2 Multi-Bearing Rig Design, Specification and Data Acquisition

The main components of the test facility are shown schematically in Figure 7.1 and specifications of the engine and main bearings are presented in Table 7.1. Bearing radial clearances were determined from dimensional data obtained using a Coordinate Measuring Machine (CMM). The crankshaft was replaced with a straight shaft (no crank throws) with the same main bearings but with big end bearings replaced with low-friction needle roller bearings. The pistons were inserted in the

cylinders with a standard ring pack and the top of the block closed with a blanking plate. Air was supplied to the cylinders through tappings in the plate. The air pressure was regulated to achieve a target pressure on the pistons and a load on the shaft, and hence load the main bearings of this. The applied main bearing load was, therefore, steady in nature. The assembly of the crankshaft, main bearings and block was enclosed in a thermally insulating cell and could be chilled from laboratory ambient temperature to a temperature of -10 ˚C in approximately 4 hours by circulating chilled ethylene glycol around the engine coolant circuit. A small refrigerant plant of typically 2.5 kW heat rejection rate at the minimum rated temperature of -30 ˚C was used. The engine could also be cooled externally using the cold circulated air to -10 ˚C, however, this took substantially longer, typically 12 hours.

The crankshaft was driven by a 24 kilo Watt DC motor outside the refrigerated enclosure via a toothed belt. A torque transducer was positioned between the drive and the crankshaft. Engine gas load was controlled via a valve on the compressed air line to the cylinders.

Table 7.1: Multi-bearing engine rig and main bearing specifications

Engine				
Engine type		In-line, 4-cylinder, diesel		
Displaced volume		2200cc		
Stroke		94.6mm		
Bore		89.9mm		
Number of main bearings		5		
Main bearings 1,2,4 groove width		5mm		
Main bearings 3,5 groove width		2.2mm		
Groove angular extent		180˚		
Bearing Number	Bearing Length	Bearing Diameter	Length/Diameter	Radial Clearance
1	23mm	65.02mm	0.354	37.78µm
2				37.13µm
3				35.84µm
4				39.04µm
5	18mm	72.03mm	0.257	39.12µm

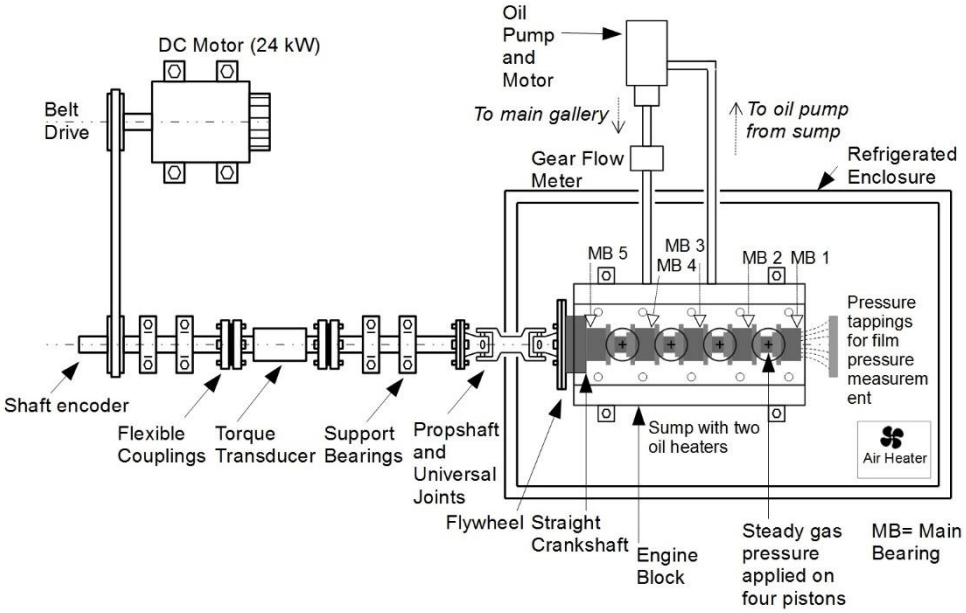


Figure 7.1: Schematic of the multi-bearing engine rig

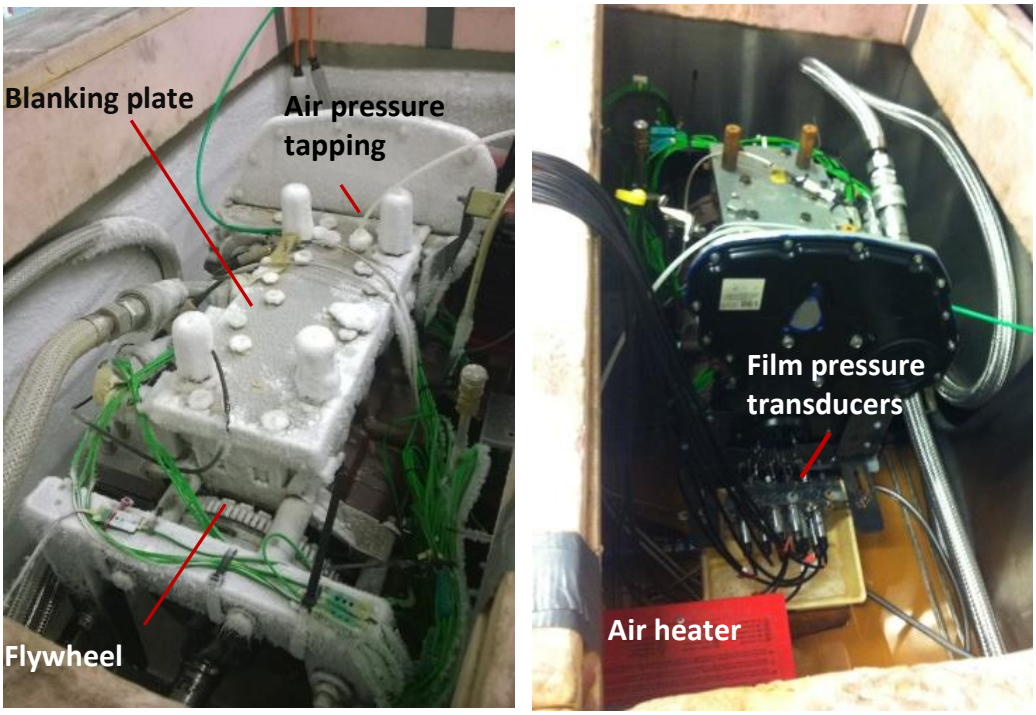
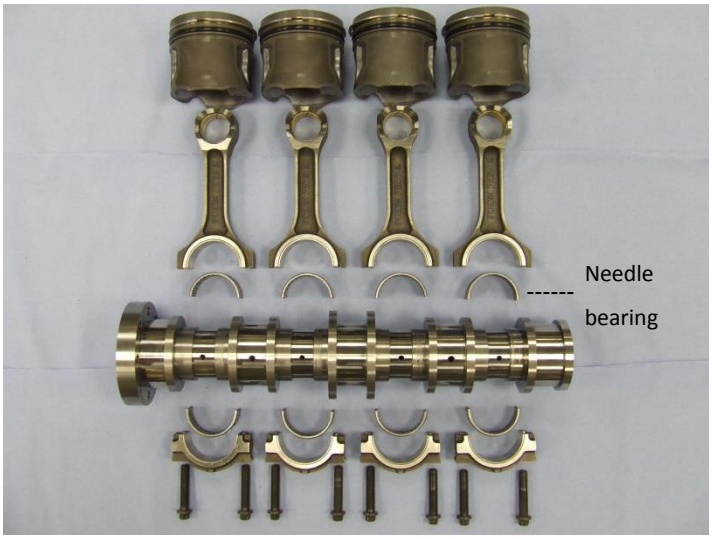
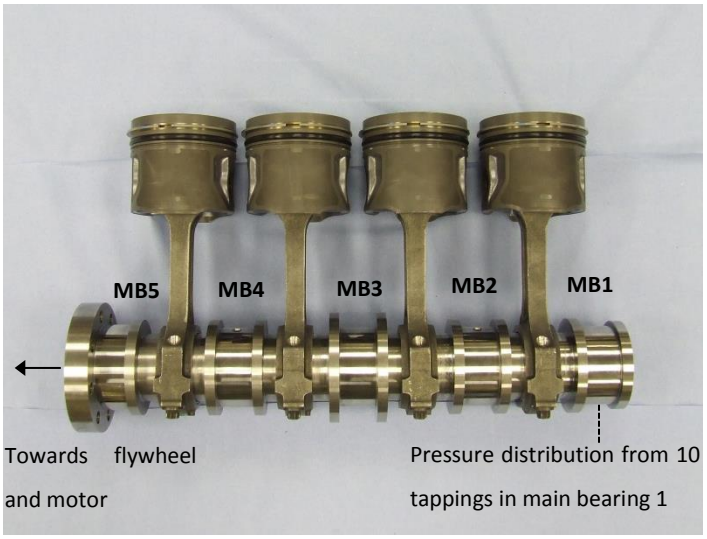


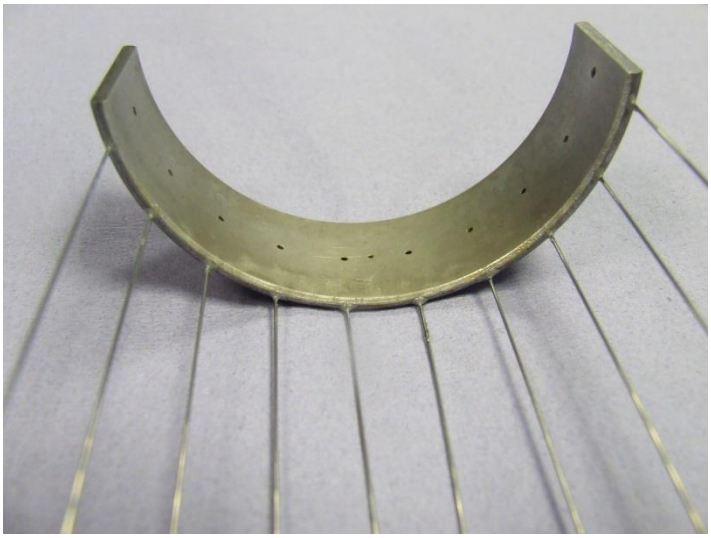
Figure 7.2: Photos of the multi-bearing rig setup (a) front view when chilled (b) rear view



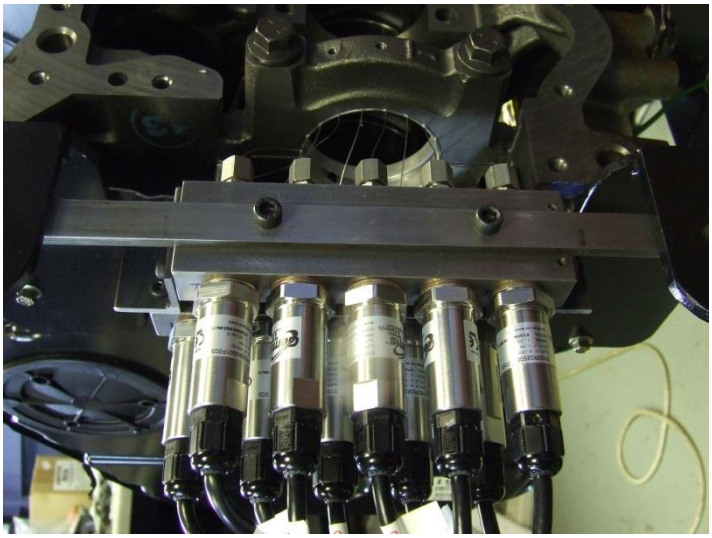
(a)



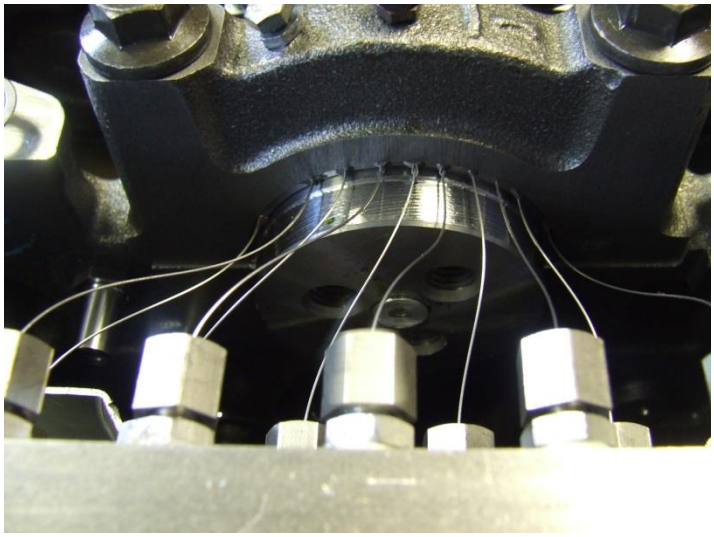
(b)



(c)



(d)



(e)

Figure 7.3: (a) Exploded view of the rig crankshaft assembly (b) Straight shaft with the connecting rods and pistons assembled (c) Main bearing 1 instrumented for film pressure (d) Pressure transducer manifold (e) Main bearing 1 film pressure pipes

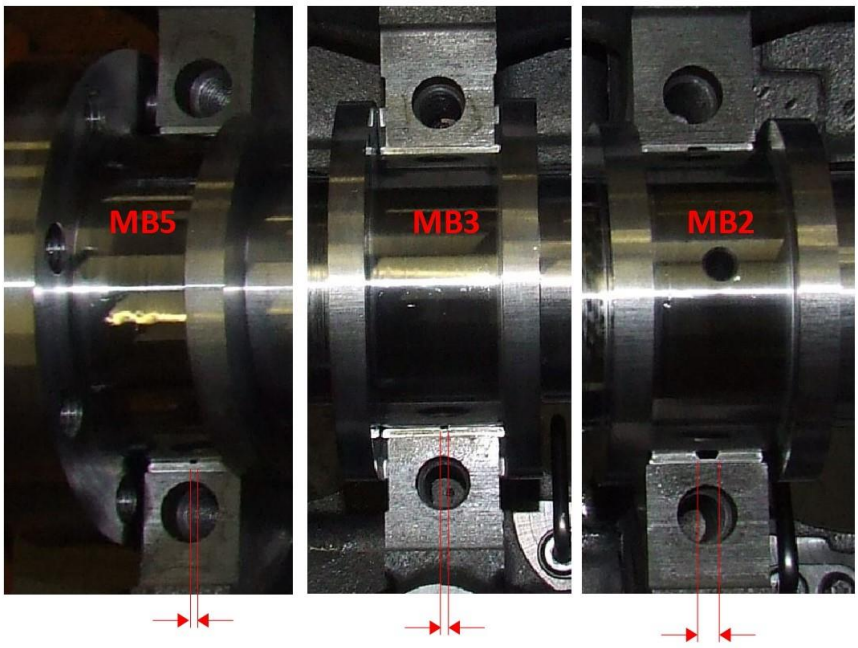


Figure 7.4: Groove widths of bearings 1,2 and 4 are larger than 3 and 5 due to oil supply to big end bearings via drillings in crankshaft

7.2.1 Test Rig Instrumentation and Calibration

The data recorded included crankshaft friction torque, speed and various pressures and temperatures. Oil pressure was measured at the pump outlet, in the main gallery and in the first main bearing film. The film pressure was measured using Gems 3100 series compact pressure transducers which measure gauge pressure. The film pressure distribution is similar to the one employed in the previous test rig. A pressure transducer was also used to measure the piston gas pressure. The pressure transducers were calibrated using a Budenberg dead-weight tester to give a linear relationship between pressure and output voltage as shown in Figure 7.5. The calibration equations have been used in the LabVIEW data acquisition system software.

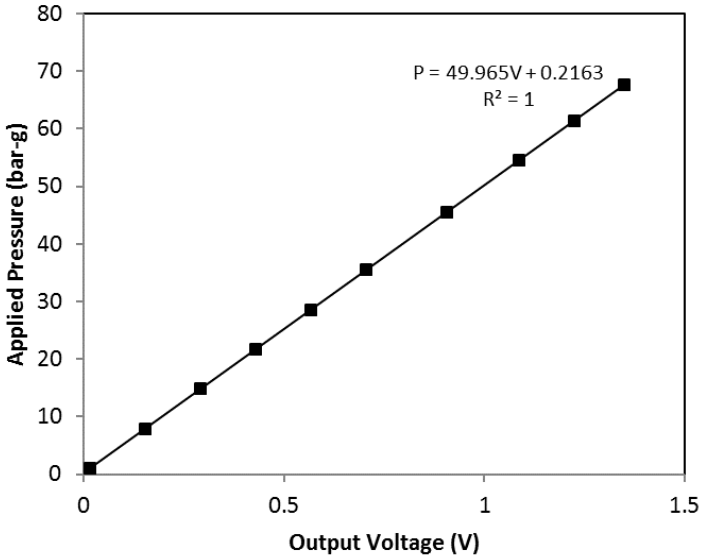


Figure 7.5 Calibration of a film pressure transducer

13 K-type Nickel-Chromium/Nickel-Aluminium thermocouple probes were fitted to the engine oil circuit in different locations to monitor the thermal state. Film and bearing shell temperature was measured in each of the five main bearings. The thermocouples were inserted through the bearing lower shells until flush with the inner surface of the shell. A thermocouple was also located at the back of each bearing shell to measure shell temperature. Temperatures were also measured downstream of the oil pump and in the main oil gallery. Thermocouple signals were amplified via AD595AQ thermocouple amplifiers, giving 10mV/˚C.

The applied gas load on the pistons was controlled via valves on a pressurised airline to the modified engine head. Crankshaft motor speed control was achieved via a speed control knob on the rig control panel.

Flow rate to the crankshaft bearings was measured using a Titan OG3 oval gear flow meter which has a range of up to 10 litres per minute. The flow meter was positioned at the outlet of the externally driven oil pump.

The data acquisition (DAQ) hardware consisted of a National Instruments (NI) AMUX-64T analogue multiplexer board, a NI CB-68LP board and a PCI-6036E DAQ board in the PC. A schematic of the hardware is shown in Figure 7.6. LabVIEW was installed on

the lab PC to visually monitor and control the data acquisition. It allowed interaction between the data acquisition devices and the PC.

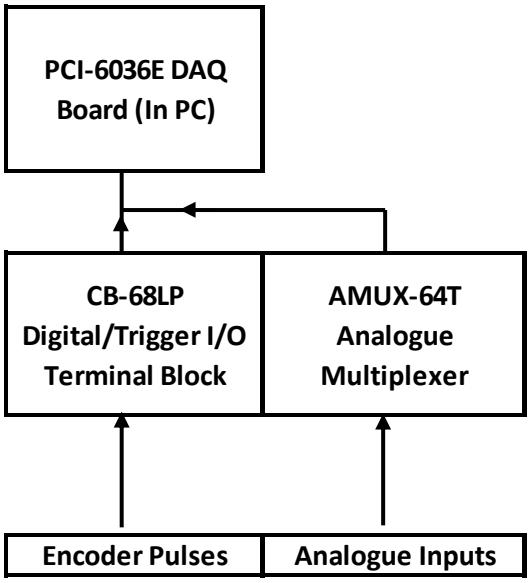


Figure 7.6: Schematic of data acquisition hardware

7.2.2 Friction Measurement

The work input required to motor the straight crankshaft assembly was measured using a strain gauge torque transducer which had a range of 0 to 160 Nm. To isolate flow to the main bearings, the piston cooling jets (PCJs) were blocked which required use of a smaller capacity pump than the original fitted on the engine to drive the oil around the modified lubricant circuit. Normally flow through the PCJs is much higher than through the bearings because of the small bearing clearances and having the PCJs open would have made it difficult to observe changes in bearing flow rate with feed pressure. The oil pump was remotely driven using an ABB inverter drive. The crankshaft oil seals were removed. Therefore, the motoring torque was required to overcome friction in the five main bearings and four needle roller bearings. The friction contribution from the needle bearings was determined using an empirical torque relationship developed by Timken [146]. It is found from this relationship that the total contribution from the four needle bearings is about 7 percent of the total crankshaft motoring torque under warm conditions which makes it a relatively small amount compared with the 5 journal bearing contributions.

The torque required to motor the main bearings is determined by:

$$\mathrm{T}_{5\ main\ bearings} = \mathrm{T}_{total} - (\mathrm{T}_{needle\ bearing} \times 4) \quad (7.1)$$

The friction contribution from the 5 main bearings can then be represented in terms of fmep by using Equation 7.2.

$$fmep = \frac{4\pi \mathrm{T}}{V_s} \quad (7.2)$$

7.2.3 Main Bearing Gas Load Distribution

The multi-bearing crankshaft rig allows application of a steady load on the crankshaft main bearings and individual main bearing loads have been calculated from in-cylinder gas pressure values using a statically determinate method. Assuming the shaft to be stiff, the distribution of load on the main bearings is shown diagrammatically in Figure 7.7. The main bearings spread the load symmetrically, such that the centre 3 take the same load (a quarter of the total each) and the outer 2 take the same (an eighth each). The calculated specific bearing loads for various steady gas pressures are shown in Figure 7.8. Specific loads for bearing 5 are slightly higher than bearing 1 due to a smaller projected area.

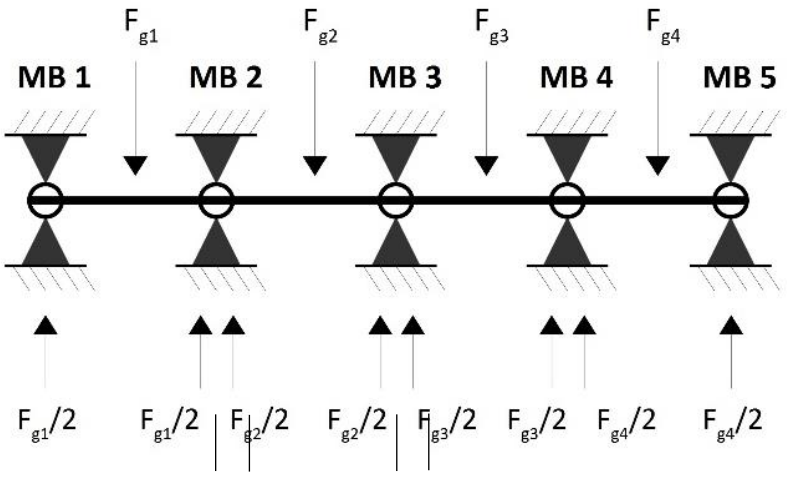


Figure 7.7: Main bearing load distribution (statically determinate method). Here F_g is the gas load.

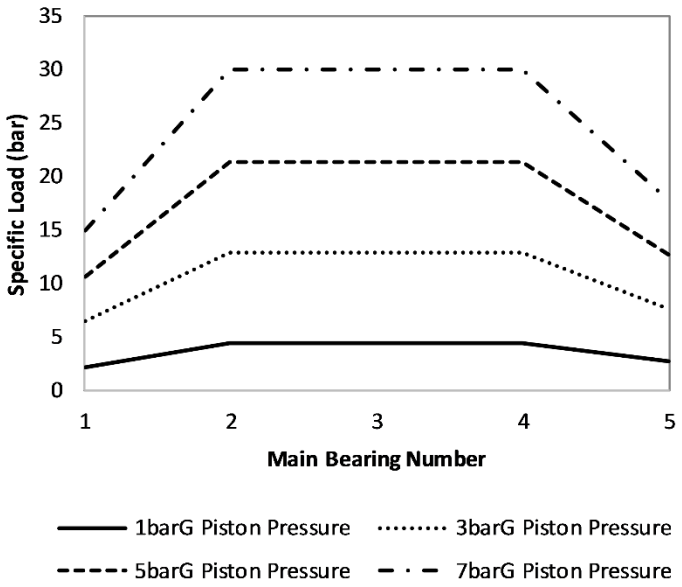


Figure 7.8: Main bearing loads for various applied in-cylinder steady pressures

7.3 Crankshaft Friction and Warm-Up Results under Reduced Oil Supply Pressures

The results presented in this section concern main bearing friction during warm-up. Initial tests investigating the effects of reduced feed pressure on motored crankshaft friction were carried out from a baseline main gallery pressure (abbreviated to **FP**) of 7.5 bar absolute down to no flow at load values of 1 (light load) and 5 (medium load) bar gauge cylinder pressure (labelled hereon as **PL**).

7.3.1 Crankshaft Bearing Friction Variation with Feed Pressure

A comparison of engine fmep variation during warm-up at the tested main gallery pressures and a light piston load of 1bar (SL=4bar) is shown in Figure 7.9. The mechanism by which the friction reduction is achieved is not solely or even mostly due to higher film temperatures reducing viscosity. To show this variation of fmep is plotted against the average oil film viscosity and this allows comparison in fmep due to feed pressure only (the effect of film temperature on bearing friction is excluded by this process). When plotted against viscosity the graph is read from right/cold end to left/warm end. Oil film viscosity is used since gallery oil viscosity poorly characterizes friction during early warm-up. The rate at which bulk oil temperature

(represented by main gallery temperature) rises during the first few seconds is much smaller than the local oil film temperatures where significant rises occur due to frictional dissipation. This is shown graphically later in Figure 7.14.

During the warm-ups, the average dynamic film viscosity decreased from 160 mPas to 50 mPas and fmep approximately halved in value. This shows a strong dependence of engine rubbing friction on oil viscosity. There is a clear drop in fmep as the feed pressure is reduced from a baseline of 7.5barA down to 1.2barA. The experimental friction characteristic is linearly dependent on viscosity and gives a higher value than the theoretical prediction considering a concentric bearing. The theoretical estimate does not truly apply to the case as there are a number of bearings considered in the crankshaft rig involving a few uncertainties, for example distortion of the engine block due to thermal changes and effects of misalignment. The experimental fmep does not pass through zero if extrapolated and an explanation for this has been addressed previously in Section 6.7.

Figure 7.10 shows the percentage fmep reduction from baseline against viscosity and a fairly constant reduction in fmep is observed over the test viscosity range down to a gallery pressure of 1.2 barA. The mean percent benefit is calculated and is plotted against gallery pressure in Figure 7.11. The response of fmep to reductions in gallery pressure/oil supply rate was linear from 7.5barA to 2barA achieving a fmep reduction of 10% at 2barA (30% baseline flow). Further reduction in gallery pressure and flow produced a more significant and non-linear drop in fmep with the benefit reaching 13% at 1.2barA gallery pressure (20% baseline flow). This is a similar observation to the results obtained on the isolated bearing rig. The test performed at no flow condition (oil pump completely turned off) showed fmep behaviour different from the rest in that the initial benefit at no flow was 35% (Figure 7.10) which diminished down to 5% as the average film temperature reaches around 35 ˚C. An average percent fmep benefit of 23% is calculated for the no flow case over the viscosity range from 180 to 60 mPas.

When plotted against time, as shown in Figure 7.12, the results again showed that substantial and early reductions in friction torque could be achieved from cold

soaked start conditions by restricting the flow to the main bearings. The friction torque was highest immediately after the start of the test and dropped at a diminishing rate as the test continued and film temperature increased. The form of the torque variation with time reflects the reduction in oil viscosity with increasing temperature and possibly increases in clearance. The oil viscosity is especially sensitive to changes in temperature at low temperatures, therefore, the changes in friction are also more pronounced.

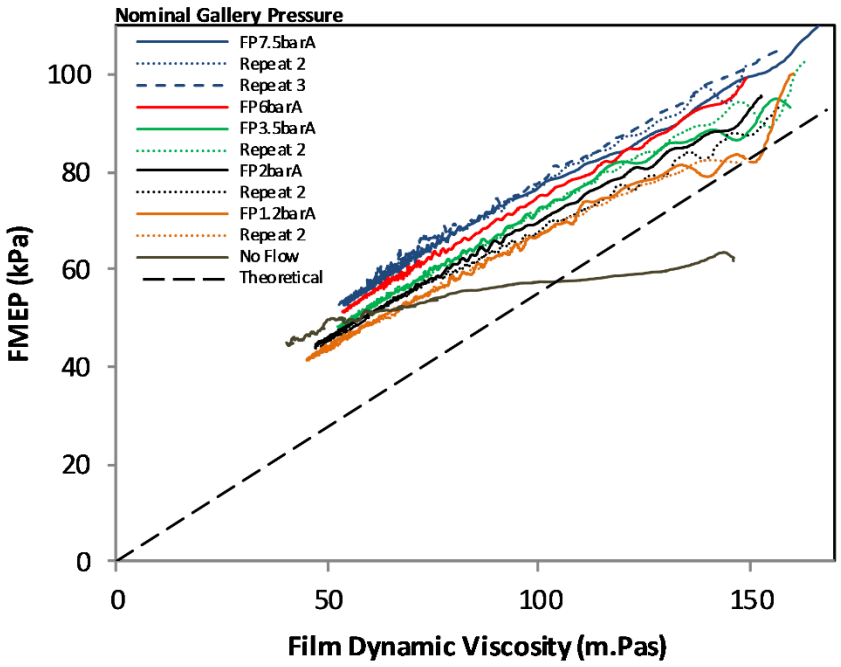


Figure 7.9: Fmep vs. film viscosity for decreasing gallery pressures

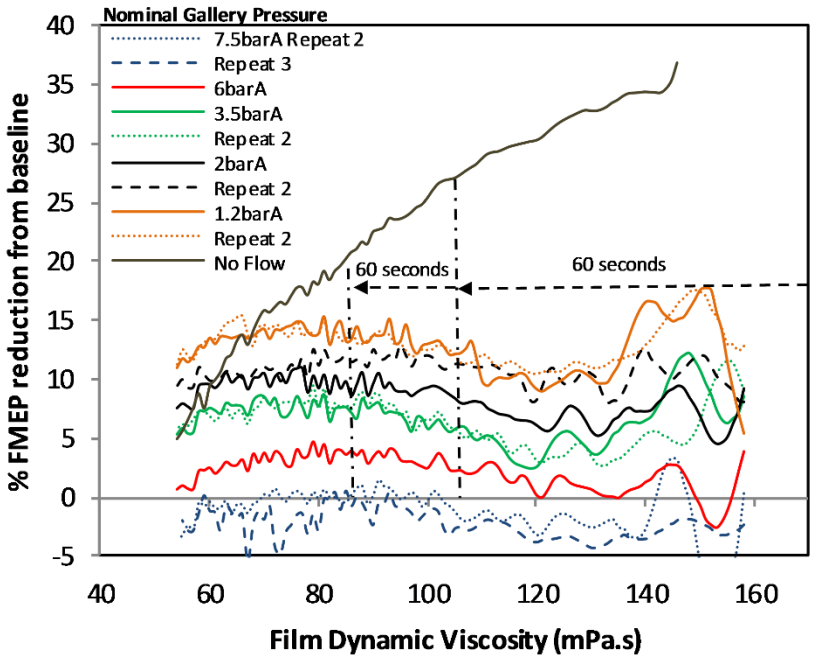


Figure 7.10: Percentage FMEP reduction from baseline test (PL=1barG, N=1000rpm and initial gallery temperature=5˚C)

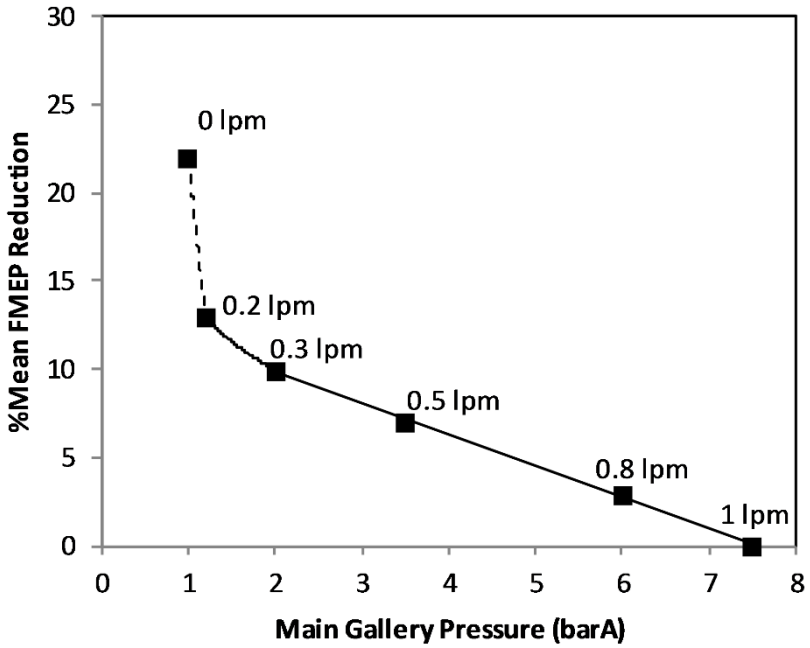


Figure 7.11: Mean percentage FMEP reduction from baseline over warmup from film temperature ~5->~35 ˚C (PL=1barG, N=1000rpm and initial gallery temperature=5˚C)

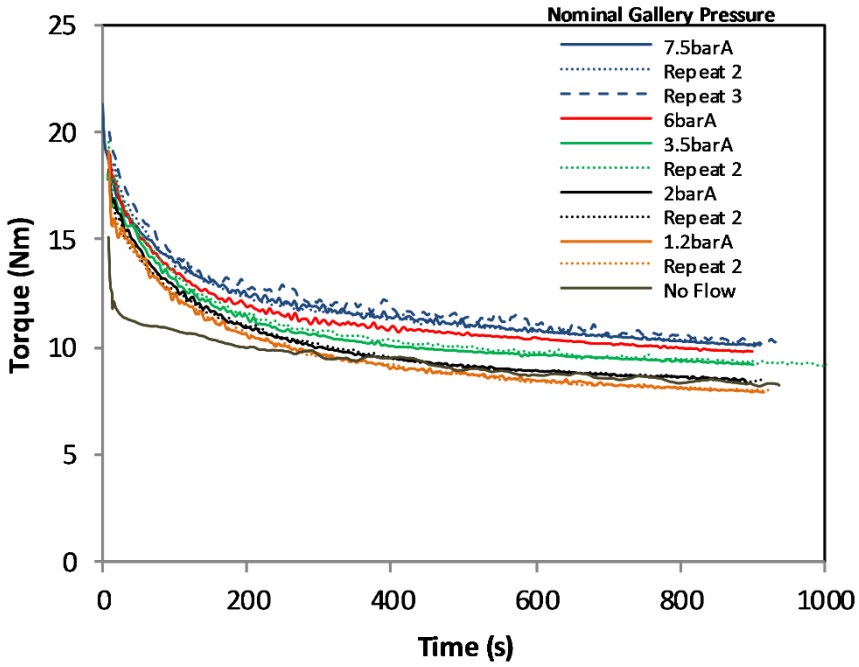


Figure 7.12: Comparison of motoring torques from start of test (PL=1barG, N=1000rpm and initial gallery temperature=5˚C)

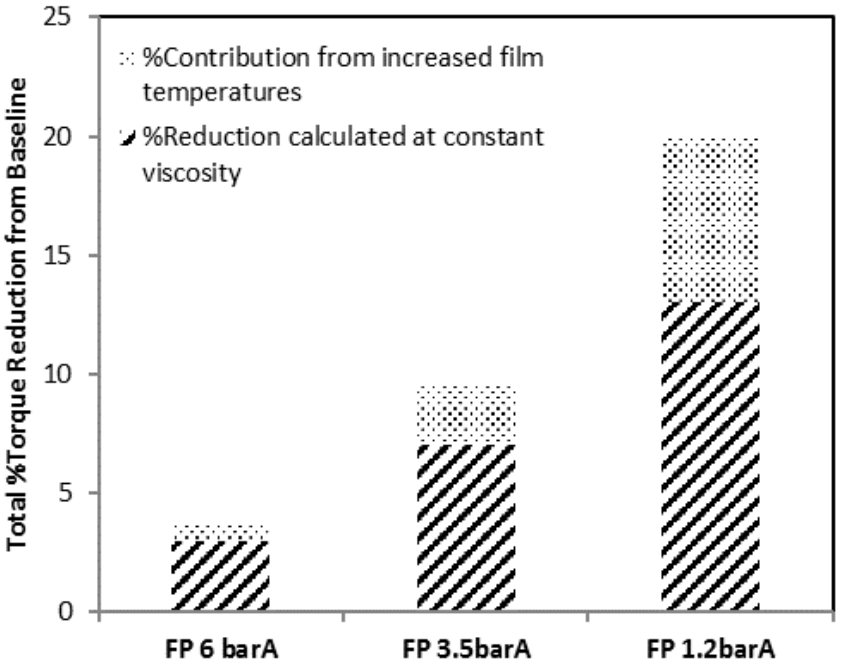


Figure 7.13: Relative contributions towards total %torque reduction (PL=1barG, N=1000rpm and initial gallery temperature=5˚C)

By plotting torque against time, the effects of increased film temperature are included in the torque reduction analysis and a higher total percentage friction reduction is observed than that calculated by the friction versus viscosity curve because of the reduction in oil viscosity associated with the increase in film

temperature. The individual contributions from increased film temperature and effects other than that under reduced flow conditions at the end of test are summarised in Figure 7.13. As feed pressure is reduced both iso-viscous contributions and increased film temperature contributions towards total torque reduction increase during early warm-up.

7.3.2 Main Bearing and Bulk Oil Thermal Interaction with Feed Pressure

The thermal interaction between lubricant oil and engine structure can influence the overall torque reduction that is obtained during warmup with supply oil pressure reduction. During the early phase of warm-up, as feed pressure is reduced, increases in local film temperatures provide additional torque reductions. Average film temperatures of the 5 main bearings at a light load of 1 barG load are presented in Figure 7.14. The maximum average film temperature increase at light load due to feed pressure reduction was ~10 ˚C at the no flow condition at the end of the motoring test. In these tests heat input to the lubricant was due to frictional dissipation within the bearing films only.

Here the highest differences between film and metal are found during the first few seconds due to heat from friction at the rubbing surfaces when the adjacent structure is still cold. Heat is conducted outwards into the surrounding structure, then the film warm ups together with the engine structure at less steep temperature gradients. During the early few seconds of the cold start, heat transfer is dominated by conduction [3] and the modest increases in film temperature occur as a result of decrease in convective heat transfer due to lower oil flow rates.

Further warm-up tests were performed with the use of electrical heating in the form of oil heaters placed in the sump to achieve higher film temperatures because friction heating alone was insufficient to achieve this. Variations in film temperature and torque are presented for a high and low feed pressure in Figure 7.15. The results show, similar to the previous test results, that film temperatures increase, though not very significantly, during the initial phase of warm-up due to reduced flow rates and reduction in convective heat transfer. However, as the warm-up progresses, bulk oil (represented by main gallery temperature) is seen to warm-up faster at the higher

flow rate. At higher flow rates, the rate of heat input from the oil heaters to the bulk oil is higher and furthermore the pump work is higher leading to faster oil warm-up. Around 60% of the structure mass is thermally connected with engine oil [147] resulting in a good thermal coupling with the structure. The faster warm-up of the bulk oil thus leads to a faster warm-up of the engine structure. Since the film temperatures are thermally clamped to the surrounding metal temperatures after the steep initial rise in temperature, a faster rise in film temperatures occurs at the higher flow rate.

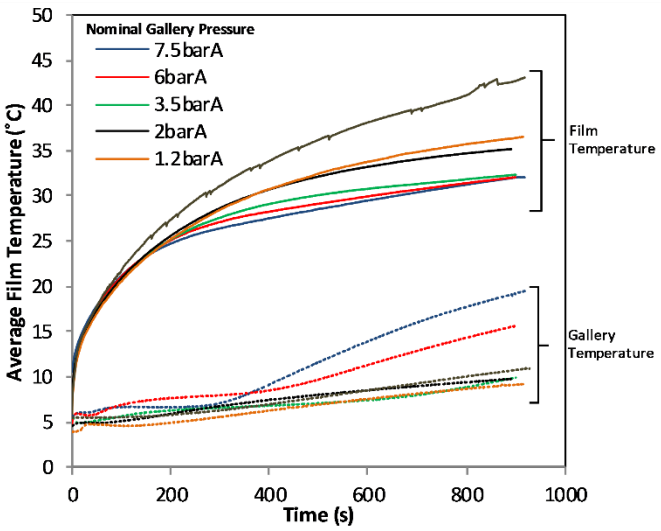


Figure 7.14: Comparison of average film and gallery temperatures from start of test (PL=1barG, N=1000rpm and initial gallery temperature=5˚C)

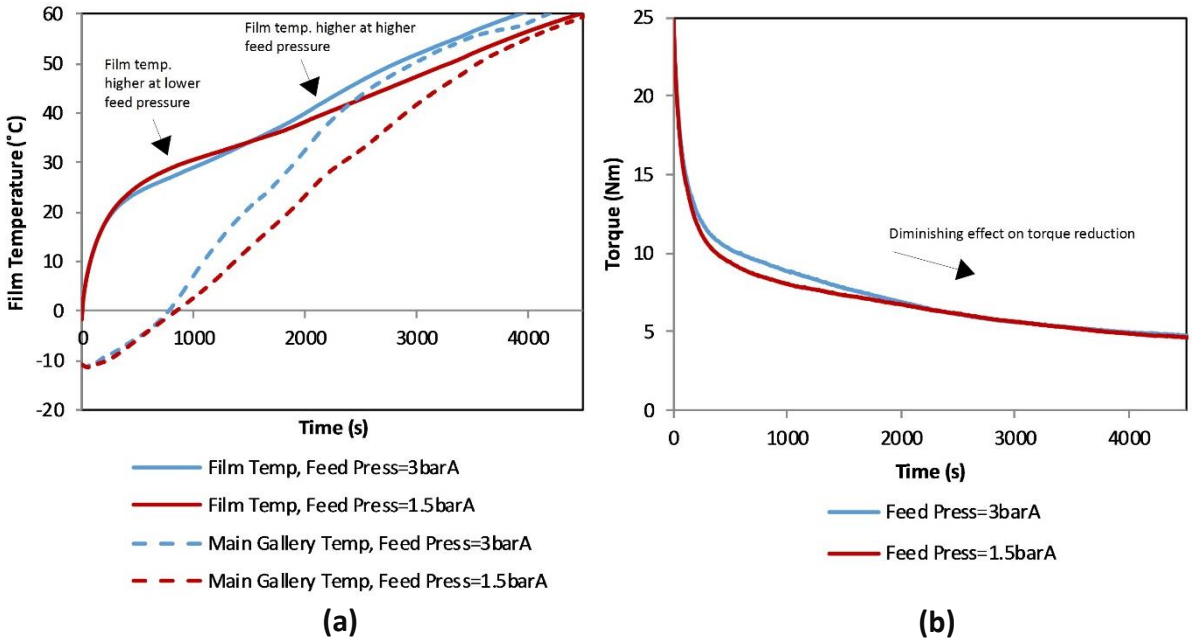


Figure 7.15: Tests with oil heaters (a) comparison of film and gallery temperatures at two supply pressures (b) crankshaft torques (PL=1barG, N=1000rpm and initial gallery temperature=-10˚C)

7.3.3 Film Pressure Variation

Experimental film pressure profiles for main bearing 1 are plotted in Figure 7.16 for a film temperature of 30 ˚C. The results show similar trends to data obtained on the isolated bearing rig and suggest an increase in cavitation as the supply pressure is reduced.

A higher peak pressure is observed at the higher feed pressure because of the significance of the hydrostatic force due to groove pressure compared with the hydrodynamic film pressure as has been previously explored. The groove pressure pushes down on the journal, therefore leading to a higher eccentricity and a higher peak film pressure.

For the no flow case, film pressure results indicate increases in eccentricity which can explain the diminishing of the torque reduction as previously presented. It is observed that peak film pressures increase and pressure transducers in the loaded region near the film reformation point start registering cavitation as the test progresses (Figure 7.16(b)). The increase in peak film pressures and eccentricity is due to a significant reduction in the load bearing film extent.

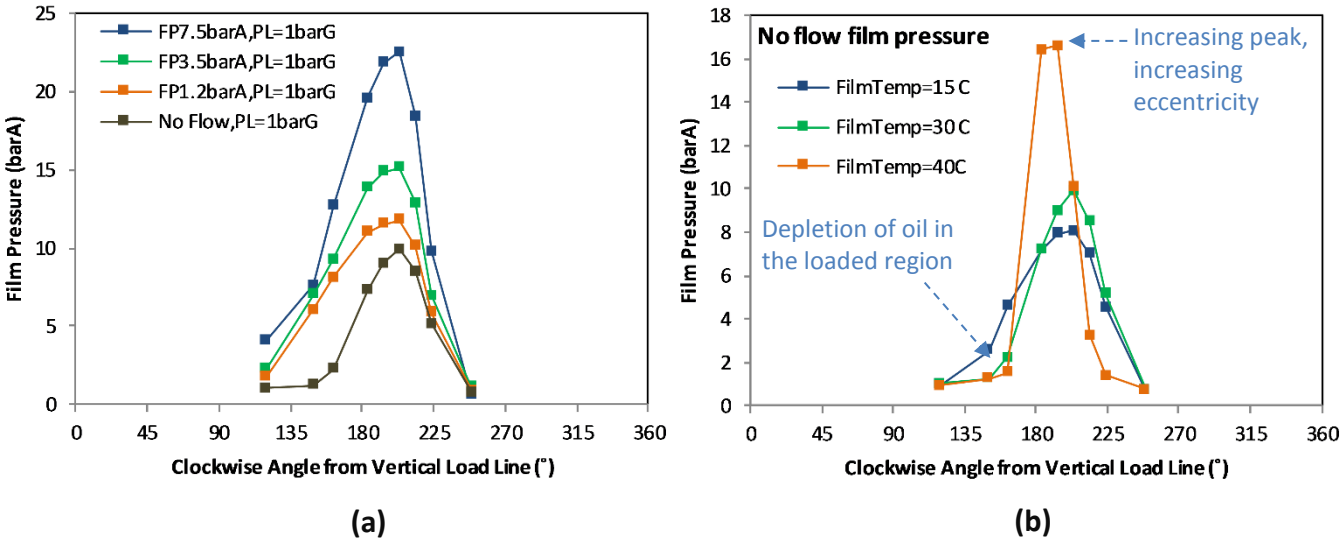


Figure 7.16: (a) Circumferential film pressure profiles (PL=1barG, N=1000rpm and Film Temp=30 °C) (b) No flow film pressure history

7.3.4 Bearing Friction and Failure at No Flow Condition

Tests performed with a piston load of 5 barG (SL=17 bar) show torque reduction benefits were obtained down to a feed pressure of 1.2 barA (20% baseline flow) without signs of bearing overheating or damage. For the same load with zero oil delivery (Figure 7.17), the oil film temperature and bearing torque showed no signs of distress before ~45s into the test but subsequently the turning torque remained at a steady value close to 17 N m and the film temperature gradient for film 3 started to increase. At ~70s, the film temperature rose very rapidly, from ~40 to >200 ^{o}C at which point the test was ended. The friction torque also rose significantly at this point. Post-test inspection of the bearing showed some burnishing and scoring damage to the shells occurred, as can be seen in Figure 7.18. The damaged shaft was replaced before conducting further tests.

Failure occurred in the central bearing first most likely because under high gas pressures it is the most critically loaded bearing (since it carries twice the gas load compared with the end main bearings) and has a small groove width.

The time taken for failure reflects the time taken for oil to be depleted from the main gallery, and subsequently from the bearing, resulting in contact. The increases in film temperature before contact occur due to high eccentricity ratios/high shear for bearing 3 as the film extent becomes smaller. At the higher load, the critical film

extent required to safely support the load is larger and oil side leakage occurs at a faster rate due to greater axial film pressure gradients. Both these factors contribute to an early failure at the higher load.

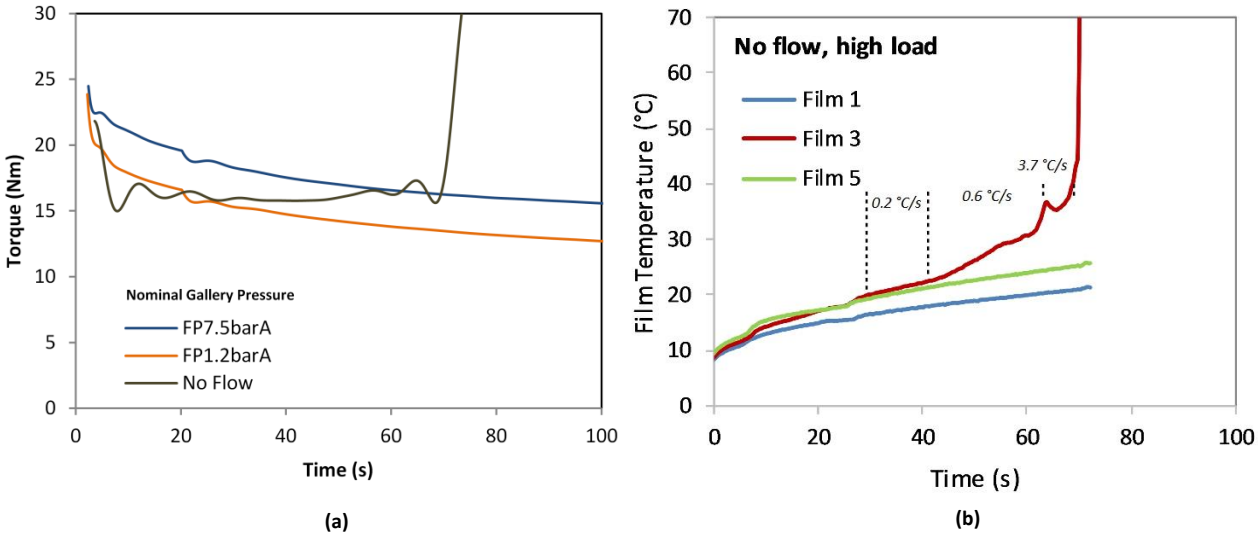


Figure 7.17: Failure at no flow, PL=5barG and N=1000rpm (a) Torque (b) Individual film temperatures at no flow and change in film temperature gradients before failure

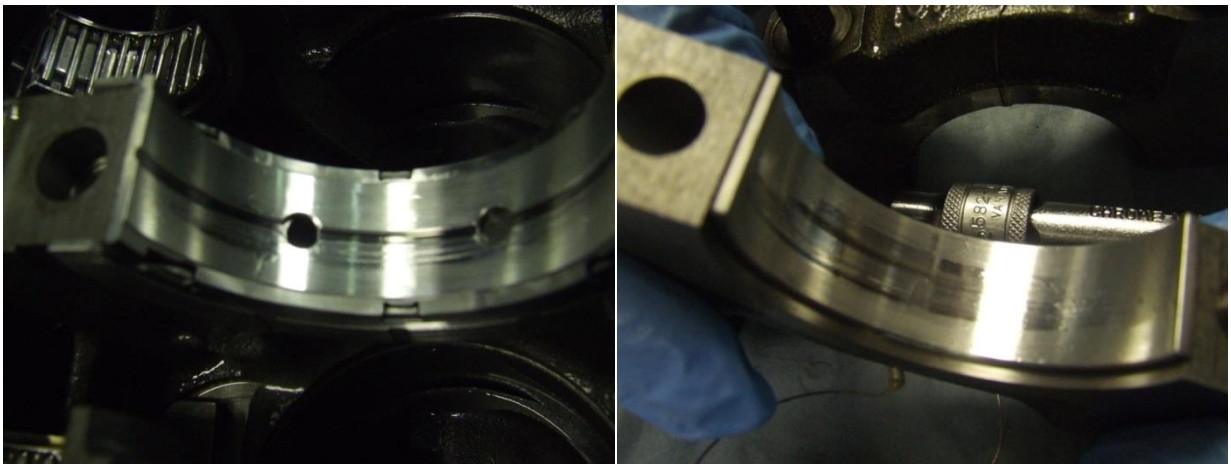


Figure 7.18: Shell scoring and burnishing damage produced during the failure of main bearing number 3

7.4 Response of Oil Film Temperature and Pressure to Increase in Main Gallery Pressure

Operating in starved oil flow conditions runs the risk of oil film temperatures rising at high rates especially at high oil supply temperatures. In the application of flow

control to engine bearings, a feedback mechanism could be employed to anticipate and prevent failure whereby film temperatures and temperature gradients are monitored and if they exceed safe values then increases in oil feed pressure can be used to bring the temperatures back under control.

For application of such a feedback system it is useful to know the time taken for the film temperatures and pressures to respond to changes in increased supply oil pressure. A test was performed at a steady piston load of 1 bar (SL=4 bar) where the oil pressure was varied between ~3 barA and no flow by turning the oil pump on for 5 seconds and keeping it off for 45 seconds.

Responses to oil pressure perturbations show small changes in film temperature especially under cold conditions (Figure 7.19(a)). This demonstrates a strong thermal coupling of the film to the surrounding metal temperatures. Film temperatures only start to rise steeply once the bearing film extent significantly reduces resulting in increases in eccentricity and local shear rates. This is evidenced in the film temperature trace under warm conditions where film temperatures in bearing 5 start rising steeply after 30 seconds of turning the oil pump off. Film pressure traces presented in Figure 7.19(b) confirm increases in peak film pressure and reduction in film extent due to oil starvation. This represents a state where the bearings are extremely starved and run the risk of contacting the journal.

Sudden increases in main gallery pressure to 3 barA brought the rate of temperature rise under control within 3 seconds. Film pressures recovered fully within 4 seconds of switching on the oil pump. Film temperature and pressure recoveries can be made even more quickly by improving the rate at which the main gallery pressure rises.

Overall the results indicate that film temperatures are thermally coupled to the surrounding structure and in the case of extreme oil starvation where film temperature gradients start to increase significantly, film temperatures can be brought back to safe limits quickly by increasing the supply oil pressure. The response time of oil film temperatures and pressures to oil feed pressure is small making a

temperature feedback oil pressure control system a viable option for preventing bearing failure under reduced oil flow rates.

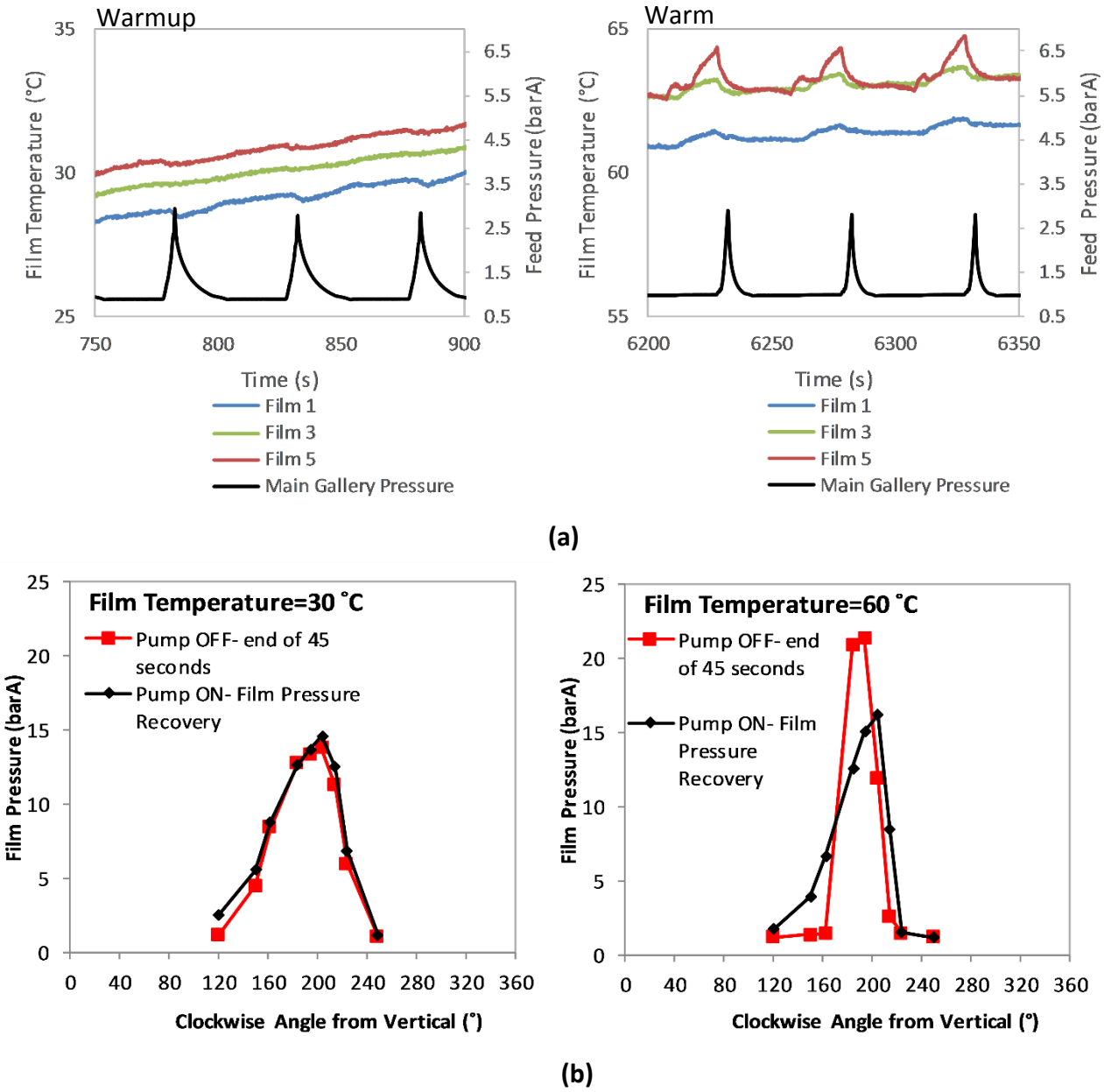


Figure 7.19: (a) Variation in film temperatures with main gallery oil pressure (b) Variation in film pressures with main gallery oil pressure. Test results at PL=1bar, N=1000rpm

7.5 Effect of Load and Reduction in Oil Supply Pressures on Crankshaft Friction

Further warm-up tests were performed covering a load range of PL=1 bar to 7 bar (SL=4 bar to 30 bar) and film temperatures of -10 ˚C to 65 ˚C at a shaft speed of 1000 rpm to investigate the influence of load on friction reduction with supply oil pressure.

Fmep variations with drop in supply oil pressure from 5 barA to 1.5 barA are presented in Figure 7.20 for increasing load values. Approximate %fmep reductions from baseline are illustrated in Figure 7.21 for cold and warm running conditions. Under cold conditions of sub-zero to temperatures of ~15 °C (Figure 7.20(a)), a friction reduction is observed at all loads tested. With increasing load, the %friction reduction is seen to diminish, most significantly at high temperature. The diminishing torque reductions can be indicative of increasing eccentricity ratios in bearings with reduction in supply pressure as a result of reduced film extents.

The film temperature gradient in the central bearing number 3 at a test condition of PL=5 bar and feed pressure=1.5 barA started to increase where the %fmep benefit had diminished at high temperature. This indicates levels of increased eccentricity and stress. The reduction in torque benefit could be attributed to a reduction in film extent in bearing 3 (which is carrying the critical gas load and is supplied by a small groove width) leading to increased eccentricities and shear rates contributing negatively towards friction reduction.

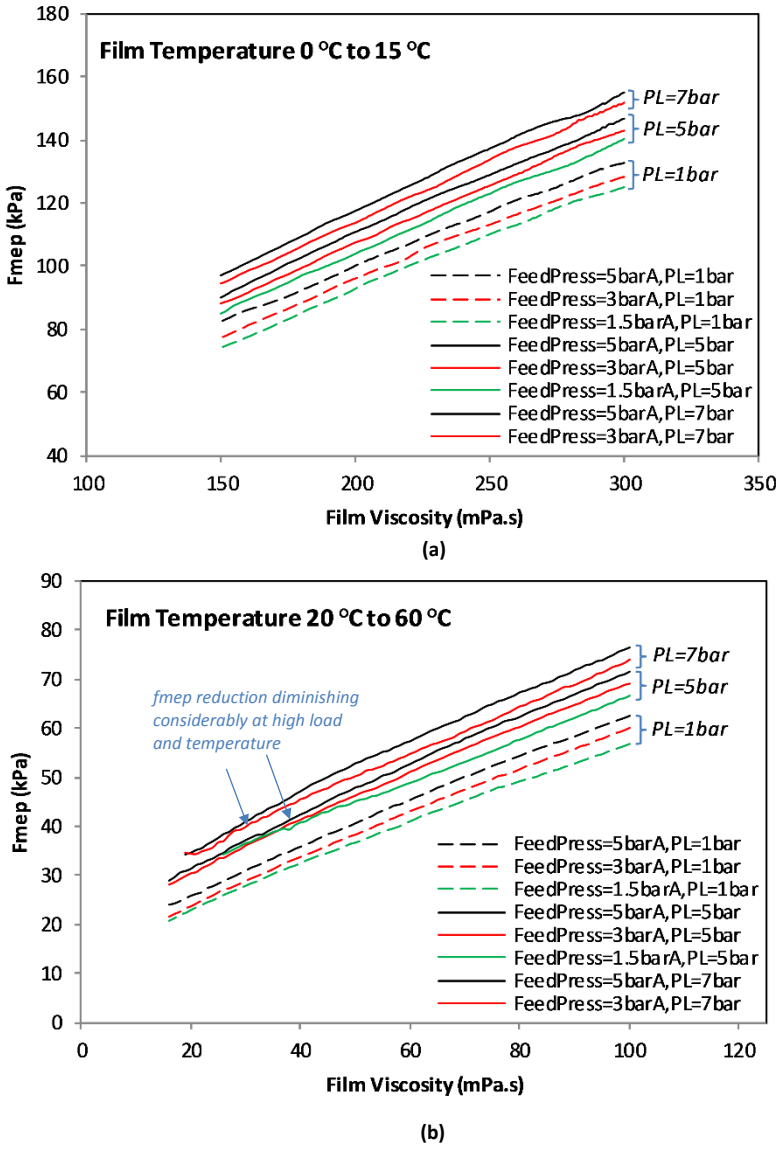


Figure 7.20: Fmep variation with film viscosity at increasing load values (a) Cold start region (b) Warm region

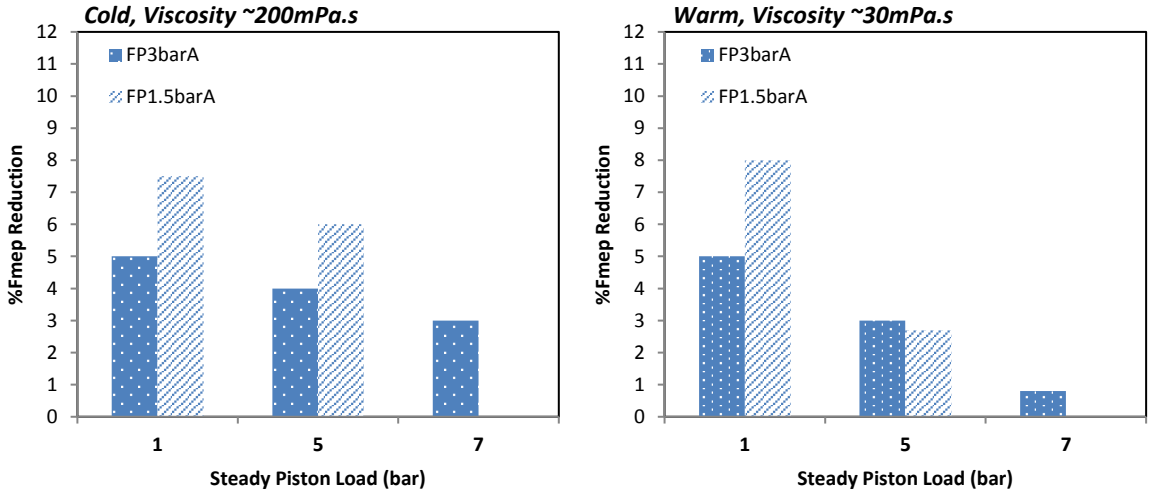


Figure 7.21: %Fmep reduction with load and feed pressure for cold and warm running conditions

7.6 Reductions in Oil Pump Work

On the test set-up employed, the oil pump was located off the engine and driven by a mains powered electric motor. Any change in oil pump work made no contribution to the reduction in measured crankshaft friction since the electric motors driving the crankshaft and the oil pump were both separate. Nonetheless, it is informative to consider the variation in pump work since it makes a significant contribution towards the engine ancillary load when it is mounted on the engine and driven off the crankshaft.

The pumping pressure in the warmup test cases was varied from 5 barA to 1.5 barA and this resulted in a variation in the pump flow delivery. The change in hydraulic power required results because of both changes in the pumping pressure and flow rate as given by the equation below:

$$\dot{W}_h = \Delta p \times \dot{V} \qquad (7.3)$$

In the current setup the piston cooling jets were blocked and reduction in total flow delivery was caused by reduction of flow and oil pressure to the main bearings and big-end needle bearings only. The variation in measured flow rate with main gallery pressure for increasing oil temperatures at pump outlet is shown in Figure 7.22. The reductions in pumping work from the baseline main gallery pressure are shown in Figure 7.23 against pump outlet oil temperature. For constant supply pressures, a bigger percentage reduction in pump work is achieved under warmer conditions since the difference in flow rates for different main gallery pressures is bigger. For conventional lubrication systems though, oil pressures are high under cold conditions and drop down as the engine warms-up. Reducing oil pressures with improved oil flow control can therefore potentially provide greater pump work reductions when the engine is cold.

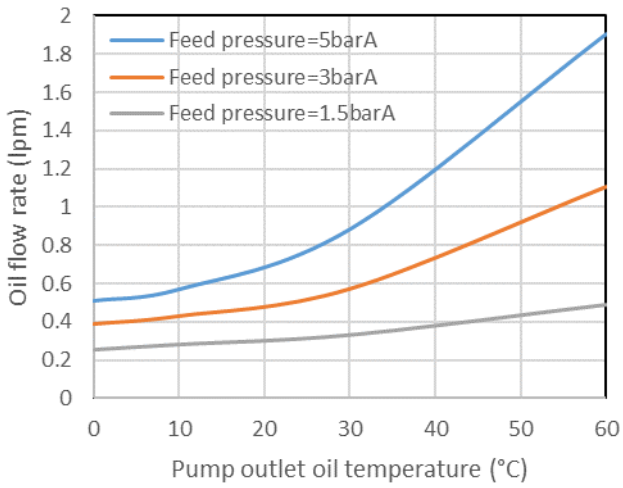


Figure 7.22: Variation in oil flow rate with pump outlet temperature

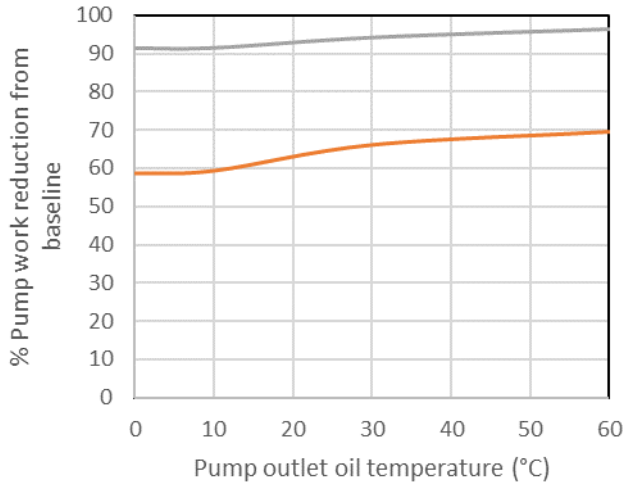


Figure 7.23: %Reduction in pump work as main gallery pressure is reduced

7.7 Discussion

Film viscosity characterizes crankshaft friction better than main gallery oil viscosity during early stages of warm-up. Film viscosities were calculated using the modified Vogel equation which better accounted for the effects of shear on oil viscosity compared with the standard Vogel equation. Comparisons of friction were made at fixed speed therefore influences of shear on viscosity would be similar in the tests. The effects of supply pressure on fmep at fixed viscosities are consistent with the results obtained on the isolated bearing rig. A reduction in friction was observed where the increases in the torque reductions became more significant at low supply

pressures at light loads. Film pressure data also confirms the findings presented in the previous chapter where peak film pressures reduced with reduction in supply pressure indicating a reduction in eccentricity and shear stresses within the film. This is again a consequence of reduced hydrostatic load on the crankshaft from the pressurised oil in the supply groove. Increases in cavitation area are also confirmed, especially under the no flow condition where pressure transducers registered cavitation pressures in the film reformation zone.

During warm-up, supply oil pressure affects the temperature variation of the main bearings. Film temperatures in crankshaft main bearings have a strong thermal coupling to the surrounding metal in the bearing support plates and the thermal mass of the crankshaft. During the first few seconds of running, film temperatures rise substantially due to frictional dissipation but then the rate of temperature rise is slower and is dictated by the temperature of the adjacent metal [148]. Increasing the bearing shell contact resistance has been shown to be a way to increase local film temperatures by reducing conductive heat transfer thus providing a friction benefit of up to 27% during cold starts [3]. In the present research, results have similarly shown that film temperatures are strongly coupled to the engine structure during early warmup. Reductions in oil pressure result in modest increases in film temperature during the early few seconds of warm-up as a result of lower convective heat transfer rates. These increases in film temperature add to the torque reductions obtained as a result of lesser film areas. The engine structure warms-up at a slower pace at lower oil pressures which results in the main bearings warming-up at a slower pace as well as the warm-up progresses. This can cause a penalty on the torque reduction that is obtained by reducing the oil feed pressure. Faster rates of oil warm-up at higher oil pressures have also been demonstrated on tests carried out on a firing diesel engine at the University of Nottingham. Here a drop in main bearing feed pressure from 3 barA to 1.5 barA yielded slower warm-up by a maximum of 5 °C when fully warm. Overall, however, an fmep reduction of ~15% was still maintained due to oil feed pressure reduction.

Responses to feed pressure perturbations show small changes in film temperatures also indicating a strong thermal coupling of the film to the surrounding metal. Film temperatures only start to rise at steeper rates when the film is extremely starved (also demonstrated in the no flow tests) and is approaching failure by contact as shown by increased cavitation and rise in peak film pressures. The quick recovery of film temperatures and pressures with increases in supply pressure indicates that a feedback mechanism can be implemented to maintain temperatures of the main bearings within safe limits at reduced levels of oil flow.

The effect of load on crankshaft fmep reduction with feed oil pressure was further explored for a wide range of film temperatures. %fmep reductions decreased as load increased- a similar observance to the single bearing results as well as that in reported literature [20, 66]. This could be a consequence of the reducing contribution from reduction in film shear towards total torque reduction as described in Chapter 5. The decreases in %fmep reduction become more significant at higher loads and temperatures especially at the lowest feed pressure of 1.5 barA. Under conditions of high load and temperature, operating eccentricities are very high reaching values close to 0.9. The high axial pressure gradients result in less oil recirculation within the bearing and hence a higher feed flow requirement to maintain sufficient film extent. When the feed pressure is low, oil starvation can occur in the bearings- the most prone being the central bearing which is supplied by a small groove width and is highly loaded. As a result eccentricity ratios can increase (rather than decreasing with supply pressure) causing large velocity gradients through the film thickness which offsets the friction benefit arising from decreasing film area (i.e. negative contribution from the shear term towards torque reduction).

The results indicate it is safer to operate under reduced flow conditions when engine and bearing film temperatures are cold and operating eccentricities are low. This is also more beneficial because friction losses are greatest when the engine is cold and therefore the reductions in friction are also more substantial compared with warm running conditions.

Reductions in hydraulic pump work are achieved by reducing the pump outlet fluid pressure and flow rate. It has been shown that operating at a feed pressure of 1.5 barA can result in pump work reductions of up to 97% when compared with a baseline of 5barA. Ancillary work is a penalty on the energy produced in the combustion chamber and by use of electric oil pumps operating at reduced oil supply pressures, not only is a friction reduction achieved within the bearing films but mechanical losses in pumping oil are also reduced.

7.8 Conclusions

- The effects of feed pressure reduction on bearing friction observed on the cylinder block rig are similar to that measured on the single bearing rig. Friction reductions are most significant under cold start conditions where oil viscosity is high.
- Fmep reductions with feed oil pressure reduction decrease as load increases. Fmep reductions diminish most significantly under high load, high temperature conditions.
- Trends in film pressures are also consistent with the isolated bearing rig results. Peak film pressures are observed to increase with feed oil pressure unless the bearing is starved of oil.
- In the case of oil starvation, full film reformation occurs in the load bearing region of the film leading to increases in peak film pressure, film temperature gradients and eccentricity. This leads to diminishing torque reductions and eventual bearing failure due to boundary contact.
- During warm-up, film temperatures and friction torque are influenced by oil feed pressure. As feed pressure is reduced, film temperatures initially increase but later rise at a slower rate as a result of the engine structure warming up slower at lower oil pressure and a strong thermal coupling between the bearing films and surrounding metal structure.
- Responses to oil perturbations show small changes in film temperatures demonstrating strong thermal coupling to surrounding metal.
- Oil pumping work and friction dissipation can be significantly reduced by reducing the oil supply pressure.

Chapter 8- Discussion and Conclusions

8.1 Discussion

The investigations reported in this thesis have quantified the friction reductions possible with reduction in pressure of the oil supply to plain bearings. The mechanisms which lead to these friction reductions, and the role of cavitation, have been explored.

The focus of the thesis has been bearing behaviour under steady applied loads. For a given supply pressure and oil viscosity, film patterns and friction torque were steady under steady loads. The dynamic effects of periodic load variations pertinent to bearing conditions in engines have not been examined and this is a limitation of the work for application to engine bearings subject to dynamic loading conditions. Under steady load conditions hydrodynamic lubrication and friction is due to the wedge effect only. Under dynamic load conditions, such as in crankcase main bearings, the squeeze mechanism adds to the wedge effect. The squeeze effect results in a substantial increase in bearing load capacity allowing crankshaft bearings to support large gas loads for short periods of time. Fired engine data acquired at the University of Nottingham on a diesel engine [97] has shown that the peak gas loads last for a short period of ~0.025 s where the main bearings sustain loads of the order 10^4 N. Here if the squeeze action did not exist, bearing eccentricities would reach values close to 1 i.e. failure by contact per short bearing steady load analytical calculation. Furthermore, literature presented in Chapter 2 suggests that the squeeze term provides a relatively smaller contribution towards the total bearing friction loss averaged over an engine cycle and becomes of less significance as the engine speed increases [44]. Since bearing friction losses are anticipated to be dominated by the wedge effect, friction reductions measured using these steady load test rigs are expected to be comparable to the dynamically loaded case. Still some caution needs to be taken when interpreting the results for the dynamic load case of a firing engine as the steady load rigs have not accounted for dynamic effects.

One of the main themes of investigation in this thesis was the cavitation behaviour of fluid films in bearings and the role of increased cavitation on friction losses as the

supply pressure is reduced. As described in Chapter 4, visualisation of the film revealed that for a 180° circumferentially grooved bearing when loaded, steady gas cavities occurred between streamers of oil in the unloaded region of the bearing on either side of the feed groove. Reductions in oil supply pressure led to increases in the areas of these cavitation zones in the unloaded region and gradually to the loaded region when extremely starved, particularly due to the movement of the film reformation point. Increases in cavitation have also been confirmed by film pressure measurements on both test rigs. A fully-flooded condition (zero cavitation) was not observed under loaded conditions for the maximum tested supply pressures of 3barA. This occurred due to the presence of negative film pressures leading to the formation of gas cavities which were not fully suppressed at the maximum oil supply pressure tested. A fully flooded condition was only observed for the unloaded case. For loaded conditions, a fully flooded condition is likely to be achieved by further increasing the supply pressure allowing the oil film to spread further backwards into the sub atmospheric film pressure zone eliminating cavitation areas. The flow/feed pressure requirement to maintain a bearing fully flooded is expected to become higher as load and speed increase since increases in both these parameters lead to shorter film extents and increases in cavitation area (indicating a greater hydrodynamic requirement). Forcing the bearing in a fully flooded condition is not ideal as increasing the film extent in the unloaded bearing region does not increase load capacity and only leads to increased frictional losses and additional pumping work.

Lubricant oils generally contain dissolved gas at atmospheric pressure. The amount of dissolved gas is dictated by Henry's law [149] which states that the solubility of a dissolved gas in a liquid at constant temperature is proportional to the partial pressure of the gas above the liquid. When the fluid pressure drops below gas saturation pressure, the dissolved gas diffuses out of the liquid leading to gaseous cavitation. As temperature increases, solubility of gas in liquid decreases hence more gas diffusion could be expected at higher lubricant temperatures.

Experimental evidence suggests that, under steady load conditions, the nature of cavities in the bearing film is likely to be gaseous rather then vapour. The cavities were stable and the recorded film pressures in the cavitation zone did not reach values close to lubricant vapour pressure. Furthermore, there were no signs of erosion damage which might be associated with vapour bubble implosion. For vaporous cavitation to occur, the fluid pressure has to fall below vapour pressures of its fractional components. This leads to instantaneous cavity formation. The 'cavitation number' is used for predicting the incipience of vaporous cavitation, for bearings, at given temperature, the equation is given as:

$$Ca = \frac{p_{\infty} - p_{vap}}{\frac{1}{2}\rho U^2}$$

where p_{∞} is the film pressure, p_{vap} is the fluid vapor pressure and U is the journal surface velocity. As cavitation number drops to a critical value, vaporous cavitation ensues. From the above equation a reduction in film pressure or increase in speed both reduce the cavitation number. This agrees with the experimental findings as increases in speed led to increases in observed cavitation on the Perspex bush.

Increases in cavitation area were found to have a significant impact on torque reductions as supply oil pressure was decreased. This is because of the significant difference in viscosities of the lubricant and expelled gas. Reductions in friction torque were calculated at fixed film viscosities to demonstrate that friction reductions occurred due to mechanisms apart from changes in film temperature. The reductions in friction have been shown to be associated with both decreases in film area and circumferential average shear stress. For the high loads experienced during typical engine operation, friction reductions are expected to be mostly due to reductions in film shear area.

The tests performed showed that grooving arrangement can play a significant role in the response to changes in supply pressure. For axial feeding grooves located perpendicular to the load line, increases in eccentricity and peak film pressures have been reported with supply pressure reduction. On the other hand, with a 180°

circumferential groove, a reduction in eccentricity has been found as confirmed by peak film pressure reduction on both test rigs. The large groove extent helps maintain large film extents even at low supply pressures preventing starvation damage in addition to its role of distributing oil to the big end bearings via crankshaft drillings in an engine.

Investigations of the effects of oil viscometrics, described in Chapter 6, show that significant reductions in rubbing friction are achievable by lowering the oil viscosity at a given temperature. Varying the grade of oil from a standard 5W-30 to lower viscosity lubricants resulted in up to 45% reduction in friction. Since engine bearings operate in the hydrodynamic regime, viscosity plays an important role in determining their frictional dissipation. From the data recorded in the tests, friction torque was shown to exhibit a linear relationship with the oil film viscosity. The effect of increases in feed pressure at the tested viscosities was to increase the friction torque which results predominantly because of increased shear area of lubricant in the bearing. The gradient of the best-fit lines through torque and viscosity points remained similar with increases in feed pressure, however, increases in absolute values occurred. Overall, the effect of changes of viscosity on friction dominated the effect of changes in feed pressure.

When selecting a low-viscosity lubricant, it is important to consider that the same oil is used to lubricate various engine components, some of which operate in the mixed/boundary lubrication regime e.g. the piston assembly, valve train. Since lower viscosity oils result in thinner hydrodynamic oil films, excessively low viscosities could increase boundary friction contribution elsewhere. The viscosity of the lubricant should ideally be such to minimize hydrodynamic friction while keeping boundary friction to a minimum as well. Viscosity modifiers are added to thinner base oils to make them more viscous under high temperatures and alter the viscosity-temperature relationship. Under conditions of high shear, viscosities can reduce further due to shear thinning leading to friction reductions. It is important to select appropriate viscosity modifiers to prevent irreversible viscosity loss due to disintegration of polymer chains.

Bearing failure due to oil starvation occurs as a result of the collapse of the hydrodynamic film and subsequent loss in load bearing capacity. If the full width oil film extent reduces sufficiently due to oil flow reduction that the film reformation point moves into the loaded region of the bearing, the minimum film thickness begins to gradually decrease. At the same time the film pressure profile becomes spiked as was shown on the crankshaft rig results for the no flow condition. The reductions in film thickness lead to increased shear stresses within the film which tend to negate the effects of increased cavitation on friction reduction. Due to an inadequate film thickness, asperity to asperity contact eventually occurs leading to a mixed and ultimately boundary lubrication regime. Under high loads, heat generation at the asperities becomes excessive. This can lead to welded joints being formed in isolated places causing scoring and roughening of the surfaces. Bearing wear leading to increases in surface roughness reduces the load capacity of the journal bearing. If the shaft is allowed to rotate under boundary conditions, welding between contacting asperities can lead to bearing seizure.

For journal bearings operating under reduced oil flow conditions, the minimum film thickness is the critical parameter for safe operation. The criteria for minimum film thickness or the critical eccentricity ratio for safe operation is dependent on the surface roughness which itself is dependent upon the machining process and journal bearing diameter. The surface roughness of the journal is more critical since it is hardened and polishes the softer bearing surface. According to the works presented in [84] and [85], the value of film thickness at which asperity contact is expected is where the peak roughness's of mating surfaces come intact. A safe value accounting for the effects of slight misalignment and debris in lubricating oil results is taken to be 2 or 3 times the failure value of film thickness. An approximate value of minimum allowable film thickness for a ground shaft of 50 mm diameter with a centre line average surface roughness of 0.2 µm is expected to be around 7 µm. This translates to a maximum safe operating eccentricity ratio of ε=0.86 (including the safety factor) with failure expected at ε=0.95 for a radial clearance of 50 µm.

It was also shown on the motored engine friction rig that during the first few tens of seconds, main bearing film temperatures rise rapidly due to frictional dissipation while the surrounding metal is still cold. As time progresses, the rate of film temperature rise decreases and is closely coupled to the surrounding structure.

Conventional engine oil pumps are designed to typically deliver oil at 4 barA under fully warm conditions. This results in the main gallery oil pressures being very high under cold conditions, around 7 barA limited with the use of relief valves. The studies carried out in this thesis have demonstrated that reducing oil supply pressures, especially under cold start conditions at low loads can provide substantial friction reductions (~15-20%) during warm-up. This would be most suitable for instance when the engine is idling under cold conditions. Though the rate of bulk oil and film warm-up is hampered to some extent by reducing flow rates, warm-up tests on a firing diesel engine have confirmed that friction reductions are still dominant. Passenger cars in Europe spend a significant amount of time in the warm-up phase as average journey lengths are small. A study carried out by Jarrier et al. [150] stated that the average car trip length in Europe is approximately 10 km. Another study carried out by Andre [151] in three European countries suggested that most journeys performed in Europe are completed before the engine reaches fully warm temperatures. The application of low oil supply pressure systems can therefore have a wide impact on improving fuel economy of passenger vehicles and yield substantial reductions in CO_2 emissions.

The extent of cavitation in a bearing was found to show a quick response to increases in oil feed pressure. Visual tests have demonstrated that recovery of a starved bearing film can be achieved in two seconds while temperature measurements show that the increases in film temperature gradients due to oil starvation can be brought back under control within three seconds. A similar observation was found on the fired diesel engine tests performed at the University of Nottingham. A closed loop control system can therefore be used to monitor film temperatures and increase oil feed pressures when temperature gradients or absolute temperatures reach critical values to prevent irreversible damage to the engine. This system could be

implemented on a prototype engine to map out the limits of pressure reduction for a range of load and speed conditions.

For a conventional oil circuit, if the oil pressure in the lubrication system is reduced, the oil supply to the valve train and turbocharger will be affected as well. To allow these subsystems to receive lubricant at high oil pressure whilst maintaining reduced pressure to the main bearings, modifications to the oil circuit are required. Such a modification has been demonstrated on the prototype diesel engine at the University of Nottingham [137] where low feed pressure oil was only supplied to the oil gallery feeding the crankshaft main bearings, big end bearings and piston cooling jets whilst supplying the valve train and turbocharger at high oil pressure. Further modifications are also possible, for example, the nozzle size and threshold pressure of the oil jets can be varied to prevent over-heating of the piston assembly in case of high loads.

Since oil is quite viscous, especially when cold, significant reductions in parasitic oil pump work losses are possible by reducing the oil flow rate. More than 50% reduction in pumping loss is achievable by reducing main gallery pressures from 5 barA to 1.5 barA during a cold start warm-up as demonstrated in the test results shown in Chapter 7. Zhao [147] has previously reported a 2% reduction in fuel consumption by reducing main gallery oil pressures from baseline NEDC values to a constant value of 3barA over a NEDC test cycle using an electric oil pump. Electrification of the oil pump allows speed independent pump operation [107] and with the advent of 48V pumps [152], the application of these is becoming more practical and efficient in a 48V mild hybrid vehicle architecture. Energy recovery technologies such as kinetic energy recovery (KERS) during braking and exhaust heat energy recovery can be used to supply energy to a 48V lithium ion battery from which the oil pump is driven to further improve the fuel economy. One of the disadvantages of using electric oil pumps is the increased cost as its function essentially requires more sensors and measurements to monitor engine parameters such as oil pressure and temperature.

8.2 Future Work

The experimental film pressure and visual data acquired as well as evidence provided in literature point towards a gaseous nature of cavitation under steady load conditions. This could be demonstrated with more certainty in the future by increased film pressure instrumentation in the cavitation zone both on the centreline and at some axial distance from the centre. The pressure variation within the cavitation zone would help establish with more confidence the nature of cavities and whether pressures equal to lubricant vapor pressure are reached at some point in the cavitation zone. Test bushes with increased instrumentation for film pressure have been manufactured for future testing.

Increases in cavitation area have been identified as a major source of reductions in friction torque with reductions in supply oil pressure. It is of great interest to explore methods other than feed pressure control to vary the amount of degassing and extent of cavitation. One area of exploration is the influence of the aeration content of oil on cavitation, friction torque and film pressure distribution and whether increased levels of aeration lead to an accelerated rate of erosion damage. The setup which allows oil to be aerated has already been commissioned on the single bearing rig and consists of an aeration stone in the oil tank connected to a line of compressed air which aerates the oil. A sight glass is used to visually observe the feed oil bubble consistency. Oil samples are taken at time intervals to estimate the percentage aeration by virtue of change in volume of the oil sample as it loses entrained air with time.

Apart from cavitation area, variations in journal eccentricity have also been shown to influence the total friction reduction with changes in oil pressure. In this thesis, a numerical method has been used to calculate the changes in eccentricity ratio with supply oil pressure. The bush can be instrumented with proximity probes in the horizontal and vertical planes which can provide data on bush displacement. The changes in eccentricity with variations in operating conditions as well as other parameters including surface roughness can then be experimentally measured.

Future work on the influence of dynamic loads on bearing friction to better match the conditions of an automotive main bearing and account for squeeze film effects should be considered. Dynamic loading might be achieved by employing a cam driven load mechanism to apply an oscillating force on the test bush. By use of a dynamic loading setup the response of cavitation to dynamic loads could also be investigated and with the measurement of cavitation pressures, the effect of dynamic loads on the nature of the cavities could also be established to some certainty.

In an engine structure, automotive main bearings consist of two shells which are assembled together by clamping the main bearing cap to the engine frame. The clamping force is essential to keep the shells firmly in place and allow maximum heat transfer to surrounding metal structure. Due to this clamping force the circularity of the bearing is distorted to an elliptic 'lemon-bore' shape with increases in clearance near the split line. This can influence flow rate into the bearing and the split line can disrupt the hydrodynamic film. The effect of the split line and elliptic clearance shape on friction, film pressure distribution and flow rate can be studied on the single bearing rig which can provide guidance on whether changes in the bearing shape could be exploited to improve performance.

As detailed in the literature review, improvements in load capacity and friction coefficient in tribological contacts are possible by introducing controlled micro textures on the surfaces. The effects of surface texturing have been experimentally researched more extensively on the piston ring-cylinder liner interface compared with journal bearing thin films. The single bearing test rig can be used in the future to investigate the influence of texture design on the hydrodynamic performance of plain bearings. Laser surface texturing offers an accurate method to create texture patterns on test shaft and bushes.

8.3 Conclusions

Major findings from the work carried out in this thesis are presented below. They have been divided into two sections. The first one relates to the more fundamental aspects mostly drawn from the work on the single bearing rig. The second set of findings focuses on journal bearings in an engine block environment. The most substantial contributions to knowledge derived from the work presented in this thesis are highlighted in bold.

Fundamental Findings

- **Reducing the pressure of the oil feed to a plain short bearing can reduce the friction torque substantially.** For an automotive crankshaft main bearing with a 180^{o} circumferential groove, reducing pressure from 3 barA to 1.1 barA reduced the friction torque by up to 20% under light steady loads. The potential to reduce running losses is therefore substantial.
- **Reducing feed pressure increases the cavitation area and reduces pressure in the low-pressure zone of the film. These changes reduce friction torque by reducing the film area and eccentricity ratio.** The reduction in eccentricity ratio contributes to the reduction in friction torque by reducing the circumferential-average surface shear stress.
- Under steady load conditions, experimental evidence (stable cavitation pattern and slightly sub-atmospheric pressure in cavitation zone) suggests that cavitation most likely consists of degassed air.
- The influence of oil feed pressure and friction reduction is sensitive to load and less sensitive to speed. As load increases, reducing oil feed pressure produces a diminishing reduction in friction. The reduction in film area due to increased cavitation becomes the dominant mechanism producing a reduction in friction. This can be attributed to the diminishing contribution from the reduction in average surface shear stress with feed pressure reduction.
- Increases in load, supply pressure (unless extremely starved) and radial clearance (unless extremely tight) lead to increases in peak film pressures and eccentricity

ratio. Increases in speed and oil viscosity result in reduced peak film pressures and eccentricity ratio.

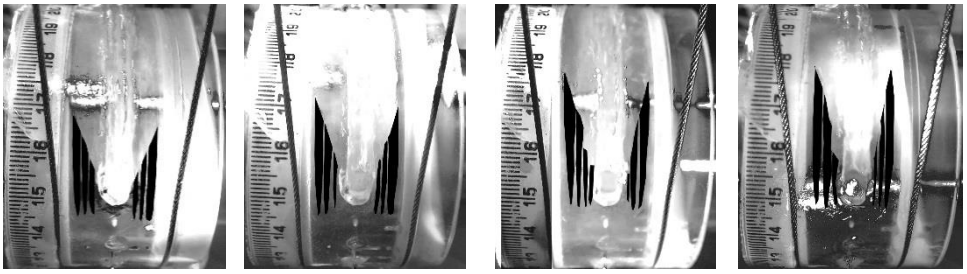
- Under conditions of oil starvation such as oil supply shut off, the film reformation point extends into the load bearing region of the film resulting in increased eccentricity (as reflected by increases in maximum film pressures) which results in diminishing torque reductions, increasing film temperature gradients and eventual failure by boundary contact.

Engine Block Findings

- The trends obtained for fmep reduction with supply pressure at given film temperatures on the motored engine rig were consistent the results obtained on the isolated bearing rig. Oil pressure reduction under cold start conditions provides the greatest reduction in friction within the bearings as well as parasitic pump work losses. Increases in load similarly led to smaller %fmep reductions.
- **Engine main bearings have strong thermal coupling with the surrounding metal structure. The thermal interaction of the main bearing films with the engine structure influences bearing warm-up and the overall torque reduction that can be achieved- higher oil flow rates result in faster warm-up of the engine structure and main bearings which lowers the oil film viscosity.**
- Oil pressure perturbations result in small changes to the main bearing film temperatures also demonstrating a strong thermal coupling of the film temperatures with the surrounding metal. When approaching high eccentricities due to oil starvation, increases in oil pressure to baseline values results in quick recovery (<2 seconds) of film temperatures and pressures.
- **Significant reductions in oil pumping work (>50%) are achievable by operating at reduced feed pressures especially under cold start conditions when oil is more viscous.** This leads to reduced parasitic losses apart from the reduced mechanical losses experienced within the bearings. Losses from oil splash and crankshaft windage are also reduced.

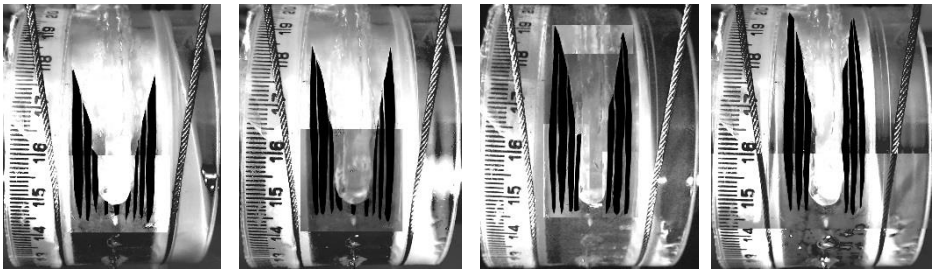
Appendix

SL=4.3bar, Feed Pressure=3barA



400rpm *600rpm* *1000rpm* *2000rpm*

SL=4.3bar, Feed Pressure=1.5barA



400rpm *600rpm* *1000rpm* *2000rpm*

Figure A1: Variation in cavitation patterns with increase in speed

References

1. Reynolds, O., *On the Theory of Lubrication and Its Application to Mr. Beauchamp Tower's Experiments, Including an Experimental Determination of the Viscosity of Olive Oil.* Philosophical Transactions of the Royal Society of London, 1886. **177**: p. 157-234.
2. Lang, O.R., *Friction Losses in Combustion Engines*, in *Limits of Lubrication*. 1982: London.
3. Shayler, P.J., Baylis, W.S., and Murphy, M., *Main Bearing Friction and Thermal Interaction During the Early Seconds of Cold Engine Operation.* Journal of Engineering for Gas Turbines and Power, 2005. **127**: p. 197-204.
4. Heywood, J.B., *Internal Combustion Engine Fundamentals*. International ed. 1988: McGraw-Hill.
5. Braun, M.J. and Hannon, W.M., *Cavitation Formation and Modelling for Fluid Film Bearings: A Review.* Journal of Engineering Tribology, 2010. **224**(Part J): p. 839-862.
6. *Road transport: Reducing CO2 emissions from vehicles*. Climate Action 2016; Available from: http://ec.europa.eu/clima/policies/transport/vehicles/index_en.htm.
7. Commission, E. *Climate Action: Reducing CO2 emissions from passenger cars*. 2008 13/01/2017; Available from: http://ec.europa.eu/clima/policies/transport/vehicles/cars_en#tab-0-0.
8. Stribeck, R., *Characteristics of plain and roller bearings.* Zeit. VDI, 1902. **46**.
9. Coy, R.C., *Practical Applications of Lubrication Models in Engines.* Tribology International, 1999. **31**: p. 563-571.
10. Taylor, R.I., *Engine Friction: The Influence of Lubricant Rheology.* Proceedings of the Institution of Mechanical Engineers Journal of Engine Tribology, 1997. **211**: p. 235-246.
11. Leong, D., *Investigations of Friction Losses in Automotive Internal Combustion Engines*. 2004, University of Nottingham.
12. Ferguson, C.R. and Kirkpatrick, A.T., *Internal Combustion Engines: Applied Thermosciences*. 3rd ed. 2016, Chichester: John Wiley and Sons Ltd.
13. Rosenberg, R.C., *General Friction Considerations for Engine Design*. 1982, SAE International.
14. Bhushan, B., *Introduction to Tribology*. 2002, New York: John Wiley and Sons, Inc.
15. Bouyer, J. and Fillon, M., *Experimental Measurement of the Friction Torque on Hydrodynamic Plain Journal Bearings during start-up.* Tribology International, 2011. **44**: p. 772-781.
16. Williams, J.A., *Engineering Tribology*. 1994, Oxford: Oxford Science Publications.
17. Taylor, C.M., *Automotive Engine Tribology-Design Considerations for Efficiency and Durability.* Wear, 1998. **221**: p. 1-8.
18. Costa, L., Fillon, M., Miranda, A.S., and Claro, J.C.P., *An Experimental Investigation of the Effect of Groove Location and Supply Pressure on the THD Performance of a Steadily Loaded Journal Bearing.* ASME Journal of Tribology, 2000. **122**: p. 227-232.

19. Costa, L., Miranda, A.S., and Claro, J.C.P., *Temperature, Flow and Eccentricity Measurements in a Journal Bearing with a Single Axial Groove at 90° to the Load Line.* Lubrication Science, 2003. **15**(2): p. 147-161.
20. Brito, F.P., Miranda, A.S., Bouyer, J., and Fillon, M., *Experimental Investigation of the Influence of Supply Temperature and Supply Pressure on the Performance of a Two Axial Groove Hydrodynamic Journal Bearing.* ASME Journal of Tribology, 2007. **129**: p. 98-105.
21. Brito, F.P., Miranda, A.S., Claro, J.C.P., and Fillon, M., *Experimental Comparison of the Performance of a Journal Bearing with a Single and a Twin Axial Groove Configuration.* Tribology International, 2012. **54**: p. 1-8.
22. Tanaka, M., *Journal Bearing Performance under Starved Lubrication* Tribology International, 2000. **33**: p. 259-264.
23. Okamoto, Y., Mochizuki, M., Mizumo, Y., and Tanaka, T., *Experimental Study for the Oil Flow Supplied from Oil Hole on Statically Loaded Bearings.* SAE Techinical Paper Series, 1995.
24. Costa, L., Miranda, A.S., Fillon, M., and Claro, J.C.P., *An Analysis of the Influence of Oil Supply Conditions on the Thermohydrodynamic Performance of a Single-Groove Journal Bearing.* Proceedings of the Institution of Mechanical Engineers Part J, 2002. **217**: p. 133-144.
25. *Handbook of Diesel Engines*. 1 ed. 2010: Springer-Verlag Berlin Heidelberg. 634.
26. DuBois, G.B. and Ocvirk, F.W., *Analytical Derivation and Experimental Evaluation of Short-Bearing Approximation for Full Journal Bearings*. 1953, NACA: Washington.
27. Fenton, M.B.M., *Flow and Heat Transfer Modelling of an Automotive Engine Lubrication System*. 1994, University of Warwick: Coventry. p. 404.
28. Clayton, D., *An Exploratory Study of Oil Grooves in Plain Bearings.* Proceedings of the Institution of Mechanical Engineers, 1946. **155**(1): p. 41-49.
29. Wang, J.K. and Khonsari, M.M., *Effects of Oil Inlet Pressure and Inlet Position of Axially Grooved Infinitely Long Journal Bearings. Part 1: Analytical Solutions and Static Performance.* Tribology International, 2007. **41**: p. 119-131.
30. Baylis, W.S., *An Investigation of Heat Transfer and Friction in Turbocharged Diesel Engines*, in *Mechanical Engineering*. 1999, University of Nottingham: Nottingham.
31. Mufti, R.A. and Priest, M., *Theoretical and Experimental Evaluation of Engine Bearing Performance.* Proceedings of the Institution of Mechanical Engineers, Part J : Journal of Engineering Tribology, 2009. **223**: p. 629-644.
32. Yang, L.S., *Friction Modelling for Internal Combustion Engines*, in *Mechanical Engineering*. 1992, University of Leeds.
33. Martin, F.A. and Lee, C.S., *Feed-Pressure Flow in Plain Journal Bearings.* ASLE Transactions, 1983. **26**(3): p. 381-392.
34. Stachowiak, G.W. and Batchelor, A.W., *Engineering Tribology: Third Edition*. 2005: Butterworth-Heinemann.
35. Hutchings, I.M., *Tribology: Friction and Wear of Engineering Materials*. 1992, Great Britain: Edward Arnold.
36. Taylor, R.I., *Lubrication, Tribology and Motorsport.* SAE Techinical Paper Series, 2002.

37. Park, S., Cho, Y., Sung, K., and Han, N., *The Effect of Viscosity and Friction Modifier on Fuel Economy and the Relationship Between Fuel Economy and Friction.* SAE International, 2009.
38. Andres, L.S. *Modern Lubrication Theory*. 2012.
39. Gumbel, L. and Everling, E., *Monatsblatter Berliner Bezirksver.* VDI, 1914(5): p. 87-104.
40. Martin, F.A., *Minimum Allowable Oil Film Thickness in Steadily Loaded Journal Bearings.* Proceedings of the Institution of Mechanical Engineers, 1964. **178**: p. 161-170.
41. Cameron, A., *Principles of Lubrication*. 3rd ed. 1966: John Wiley & Sons Inc. 256.
42. Petroff, N., *Friction in Machines and the Effect of the Lubricant (in Russian).* Inzh. Zh. St. Petersburg, 1883: p. 71-140.
43. Martin, F.A., *Friction in Internal Combustion Engine Bearings.* Proceedings of the Institution of Mechanical Engineers, 1985. **3**: p. 1-17.
44. Ozasa, T., Maitani, K., Fujimoto, Y., and Yorizane, K., *Simplified Estimation Method of Bearing Friction for Engines.* Internation Journal of Engine Research, 2016. **17**(8): p. 886-896.
45. Cole, J.A. and Hughes, C.J., *Oil Flow and Film Extent in Complete Journal Bearings.* Proceedings of the Institution of Mechanical Engineers, 1956: p. 499-510.
46. Dellis, P. and Arcoumanis, C., *Cavitation development in the lubricant film of a reciprocating piston-ring assembly.* Proceedings of the Institution of Mechanical Engineers, Part J: Journal of Engineering Tribology, 2004. **218**(3): p. 157-171.
47. Dhunput, A., Teodorescu, M., and Arcoumanis, C., *Investigation of cavitation development in the lubricant film of piston-ring assemblies.* Journal of Physics: Conference Series, 2007. **85**(1): p. 012005.
48. Brewe, D.E., *Current research in cavitating fluid films*, in *NASA Technical Memorandum*. 1990.
49. Braun, M.J. and Hendricks, R.C., *An Experimental Investigation of the Vaporous/Gaseous Cavity Characteristics of an Eccentric Journal Bearing.* ASLE Transactions, 1984. **27**(1): p. 1-14.
50. Dowson, D. and Taylor, C.M., *Cavitation in Bearings.* Annual Review Fluid Mechanics, 1979. **11**: p. 35-66.
51. Hamrock, B.J., *Fundamentals of Fluid Film Lubrication*. 1990, Ohio: CRC Press.
52. Floberg, L., *On the Tensile Strength of Liquids*, in *Transactions of Machine Elements Division*. 1973, Lund Technical University: Lund, Sweden. p. 1-13.
53. Wilson, R.W. *Cavitation Damage in Plain Bearings*. 1974. Leeds-Lyon: Inst. Mech. Engrs.
54. Sun, D.C. and Brewe, D.E., *A High Speed Photography Study of Cavitation in a Dynamically Loaded Journal Bearing.* Journal of Tribology, 1991. **113**(2): p. 287-294.
55. Sun, D.C. and Brewe, D.E., *Two Reference Time Scales for Studying the Dynamic Cavitation of Liquid Films.* Journal of Tribology, 1992. **114**(3): p. 612-615.

56. Dowson, D. and Taylor, C.M., *Fundamental Aspects of Cavitation in Bearings*, in *Proceedings of the 1st Leeds-Lyon Symposium on Tribology*, D. Dowson, M. Godet, and C.M. Taylor, Editors. 1974, Mechanical Engineering Publications Ltd, London, UK: University of Leeds, Leeds, UK. p. 15-25.
57. Soda, N. and Yasuhisa, T., *Cavitation Erosion of a Flat Surface Near a Rotating Shaft.* Wear, 1982. **74**: p. 275-286.
58. Heshmat, H., *The Mechanism of Cavitation in Hydrodynamic Lubrication.* Tribology Transactions, 1991. **34**: p. 177-186.
59. Mokhtar, M.O.A. and Ameen, M.E., *An Experimental Study of Cavitation in Hydrodynamically Lubricated Journal Bearings- Part 1: Oil Film Behaviour.* SAE Technical Paper Series, 1983(830305).
60. Wang, L., Lu, C., and Ge, P., *Theoretical and Experimental Study on the Cavitation Mechanism of a Low Viscosity Spiral Oil Wedge Journal Bearing.* Proceedings of the Institution of Mechanical Engineers, Part J : Journal of Engineering Tribology, 2014. **228**(9): p. 947-954.
61. Mitsui, J., Hori, Y., and Tanaka, M., *Thermohydrodynamic Analysis of Cooling Effect of Supply Oil in Circular Journal Bearing.* Journal of Lubrication Technology, 1983. **105**(3): p. 414-420.
62. Dowson, D., Taylor, C.M., and Miranda, A.A.S., *The Prediction of Liquid Film Journal Bearing Performance with a Consideration of Lubricant Film Reformation Part 2: Experimental Results.* Proceedings of the Institution of Mechanical Engineers, 1985. **199**: p. 103-111.
63. Dowson, D., Taylor, C.M., and Miranda, A.A.S., *The Prediction of Liquid Film Journal Bearing Performance with a consideration of Lubricant Film Reformation Part 1: Theoretical Results.* Proceedings of the Institution of Mechanical Engineers, 1985. **199**: p. 95-102.
64. Heshmat, H. and Pinkus, O., *Performance of Starved Journal Bearings with Oil Ring Lubrication.* Journal of Tribology, 1985. **107**: p. 23-31.
65. Heshmat, H., *Starved Bearing Technology Theory and Experiment*. 1988, Troy: Rensselaer Polytechnic Institute
66. Vijayaraghavan, D. and Keith, T.G., Jr, *Effect of Lubricant Supply Starvation on the Thermohydrodynamic Performance of a Journal Bearing.* Tribology Transactions, 1996. **39**: p. 645-653.
67. Ha, K.-P., Lee, H.W., Oh, D.Y., and Kim, W.T., *Development of Oil Aeration Meter for Internal Combustion Engine.* SAE Techinical Paper Series, 2005.
68. He, M., Allaire, P., Barrett, L., and Nicholas, J., *Thermohydrodynamic Modeling of Leading-Edge Groove Bearings under Starvation Condition.* Tribology Transactions, 2005. **48**(3): p. 362-369.
69. Vincent, B., Maspeyrot, P., and Frene, J., *Starvation and Cavitation Effects in Finite Grooved Journal Bearing.* Lubricants and Lubrication, 1995: p. 455-464.
70. Brito, F.P., Miranda, A.S., Claro, J.C.P., Teixeira, J.C., Costa, L., and Fillon, M., *The Role of Lubricant Feeding Conditions on the Performance Improvement and Friction Reduction of Journal Bearings.* Tribology International, 2014. **72**: p. 65-82.
71. Elrod, H.G., *A Cavitation Algorithm.* ASME Journal of Lubrication Technology, 1981. **103**: p. 350-354.

72. Jakobsson, B. and Floberg, L. *The Finite Journal Bearing Considering Vaporization*. Transactions of Chalmers University Technology, 1957. **190**, 1-119.
73. Olsson, K.O. *Cavitation in Dynamically Loaded Bearings*. Transactions of Chalmers University Technology, 1965. **308**.
74. Sommerfeld, A., *The Hydrodynamic Theory of Lubrication Friction.* Zs. Math. und Phys., 1904. **50**: p. 97-155.
75. Swift, H.W., *The Stability of Lubricating Films in Journal Bearings. (Includes Appendix).* Minutes of the Proceedings of the Institution of Civil Engineers, 1932. **233**(1932): p. 267-288.
76. Stieber, W., *Das Schwimmlager.* V.D.I., Berlin, 1933.
77. Floberg, L. *On Journal Bearing Lubrication Considering the Tensile Strength of the Liquid Lubricant*. Transactions of the Machine Elements Division, 1973. 1-26.
78. Elrod, H.G. and Adams, M.L., *A Computer Program for Cavitation and Starvation Problems.* Cavitation and Related Phenomena in Lubrication, Mechanical Engineering Publications, 1974: p. 37-41.
79. Brewe, D.E., *Theoretical Modeling of Vapor Cavitation in Dynamically Loaded Journal Bearings*, in *NASA Technical Memorandum*. 1985, NASA: Cleveland, Ohio.
80. Woods, C.M. and Brewe, D.E., *The Solution of the Elrod Algorithm for a Dynamically Loaded Journal Bearing Using Multigrid Techniques.* Journal of Tribology, 1989. **111**(2): p. 302-308.
81. Vijayaraghavan, D. and Keith, T.G., *Development and Evaluation of a Cavitation Algorithm.* Tribology Transactions, 1989. **32**(2): p. 225-233.
82. Ahmad, M.A., Kasolang, S., Dwyer-Joyce, R., and Abdullah, N.R., *The Effect of Oil Supply Pressure on the Circumferential Pressure Profile in Hydrodynamic Journal Bearing.* Applied Mechanics and Materials, 2013. **315**: p. 809-814.
83. King Engine Bearings, I. *Engine Bearings and How They Work*.
84. Garner, D.R., *Designing a Plain Bearing*, in *GLACIER*. 1975, The Glacier Metal Company Limited: University of Leeds.
85. Garner, D.R., *The Use of Design Procedures for Plain Bearings*, in *GLACIER*. 1980, The Glacier Metal Company: University of Leeds.
86. Rizvi, S.Q.A., *A Comprehensive Review of Lubricant Chemistry, Technology, Selection and Design*. 2009, Pensylvania, USA: ASTM International.
87. He, M., Cloud, C.H., and Byrne, J.M., *Fundamentals of Fluid Film Journal Bearing Operation and Modeling.* Proceedings of the Thirty-Fourth Turbomachinery Symposium, 2005: p. 155-176.
88. SAE International, *Engine Oil Viscosity Classification*. 2015: SAE International, 400 Commonwealth Drive, Warrendale, PA 15096-0001, USA.
89. ASTM D5293-15, *Standard Test Method for Apparent Viscosity of Engine Oils and Base Stocks between -10 ˚C and -35 ˚C using Cold-Cranking Simulator*. 2015: ASTM International, 100 Barr Harbor Drive, PO Box C700, West Conshohocken, PA 19428-2959, USA.
90. ASTM D4683-13, *Standard Test Method for Measuring Viscosity of New and Used Engine Oils at High Shear Rate and High Temperature by Tapered*

Bearing Simulator Viscometer at 150 ˚C. 2013: ASTM International, 100 Barr Harbor Drive, PO Box C700, West Conshohocken, PA 19428-2959, USA
91. ASTM D341-09 (Reapproved 2015), *Standard Practice for Viscosity-Temperature Charts for Liquid Petroleum Products*. 2015: ASTM International, 100 Barr Harbor Drive, PO Box C700, West Conshohocken, PA 19428-2959, USA.
92. Cross, M.M., *Rheology of non-Newtonian Fluids: a new flow equation for pseudo plastic systems.* Journal of Colloid Science, 1965. **20**.
93. Taylor, R.I., *The Inclusion of Lubricant Shear Thinning in the Short Bearing Approximation.* Proceedings of the Institution of Mechanical Engineers Part J, 1997. **213**.
94. Sorab, J., Holderman, H.A., and Chui, G.K., *Viscosity Prediction for Multigrade Oils.* SAE Paper 932833, 1993.
95. Watson, R.W. and McDonnell, T.F., *Additives-The Right Stuff for Automotive Enigne Oils*, in *International Off-Highway and Powerplant Congress and Exposition*. 1986: Milwaukee, Wisconsin.
96. P.J. Shayler, A.J.A., D.K.W. Leong, I. Pegg, A.J. Brown, J-C. Dumenil, *Characterising Lubricating Oil Viscosity to Describe Effects on Engine Friction.* SAE Paper 2007-01-1984, 2007.
97. Zammit, J.-P., *Managing Engine Thermal State to Reduce Friction Losses during Warm-up*, in *Mechanical Engineering*. 2012, University of Nottingham.
98. Wu, C.S., Klaus, E.E., and Duda, J.L., *Development of a Method for the Prediction of Pressure-Viscosity Coefficients of Lubricating Oils Based on Free-Volume Theory.* Journal of Tribology, 1989. **111**(1): p. 8.
99. Morita, A., Hosoi, A., Harada, T., Uchida, M., Kodama, Y., and Maegawa, H., *Study of the vehicle thermal management focused on the engine lubricant oil*, in *Vehicle Thermal Management Systems Conference Proceedings (VTMS11)*. 2013, Woodhead Publishing. p. 3-13.
100. Burke, R.D., Lewis, A.J., Akehurst, S., Brace, C.J., Pegg, I., and Stark, R., *Systems Optimisation of an Active Thermal Management System During Engine Warm-up.* Proceedings of the Institution of Mechanical Engineers, Part D: Journal of Automobile Engineering, 2012. **226**(10): p. 1365-1379.
101. Luff, D.C., Law, T., Shayler, P.J., and Pegg, I., *The Effect of Piston Cooling Jets on Diesel Engine Piston Temperatures, Emissions and Fuel Consumption.* SAE Int. J. Engines, 2012. **5**(3): p. 1300-1311.
102. Manning, J., *Internal Combustion Engine Design*. 2012: Ricardo UK Limited.
103. Staley, D., Pryor, B., and Gilgenbach, K., *Adaptation of a Variable Displacement Vane Pump to Engine Lube Oil Applications.* SAE International, 2007.
104. Toyoda, F., Kobayashi, Y., Miura, Y., and Koga, Y., *Development of Variable Discharge Oil Pump.* SAE International, 2008.
105. Neukirchner, H., Kramer, M., and Ohnesorge, T., *The Controlled Vane-Type Oil Pump for Oil Supply on Demand for Passenger Car Engines.* SAE International, 2002.
106. Rundo, M. and Squarcini, R., *Experimental Procedure for Measuring the Energy Consumption of IC Engine Lubricating Pumps during a NEDC Driving Cycle.* SAE Int. J. Engines, 2009. **2**(1): p. 1690-1700.

107. C. J. Brace, J.G.H., A. Cox, I. G. Pegg, R. Stark, *The Effect of Variable Flow Oil Pumps on Vehicle Fuel Economy.* 2009: p. 219-226.
108. J. Chisaki, K.Y., T. Kikuchi, S. Morinaka, K. Yamada, M. Okamoto, T. Oda, K. Manabe, *Development of a New 2.0-Liter Fuel-Efficient Diesel Engine.* SAE International, 2013.
109. Loganathan, S., Govindarajan, S., Suresh Kumar, J., Vijayakumar, K., and Srinivasan, K., *Design and Development of Vane Type Variable flow Oil Pump for Automotive Application*. 2011, The Automotive Research Association of India.
110. Arata, T., Novi, N., Ariga, K., Yamashita, A., and Armenio, G., *Development of a Two-Stage Variable Displacement Vane Oil Pump*. 2012, SAE International.
111. Ribeiro, E.G., Melo, W.B., and Filho, A.P.A., *Application of electric oil pumps on automotive systems*. 2005, SAE International.
112. Priest, M. and Taylor, C.M., *Automobile Engine Tribology - approaching the surface.* Wear, 2000. **241**: p. 193-203.
113. Bolander, N.W., Steenwyk, B.D., Sadeghi, F., and Gerber, G.R., *Lubrication Regime Transitions ar the Piston Ring-Cylinder Liner Interface.* Proceedings of the Institution of Mechanical Engineers, Part J : Journal of Engineering Tribology, 2004. **219**: p. 19-31.
114. Burrows, J.A., *An Investigation of Heat Transfer and Friction in Turbocharged Diesel Engines*. 1998, University of Nottingham.
115. Choukroun, A. and Chanfreau, M., *Automatic Control of Electronic Actuators for an Optimized Engine Cooling Thermal Management*. 2001, SAE International.
116. Cortona, E., Onder, C.H., and Guzzella, L., *Engine Thermomanagement with Electrical Components for Fuel Consumption Reduction.* Internation Journal of Engine Research, 2001. **3**: p. 157-170.
117. Law, T., Shayler, P., and Pegg, I., *Investigations of Sump Design to Improve the Thermal Management of Oil Temeprature during Engine Warm-up*, in *VTMS 8*. 2007: Nottingham.
118. J. Zammit, P.S., R. Gardiner, I. Pegg, *Investigating the Potential to Reduce Crankshaft Main Bearing Friction During Engine Warm-up by Raising Oil Feed Temperature.* SAE Paper 2012-01-1216, 2012.
119. Taylor, R.I. and Coy, R.C., *Improved Fuel Efficiency by Lubricant Design: A Review.* Proceedings of the Institution of Mechanical Engineers, Part J : Journal of Engineering Tribology, 1999. **214**: p. 1-15.
120. Allmaier, H., Priestner, C., Sander, D.E., and Reich, F.M., *Tribology in Engineering Chapter 9: Friction in Automotive Engines*, ed. H. Pihtili. 2013.
121. Sutton, M., Kocsis, J.A., and Nakagawa, I., *Improved Friction Modifiers to Aid in Future Fuel Economy Targets*. 2007, SAE International.
122. Ryk, G. and Etsion, I., *Testing Piston Rings with Partial Laser Surface Texturing for Friciton Reduction.* Wear, 2006. **261**: p. 792-796.
123. Ryk, G., Kligerman, Y., Etsion, I., and Shinkarenko, A., *Experimental Investigation of Partial Laser Surface Texturing for Piston-Ring Friction Reduction.* Tribology Transactions, 2005. **48**: p. 583-588.
124. Holmberg, K., Andersson, P., and Erdemir, A., *Global Energy Consumption due to Friction in Passenger Cars.* Tribology International, 2012. **47**: p. 221-234.

125. Etsion, I. and Sher, E., *Improving Fuel Efficiency with Laser Surface Textured Piston Rings.* Tribology International, 2009. **42**: p. 542-547.
126. Wang, X., Yu, H., and Huang, W. *Surface Texture Design for Different Circumstances*. in *Proceedings of the 1st International Brazilian Conference on Tribology*. 2010. Rio de Janeiro.
127. Cupillard, S., Glavatskih, S., and Cervantes, M.J., *Computational Fluid Dynamics Analysis of a Journal Bearing with Surface Texturing.* Proceedings of the Institution of Mechanical Engineers, Part J : Journal of Engineering Tribology, 2008. **222**: p. 97-107.
128. Tala-Ighil, N., Maspeyrot, P., Fillon, M., and Bounif, A., *Effects of Surface Texture on Journal Bearing Characteristics under Steady State Operating Conditions.* Proceedings of the Institution of Mechanical Engineers, Part J : Journal of Engineering Tribology, 2007. **221**: p. 623-633.
129. Cameron, A., *Basic Lubrication Theory*. 1971, London: Longman.
130. Wada, S., Hayashi, H., and Haga, K., *Behaviour of a Bingham Solid in Hydrodynamic Lubrication.* Bulletin of the Japan Society of Mechanical Engineers, 1974. **17**(111): p. 1182-1191.
131. Savaskan, T., Purcek, G., and Murphy, S., *Sliding Wear of Cast Zinc-Based Alloy Bearings under Static and Dynamic Loading Conditions.* Wear, 2001. **252**: p. 693-703.
132. Dowson, D., Hudson, J.D., Hunter, B., and March, C.N., *An Experimental Investigation of the Thermal Equilibrium of Steadily Loaded Journal Bearings.* Proceedings of the Institution of Mechanical Engineers Part 3B, 1966-67. **101**: p. 70-80.
133. Okamoto, Y., Kitahara, K., Ushijima, K., Aoyama, S., Xu, H., and Jones, G., *A Study for Wear and Fatigue on Engine Bearings by using EHL Analysis.* JSAE Review 2000. **21**: p. 189-196.
134. Jiang, G.D., Hu, H., Xu, W., Jin, Z.W., and Xie, Y.B., *Identification of Oil Film Coefficients of Large Journal Bearings on a Full Scale Journal Bearing Test Rig.* Tribology International, 1997. **30**: p. 789-793.
135. Tomimoto, M., *Experimental Verification of a Particle Induced Friction Model in Journal Bearings.* Wear, 2003. **254**: p. 749-762.
136. Brito, F.C.P., *Thermohydrodynamic Performace of Twin Groove Journal Bearings Considering Realistic Lubricant Supply Conditions: A Theoretical and Experimental Study (PhD Thesis)*. 2009: Universidade do Minho.
137. Shayler, P.J., Cheng, L., Li, Q., and Wahab, E., *A Modified Oil Lubrication System with Flow Control to Reduce Crankshaft Bearing Friction in a 1.4 Litre 4 Cylinder Diesel Engine*, in *SAE 2016 World Congress and Exhibition*. 2016, SAE International: Detroit, USA.
138. Majumdar, B.C. and Saha, A.K., *Temperature Distribution in Oil Journal Bearing.* Wear, 1974. **28**(8).
139. Swales, P.D. *A Review of Cavitation Phenomena in Engineering Situations*. in *Proceedings of the 1st Leeds-Lyon Symposium on Tribology*. 1974. Leeds.
140. *Chevron Supreme Motor Oil Material Safety Data Sheet*. 2010, Chevron Energy Technology Company Richmond.

141. Ahmad, M.A., Kasolang, S., Dwyer-Joyce, R.S., and Jumahat, A., *The Effects of Oil Supply Pressure at different Groove Position on Temperature and Pressure Profile in Journal Bearing.* Jurnal Teknologi, 2014. **66**(3): p. 113-119.
142. *Performance Curves-L Series Metric*. 2013, Tuthill Pump Company.
143. Miura, A. and Shiraishi, K., *Investigation of Main Bearing Friction in a Diesel Engine*. 1989, SAE International.
144. Shayler, P.J., Leong, D.K.W., and Murphy, M., *Contributions to Engine Friction During Cold, Low Speed Running and the Dependence on Oil Viscosity*. 2005, SAE International.
145. Islam, M.R., *A Floating Liner Facility and Studies of Friction at a Reciprocating Piston-Cylinder Wall Interface*, in *Mechanical Engineering*. 2016, University of Nottingham: Nottingham.
146. Company, T.T., *Timken Products Catalog*. 2012. p. A173.
147. Zhao, C., *Thermal Systems Behaviour and Exhaust Energy Recovery of a Spark Ignition Engine*, in *Mechanical Engineering*. 2015, University of Nottingham.
148. Gardiner, R., Zhao, C., Addison, J., and Shayler, P.J., *Investigations of Thermal State Changes during Warm up of a Spark Ignition Engine*, in *Proc. of IMechE Int Conf C1365, VTMS 11, paper C028*. 2013: Coventry.
149. Henry, W., *Experiments on the quantity of gases absorbed by water, at different temperatures, and under different pressures.* Philosophical Transactions of the Royal Society of London, 1803. **93**: p. 29-274.
150. Jarrier, L., Champoussin, J.C., Yu, R., and Gentile, D., *Warm-Up of a D.I. Diesel Engine: Experiment and Modeling*. 2000, SAE International.
151. André, M., *In Actual Use Car Testing: 70,000 Kilometers and 10,000 Trips by 55 French Cars under Real Conditions*. 1991, SAE International.
152. Malvasi, A., Squarcini, R., Armenio, G., and Brommel, A., *Design Process of an Electric Powered Oil Pump.* Autotechreview, 2014. **3**(3): p. 36-39.